ELECTROSPRAY IONIZATION TANDEM-MS OF AMMONIUM AND ALKALI METALS OF TAGS AND THEIR OXIDATION PRODUCTS WITH FRACTIONATION BY LC-MS AND FAIMS

by

EmmaRae Murphy

Submitted in partial fulfilment of the requirements
for the degree Masters of Applied Science

at

Dalhousie University
Halifax, Nova Scotia
July 2022

TABLE OF CONTENTS

LIST OF TABLES ..... **v**

LIST OF FIGURES ..... **vi**

ABSTRACT ..... **xi**

LIST OF ABBREVIATIONS AND SYMBOLS USED ..... **xii**

ACKNOWLEDGEMENTS ..... **xiv**

CHAPTER 1 INTRODUCTION **1**

1.1.Lipid Classes/Nomenclature 1

1.2.TAG Oxidation Products 4

1.3.Chromatographic Methods for TAG and TAG Oxidation Products 8

1.4.Mass Spectrometry 8

1.5.Ionization Mechanisms 15

1.6.ESI-MS Analysis of TAG Standards using NH_4^+ 19

1.7.Tandem-MS of TAG and TAG Degradation Products 23

1.8.Liquid Chromatography (LC) 27

1.9.FAIMS 33

1.10. Research Goals 34

CHAPTER 2 ELECTROSPRAY IONIZATION TANDEM-MS OF TAG AND TAG OXIDATION PRODUCTS **35**

2.1 Introduction 35

2.2 Experimental 38

2.2.1 Materials 38

2.2.2 Sample Preparation 38

2.2.3 Mass Spectrometry 40

2.3 Results and Discussion 41

2.3.1 Ionization of TAG Standard Using Ammonium Acetate 41

2.3.2 Tandem-MS of TAG Standards 44

2.3.3 Ionization of TAG With Cation Adducts 48

2.3.4 Competitive Ionization of TAG With Alkali Metal and Ammonium Adduct 51

2.3.5 Thermal Degradation of Intact TAG Standards 60

2.3.6 Ionization of TAG Oxidation Products (Hydroxy Trilinolein, Hydroperoxy Trilinolein and Epoxy Trilinolein) at 25°C ……..…….64

2.3.7 Tandem-MS of Oxidized Trilinolein With Cation Adducts...……..71

2.3.8 MS^3 Analysis of Ammoniated TAG Degradation Products.…….…..…….84

2.3.9 Thermal Fragmentation of TAG Oxidation Products...…..……..…….86

2.4 Conclusion……...91

CHAPTER 3 HIGH-FIELD ASYMMETRIC WAVEFORM ION MOBILITY SPECTROMETRY ANALYSIS OF TAGS AND THEIR OXIDATION PRODUCTS……93

3.1 Introduction……..93

3.2 Experimental……....99

3.2.1 Materials and Methods……..99

3.2.2 Instrumentation…..……..……100

3.3 Results and Discussion……..103

3.3.1 Effect of Dispersion Voltage (DV) on Compensation Voltage (CV)…….103

3.3.2 Transmission of (54:6) Versus (54:3) TAG……..……..106

3.3.3 Ion-selective Compensation Voltage Spectra of TAG and TAG Oxidation Products Using Alkali Metal Adducts……108

3.3.4 Thermal Degradation of Oxidized TAG at High Inlet Temperatures.……113

3.4 Conclusion.……117

CHAPTER 4 LIQUID CHROMATOGRAPHY MASS SPECTROMETRY OF TAG AND TAG DEGRADATION PRODUCTS……..119

4.1 Introduction……119

4.2 Experimental……..122

4.2.1 Materials……122

4.2.2 Liquid Chromatography……...……...…..123

4.2.3 Mass Spectrometry……126

4.2.4 Sample Preparation……126

4.3 Results and Discussion……..126

4.3.1 Isocratic Elution of TAG and TAG Oxidation Products……126

4.3.2 Calibration Curves for TAG Degradation Products……135

4.4 Conclusion……138

CHAPTER 5 IDENTIFICATION OF TAG DEGRADATION IN CANOLA OIL USING LC-MSMS……140
5.1 Introduction……..…140
5.2 Experimental……..142
5.2.1 Materials……142
5.2.2 Mass Spectrometry……..142
5.2.3 Liquid Chromatography……..142
5.2.4 Sample Preparation……143
5.3 Results and Discussion……..144
5.3.1 Identification of Unoxidized TAG in Canola Oil……...144
5.3.2 Thermal Oxidation of TAG in Canola Oil……..154
5.3.3 Mono-oxygenated Degradation Products of 54:3 TAG……..161
5.3.4 Di-oxygenated Products of 54:3 TAG……166
5.3.5 Identification of Multiple Oxidation Products on 54:3 TAG……..170
5.4 Conclusion……178
CHAPTER 6 CONCLUSIONS……180
6.1 General Conclusions……..180
6.2 Future Work……..183
BIBLIOGRAPHY……..186
APPENDIX A……196

LIST OF TABLES

Table 2.1 Comprehensive list of all chemicals and reagents used throughout this study……..38

Table 2.2 List of L-QIT mass spectrometry parameters used in this study……..41

Table 2.3 List of Q-OT mass spectrometry experimental details used in this study……41

Table 2.4 Fragmentation for mono-oxygenated products of trilinolein showing the difference between possible unique fragments using lithium, sodium and ammonium adducts……..…….……75

Table 2.5 Fragmentation for hydroperoxide trilinolein, di-epoxy trilinolein and di-hydroxy trilinolein showing the difference between possible unique fragments using lithium, sodium and ammonium adducts…….81

Table 2.6 Direct-infusion MS was performed on the L-QIT MS to employ MS^3 on target TAG precursor oxidation products. Un-oxidized DAG product ions from MS^2 were further targeted for MS^3 analysis to yield MAG product ions……..86

Table 3.1 List of FAIMS parameters used for this study……103

Table 4.1 Agilent 1260 Infinity II, LC parameters used in this study……123

Table 4.2 Epoxy, hydroxy and hydroperoxy trilinolein standard retention times. XIC for each oxidation product was done using a 10 ppm window……...132

Table 5.1 Agilent 1260 Infinity II, LC parameters used in this study……143

Table 5.2 Endogenous TAG of canola oil and the proposed empirical formulae. t_R are determined by the proposed empirical formula m/z to within 10 ppm. Tandem-MS using a CE of 27 eV shows fragment ions……..152

Table 5.3 Predicted m/z values and empirical formula for mono-, di-, tri-, tetra-, penta- and hexa- oxygenated products of 54:3 TAG……...157

LIST OF FIGURES

Figure 1.1 Diagram of a triacylglycerol structure where R represents the acyl chain. The possible positions within the glycerol backbone are highlighted by sn-1, sn-2 and sn-3……2

Figure 1.2 Chemical diagrams of the general structures of MAGs (A), DAGs (B) and TAG (C)……4

Figure 1.3 Mechanisms of lipid oxidation from an unsaturated site in a TAG molecule……..6

Figure 1.4 Mechanisms of lipid oxidation from two unsaturated sites in a TAG molecule……..7

Figure 1.5 Block diagram of mass spectrometer parameters highlighting the ion source, mass analyzer, collision cell and detector/readout in vacuum…….10

Figure 1.6 Diagram of an orbitrap mass analyzer and an example of ion trajectory…....12

Figure 1.7 Trilinolein standard analyzed by direct-infusion on the L-QIT mass spectrometer (A), and the Q-OT mass spectrometer (B). Panel (A) resolution is set at "enhanced" while (B) is at a resolution of 140,000…….13

Figure 1.8 Tandem-MS mechanism of parallel reaction monitoring (PRM)……15

Figure 1.9 Diagram of atmospheric pressure chemical ionization mechanism……16

Figure 1.10 Diagram of electrospray ionization mechanism……17

Figure 1.11 Trilinolein mass spectrometry spectra displaying the simulated mass spectra from the Q-OT HR/AM using the empirical formula $C_{57}H_{98}O_6NH_4$……21

Figure 1.12 Magnified full-MS spectra of ammoniated trilinolein collected on the Q-OT at a mass range of 400-2000 m/z, showing the TAG sodium peak in red…..……..22

Figure 1.13 MSMS spectra of precursor $[M+Li]^+$ TAG (16:0/18:1/18:0) at m/z 867….24

Figure 1.14 Proposed structure of FA +74 by Kalo et al, (2006) from degradation of R_1R_3 DAG product ion……..25

Figure 1.15 Liquid chromatographic separation of triolein (18:1/18:1/18:1) and trilinolein (18:2/18:2/18:2) on a C8 column with an isocratic mobile phase of 95 % ethanol……....31

Figure 2.1 Spectra of ammoniated trilinolein showing the DAG (A) and dimer (B) that appear in the spectra resulting from analysis on the Q-OT mass spectrometer with the inlet set to RT……...43

Figure 2.2 Ammoniated 54: 6 TAG showing Q-OT full MS scan (A), isolation of precursor ion m/z 896.78 at CE 10 eV in panel (B), CE of 30 eV in panel (C) and 50 eV in panel (D)….……44

Figure 2.3 Q-OT MSMS spectra of precursor dimer ion 1776.5 [2TAG+NH_4] at an applied CE of 27 eV……...47

Figure 2.4 Direct-infusion ESI on the Q-OT MS of 5 ug mL^{-1} 54:6 TAG with alkali salts LiCl, NaCl, KCl, RbCl and CsCl…….49

Figure 2.5 Competitive ionization of alkali metal and ammonium with 54:6 TAG prepared in binary mixtures…….53

Figure 2.6 ESI-MSMS of ammonium and alkali metal adducts of 54:6 performed on the Q-OT MS. A CE of 27 eV was used……..55

Figure 2.7 Proposed pathway to generate the protonated DAG ion from lithiated 54:6. Rationalizes the formation of DAG ion arising from elimination of the *sn*-2 FA as a lithiated salt……..57

Figure 2.8 Proposed structural diagram of m/z 337.27 MAG derivative by Kalo et al. (2006) representing RCO+74……..58

Figure 2.9 Thermal degradation of ammoniated 54:6 in the heated transfer capillary of the L-QIT. Spectra collected with the transfer capillary at room temperature (A) were compared to those at 275 °C…….61

Figure 2.10 Thermal degradation of sodiated 54:6 in the heated transfer capillary of the L-QIT. Spectra collected with the transfer capillary at room temperature (A) were compared to those at 275 °C……..63

Figure 2.11 Plots of m/z 896.67 $[TAG + NH_4]^+$ in red, m/z 901.67 $[TAG+Na]^+$ in black and 599.67 DAG ion $[TAG + NH_4 - FA - NH_3]^+$ in blue. Analysis was done on the L-QIT at temperature intervals of 30 °C, 50 °C, 100 °C, 150 °C, 200 °C, 250 °C and 300 °C…….64

Figure 2.12 Hydroperoxy 54:6 on the Q-OT with each alkali metal and ammonium……65

Figure 2.13 Ionization of hydroxy 54:6 on the Q-OT with each alkali metal and ammonium……67

Figure 2.14 Hydroperoxide decomposition mechanism to generate secondary oxidation products, epoxides……69

Figure 2.15 Ionization of epoxy 54:6 on the Q-OT with each alkali metal and ammonium……69

Figure 2.16 Tandem-MS of mono-hydroxy 54:6 with alkali metals and ammonium at a collision energy of 33 eV……73

Figure 2.17 Q-OT MS spectra highlighting the unique fragment ions of mono-hydroxy and mono-epoxy 54:6 with ammonium. Both precursor ions were at m/z 912.671 and targeted at a CE of 27 eV……..77

Figure 2.18 Ammoniated mono-hydroxy trilinolein (A) targeted at increasing CE. Product ions 877.7 (black), [M+NH_4+O-NH_3OH_2] and 597.5 (blue), [M+NH_4+O-$C_{18}H_{35}O_2NH_3O$] are plotted as signal intensity versus increasing CE……..….78

Figure 2.19 Precursor mono-hydroxy 54:6 was targeted at increasing CE. (A) represents lithiated mono-hydroxy precursor with corresponding product ions, and (B) represents sodiated mono-hydroxy 54:6 with corresponding product ions. Panel (C) represents rubidiated 54:6 with corresponding product ions…….80

Figure 2.20 Thermal degradation of ammoniated hydroxy 54:6 where panel (A) represents spectra collected at room temperature and panel (B) shows spectra collected at 275 °C…….87

Figure 2.21 Hydroxy 54:6 at 275 °C as the inlet temperature with each of the alkali metals and ammonium…….89

Figure 3.1 Hypothetical dependence of ion mobility on electric field strength for three different type of ions. K_h is ion mobility at high electric fields and K is low-field ion mobility..……..……94

Figure 3.2 Illustration of the ion movement between two plates during an applied electric field shown as $V(t)$. The ion is transported horizontally by a gas flow (distance is not to scale)…….96

Figure 3.3 Asymmetric waveforms used in FAIMS. The maximum value of the waveform is called the dispersion voltage (DV)……...97

Figure 3.4 A front-on view of cylindrical FAIMS geometry highlighting the inner and outer electrodes and the gas inlet. Ion trajectory direction is highlighted by green arrows……..99

Figure 3.5 Diagram of the experimental setup of the dome-style FAIMS device mounted on the L-QIT MS interface……...102

Figure 3.6 In panel (A) CV is plotted as DV values increase for ammoniated 54:6 monomer (black) and ammoniated dimer (blue). Panel (B) shows CV ionograms of 54:6 monomer at increasing DV values……..106

Figure 3.7 (A) Full MS spectra acquired on the L-QIT of ammoniated hydroxy 54:6 versus (B) ammoniated hydroxy 54:6 at a DV of -4.2 kV……..107

Figure 3.8 CV ionograms of 54:6 and 54:3 using FAIMS…….108

Figure 3.9 54:6 CV scans using different alkali metals and ammonium using FAIMS. CV chromatograms were extracted for the ion $C_{57}H_{98}O_6A$ where A represents the cation…….....110

Figure 3.10 Comparison of lithiated 54:6 (black), lithiated hydroxy 54:6 (blue) and lithiated hydroperoxy 54:6 (red) CV traces at DV -4.25 kV……...…….…111

Figure 3.11 Hydroperoxy 54:6 CV scans using different alkali metals and ammonium using FAIMS……....112

Figure 3.12 Comparison of CV profiles with mono-hydroxy trilinolein (black), mono-hydroperoxy 54:6 (blue) and mono-epoxy 54:6 (red) at a DV of -4.25 kV..…....113

Figure 3.13 FAIMS analysis of peroxy-trilinolein with each alkali metal and ammonium at 25 °C and 275 °C……..117

Figure 4.1 LC chromatograms of 54:6 TAG using a 10-minute 95 % ethanol method with 0.1 mM ammonium acetate and 0.1 % formic acid and a C8 column. Scan filters are shown as a TIC in (A), and base peak (BP) filter in (B), and extracted ion chromatogram (XIC) in panel (C) and selected reaction monitoring scan of precursor 896.771 in (D)……..125

Figure 4.2 54:6 (black) and 54:3 (red) standards on LC coupled to Q-OT. the chromatograms are extracted with the corresponding MS spectra……128

Figure 4.3 Epoxidized 54:6 TAG with 0.1 mM ammonium acetate. LC separation of the six oxidation products is shown over an isocratic (95 % ethanol) period of 10 minutes……130

Figure 4.4 Separation of mono-epoxy 54:6 (red) and mono-hydroxy 54:6 (black). The molecules were injected separately and extracted with a m/z of 912.67 within 10 ppm…….131

Figure 4.5 Hydroxy and hydro-peroxy 54:6 TAG. XIC for mono-hydroxy (black), di-hydroxy (red) and tri-hydroxy (brown). XIC for mono- (blue), di- (green) and tri-hydroperoxy (orange) were also plotted…….134

Figure 4.6 Calibration curve of hydroxy 54:6 from 0.001 ug mL^{-1} – 5ug mL^{-1} where mono-hydroxy 54:6 at m/z 912.67 is extracted and plotted……..136

Figure 4.7 Hydroxy 54:6 TAG at concentrations from 0.001 ug mL-1 to 1 ug mL-1 where m/z 912.78 is plotted in (A) and hydro-peroxy 54:6 at m/z 928.76 in (B)……138

Figure 5.1 Comparison of 54:3 TAG of canola oil (blue) to triolein standard (green) in panel (A). Ions are extracted as $[TAG+NH_4]^+$ adducts. At a collision energy of 30 eV, product ions from precursor 54:3 TAG in canola (B) and precursor triolein (C). The corresponding m/z spectra are displayed in panels (D) and (E)……146

Figure 5.2 Un-oxidized canola oil analyzed on the L-QIT MS using MS^3 to target 54:3 TAG……..…….148

Figure 5.3 Endogenous TAG identified in un-oxidized canola oil analyzed using the 10-minute isocratic method. Panel (A) shows the 5 most abundant TAG identified, where the colour corresponds to that in the legend. Panel (B) highlights less abundant TAGs identified……150

Figure 5.4 Base peak chromatograms of un-oxidized canola oil (A), canola oil heated (60 °C) for 24 hours (B) and heated for 15 days (C)……155

Figure 5.5 Proposed mechanism for the decomposition of hydroperoxy triolein (A) to form epoxy TAG (B), epoxy DAG (C) and DAG (D)……..158

Figure 5.6 MSMS PRM channel of precursor ion m/z 934 at CE =27 eV…...……..160

Figure 5.7 XIC of mono-oxygenated 54:3 after 24 hours, 48 hours, 72 hours, 96 hours, 102 hours and 504 hours……..162

Figure 5.8 m/z 918.81 mono-oxygen product after three days of heating at 60 °C (A). MSMS on precursor m/z 918 with a CE of 30 eV, where the product ions from the two peaks are presented in (B) and (C)…….164

Figure 5.9 Proposed mono-hydroxy 54:3 TAG in canola represented by diagonal grey stripes versus propose mono-epoxy 54:3 TAG in canola represented by solid black……165

Figure 5.10 XIC of di-oxygenated 54:3 TAG of canola after heating at 60 °C for 24 hours, 48 hours, 72 hours, 96 hours, 102 hours, 144 hours, 168 hours and 504 hours……..167

Figure 5.11 Panel (A) MSMS PRM window of m/z 934 at 504 hours of heating. Corresponding MSMS spectra are shown in panel (B) for 3.75 minutes and panel (C) for 4.25 minutes…….170

Figure 5.12 XIC of un-oxidized 54:3 TAG and the six oxidation products……...172

Figure 5.13 MSMS of precursor ions m/z 950.8 (A), m/z 966.5 (B), m/z 982.5 (C) and m/z 998.5 (D)……..174

Figure 5.14 Absolute signal intensities for six potential oxidation products of 54:3 TAG in canola oil over a period of 504 hours…….176

Figure 5.15 Relative amounts of six potential oxygen atoms onto 54:3 TAG in canola oil……..177

ABSTRACT

Triacylglycerols (TAGs) are the main component of edible oils, where unsaturated TAGs are easily oxidized, leading to toxicity and negative health effects. The analysis of TAG and TAG oxidation products is an ongoing analytical challenge due to the immense complexity within the molecules. Previous studies on TAG oxidation focused on hydroperoxide products to measure oxidation. There are few studies that address the importance of hydroxide and epoxide formation and their effect on health and nutritional deterioration. In this thesis, a longitudinal liquid chromatography- tandem mass spectrometry (LC-MSMS) study was presented for the simultaneous qualification and quantification of TAGs and their oxidation products in canola oil. The method allowed the oil sample to be diluted 100,000-fold, while avoiding other sample preparation steps and reducing variability in results.

Ionization of TAG and TAG oxidation products was observed using alkali metal and ammonium adducts on a high resolution/ accurate mass, mass spectrometer. Ionization was successful with each potential charge carrier; however, tandem-MS analysis favoured the use of ammonium which produced unique product ions for overlapping m/z oxidation products. It was critical to acidify ammonia in order to produce the adduct species. The unique product ions from ammonium were easily identifiable and can be applied to interpret complex samples.

The ionization method presented an unexpected effect of MS inlet temperature with TAGs and their oxidation products. Using a novel high-filed asymmetric waveform ion mobility spectrometry (FAIMS) device, it was determined that MS inlet temperatures greater than 150 °C led to decomposition of the TAG monomer into DAG, and decomposition of the dimer ion into a monomeric species. FAIMS was used to determine the decomposition pathways and led to the conclusion that the effect of temperature was adduct dependent. It is ironic that heat degrades TAGs and causes the oxidation product to leave, as the oxidation initially arises under the presence of heat.

A quick and simple isocratic LC method was coupled with MSMS for reproducible resolution of TAGs and their oxidation products. The method successfully resolved overlapping m/z oxidation products, where hydroxy TAGs were found to be more polar than epoxides. A linear response was achieved over a 1000-fold region with approximate limit of detection (LOD) of 24 pg mL^{-1}. The quick and simple analytical method can be easily incorporated for analysis of a complex sample.

LIST OF ABBREVIATIONS AND SYMBOLS USED

amu	Atomic mass unit
APCI	Atmospheric pressure-chemical ionization
APPI	Atmospheric pressure photoionization
BP	Base peak
CE	Collision energy
CID	Collision-induced dissociation
CRM	Charge residue model
C-trap	Curved linear trap
CV	Compensation voltage
Da	Dalton
DAG	Diacylglycerol
DB	Double bond
DV	Dispersion voltage
ECN	Equivalent carbon number
EI	Electron ionization
ESI	Electrospray ionization
ESI-MS	Electrospray ionization mass spectrometry
eV	Electron volt
FA	Fatty acid
FAIMS	High-field asymmetric waveform ion mobility spectrometry
FAME	Fatty acid methyl esters
FID	Flame ionization detector
FTICR	Fourier transform ion cyclotron resonance
GC	Gas chromatography
GC-FID	Gas chromatography flame ionization detector
GC-MS	Gas chromatography mass spectrometry
HCD	Higher-energy C-trap dissociation
HPLC	High performance liquid chromatography

HR/AM	High-resolution accurate mass
IET	Ion evaporation theory
IMS	Ion mobility spectrometry
LC	Liquid chromatography
LC-MS	Liquid chromatography mass spectrometry
LDI	Laser desorption ionization
LQIT	Linear ion trap mass spectrometer
m/z	Mass to charge ratio
MAG	Monoacylglycerol
MIPS	Modular intelligent power sources
MS	Mass spectrometry
MS/MS	Tandem mass spectrometry
MS^n	Multi-stage mass spectrometry
NPLC	Normal phase liquid chromatography
OBV	Outer bias voltage
OT	Orbitrap
ppm	Parts per million
PRM	Parallel reaction monitoring
Q-OT	Quadrupole orbitrap mass spectrometer
RPLC	Reversed phase liquid chromatography
SIM	Selected ion monitoring
sn	Stereochemical numbering
SRM	Selected reaction monitoring
TAG	triacylglycerol
Th	Thomsons
TIC	Total ion chromatogram
TLC	Thin-layer chromatography
tR	Retention time
XIC	Extracted ion chromatograms

ACKNOWLEDGEMENTS

I would like to firstly express my deepest appreciation to my two supervisors, Dr. Suzanne Budge and Dr. Dave Barnett for their endless support, guidance, encouragement and friendship along this journey. Thank you for all your time and dedication spent working with me on this thesis. Dave, thank you for your endless knowledge on mass spectrometry and FAIMS. Sue, thank you for introducing and teaching me the field of lipids and their diversity. The combination of the two fields made for a great project. Thank you to Dr.Azadeh Kermanshahi pour for your commitment and help with this project. I would also like to thank my lab-mates, Andrew, Katie and Victoria for their help and friendship along the way.

This endeavor would not have been completed without the continued love and support of my amazing parents. To my best friends and partner Taylor, thank you for always being there for me. This would not have been completed without all of the amazing people in my life that continue to support me, words cannot express my gratitude.

Thank you.

CHAPTER 1 INTRODUCTION

1.1 LIPID CLASSES/NOMENCLATURE

Although the term 'lipid' is widely recognized and seemingly understood by many, a single and accepted definition does not exist. A definition was proposed by William Christie in 1987 which stated, "Lipids are fatty acids and their derivatives, and substances related biosynthetically or functionally to these compounds" (Christie, 1987) and many people use this as the definition of lipids. However, he later deemed his initial definition too short and vague, instead proposing a more thorough explanation of the term as "Lipids compromise a heterogeneous class of predominantly hydrophobic organic molecules of relatively low molecular weight (commonly <1000), that are defined by the presence either of linear alkyl chains, usually with even-numbers of carbon atoms and saturated or unsaturated with double bonds in characteristic positions, or of isoprene units in linear or cyclic structures. These can contain variable numbers of oxygenated substituents such as carboxylic acid or hydroxyl groups, and/or other heteroatoms, but especially nitrogen in amines. Often, these are linked covalently to glycerol, carbohydrates, phosphate and other small polar entities, which can render the molecules more amphiphilic" (Christie, 2009). Christie incorporates the term 'amphiphilic' which defines a chemical compound with both hydrophilic and lipophilic properties. The struggle of defining lipids and lipid classes highlights the complexity of these molecules. Lipids are often separated into either simple or complex groups; this study will focus on the simple lipid group of triacylglycerols (TAGs) (Christie, 2010).

Essentially all commercially important fats and oils of animal or plant origin are composed of TAGs (Kato et al. 2017). TAGs consist of a glycerol backbone esterified to

three fatty acid (FA) chains (Figure 1.1). Although their analysis presents a magnitude of complexity, TAGs are considered simple lipids because they yield two primary products per molecule in hydrolysis: glycerol and FAs (Christie et al. 2010).

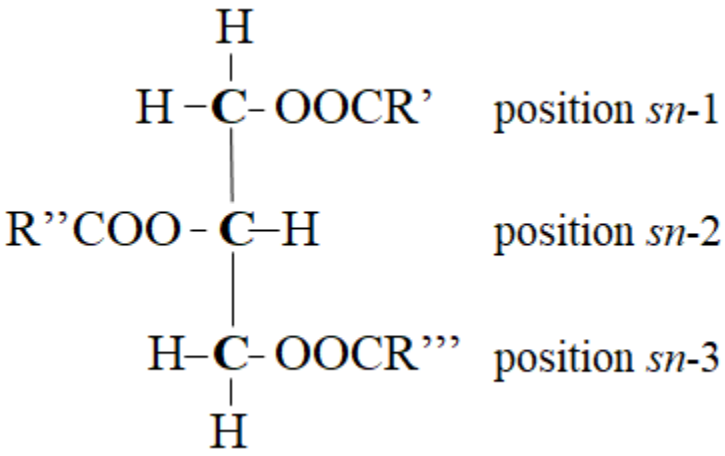

Figure 1.1 Diagram of a triacylglycerol structure where R represents the acyl chain. The possible positions within the glycerol backbone are highlighted by *sn*-1, *sn*-2 and *sn*-3.

TAGs are energy storing molecules and as such are one of the main sources of energy for living organisms. TAGs are also an important source of FAs that are essential for human health where their structure affects digestibility and metabolism of dietary FAs (White, 2009). The FAs within the TAG can be saturated or unsaturated, where unsaturated FAs contain double bonds within the chain. FAs within TAGs can be of different chain lengths and have different amounts/positions of double bonds (Frankel, 1999). Food oils are largely composed of unsaturated TAGs. The presence of a double bond within an unsaturated FA causes a 'kink' or bend in the chain that prevents the molecules from tightly packing (Pelley et al. 2012). The inability to tightly pack the TAG molecules results in liquid oils at room temperature in comparison to solid butter, which is largely composed of saturated TAGs (Echegaray et al. 2022). The possibility of

multiple FA conformations within TAG species presents numerous potential structures and isomers, creating a challenge when determining their molecular structures.

TAGs are commonly represented by the total number of carbon atoms in the molecule followed by the total number of double bonds in the three acyl chains (Liebisch et al. 2020). For example, trilinolein, a commonly identified TAG, has a total of 54 carbon atoms and 2 double bonds on each FA chain. Therefore, trilinolein is represented as 54:6. TAGs can also be described by explicitly defining the number of carbons and double bonds in each of the FAs separately. For example, using this notation trilinolein is defined as (18:2/18:2/18:2) (Liebisch et al. 2020) where the 18 gives the number of carbon atoms in each chain and the 2 indicates the number of double bonds in each chain. The three carbon atoms in the glycerol backbone can also be labeled "*sn*" which stands for stereochemical numbering and are referred to as *sn*-1, *sn*-2 and *sn*-3 (Figure 1.1). It was determined that the FA at the central position (*sn*-2) dissociates less favourably during hydrolysis than FAs in *sn*-1 and *sn*-3 positions (Renaud et al. 2013). The FA positions in the glycerol backbone are often referred to as *sn*-1/*sn*-3 and *sn*-2 due to the inability to differentiate between *sn*-1 and *sn*-3 positions. A TAG molecule who's FAs differs in *sn*- position are regioisomers (Frankel, 1984). Thus, the complexity of TAG molecules is further increased by the number of potential isomers that can arise.

It is important to gain a better understanding of the structural characteristics of TAGs as they are responsible for the chemical and physical properties of oil, as well as increasing risk of certain health conditions such as stroke, heart attack and heart disease (Kato et al. 2017). DAG and MAG molecules are structurally similar to TAGs except

they only contain two (DAG) or one (MAG) FA attached to the glycerol backbone (Figure 1.2).

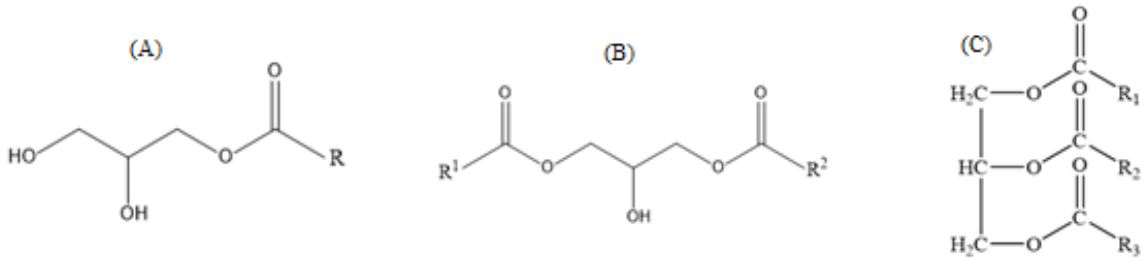

Figure 1.2 Chemical diagrams of the general structures of monoacylglycerols (A), diacylglycerols (B) and triacylglyceols (C).

DAG and MAG molecules are often found in oil samples along with TAGs (Christie, 1982). They are also important decomposition compounds of TAGs that can be produced during instrumental analysis that help determine the structure of the TAG molecule.

1.2 TAG OXIDATION PRODUCTS

Oxidized TAGs are responsible for food deterioration and the effect of degradation on nutritional value. TAG oxidation also leads to off-flavours, foul smells and odours (Simas et al. 2011). Oxidation levels increase when oils are repeatedly heated or stored for long periods of time, creating a major issue in the food industry in terms of financial cost associated with lost product. Aside from physical property changes of oils, oxidized TAG have been associated with diseases such as cancer, atherosclerosis, heart attacks and chronic inflammatory diseases (Cohn et al. 2002; Saguay et al. 2003; Kanner, 2007). Thus, it is important to understand oxidation pathways in order to limit or prevent oxidation.

TAG oxidation in oils and fats is assumed to follow a radical chain mechanism composed of three stages: initiation, propagation and termination (Hamilton et al. 1997). Hydroperoxide radicals are formed during the initiation stage usually with an initiator present, such as heat, light or alkali metals (Neff et al. 1988). The role of the initiator is to remove electrons from lipids and oxygen to create radicals. The free radicals produce more oxidation products by participating in further reactions in the propagation stage (Schaich, 2005). Reactions will continue until all radicals are consumed, leading to the termination stage (Frankel, 1998).

Hydroperoxides are known as primary oxidation products since they are often the first oxidation products to form. Secondary oxidation products are formed in the propagation stage from reactions with the oxygen radicals (Frankel, 1998). Common secondary oxidation products include epoxides, ketones, aldehydes, hydroxides and polymers (Frankel et al. 1987). Generation of epoxide products occurs from a peroxy radical attacking a double bond to result in an epoxide and an alkoxy radical. They can also form from a rearrangement of alkoxy radicals (Hamilton et al. 1997). It was determined that the formation of epoxides from hydroperoxide decomposition leads to the epoxide being in the same location as the original double bond (Figure 1.3). However, the formation of epoxides from alkoxy radicals can also create isomers due to rearrangements of alkoxy radicals (Figure 1.3) (Neff et al. 1998). The formation of hydroxy oxidation products was mainly determined to occur via hydrogen abstraction mechanisms between the alkoxy radical and hydroperoxide groups (Frankel, 1984). Hydroxides can also be formed from the decomposition of hydroperoxide products (Figure 1.3) (Schaich, 2012). Aldehydes form on the end of an acyl chain, commonly from decomposition of

hydroperoxides. Aldehydes and ketones result in a double bond to the oxygen product which results in the formation of a double bond, and a mass shift of 14 m/z in comparison to 16 m/z for hydroxides and epoxides.

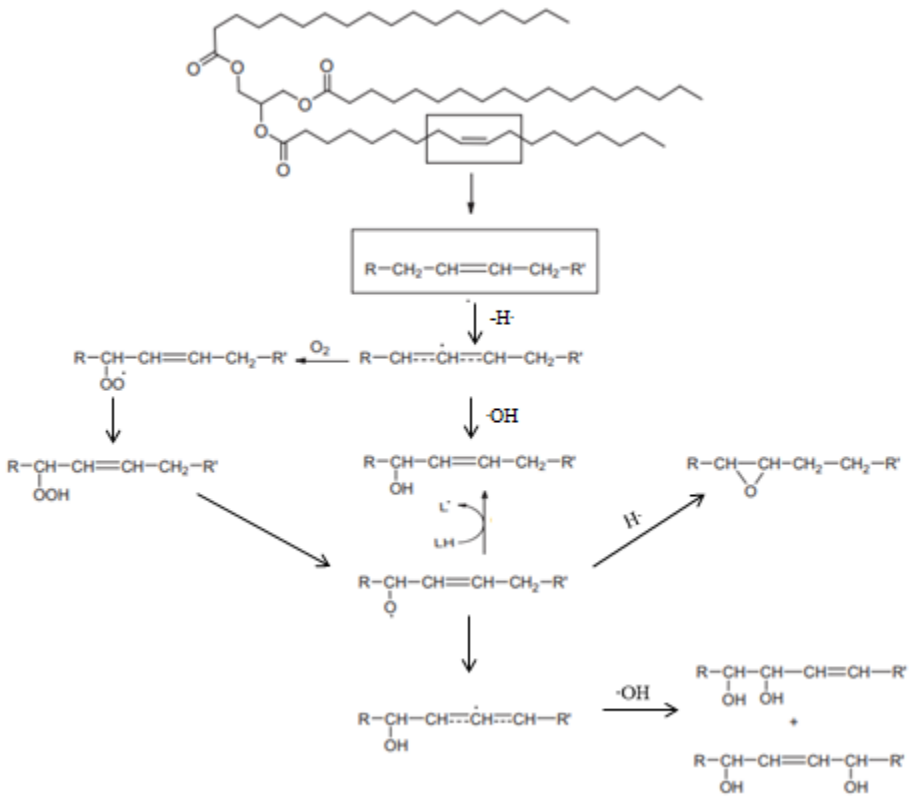

Figure 1.3 Mechanisms of lipid oxidation from an unsaturated site in a TAG molecule. Oxidation mechanisms are adapted from Xia et al., (2017). Formation of oxidation products are shown for hydroperoxy products (left), epoxy products (right) and hydroxy products (center). Two hydroxy products are also referred to as a diol.

The location of oxidation products on unsaturated TAG is largely due to the position of the original double-bond (Neff et al. 1998). However, there is potential for migration of the double bond and alkoxy radicals which would lead to different oxidation positions (Neff et al. 1998). For this study, oxidation products will be focused on 54:3 and 54:6 TAG molecules containing one and two double bonds per FA chain,

respectively. There are often multiple oxidation products that can occur within the same TAG molecule in the presence of multiple double bonds (Figure 1.4) (Xia et al. 2017). Analytical methods are used to qualitatively understand the oxidation mechanisms that occur; however, the ability to form multiple oxidation products by numerous mechanisms creates a significant challenge.

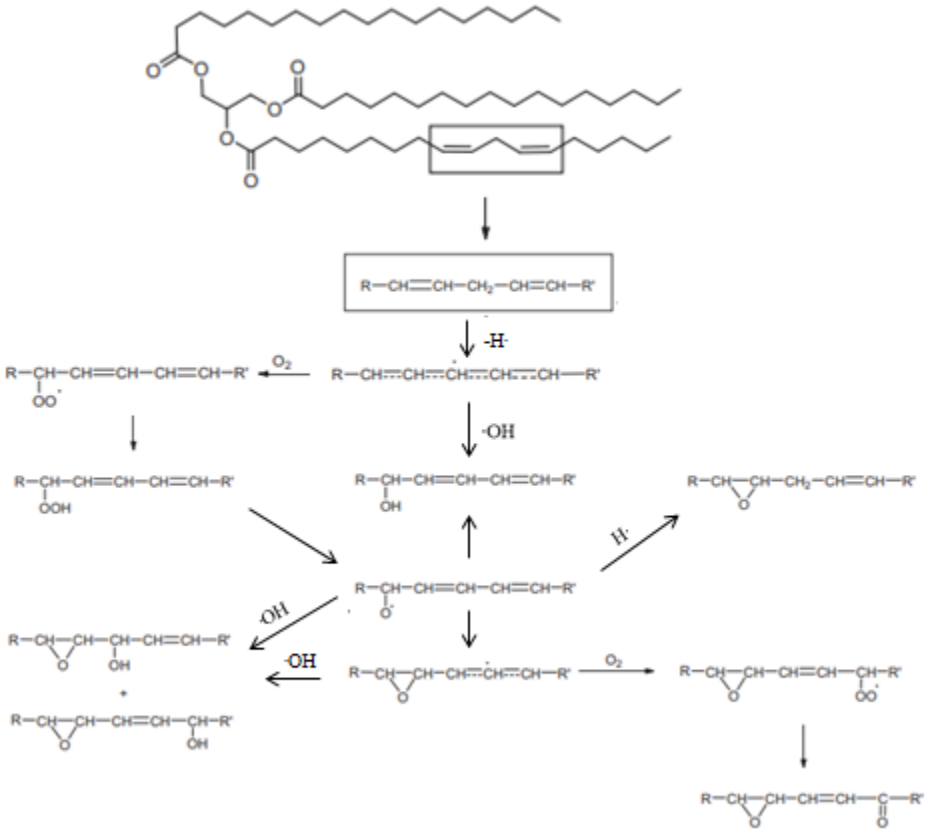

Figure 1.4 Mechanisms of lipid oxidation from two unsaturated sites in a TAG molecule. Oxidation mechanisms are adapted from Xia et al. (2017).

The identification and general understanding of lipid oxidation products is a challenging task due to the complexity of the compounds formed, the effect of variable reaction time, the extent of oxidation, and the complex reaction mechanisms involved (Schneider, 2009). Due to these contributing factors, it is difficult to arbitrarily select the

time points to measure, and to decide whether primary or secondary oxidation products provide a better degradation profile. Often the primary oxidation product class of hydroperoxides are used to determine the extent of oxidation, although more recently incorporation of secondary products has been done (Gruneis et al. 2012).

1.3 Chromatographic Methods for TAG and TAG Oxidation Products

Chromatographic techniques for TAG separation were classically performed by gas chromatography (GC) through indirect analysis of their methyl esterified FAs. GC of TAG is limited due to their low volatility which requires de-esterification followed by the formation of FA methyl esters (FAMEs). Loss of fundamental structural information is inherent to the sample preparation steps. In more recent years, HPLC has been used for the direct analysis of intact TAGs.

GC coupled to a flame ionization detector (FID) is frequently used for quantitative analysis of FA methyl esters (FAME) while GC-MS is important for qualitative analysis. GC-MS gives you a potential chemical formula that GC-FID cannot. GC-FID lacks selectivity and analysis of oxidation products is limited due to the lack of authentic standards (retention time). Information about the structure of TAGs is still lost due to derivatization requirements in both GC-FID and GC-MS.

HPLC has become a widely used chromatographic method for TAG analysis due to its good reproducibility and selectivity (Jurowski et al. 2017). HPLC is more popular than GC due to the ability to analyze intact TAG molecules, without prior sample preparation steps. Both LC and GC benefit by coupling with MS to increase specificity.

1.4 Mass Spectrometry

Mass spectrometry (MS) is an invaluable tool for the identification and quantitation of organic molecules as ions in the gas-phase according to their mass-to-charge (m/z) ratio. MS platforms consist of five basic components: ion source, mass analyzer, collision cell, detector/readout and vacuum system (Figure 1.5). MS systems are generally defined by the type of mass analyzer; these include quadrupole, time-of-flight, ion traps, sectors and hybrid combinations of multiple analyzers. Triple quadrupoles, quadrupole-Orbitrap and quadrupole/time-of-flight systems can be used for beam-type ion fragmentation studies, also referred to as tandem-in-space analysis. Quadrupole and linear quadrupole ion traps offer multiple sequential rounds of ion fragmentation (i.e., MS^n) within one analyzer, referred to as tandem-in-time analysis.

The inlet system is responsible for introducing the sample to the mass spectrometer. Two inlet systems are used throughout this study: liquid chromatography (LC) and direct infusion via syringe. Infusion provides a continuous sample introduction to the MS and is useful for optimizing various parameters including lens voltages, temperature and collision energies. While infusion gives an immediate readout, it requires much higher sample volumes, suffers from sample suppression and competition, and requires dilution in an organic solvent. Quantitative analysis by infusion is impractical mainly due to carry-over and suppression effects from salts and other analytes. LC serves as a prior separation mechanism before the sample is introduced to the ion source, permitting sample components to ionize at different times. The MS data is characteristic to the combination of ion source and mass analyzer. Infusion is typically performed at lower sample flow rates than LC.

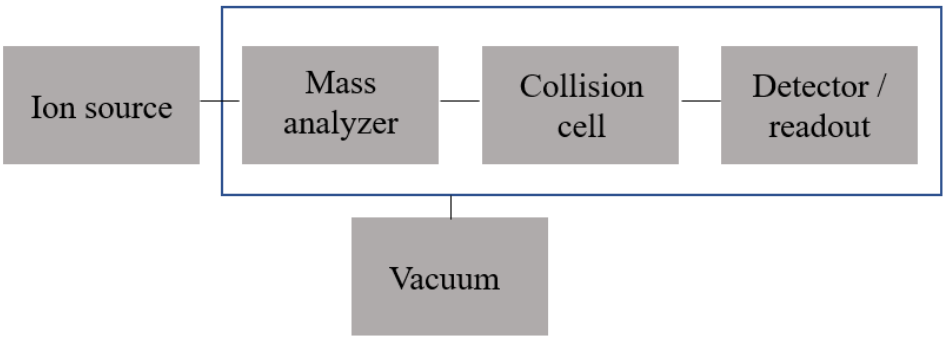

Figure 1.5 Block diagram of mass spectrometer parameters highlighting the ion source, mass analyzer, collision cell and detector/readout in vacuum.

The ion source is where a liquid sample is ionized. There are multiple different ion sources, including electrospray ionization (ESI), atmospheric pressure chemical ionization (APCI), atmospheric pressure photoionization (APPI) and laser desorption ionization (LDI) (Li et al. 2014).The most commonly used ion sources for TAG analysis are ESI and APCI. Both are considered "soft ionization" techniques that are beneficial for high molecular weight compounds of low volatility.

While mass spectrometers are available in many different forms, most contemporary instruments are based on quadrupole, time-of-flight and ion-trap platforms (Li et al. 2014). Classical sector (magnetic or electronic) and FTICR (Fourier Transform Ion Cyclotron Resonance) instruments are less common. The present study focuses on two mass spectrometers with different mass analyzers: a Linear Quadrupole Ion Trap (LQIT) and a Quadrupole-Orbitrap (Q-OT). The mass analyzer is the component of the mass spectrometer that separates ions based on their mass and then sends them to the detector (Figure 1.5) (Watson, 1997). In the orbitrap, all ions are detected simultaneously.

The LQIT-MS uses quadrupole rods to confine ions into the trap using oscillating electric fields. In the linear ion trap, ions are confined radially where a two-dimensional RF field is applied while stopping potentials are applied to two end electrodes (Douglas

et al. 2004). The potential that is applied to the end electrodes controls the ions that are trapped in the cage. The specific applied potential permits ions of a specific m/z range to be trapped while releasing other ions not having the selected m/z value (Watson, 1997). An advantage of using a linear trap is that it can be used as a mass filter and as a trap, as well as leading to increased ion storage and faster scan times.

The Q-OT-MS uses a high-performance quadrupole coupled with high-resolution, accurate-mass (HR/AM) orbitrap detection. Ions are introduced into the quadrupole where it functions as an ion transmission element with the ability to transmit all ions or filter (select) ions according to their mass-to-charge ratios (Denisov et al. 2012). RF and DC voltages are applied to opposite rods in the quadrupole where the same amplitude and sign are applied to each pair of rods, but the voltages are opposing signs between the different rods (Li et al. 2014). The RF and DC voltages determine the m/z range that is transmitted. From the quadrupole, the ions are transferred to the C-Trap (curved linear trap for ion injection) where they are met with a nitrogen gas and then injected into the orbitrap mass analyzer (Denisov et al. 2012). The orbitrap is composed of a spindle-shape central electrode surrounded by a pair of bell-shaped outer electrodes (Figure 1.6). The ions rotate around the central electrode with harmonic oscillations (Zubarev et al. 2013). The frequency of oscillations is dependent on the ion's m/z and detection is based on the frequency (Zubarev et al. 2013).

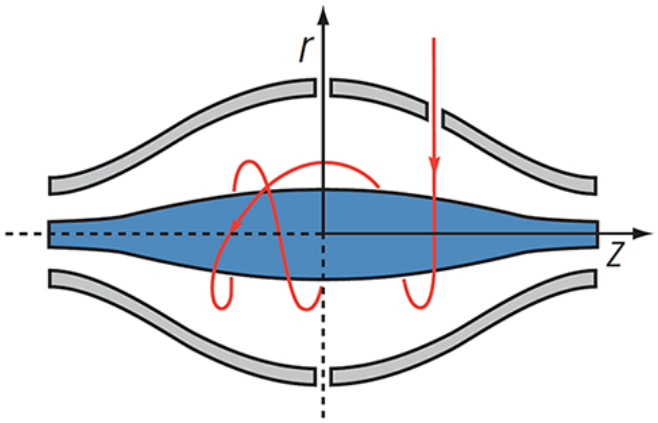

Figure 1.6 Diagram of an orbitrap mass analyzer and an example of ion trajectory (Michalski et al. 2011).

The two mass spectrometers presented differ in terms of resolution, mass accuracy, sensitivity and fragmentation. Perhaps the most striking difference between the two instruments is the mass resolution. The Q-OT is a HR/AM mass spectrometer that can separate compounds having very small differences in m/z compared to the lower-resolution L-QIT. The high mass resolution of the Orbitrap translates directly into improved selectivity while its mass accuracy offers better specificity (Zubarev et al. 2013). The term resolution, *R*, in mass spectrometry defines the ability to differentiate between m/z, and can be further defined by Equation 1.1 below.

$$R = m/\Delta m \qquad \text{Equation 1.1}$$

In Equation 1.1, Δm is the peak width at half height of an m/z peak.

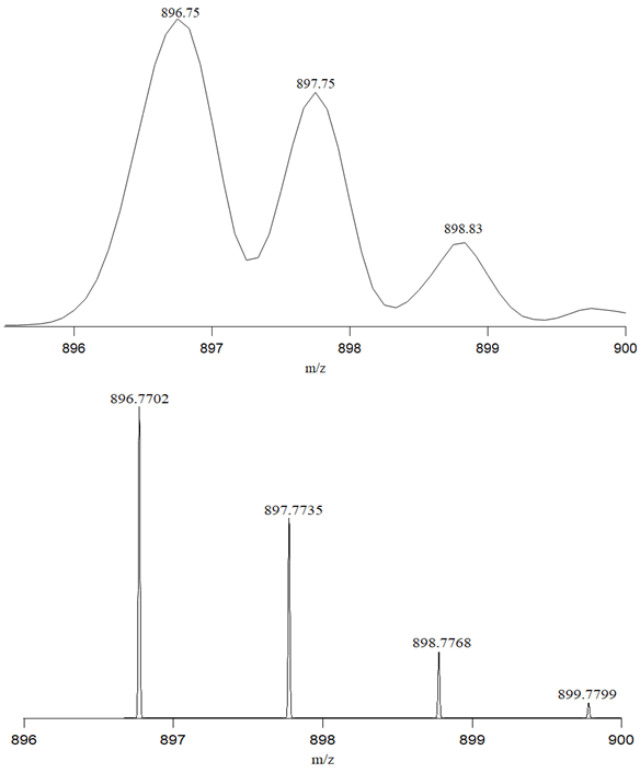

Figure 1.7 Trilinolein standard analyzed by direct-infusion on the L-QIT mass spectrometer (A), and the Q-OT mass spectrometer (B). Panel (A) used "enhanced" resolution while panel (B) used a resolution setting of 140,000 (the highest available).

Figure 1.7 demonstrates the difference in high resolution mass spectrometry (panel B) versus low- resolution mass spectrometry (panel A). It is obvious that panel (B) has better resolution as each mass peak is defined and well-separated from the neighbouring peak. In panel (A) the peak widths are wider and run into each other, indicating low resolution. Calculating *R* for panel (B) resulted in a value of 73,505, in contrast to the theoretical setting of 140,000. The MS resolution is reported for a m/z of 200; as the m/z increased the measured resolution value decreased. Doing the same calculation for panel (A) yields an *R* value of 1,345. Thus, the HR/AM Q-OT provided 50-fold greater resolution. The advantage of HR/AM is the superior specificity and selectivity that it can provide.

Tandem-MS (Fragmentation, MSMS) is a MS technique that breaks down precursor ions into product ions (fragments). Ions of a certain m/z value are selected as precursor ions, and broken into smaller fragment ions. The fragmentation process can vary depending on the type of mass spectrometer (Watson, 1997). Linear ion traps perform collision induced dissociation (CID) that is different from orbitrap tandem-MS due to it being a tandem-in-time technique (Watson, 1997). Tandem-in-time fragmentation techniques allow dissociation to occur in the same place, with the potential for multiple dissociation steps to take place over time. With CID, ions are generated and trapped within the ion trap, where a precursor ion can be isolated using rf voltages (Somogyi, 2008). An inert gas (helium) is introduced that collides with the ions, increasing the internal energy of the ion to simulate its dissociation.

Higher-energy C-trap dissociation (HCD) is used in an orbitrap mass spectrometer. HCD is specific to the orbitrap instrument where it takes place within the octopole HCD cell and is more energetic than CID. HCD is referred to as a trap-type fragmentation that also possesses beam-type characteristics (Jedrychowski et al. 2011). HCD is a tandem in space technique where separation happens at a different location (HCD cell). The limitations to this type of fragmentation compared to the L-QIT is the inability to perform MS^n analysis. The L-QIT performs fragmentation where the ions are trapped and multiple fragmentation steps can be performed over time (residing in the same location) (Jedrychowski et al. 2011). The ability to perform multiple rounds of fragmentation can be useful in the analysis of TAGs where a TAG can be fragmented to its corresponding diacylglycerol (DAG) which can then be targeted to give the resulting monoacylglycerol (MAG).

The present study will focus on the scan function parallel reaction monitoring (PRM). A PRM scan targets a precursor ion and scans all of the resulting product ions simultaneously unlike a slower scanning triple quadrupole mass spectrometer (Figure 1.8). Qualitative information can be acquired using a PRM and is often the method of choice for TAG analysis to identify DAG product ions.

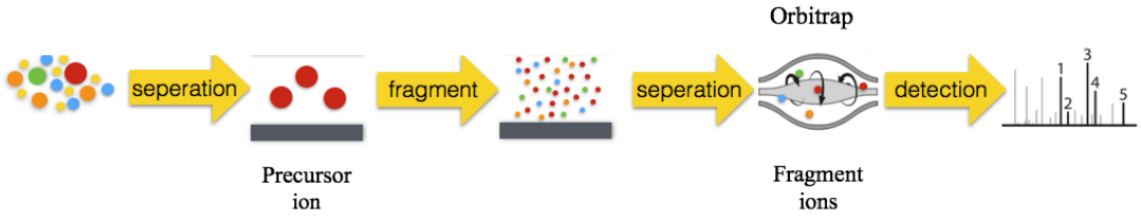

Figure 1.8 Tandem-MS mechanism of parallel reaction monitoring (PRM) (Brzhozovskiy, 2022).

Lipid analysis by mass spectrometry without prior separation is referred to as "shotgun lipidomics". Results are obtained within seconds with shotgun lipidomics and abundant precursor ions can be selected for MSMS analysis. However, limitations to shotgun lipidomics includes the inability to differentiate isomers, ion suppression and sample carry over.

1.5 Ionization Mechanisms

The generation of ions is critical to mass spectrometry analysis. Ionization mechanisms can involve the loss of an electron, or removal or addition of a proton on other charged entity. Each ionization technology creates ions differently. For atmospheric pressure ionization, APCI and ESI are the two most common methods for TAGs. The main difference between the two is that with APCI analytes are ionized after they are volatilized, whereas with ESI, analytes are volatilized and ionized at the same time. With APCI, the sample is introduced through a heated needle which forms the aerosol (Cai et

al. 2006). Solvent vapour is then ionized by a corona-discharge and analytes are ionized indirectly by the charged vapour (Figure 1.9). APCI is often the method of choice for ionization of non-polar compounds like TAGs, although, potential limitations of APCI include the thermal stability required of the molecules (Neff et al. 1998). TAG hydroperoxide products are often not stable and analysis by APCI produces little, if any, molecular ion information (Neff et al. 1998). Thus, APCI is limited for analysis of intact oxidized TAG molecules due to the instability of the oxidation products. Analysis by APCI focuses on fragmentation product ions to determine the corresponding oxidation groups (Neff et al. 1998).

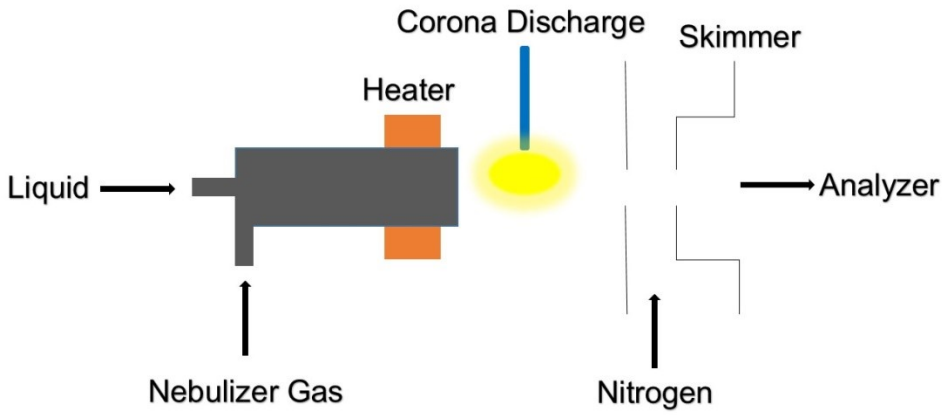

Figure 1.9 Atmospheric pressure chemical ionization mechanism (Rockwood et al. 2018).

For the present study, ESI was used for TAG ionization. ESI works by passing the solution through a capillary tube while applying a high electric field to the capillary (Gaskell, 1997). In positive ion mode, the tip of the capillary tube is positive and does not allow negatively charged ions to pass through (Cody, 2002). The positive ions exit the capillary as a mist of charged droplets dispersed using a nebulizing gas, often nitrogen or air (Figure 1.10). The increase in repulsive forces between the excess charges results in the parent droplet breaking up into smaller droplets, and this is known as Coulombic

repulsion or fission (Watson, 1997). The process is repeated until isolated ions form and are accelerated into the mass analyzer where they are analyzed according to their m/z (Figure 1.10). This theory of ion formation by ESI is called the charged residue model (CRM). An alternative to CRM is the ion evaporation theory (IET) whereby ions effectively evaporate from a charged droplet. The IET may be more applicable for TAGs due to the low affinity of the acyl chains for the polar ESI solvents such as ethanol.

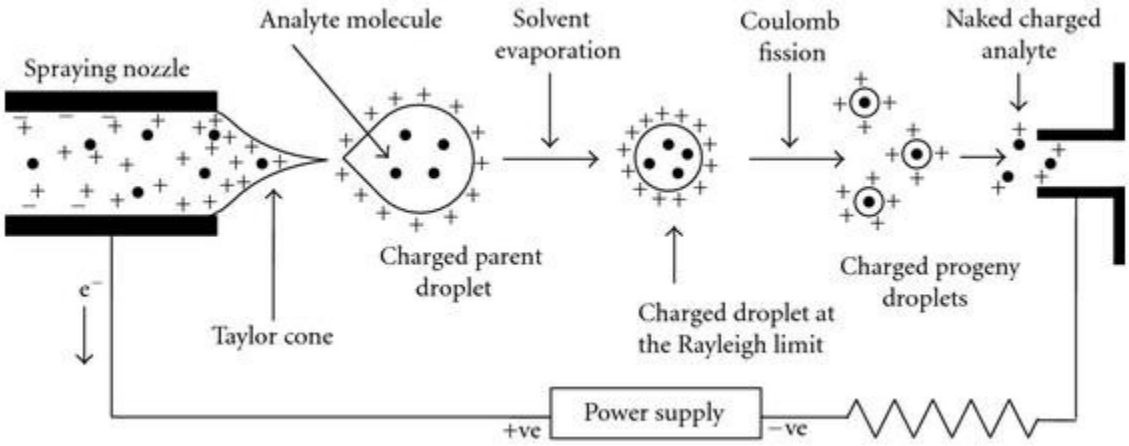

Figure 1.10 Diagram of electrospray ionization mechanism (Eberlin, 2007)**.**

A main advantage of ESI is the ability to form adduct ions of molecules that do not have ionizable sites like a primary amine or carboxylic acid. Adduct species are formed as the excess surface charge of the ESI droplets can be carried by various cationic species (Watson, 1997). Protons are the most common species, creating $[M+H]^+$ molecular ions. However, sodium, ammonium and potassium cations have also been used to create $[M+Na]^+$, $[M+NH_4]^+$ and $[M+K]^+$ ions (Hsu et al. 2010). Often, sodium and potassium ions are generated from endogenous levels of the metals present in solvent impurities, glassware or other sample preparation contaminants. Complexation of alkali metal cations and ammonium with TAGs has been previously investigated, and it was

found that the cations bind with the lone pair of electrons from carbonyl oxygen groups of the glycerol backbone (Chakrabarti, 1990). Another charge mechanism has been proposed between the double bonds in unsaturated TAGs and the metal cation groups (Grossert et al. 2014).

The use of ESI for the analysis of intact TAG molecules has previously favoured lithiated adducts due to the ability to structurally characterize TAG ions. Hsu et al. (2010) determined that tandem-MS analysis of precursor $[M+Li]^+$ (M=TAG) adducts produced product ions that can determine the FA substituents and their position on the glycerol backbone. They determined that targeting precursor $[M+Li]^+$ resulted in abundant product ions reflecting the loss of the outer, *sn*-1 and *sn*-3 FAs as both free acids ($[M+Li-R_1CO_2Li]^+$ and $[M+Li-R_3CO_2Li$) and, in lower amounts, lithium salts ($[M+Li-R_1CO_2H]^+$ and $[M+Li-R_3CO_2H]^+$). A linear ion-trap MS was used for their analysis to further determine the position of double bonds in the TAG by using MS^3 to target DAG precursor ions. They also showed MS^3 analysis of $[M+Na]^+$ and $[M+NH_4]^+$ to determine the position of the FA on the glycerol backbone but did not provide information about double bond location. Hsu et al. (2010) briefly mention $[M+K]^+$ and $[M+Cs]^+$ adducts; however, they fail to show successful adduct formation. They stated that the Cs adduct showed a dominant free cesium ion at m/z 133 and no $[M+Cs]^+$ ion. Han et al. (2001) also investigated lithiated TAG species in biological samples where they used the neutral losses from tandem-MS with a triple quadrupole MS to quantify intact TAG species. A more recent study on ESI of lithiated TAGs focused on MS^3 analysis to separate regioisomers by identifying monoacylglycerol derivatives (Lin et al. 2008). Duffin et al. (1991) investigated ESI of MAGs, DAGs and TAGs using ammonium and sodium

adducts. They required methanol and chloroform solvents for the samples, and used high molarities of 10 mM ammonium acetate and sodium chloride for cation concentration. They concluded that Na^+ did not produce sufficient product ions and required higher collision energy for dissociation compared to ammonium. Ammonium adducts yielded protonated product ions and an ammonia leaving group. They used the protonated product ions to identify MAG derivatives from the precursor DAG and TAG ions.

1.6 ESI-MS Analysis of TAG Standards using NH_4^+

In the present study, ESI was used to ionize TAG standards. Initial attempts to ionize TAGs by protonation of an oxygen atom at low pH with formic acid resulted in near undetectable signal. One of the more commonly used adducts in lipidomics is ammonium (Dorshel et al. 2002 & Zeb et al. 2010). Native TAGs were investigated using trilinolein (18:2/18:2/18:2) standard and ammonium acetate. It is important to note that ammonium adduct formation requires the addition of formic acid to lower pH. Trilinolein has an empirical formula $C_{57}H_{98}O_6$, with a molecular weight of 879.4 g mol^{-1}. When bound to ammonium, the resulting empirical formula is $C_{57}H_{98}O_6NH_4$ with a mass-to-charge value of m/z 896.67 (Figure 1.11). Ionization is typically performed at elevated capillary temperatures between 275-300 °C as it is known to provide higher signal transmission.

Mass spectra are plots of ion abundance as their *m/z*. *m/z* represents the mass number (*m*) of a particle over the number of charges the ion has (*z*). When analyzing lipid molecules the charge is typically +1; therefore, the m/z is often referred to as just the mass of the ion. A pseudo-molecular ion is the addition of a proton or adduct that alters the molecule of interest in an identifiable way (Horman et al. 1989). For instance, the

pseudo-molecular ion with a mass-to-charge ratio of 896.67 in Figure 1.11 corresponds to the $[M+NH_4]^+$ ion of trilinolein. On the other hand a molecular ion of trilinolein would be the $M^{+\cdot}$ radical cation. An advantage of mass spectrometry compared to other analytical techniques is the ability to identify molecular species with different isotopic abundances. Molecular masses in mass spectrometry are typically expressed as Daltons (Da) or more commonly as atomic mass units (amu). Units of mass-to-charge are correctly expressed as Thomsons (Th). Mass units are based upon a relative scale with the reference of the carbon isotope ${}^{12}_{6}C$, which has an exact mass of 12 amu. Therefore, the amu is classically defined as 1/12 of the mass of one neutral ${}^{12}_{6}C$ isotope. However, also noticeable on a mass spectrum are carbon-13 isotope peaks which appear 1 amu, or the mass of a single neutron higher. The intensity of the isotope peaks is proportional to the relative abundance of the naturally occurring carbon-13 isotope. The relative abundance of the carbon-12 isotope is ~98.9 % while carbon-13 is ~1.1 %. The mass of carbon reported on a periodic table (i.e., 12.011) represents a weighted average of the two stable isotopes whereas mass spectrometry can differentiate between the isotopes. In Figure 1.11, the two magnified spectra, simulated (A) and experimental (B), clearly show the contribution of carbon-13 in the peaks approximately 1 Dalton higher than the target ion 896.7702 at 897.7729. The expected intensity of the carbon-13 isotope peak can be estimated using simulated mass spectra where the intensity for 897.7729 is 62.7 %. Knowing the actual percent contribution of carbon-13 isotope is 1.1 %, the number of carbon atoms in the molecule can be estimated by dividing the intensity of the carbon-13 peak by 1.1, for a resulting value of 57. From the collected spectra, the empirical formula can be generated from the known natural abundance of carbon isotopes.

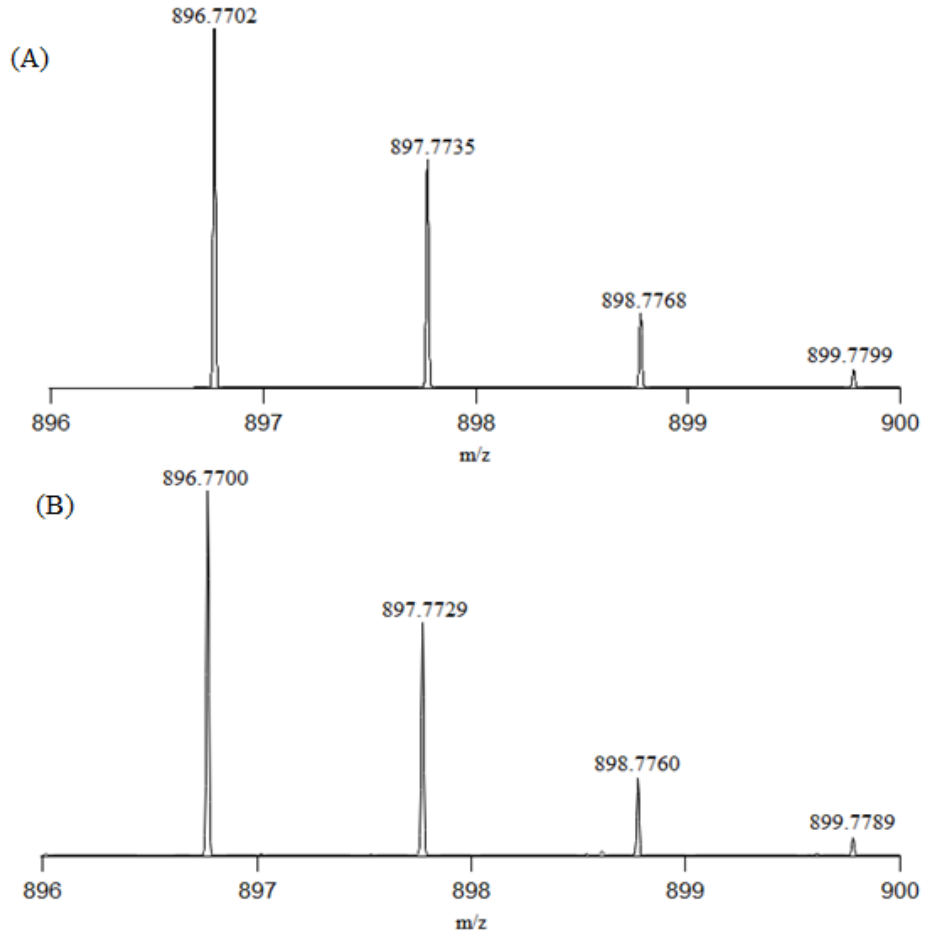

Figure 1.11 Trilinolein MS spectra displaying the simulated mass spectra (panel (A)) from the Q-OT HR/AM using the empirical formula $C_{57}H_{98}O_6NH_4$. Experimental data was collected using 5 ug mL^{-1} trilinolein standard with ammonium acetate as shown in panel (B).

The simulated mass spectra and experimental mass spectra have a mass difference of 0.2 ppm for the carbon-12 isotope peak. The carbon-13 isotope peak has a mass difference of 5.1 ppm from the theoretical predicted mass, while the other two peaks differ by 0.8 ppm and 1.0 ppm respectively. The remaining two peaks represent two and three carbon-13 isotopes at m/z 898.7760 and 899.7789, respectively.

When analyzing ammoniated trilinolein, it was noted that there was also a small amount of sodiated trilinolein ionized as well. Sodium adducts form from endogenous

sodium found in the ethanol solvent, glassware or in the environment (Zeb et al. 2010). The sodiated ion had a m/z of 901.7219, five mass units higher than the ammoniated ion (the mass difference between sodium and ammonium) (Figure 1.12).

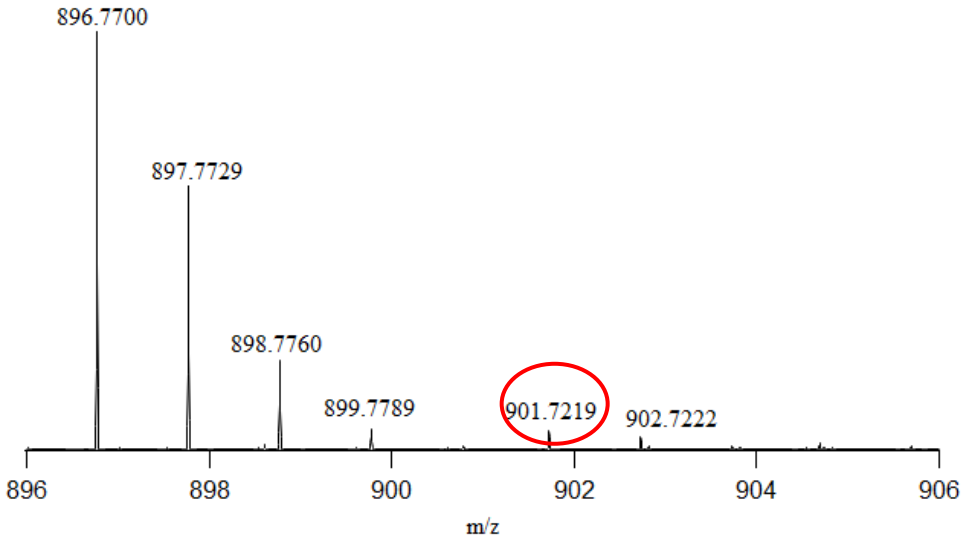

Figure 1.12 Magnified Full MS spectra of ammoniated trilinolein collected on the Q-OT at a mass range of 400-2000 m/z, showing the TAG sodium peak circled in red that appears within the same spectra as the ammoniated trilinolein sample.

Direct-infusion electrospray mass spectrometry leads to signal suppression and competition which is a major drawback of an infusion sample inlet. Although the sodium adduct is present in low amounts in this sample, it is important to note that with lower levels of added ammonium, endogenous sodium levels could compete with the target ion. Despite drawbacks, direct-infusion shotgun lipidomics is advantageous due to the ability to provide continuous introduction of the analyte from a sample syringe, providing adequate time for MS optimization. Direct infusion produces mass spectra in seconds, allowing quick identification of sample analytes. Despite the lack of chromatographic separation and associated drawbacks, infusion leads to convenient and easy sample introduction without complicated method development.

1.7 Tandem-MS of TAG and TAG Degradation Products

Tandem-MS is a popular method for TAG analysis to determine characteristic DAG and MAG product ions that can be used to determine the structure of the precursor TAG. When ammonium acetate is used as the cation adduct, ammonia cleaves at applied collision energies and product ions can be identified in their protonated form. In a TAG with three different FA constituents (i.e., ABC) three DAG ions are expected to be observed that highlight the loss of each FA (i.e., AB, AC, BC). Homogenous TAG molecules will show a single DAG ion that reflects the loss of the FA group as $[(M+NH_4)-NH_3-FA]$. The relative abundance of DAG product ions allows for regiospecific determination of the FA constituents. The positions are determined based on the knowledge that *sn*-1 and *sn*-3 (α and β-DAG fragments) are more favourable leaving groups than those in the *sn*-2 position. *sn*-1 and *sn*-3 positions are indistinguishable from each other (Zeb et al. 2010). DAG ions with the loss of *sn*-1/*sn*-3 FA appear at higher amounts than the DAG ion that loses *sn*-2 FA. For example, Hsu et al. (2010) highlight this by using a heterogeneous TAG ion with three FA constituents where DAG products at m/z 583 and m/z 611 highlight the loss of *sn*-1 and *sn*-3 FAs (Figure 1.13). They are present at higher abundance than m/z 585, which would therefore represent the loss of *sn*-2 FA as it is less common. Further identified product ions include the protonated precursor ion, resulting from the loss of free ammonia (Zeb et al. 2010 & Kalo et al. 2006).

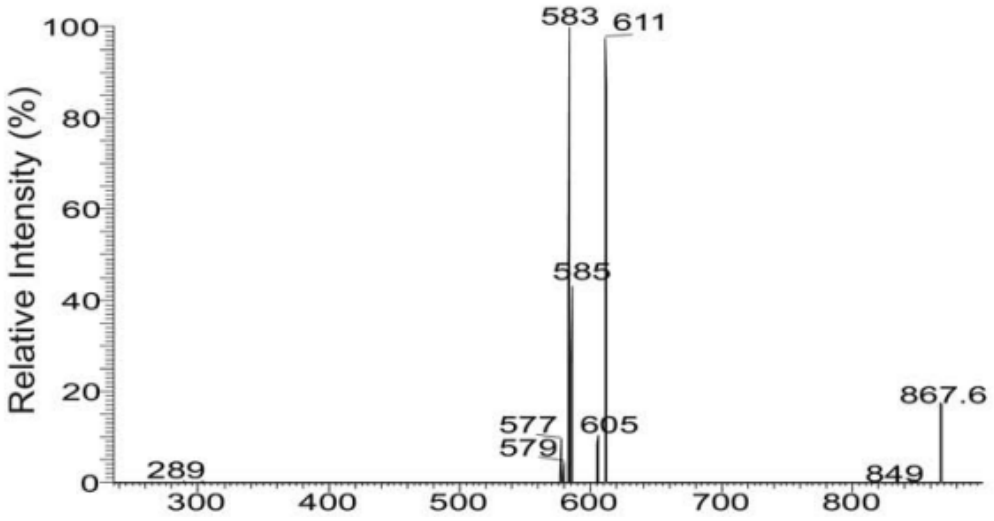

Figure 1.13 MSMS spectra of precursor $[M+Li]^+$ TAG (16:0/18:1/18:0) at m/z 867 (Hsu et al. 2010).

MAG derivative product ions have been previously used to determine the corresponding FA constituents of the TAG molecule (Kalo et al. 2006). There are two commonly identified MAG derivatives which include the protonated acyl chains $[FA]^+$ and $[FA+74]^+$. Product ions identified as $[FA+74]^+$ are proposed to be derived from DAG product ions. Kalo et al. (2006), postulated a ring formation using part of the glycerol backbone to form the product ion (Figure 1.14). Further product ions have been identified to determine the location of the double bonds within TAG molecules. Double bonds are more likely to undergo cleavage compared to single bonds; therefore DAG fragments have been identified that show partial losses of FA chains.

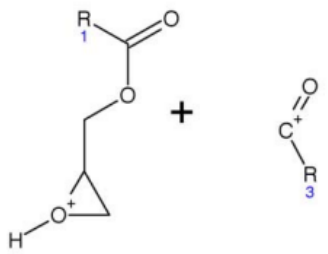

$R_1CO + 74$

Figure 1.14 Proposed structure of FA+74 by Kalo et al. (2006), from degradation of R_1R_3 DAG product ion.

Oxidized TAGs have received less attention than intact TAGs likely due to their increased complexity. All studies on TAG oxidation products included prior chromatographic separation by LC. Gruneis et al. (2019) investigated potential MSMS pathways from proposed hydroperoxy TAG and proposed mono-epoxy TAG. They did not have a method to specify the oxidation products; therefore, it was assumed that they were starting with the proposed products. They determined that hydroperoxy TAG lost a water molecule from the –OH in the peroxy product which caused the remaining oxygen to form an epoxide. This product appeared as a loss of H_2O. They further identified the loss of a FA chain that did not contain the peroxide product, to yield DAG[OOH]. The loss of H_2O from this DAG resulted in DAG[O] as a proposed epoxide product. Another product was identified as the loss of the FA including the hydroperoxide group, generating a protonated un-oxidized DAG. Their investigation into MSMS patterns of proposed mono-epoxy TAG showed the loss of the epoxide group and addition of two double bonds with the loss of H_2O. With degradation of the epoxidized TAG precursor ion, they identified both the loss of a FA without the epoxide group and the loss of FA with the epoxide group as DAG products DAG[O] and DAG, respectively. There are two other un-oxidized DAG products identified which were proposed to be from degradation

of DAG[O]. The two un-oxidized DAG show an addition of one and two double bonds. The limitation of the proposed fragmentation patterns from Gruneis et al. (2019) is their inability to identify the correct oxidation product or distribution of FAs. They state that they were unable to identify neither double bond location nor the distribution of FAs within the identified compounds. Therefore, they could not confidently confirm their proposed precursor structure as there was no proof of the FA structure. They also lacked confidence in defining the proposed oxidation products where there could be m/z overlap between other potential oxidation products.

One of the initial studies on TAG oxidation products was by Neff and Byrdwell (1998), where they mainly evaluated hydroperoxides but identified some hydroxide and epoxide products as well. Oxidation of trilinolein, triolein, and trilinolenin standards was done at 60 °C and measured after 3 weeks (no prior sampling was done). The use of TAG standards provided an advantage as the FA distribution was known. The analysis performed by Neff and Byrdwell (1998) was carried out using APCI-MS where fragment ions are produced from the applied source voltage and potential decomposition from the heated source. The identified decomposition products from mono-hydroperoxy TAG included the loss of water and rearrangement to an epoxide product, the loss of H_2O_2, and the appearance of multiple DAG product ions. Unlike Gruneis et al. (2019), Neff and Byrdwell (1998) did not identify DAG[OOH] product ions, but they did identify DAG[O] and two protonated un-oxidized DAG products. The decomposition of mono-epoxy TAG showed the same product ions as described by Gruneis et al. (2019). However, Neff and Byrdwell (1998) also identify the loss of C_9H_{18} and $C_9H_{18}O$ to identify the position of the

epoxide product on Δ9. Their study reported limited amounts of identified DAG product ions from hydroxy TAG.

Petronilho et al. (2021) studied the fragment ions of oxidized triolein after frying at 180 °C using HPLC-ESI-MSMS. They identify hydroxy, hydroperoxy and epoxy/keto products on TAG; however, they identify epoxy TAG as [TAG+14] rather than +16 and do not state whether an additional double bond had formed. They identified mono-hydroxy triolein at two retention times, identifying potential isomers, with the earlier retention time producing DAG product ion m/z 601.53. At the later eluting retention time they identified a major peak at m/z 603.53 [DAG] and m/z 619.52 [DAG+O] and product ions m/z 477.39 [DAG-$C_9H_{18}O$]$^+$ and m/z 493.39 [DAG-C_9H_{18}]$^+$ which were previously described by Neff and Byrdwell (1998). MSMS of di-hydroxy yielded DAG product ions m/z 601.51, m/z 603.51, m/z 617.51and m/z 619.52. Product ions were identified based on their neutral losses and not the FA constituents.

Hydroperoxy fragment ions were identified by Petronilho et al. (2021) in correlation with those identified by Neff and Byrdwell (1998). They identified mono-epoxy triolein at two retention times with corresponding product ions that were previously identified (Neff et al. 1998). Similar results were also identified by Zeb (2012) from autoxidized camellia oil. Zeb focused on epoxide products where he identified them as [TAG +16] and highlighted similar fragment ions to those previously mentioned.

1.8 Liquid Chromatography (LC)

Liquid chromatography (LC) is a condensed-phase separation technique based on analyte partitioning between a liquid mobile phase and a solid stationary phase. Under a defined set of conditions (i.e., solvent strength, temperature, flow rate, etc.) molecules

will elute at a characteristic retention time that may often be used to differentiate isomers and other chemicals with similar detector response (i.e., absorption wavelength, mass-to-charge, etc.). As an inlet for MS, LC has several advantages over infusion including small sample sizes, automation, resolution of isomeric species for increased selectivity, discrete sampling, reduced ion suppression and competition, and increased signal-to-noise. Despite the decreased throughput and extra method development time, LCMS is the preferred approach for qualitative and quantitative analysis of TAGs.

LC separates molecules in a liquid mobile phase using a solid stationary phase. As the sample in the mobile phase passes through the LC column, different components will interact with the stationary phase to varying degrees (Christie, 2010). LC-MS has dominated the field of TAG analysis due to the ability to monitor intact TAG species and elucidate structures in combination with MS techniques.

There are two main types of LC used for TAG analysis: normal phase LC (NPLC) and reverse phase LC (RPLC). NPLC uses a polar stationary phase and a nonpolar mobile phase for the separation of polar molecules (Jurowski et al. 2017). For analysis of lipids, NPLC separates the different molecules based on the glycerol backbone. NPLC often requires the use of non-polar solvents such as hexane and chloroform that are regarded as environmentally un-friendly, toxic solvents that are also not compatible with ESI. For these reasons, NPLC is not used as often as RPLC for TAG analysis; however Kalo et al. (2006) released a study on a gradient NPLC separation of TAG, DAG and MAG compounds in rapeseed oil. The study did not show chromatograms; however, they stated that TAG separation occurred between retention times of 21-28 minutes while

DAG separation occurred 22 minutes later. Further identification was done for MAG derivatives where they were not separated and eluted at a retention time of 67.8 minutes.

RPLC uses alkyl chains covalently bound to micro-particles in order to create a hydrophobic stationary phase which has an affinity for hydrophobic compounds (Jurowski et al. 2017). RPLC separates TAGs based on their fatty acyl composition. The order of elution is governed by the carbon-chain length and number of double bonds, where longer fatty acyl chains will elute later than shorter chains, and a higher number of double bonds results in a shorter retention time. A C18 stationary phase is most commonly used for RPLC analysis (Zeb, 2012). However, the use of C8 and C30 columns have also been reported. In C8 columns, the alkyl chains that are bound to the stationary phase are shorter at only 8 carbons in length and have a lower hydrophobicity. In comparison C30 columns have alkyl chains that are 30 carbon atoms long and are more hydrophobic than C18 columns (Petronilho et al. 2021).

There are two methods of elution used in LC: gradient elution and isocratic elution. In a gradient elution protocol, the composition of the mobile phase changes linearly over time. In comparison, an isocratic elution maintains a consistent composition of the mobile phase. Due to the change in mobile phase composition throughout the method, the end portion of a gradient method requires a column re-equilibration step. The re-equilibration time is required to recondition the column to the starting conditions before the next analysis. Gradient LC-MS is more commonly used for TAG analysis but has required long elution periods for complex samples. Fasciotti et al. (2010) combined HPLC with APCI-MS and used a 40-minute gradient with 2-proponal and acetonitrile as the mobile phase. A C18 column was used with dimensions 250 mm x 3 mm at a flow

rate of 700 uL min^{-1}. Their method successfully separated intact TAG molecules in five different oil samples. A 45-minute gradient was used by Petronilho et al. (2021) at a flow rate of 300 uL min^{-1}. They used a C30 column with dimensions 150 mm x 2.1 mm. The mobile phase was composed of 50/50 water and acetonitrile with 5 mM ammonium formate and 0.1 % formic acid and the second solvent was water. Chromatograms were not included in their study of TAG oxidation products; however, it was stated that the identified products eluted between 19-23.5 minutes. Other gradient methods included a 27-minute method by Gruneis et al. (2019) and a 30-minute method by Lim et al. (2012) separating TAG oxidation products and native TAG molecules, respectively. All of the studies focused on the separation of either native TAG molecules or their oxidation products but no one has considered both simultaneously. Due to the low amounts of oxidation products and their relatively high limit of detection, Gruneis et al. (2019) incorporated a C18 solid phase extraction step (Sep-Pak) to remove intact TAG and concentrate the oxidation products. Such additional sample preparation steps increase the analysis time, as well as increasing the uncertainty of the results due to the increased risk of sample preparation error and contamination. Zeb (2012) proposed a 35-minute isocratic elution for TAG oxidation products using 18% isopropanol in methanol with separation of oxidation products achieved between 7-30 minutes. Thus, run times for TAG and TAG oxidation products with RPLC are normally 30 minutes or more.

Extracted ion chromatograms (XIC) can be plotted based on their mass-to-charge value (Figure 1.15). Triolein (18:1/18:1/18:1, m/z=902.676) (Red), was separated from trilinolein (18:2/18:2/18:2, m/z= 896.774) (Black), using the Q-OT MS with a C8 column to demonstrate the resolution between different numbers of double bonds. A 10 minute

isocratic method was used at 95 % EtOH with 0.1 mM ammonium acetate and 0.1 % formic acid. It is evident that (18:2/18:2/18:2) and (18:1/18:1/18:1) are well resolved with no overlap between the chromatographic peaks (Figure 1.15). The increased number of double bonds in trilinolein resulted in a shorter retention time compared to triolein as expected based on their equivalent carbon number, ECN, which takes into account the influence of double bonds and chain length on elution time. TAGs with a higher number of double bonds are more polar molecules than TAGs with less double bonds.

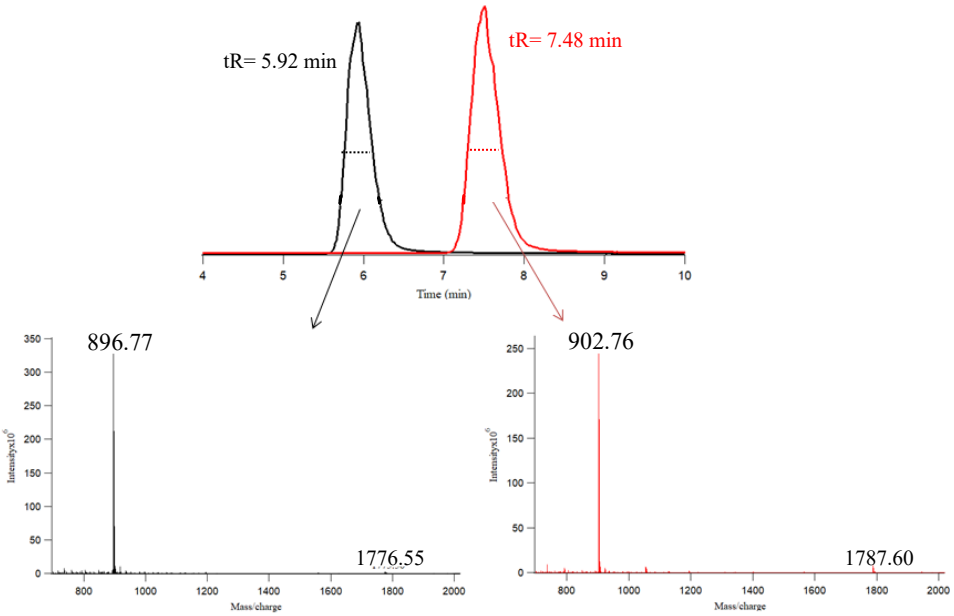

Figure 1.15 Liquid chromatographic separation of triolein (18:1/18:1/18:1), (red), and trilinolein (18:2/18:2/18:2), (black), on a C8 column with an isocratic mobile phase of 95% ethanol.

The coupling of LC with high resolution mass spectrometry allows for quick and confident assignment of ions to LC peaks (Figure 1.15). The m/z value of the molecule of interest can be selected to produce a chromatogram for the corresponding lipid where ions are of the form $[M+NH_4]^+$. Further, the known empirical formula of the molecule can be used to simulate the mass spectrum to confidently identify the molecule and to

confirm that the mass deviation between experimental and predicted is within a 10 ppm window. Accurate mass measurements at high resolution are particularly useful when working with complex samples. The extracted mass spectra for the two standard TAGs also contain low amounts of dimer, $[2TAG+NH_4]^+$, at the same retention time at m/z 1776.55 and 1787.60 for trilinolein and triolein, respectively (Figure 1.15). The levels of observed dimer ions can increase at elevated lipid concentrations and their stability can also be affected by inlet conditions, including lens voltages and the transfer capillary temperature.

It is important to evaluate the proposed LC method in order to ensure it provides sufficient retention and separation potential. A key parameter when developing an LC method is referred to as the retention factor (*k'*) and is used to evaluate whether the sample(s) are being sufficiently retained on the LC column. The retention factor is calculated by subtracting t_m (the mobile phase time) from the retention time (t_R) and then dividing by t_m as shown in Equation 1.2 below. Retention factors should be greater than 2.

$$k' = \frac{[t_R - t_m]}{t_m} \qquad \text{Equation 1.2}$$

Chromatographic resolution is defined as a measure of separation of two peaks of different retention time in a chromatogram and it differs from mass spectrometry resolution (Equation 1.3).

$$R = \frac{t_{R2} - t_{R1}}{\frac{1}{2}(W_1 + W_2)} \qquad \text{Equation 1.3}$$

Resolution is calculated using the retention time for the later eluting analyte, triolein (t_{R2}) and subtracting the earlier eluting analyte, trilinolein (t_{R1}). The two peak widths (W_1, W_2)

are summed and multiplied by ½ to achieve the peak widths at half height. Baseline resolution of Gaussian peaks is defined as greater than 1.5.

1.9 FAIMS

High-field asymmetric waveform ion mobility spectrometry (FAIMS) is an established atmospheric pressure separation technique for gas-phase ions that is often combined with mass spectrometry detection. FAIMS is positioned between the ion source and MS inlet and is often referred to as an ion filter. FAIMS separates ions based on the dependence of ion mobility on electric field strength. The separation parameter is called compensation voltage (CV). The CV can be maintained at a constant value for continuous ion transmission. Alternatively, the CV may be scanned linearly or stepped between predetermined values to transmit multiple ions in series. The mobility-based FAIMS phenomenon is complementary to both reversed-phase LC (hydrophobicity) and mass spectrometry (mass-to-charge). FAIMS can be implemented in-line with both techniques, commonly referred to as an LC-FAIMS-MS/MS platform, reducing isobaric interferences and generally improving signal-to-background in the MS measurement. It is easiest to implement FAIMS with a single, fixed CV value whereby ion transmission between the LC and MS is continuous and uninterrupted. Full CV scans are best done using an infusion inlet, whereas programmed CV stepping can be synchronized with LC elution. Synchronization of FAIMS (CV) with MS acquisition is difficult without software integration.

Thus far, the use of FAIMS has been limited for TAG analysis. Shvartsburg et al. (2011) looked at the separation within lipid classes using FAIMS. Their study concluded

that unsaturated TAG showed smaller changes in mobility for unsaturated TAG although they did not offer an explanation for the phenomena. TAG isomers were not investigated; however, they did show successful separation of DAG isomers at DV=4.0 kV. The addition of helium increased resolution between DAG regioisomers. There lacks further application of FAIMS to TAG analysis.

1.10 Research Goals

The overall goal of this thesis was to identify TAG degradation products from canola oil using tandem mass spectrometry and complementary methods of liquid chromatography and FAIMS. An instrumental method was developed using ESI-MS, MSMS, LC and FAIMS. The specific challenges I wanted to address included the resolution of positional isomers, the identification of oxidation products and the complexity of dealing with a real sample. Tools were developed using standards to later be applied to a real sample. To achieve our overarching research goal, individual goals were achieved as follows:

A) Optimizing ionization conditions for TAG and TAG degradation products

B) Applying MSMS to differentiate TAG degradation products

C) LC and FAIMS method development for TAG and their oxidation products

D) Understanding the complexity of TAG oxidation and degradation in real time

CHAPTER 2 ELECTROSPRAY IONIZATION TANDEM-MASS SPECTROMETRY OF TAG AND TAG OXIDATION PRODUCTS

2.1 INTRODUCTION

Triacylglycerol's (TAGs) are an important class of energy storing lipid molecules that consist of a glycerol backbone attached to three fatty acid chains via ester linkages. Structural information of TAG is required to determine carbon chain lengths and the number and location of double bonds (DB). TAGs are the main component of edible oils where their structures determine physical properties such as; viscosity, melting point and solubility (Foubert et al. 2007). TAGs that contain double bonds are known as unsaturated TAGs and are more susceptible to oxidative degradation compared to saturated (no double bonds) TAGs (Frankel et al. 2005). The susceptibility of unsaturated TAGs to undergo oxidation when exposed to heat, light or oxygen creates changes within their media (Neff et al. 1998). Oxidized TAGs lead to deterioration of lipid-containing foods causing foul odours and tastes as well as being linked with negative health implications including; cancer, heart disease and neurodegenerative diseases (Zeb et al. 2010).

Mass spectrometry provides a rapid method for the identification and structural characterization of TAGs. Electrospray ionization (ESI) coupled with mass spectrometry detection initiated the term 'shotgun lipidomics' which permits analysis of larger intact lipid molecules such as TAGs (Han et al. 2005). Although there are some exceptions, ionization by ESI generally involves the addition or loss of a proton at an acidic or basic site on the molecule of interest (Gaskell, 1997). The classification of a molecule as acidic or basic requires the presence of a heteroatom such as nitrogen or oxygen/sulfur/phosphorus, respectively. Although oxygen atoms are present in the

glycerol backbone, they do not possess exchangeable protons since they are all tied up in esters (Zeb, 2012). An advantage of ESI is that non-polar ions can still be ionized with the addition of a cationic adduct (Postel, 2006). TAGs have previously been shown to form successful adduct complexes with lithium, sodium, potassium and ammonium adducts of the form $[M+Li]^+$, $[M+Na]^+$, $[M+K]^+$ and $[M+NH_4]^+$ (McAnoy et al. 2005; Hsu et al. 1999). Cesium and rubidium adducts have been used for fatty acid analysis but have not been investigated for TAG analysis. The capillary inlet of a mass spectrometer is typically kept at high temperature to ensure complete desolvation of the droplets in the process of forming ions, where sample flow rate has an effect on inlet temperature and desolvation (Banerjee et al. 2019). Therefore, MS instruments are set almost to a default of 275 °C or higher (Zeb et al. 2010; Petronilho et al. 2021).

Using MSMS, fragmentation of lithiated TAGs has been shown to provide valuable structural information about TAGs and their fatty acid composition (Hsu et al. 1999). Sodium and ammonium adducts fragmented to DAG product ions as well, although there was a lack of structural information generated from the product ions in comparison to lithiated TAGs (Hsu et al. 1999). MSMS analysis of potassium, rubidium or cesium adducts with TAG have failed to produce product ions. Ammoniated oxidized TAGs fragment into protonated DAG and MAG product ions. Neff et al. (1998) showed epoxidized TAGs fragment to DAG ions with the epoxide group intact, as well as hydroperoxy TAGs fragment to DAG ions with a proposed epoxide group as well. They assumed the other oxygen present in the initial hydroperoxide product dissociated to $[TAG(OOH)-H_2O]^+$ also identified in the MSMS spectra (Neff et al. 1998). The position of the oxidation products were determined from MSMS of hydroperoxy TAG, as DAG

product ions were identified with part of an acyl chain cleaved where the oxidation product resided. MSMS of oxidized TAGs help yield structural information about the precursor molecule, however, there lacks structural information that increases specificity between potential oxidation groups.

Previous investigation into ESI-MS of TAGs focused on lithiated TAG molecules with emphasis on tandem-MS analysis (Hsu et al. 1999). There is a lack of a comprehensive overview of ESI-MS analysis of intact TAGs, comparing cation adducts such as lithium to sodium, potassium, rubidium, cesium, and ammonium, as well as their ability to help structurally determine TAG molecules using MSMS. To our knowledge there are very few, if any, previous studies focusing on ESI-MS analysis of TAG oxidation products without prior chromatographic separation. APCI-MS has been considered, although the technique is limited in its ability to analyze intact TAG molecules and it would not use alkali metal adducts for ionization (Mottram et al. 2001). A direct comparison of alkali metal adducts, and ammonium adducts has previously been made for fatty acids but has not been carried out for TAGs or TAG degradation products (Kato et al. 2021). This study investigates direct comparisons between product ions generated from precursors Li^+, Na^+, K^+, Rb^+, Cs^+ and NH_4^+ TAG ions. A comparison is also made with product ions resulting from fragmentation of primary and secondary oxidation products using the six potential adducts. Unique product ions are highlighted to distinguish between products with overlapping m/z ratios and structural determination hints are presented. The study also investigates the effect of MS inlet temperature on TAG and TAG degradation products.

2.2 EXPERIMENTAL

2.2.1 Materials

TAG standards trilinolein (18:2/18:2/18:2) and triolein (18:1/18:1/18:1) were purchased at 5 mg mL^{-1} in ethanol (EtOH) from Cayman Chemical Company (Ann Arbor, Michigan, USA) (Table 2.1). Standards of hydroxy and hydroperoxy trilinolein were purchased at 5 mg mL^{-1} in EtOH also from Cayman Chemical Company (Ann Arbor, Michigan, USA). Dry samples of lithium chloride (LiCl), sodium chloride (NaCl), potassium chloride (KCl), rubidium chloride (RbCl), cesium chloride (CsCl) and ammonium acetate were purchased from Sigma Aldrich. (St.Louis, MI, USA)

Table 2.1 Comprehensive list of all chemicals and reagents used throughout this study.

Abbreviation	Name	Molar Mass	Formula	Supplier
OOO	Triolein	885.4 Da	$C_{57}H_{104}O_6$	Cayman Chemical
LLL	Trilinolein	879.4 Da	$C_{57}H_{98}O_6$	Cayman Chemical
	Hydroxy linoleins	879.04 Da + [(1-6) x (16.001 amu)]	$C_{57}H_{98}O_6$[+(1-6)O]	Cayman Chemical
	Linoleins hydroperoxides	879.04 Da + [(1-6) x (32.002 amu)]	$C_{57}H_{98}O_6$[+(1-6)OO]	Cayman Chemical
FA	Formic acid	46.03 Da	$C_2H_2O_2$	Sigma-Aldrich
LiCl	Lithium chloride	42.39 Da	LiCl	Sigma-Aldrich
NaCl	Sodium chloride	58.44 Da	NaCl	Sigma-Aldrich
KCl	Potassium chloride	74.55 Da	KCl	Sigma-Aldrich
RbCl	Rubidium chloride	120.92 Da	RbCl	Sigma-Aldrich
CsCl	Cesium chloride	168.38 Da	CsCl	Sigma-Aldrich
H_2O	Water	18.02 Da	H_2O	Sigma-Aldrich
AA	Ammonium acetate	77.08 Da	CH_3COONH_4	Caledon
EtOH	Ethanol	46.07 Da	C_2H_5OH	Greenfield Global
H_2O_2	Hydrogen peroxide	34.015 Da	H_2O_2(3%W/V)	Health Care PLUS

2.2.2 Sample Preparation

Alkali salts and ammonium acetate

Six potential cation adducts (Li^+, Na^+, K^+, Rb^+, Cs^+ and NH_4^+) were prepared in stock solutions of 1.0 mM from stock. Using Equation 2.1, the adducts were analytically

weighed to the appropriate mass (mg) resulting in a molarity of 1.0 mM in a total volume of 1 mL based on their corresponding molar masses.

$$Molar\ mass\ \left(\frac{g}{mol}\right) x\ Volume\ (L)\ x\ Molarity\ (\frac{mol}{L}) = (mass\ (g) x\ [1x10^3]) = mass\ (mg) \quad \text{Eq. 2.1}$$

The stock solutions were stored at 5°C. The stock samples were diluted 10 fold (100 uL stock in 900 uL solution) to 0.1 mM for analysis. Formic acid (0.1 %) was added with ammonium acetate to lower the pH.

Triacylglycerol Standards

Stock solutions of trilinolein (54:6, (18:2/18:2/18:2)) and triolein (54:3, (18:1/18:1/18:1)) were prepared to 5 mg mL^{-1} in 100% EtOH. Stock solutions were stored at -30°C. TAG standards were analyzed at 10 ug mL^{-1} for either L-QIT or Q-OT infusion analysis. The stock solutions were diluted from 5 mg mL^{-1} to 10 ug mL^{-1} by pipetting 2 uL of stock into 998 uL 100% EtOH. The majority of samples were prepared to 1 mL total working volume to facilitate simple dilutions. For analysis by infusion, 0.1 mM of an alkali salt adduct or ammonium acetate was added to the sample and vortexed briefly.

Triacylglycerol Oxidation Standards

Stock solutions of hydroxy trilinolein and hydroperoxy trilinolein were purchased in solution (EtOH) at 5 mg mL^{-1}. Stock solutions were stored at -30°C. Oxidation standards were analyzed at 10 ug mL^{-1} for either L-QIT or Q-OT infusion analysis. The stock solutions were diluted from 5 mg mL^{-1} to 10 ug mL^{-1} by pipetting 2 uL of stock into 998 uL 100% EtOH. For analysis by infusion, 0.1 mM of an alkali salt adduct or ammonium acetate was added to the sample and vortexed briefly.

Commercial samples of epoxidized trilinolein were not available for purchase; therefore, epoxidized trilinolein was prepared following a method proposed by Xia and Budge (2015). Using the calculations in that method, based on the number of double bonds in trilinolein, the ratio of reagents was determined to be 1:0.5:1.5 TAG:FA:H_2O_2. Molarities of FA and H_2O_2 were calculated to 23.5 M and 0.66 M respectively. A calculated *n* value of 0.0000682 mols based on the 6 double bonds in trilinolein and volumes of formic acid and hydrogen peroxide were determined to be 1.45 uL and 155 uL respectively. The two volumes were added to 10 mg of trilinolein standard. Epoxy samples were then diluted from a stock solution of 10 mg mL^{-1}, following the same parameters as for hydroxy and hydroperoxy trilinolein.

2.2.3 Mass Spectrometry

Mass spectrometry detection was performed using either a linear ion trap (L-QIT) or a high-resolution/accurate mass (HR/AM) quadrupole-orbitrap (Q-Exactive, Q-OT), both from Thermo-Fisher Scientific (San Jose, CA). Instrumental details on the L-QIT and Q-OT mass spectrometers are listed in Tables 2.2 and 2.3 respectively. The mass spectrometers were both calibrated in positive ion mode using pre-prepared commercial solutions containing caffeine, MRFA, and Ultramark 1621 (Thermo-Fisher Scientific) once every three days. Nitrogen gas for the ESI ion source was provided from the head-space of a 230-L liquid nitrogen dewar from Linde (Moncton, NB). This dewar lasted for approximately 12 days of continuous operation of the mass spectrometer. High purity 5.0 nitrogen (i.e., 99.999% pure) was used in the octopole collision cell of the Q-OT. Helium gas was used in the linear ion trap of the L-QIT.

Table 2.2 List of L-QIT mass spectrometry parameters used in this study.

Parameter	Value
Ion source	Electrospray
Source voltage	4.5 kV
Sheath gas flow	5 arb units
Emitter diameter	Low flow
Ion transfer capillary temperature	RT to 280 ºC
Ion transfer capillary voltage	(+20)-(+140) V
Tube lens voltage	0-250 V
Ion trap resolution	Enhanced
Maximum ion injection time	500 ms
Mass accuracy	0.2 Da
Mass range	50-2000 Da
Scan functions used	Full-MS/ MSMS

Table 2.3 List of Q-Exactive mass spectrometry experimental details used in this study.

Parameter	Value
Ion Source	Electrospray
Source voltage	4.0 kV
Sheath gas flow rate	8 arbitrary units
Auxiliary gas flow rate	3
Ion transfer capillary temperature	275 ℃
Ion transfer capillary voltage	35
S-lens voltage	50
Orbitrap resolution	140,000
Orbitrap transient time	512
Maximum ion fill time	500
Mass accuracy	<10 ppm
Mass range	50-2000
Scan functions used	Full-MS/ PRM/ Targeted SIM

2.3 Results & Discussion

2.3.1 Ionization of TAG Standard Using Ammonium Acetate

An MS scan of ammoniated trilinolein standard was acquired over m/z range of 400-2000 m/z using a Q-OT MS. The analysis was done by direct-infusion MS which, is the continuous introduction of analyte to the MS source from a sample syringe. The MS inlet

was set at 25 °C. Capillary inlets are more commonly set to higher temperatures (275-300 °C); however, when infusion was carried out at 25 °C it resulted in successful ionization. Ammoniated trilinolein, $[C_{57}H_{98}O_6NH_4]^+$, has a m/z value at 896.7702 with two other ions appearing within the spectra (Figure 2.1). The ion at m/z 599.5017 (label A) is in a m/z range that suggests a diacylglycerol (DAG). HR/AM allows for predicted empirical formulas to match with experimental collected spectra; therefore, a predicted empirical formula of the 599.5017 ion was determined to be $C_{39}H_{65}O_4H$ within 10 ppm. This formula represented the loss of one of the C18:2 fatty acyl chains from the TAG molecule along with ammonia. Ammonium is a weakly bound adduct and is able to leave as neutral ammonia, leaving behind a hydrogen atom to protonate the molecule. The loss of ammonia is commonly observed when analyzing ammoniated lipids (Zeb, 2012).

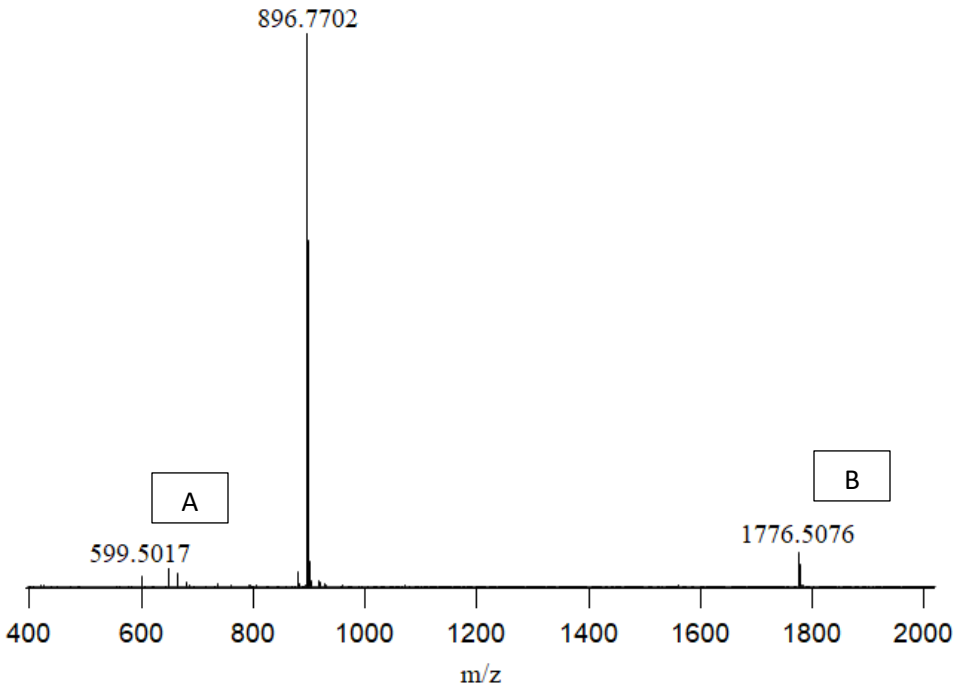

Figure 2.1 Spectra of ammoniated trilinolein showing the DAG (A) and dimer (B) that appear in the spectra, resulting from analysis on the Q-OT mass spectrometer at an inlet temperature of 25°C. The m/z scan range was set from 400-2000 m/z.

TAG molecules are also able to form non-covalently bound dimer ions. Although dimers are not often mentioned in the literature, they have been previously reported by Grossert et al. (2014), and clearly identified in Figure 2.1 as label B. The m/z 1776.5076 ion represents [2TAG+NH_4], where the TAG is 54:6. The mechanism of dimer formation between two TAGs is not well known but a high affinity between the acyl chains of two TAG molecules may be expected. Gerbig and Takats, (2010) proposed that the formation was "associated with van der Waals forces between the hydrocarbon chains of the fatty acid residues," whereas Grossert et al. (2014) suggest that the cation adducts can form tetrahedral complexes between two TAGs through the glycerol backbone. The binding mechanism cannot, however, be determined through MS analysis alone.

2.3.2 Tandem-MS of TAG Standards

Once efficient ionization of trilinolein was accomplished, the next steps to characterize the ion were to induce fragmentation and identify resulting product ions (Figure 2.2). Fragmentation using the Q-OT mass spectrometer is known as higher-energy collisional dissociation (HCD). HCD is specific to the orbitrap instrument and is a beam-type, tandem in space MS/MS mode that takes place within an octopole HCD cell.

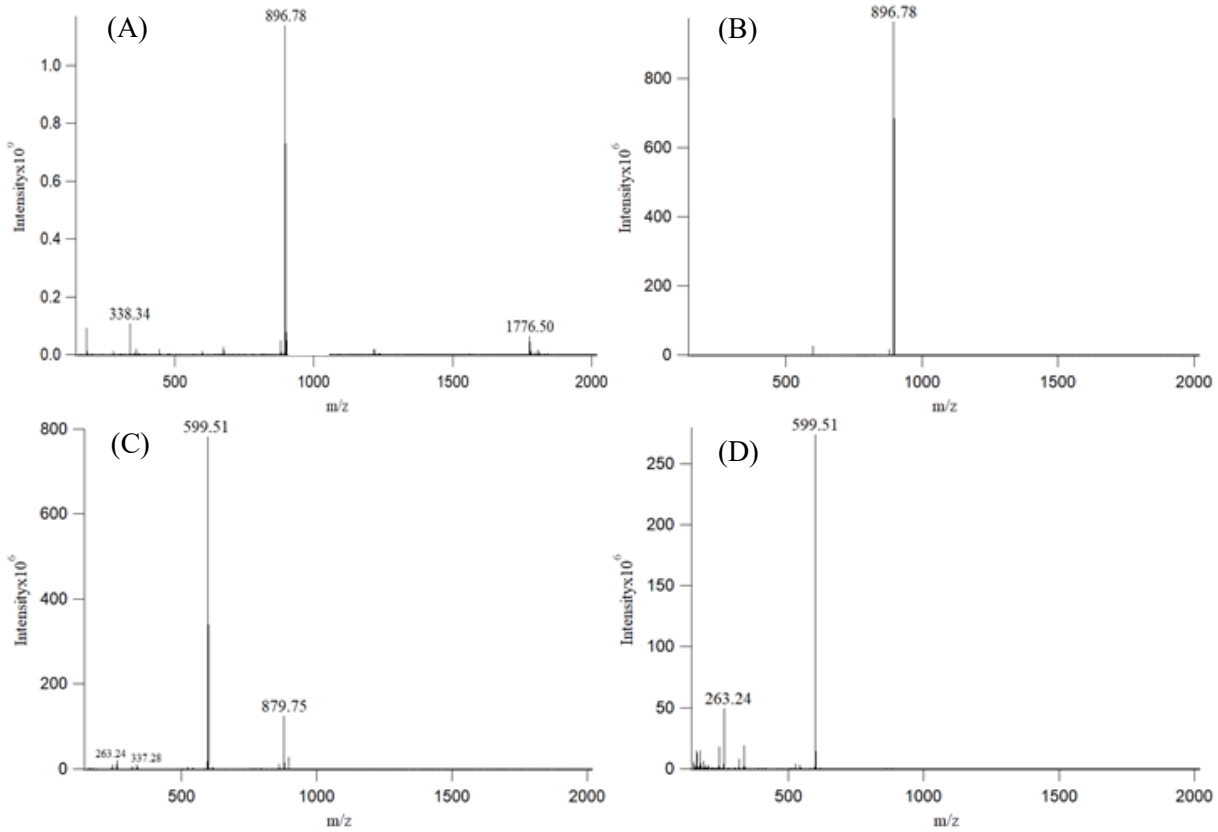

Figure 2.2 Ammoniated trilinolein infused on the Q-OT MS showing Full MS scan in panel (A). Isolation of the monomer ion 896.78, collision energy of 10 eV is applied in panel (B) compared to a collision energy of 30 eV in panel (C). An increased collision energy of 50 eV is applied in figure (D). m/z scan range was set from 200-2000 m/z.

Using ammoniated trilinolein with the previously described monomer at 896.78, the full MS spectra shows the dimer at m/z 1776.50, the protonated monomer at m/z 896.78 and a monoacylglycerol (MAG) derivative, m/z 338.34, as well as low levels of background signal (Figure 2.2, A). There is also a very small signal for the DAG ion at m/z 599.50 in the full MS spectra. As noted above, the MAG and DAG ions could be a result of degradation within the sample or degradation within the source or MS inlet. In general, the full MS scan shows the comprehensive ionization of the sample including chemical background and solvent/buffer related ions within the spectra.

In panel (B), continuing to use the Q-OT MS, m/z 896.78 monomer is isolated using the quadrupole mass filter with a m/z window of 4 to include isotopes (Figure 2.2). In panel (B) the precursor isolation is done at very low collision energy levels, resulting in minimal fragmentation. In panel (C), 30 eV was applied to m/z 896.77, causing it to break into fragment ions. Resulting fragment ions help determine structural characteristics of the target ion. Knowing the empirical formula of the parent ion and simulating the product ions, the chemical formula of the neutral loss can be determined. For example, in panel (C) the most abundant fragment, m/z 599.51 can be matched to an empirical formula of $C_{39}H_{65}O_4H$ confirmed using the simulation tool on Qualbrowser. Therefore, the monomer ion, TAG, lost one of the C18:2 fatty acid chains as well as ammonia (NH_3). Ammonia departs as a free ion, leaving the remaining hydrogen atom on the DAG. Therefore, the fragmentation reaction is: TAG +NH_4 – NH_3 – $C_{18}H_{33}O_2$. Loss of one fatty acid chain from applied collision energies is frequently stated in the literature when using ESI-MSMS for TAG analysis (Neff et al. (1998); Kato et al. (2018); Kalo et al. (2006)). Trilinolein standard had a FA distribution of (18:2/18:2/18:2) and, in a

homogenous standard, it is known that the fragment loss was an 18:2 acyl chain. It has previously been reported that TAG molecules favour the loss of FA in the *sn-1* or *sn-3* position as opposed to *sn-2*.

There is also a small amount of m/z 879.75 in panel (C). This fragment represents the loss of ammonia from the parent ion, creating a protonated TAG monomer. There is very little protonated monomer ion in the full scan (Fig 2.2, A) but a greater amount of protonated TAG, attributed to the loss of neutral ammonia, is observed at applied collision energies (Fig 2.2, C). There are also two fragment ions at lower mass values, m/z 337.28 and m/z 263.24, equating to the loss of two C18 fatty acid chains. The difference in the two fragment ions is the loss of glycerol backbone. The simulated formulas are $C_{18}H_{31}O$ for m/z 263.24 and $C_{21}H_{37}O_3$ for m/z 337.28. If a heterogeneous group of FA composed the TAG molecule, we could expect to see each of the different fatty acid groups as fragments (Zeb et al. 2010). Since the standard is a homologous set of FA, only one monoacylglycerol chain is observed.

Application of a higher collision energy of 50 eV (Fig 2.2, D) leads to an increase in collisions between the target ion and neutral gas molecules. The maximum signal intensity decreased by almost three fold as collision energy increased (Fig 2.2, C and D). As the collision energy is increased in an octopole cell, fragment ions begin to undergo further fragmentation. In panel (D) there is no protonated monomer ion left, indicating that 50 eV is too high a collision energy for that fragment. The effects of adding collision energy in the HCD are thereby specific to the precursor of interest. This process of fragmentation helps generate qualitative information surrounding the structure of the TAG and its fatty acid distribution. Tandem MS improves specificity and reduces the

chemical noise while increasing the signal-to-noise ratio and promoting improved conditions for quantitative analysis.

The previously identified dimer ion at m/z 1776.5 can also be targeted for fragmentation to yield ammoniated TAG monomer m/z 896.771. The fragmentation at collision energy of 27 eV also produced a small amount of protonated trilinolein at m/z 879.833, along with the DAG ion at m/z 599.583 (Figure 2.3).

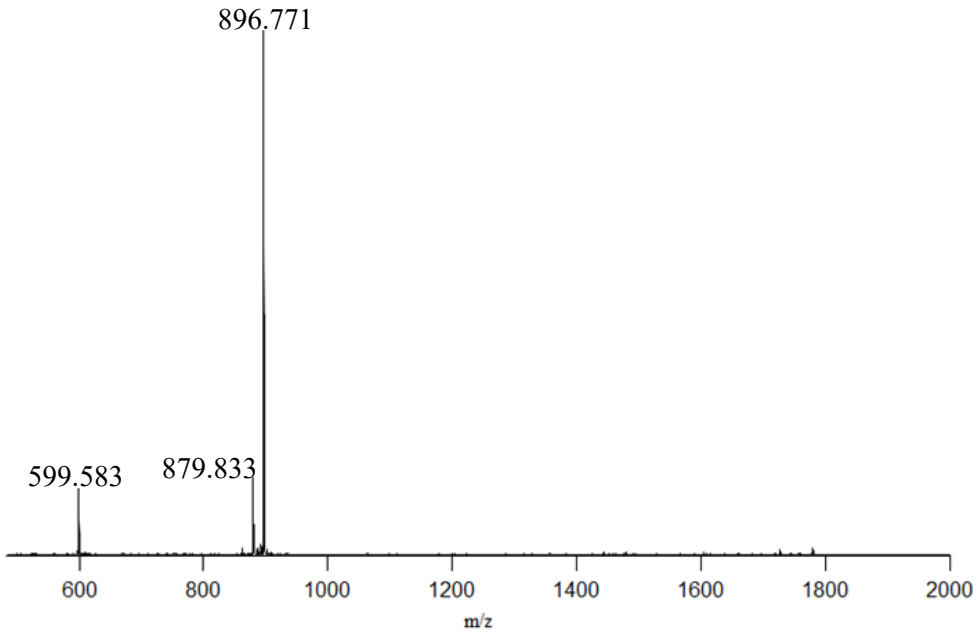

Figure 2.3 MSMS spectra of precursor dimer ion 1776.5 [2TAG+NH_4]. An applied collision energy of 27 eV is used to target 1776 (± 4 m/z).

Assuming that the dimer forms through non-covalent interactions between the ammonium ion and two TAG glycerol backbones, the easiest fragmentation process is to cleave a TAG molecule with the ammonium adduct intact. A smaller amount of the protonated monomer indicates that the ammonium adduct may be somewhat protected in the dimeric species. It is important to understand the fragmentation of a certain molecule to better understand the structure of it. Considering the complexity of TAG molecules

and the vast amount of possible conformations they can contain when thinking of a complex sample rather than a standard, it is advantageous to use tandem MS methods to get a better understanding of structural conformation.

2.3.3 Ionization of TAG with Cation Adducts

An acidic solution of 0.1% formic acid was used and enhance protonation of TAG, however the method failed to produce relevant amounts of protonated TAG in positive ion mode with low levels of sodiated TAG. Previous investigation into ESI of TAGs identified sodiated TAG adducts present from endogenous levels in the environment (Hsu et al. 1999). Our investigation into ammoniated trilinolein resulted in low amounts of sodiated 54:6 TAG. Based on this knowledge, it was of interest to investigate the adduct potential of other alkali metals. Using trilinolein standard, ionization efficiency was investigated using six potential cationic adducts (i.e., Li^+, NH_4^+, Na^+, K^+, Rb^+, Cs^+) (Figure 2.4).

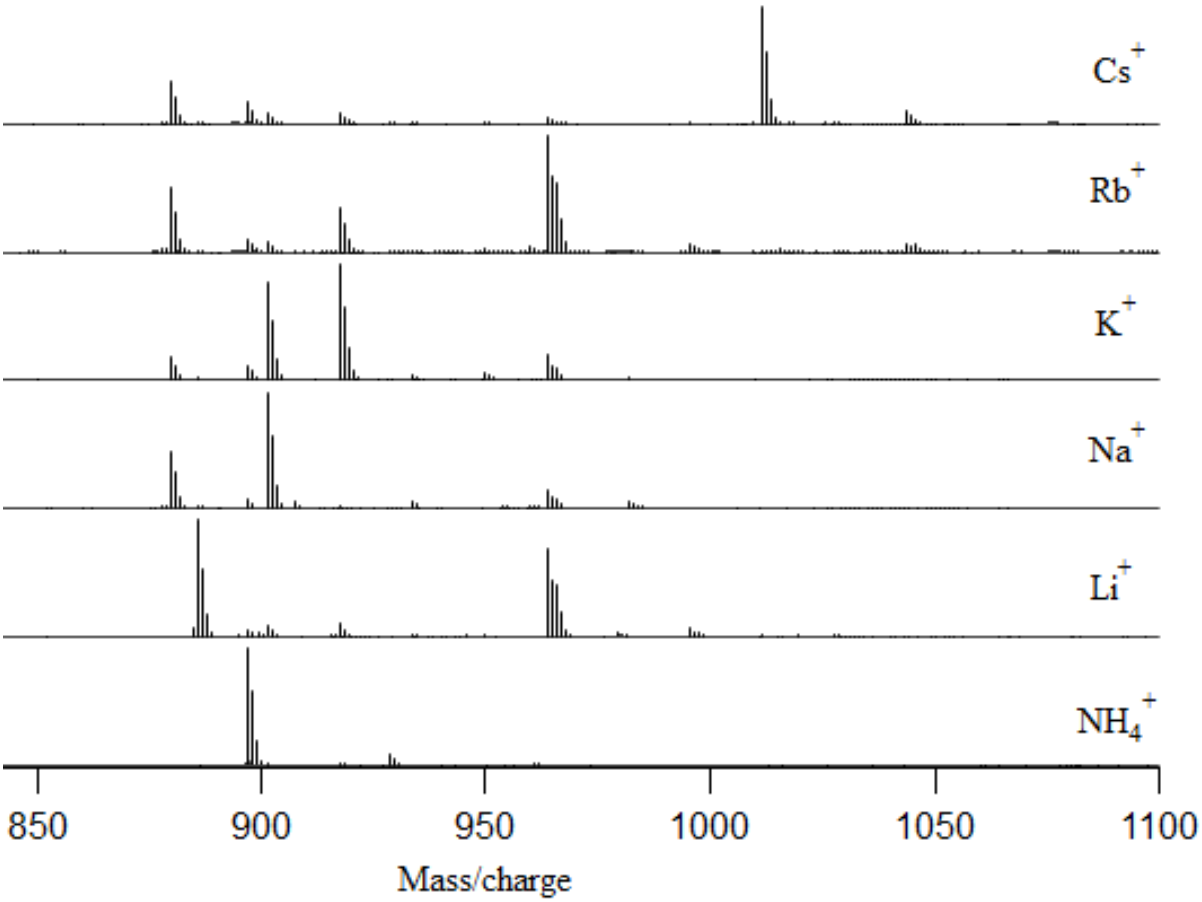

Figure 2.4 Direct-infusion ESI on the Q-OT MS of 10 ug mL^{-1} trilinolein samples in 100 % EtOH and 0.1% formic acid with the addition of one alkali metal or ammonium adduct. Alkali salts, LiCl, NaCl, KCl, RbCl, and CsCl, were added at concentrations of 0.1 mM. Ammonium acetate was also investigated as a potential adduct at a 0.1 mM. Each sample was analyzed using a Full MS scan at a m/z range of 400-2000, where the range was magnified for the current figure. The Hamilton syringe was flushed three times between each sample with 500 uL 100 % EtOH.

The adducts NH_4, Li, Na, K, Rb and Cs form $[M+adduct]^+$ ions with corresponding m/z of 896.757, 885.742, etc, respectively. Alkali metals were added in excess of the lipid. An increase in metal concentration could lead to suppression of ionization efficiency due to larger amounts of metal within the sample competing with the other analytes for ionization. The efficiency of ionization by each adduct is important

because there may be instances when the use of one adduct over another could be advantageous. For example, if an ion of interest is located in a mass-to-charge region of high noise, it could be beneficial to employ a heavier adduct such as rubidium or cesium to shift the ion to a m/z region of potentially less noise, particularly if the chemical noise is not due to isomeric TAGs. Tandem-MS data presented in the following section also suggests that ion fragmentation profiles may be adduct dependent.

It is evident that there was carry-over between the samples, where lithiated TAG can be identified in each of the other alkali metal spectra (Fig 2.4). This is a common problem with infusion techniques, even with thorough rinsing of the syringe between samples. Each adduct sample was infused separately and the Hamilton syringe and sample line was flushed three times with 250 uL of 100% ethanol between each sample. The effects of carry-over are even more troublesome for quantitative analysis. The discrete sampling and washing capabilities of a liquid chromatography autosampler are particularly valuable for quantitation but even with LC, we have found it is sometimes necessary to include a blank injection, especially after injecting a sample of high concentration. Infusion techniques also are much more limited by the detrimental effects of ion suppression. With infusion analysis, everything within the sample matrix is ionized simultaneously; therefore, the signal of the target ion can be suppressed due to contaminants within the sample. The extent of signal suppression is very dependent on sample composition so that signal response can be highly variable on a sample-to-sample basis. If possible, sample dilution can be an effective method for reducing the effects of signal suppression (Volmer and Jessome, 2006).

In comparing ionization efficiency, the six adducts produced approximately the same signal response at $2\ x\ 10^8$ for a concentration of 10 ug mL^{-1} (11.36 μM) (Figure 2.4). If it is assumed that the cations are positioned on the carbonyl groups of the glycerol backbone, it is plausible that the ionization mechanism, the ionization efficiency and the location of the charge are very similar (Hsu et al. 2010). However, there is no definitive proof of the nature of the interaction. Grossert et al. (2014) suggested that, although interaction between cation adducts and the carbonyl groups yield strong bonds, there is also an attraction to consider between the double bonds and the cations. A double bond is an alkenyl π-bond which has an affinity for cations to create cation-π interactions. Unfortunately, when ionizing TAG standards by ESI with alkali metals or ammonium cations, it is not possible to deduce the location of the charge.

2.3.4 Competitive Ionization and Tandem-MS of TAG with Alkali Metal and Ammonium Adducts

In order to identify the best adduct species in terms of ionization efficiency, competitive ionization experiments were conducted amongst ammonium and the five common alkali metals. Ionization by ammonium is enhanced by the addition of 0.1% formic acid to ensure that ammonia is in its cationic form (Kruve and Kaupmees, 2017). The data shown in Figure 2.5 is plotted as the percent signal contribution of the adduct listed on the x-axis relative to the adduct in the legend of each panel. Resulting values greater than 50 % indicate a stronger ionization efficiency of the corresponding adduct on the x-axis than the ion shown in the body of the panel. From panel A, it is clear that all alkali metals appear to bind more strongly than ammonium but it should be noted that subsequent work suggests that the ammonium adducts are susceptible to the loss of

neutral ammonia at elevated inlet temperatures and inlet voltages. The effect of thermal degradation to form a protonated product is only relevant to ammonium adducts although some release of cesium metal was observed at elevated temperatures for Cs-TAG adducts. Panel B of Figure 2.5 indicates that the heavier alkali metals are favoured over lithium and that the ionization seems to overwhelmingly favour sodium. Panel F indicates that the head-to-head comparisons favour the largest metal (cesium) in every case. A previous study by Hsu et al. (2010) stated that the strength of adducts bound to TAG is in the order of $Li^+ > Na^+ > K^+ > NH_4^+$ based on the signal response from MSMS analysis; however, the competitive ionization experiments here show the opposite effect where the heavier adducts show stronger binding ability. While competitive ionization experiments tended to favour the larger adducts, similar signal responses were observed for simple mixtures of TAGs with single adduct species.

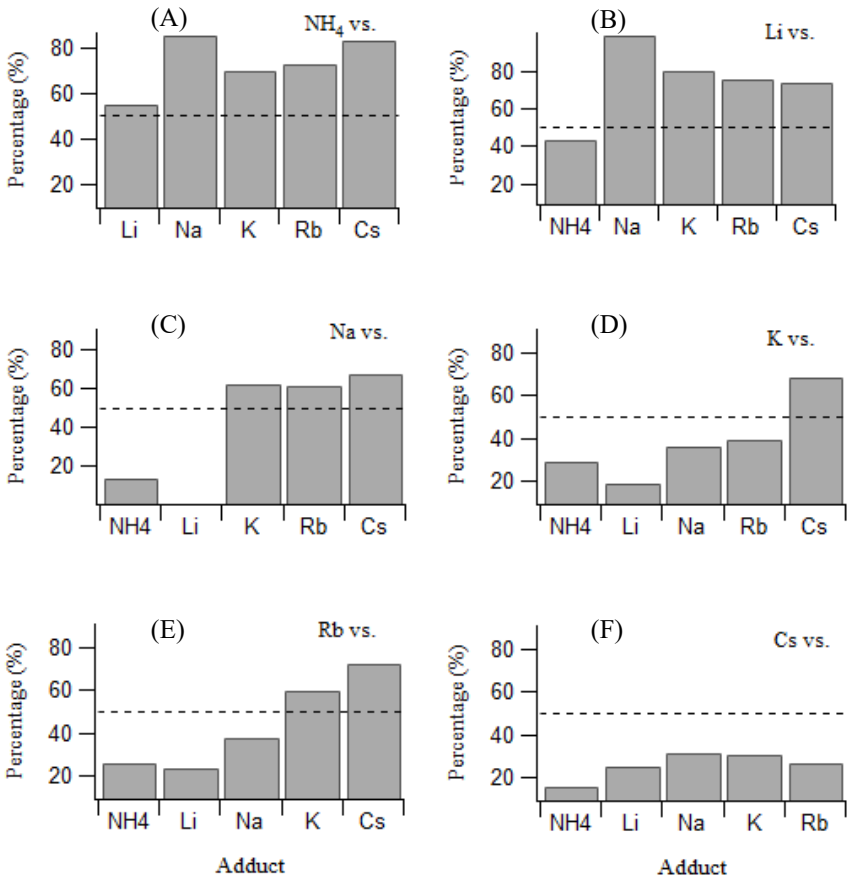

Figure 2.5 Competitive ionization of alkali metal and ammonium adducts done by infusion and tested one versus one. Each adduct was tested in the same sample as each of the other adducts, at a concentration of 0.1 mM in excess to the lipid standard trilinolein. (A) ammonium versus alkali metals, (B) lithium versus adducts, (C) sodium versus adducts, (D) potassium versus adducts, (E) rubidium versus adducts, and (F) cesium versus adducts. For example, in the first column of panel A the percent signal is calculated as follows: $\%Li\ versus\ NH_4 = \frac{Li\ signal\ intensity}{\sum Li\ signal\ intensity + NH_4\ signal\ intensity)} x\ 100$

After investigating the ionization ability and competitive ionization characteristics of each potential adduct, tandem-MS was used for further characterization of each adduct. In analytical mass spectrometry, MSMS is a very useful and powerful tool for both qualitative and quantitative analysis. MSMS data acquired for different adducts may also be expected to highlight differences in ionization mechanisms and analyte stability.

Note that the dissociation of a charged adduct species would render the molecule unresponsive to mass spectrometry if the metal adduct was to dissociate from the lipid.

The same MSMS technique can be applied to each of the TAG monomers for the alkali metal adducts using an applied collision energy of 27 eV (Figure 2.6). There are a few important features to note in these TAG fragmentation spectra, including (1) the variable complexity of the spectra, (2) the 16 Th mass-to-charge shifts in DAG products for lithium (7 amu) , sodium (23 amu) and potassium (39 amu), (3) the unanticipated appearance of protonated DAG fragments (m/z 599) originating from alkali adduct parent ions, (4) a variety of MAG fragment masses and (5) the relative ion abundance on the y-axes. There are also small peaks that represent the TAG+A, (A=adduct), for sodium, potassium and rubidium adducts (Figure 2.6, C, D, E). This is because some of the precursor ion is still intact at that CE, and requires a higher CE than NH_4, Li and Cs to completely fragment. The 16 Th mass-to-charge difference becomes important when oxidation products are present.

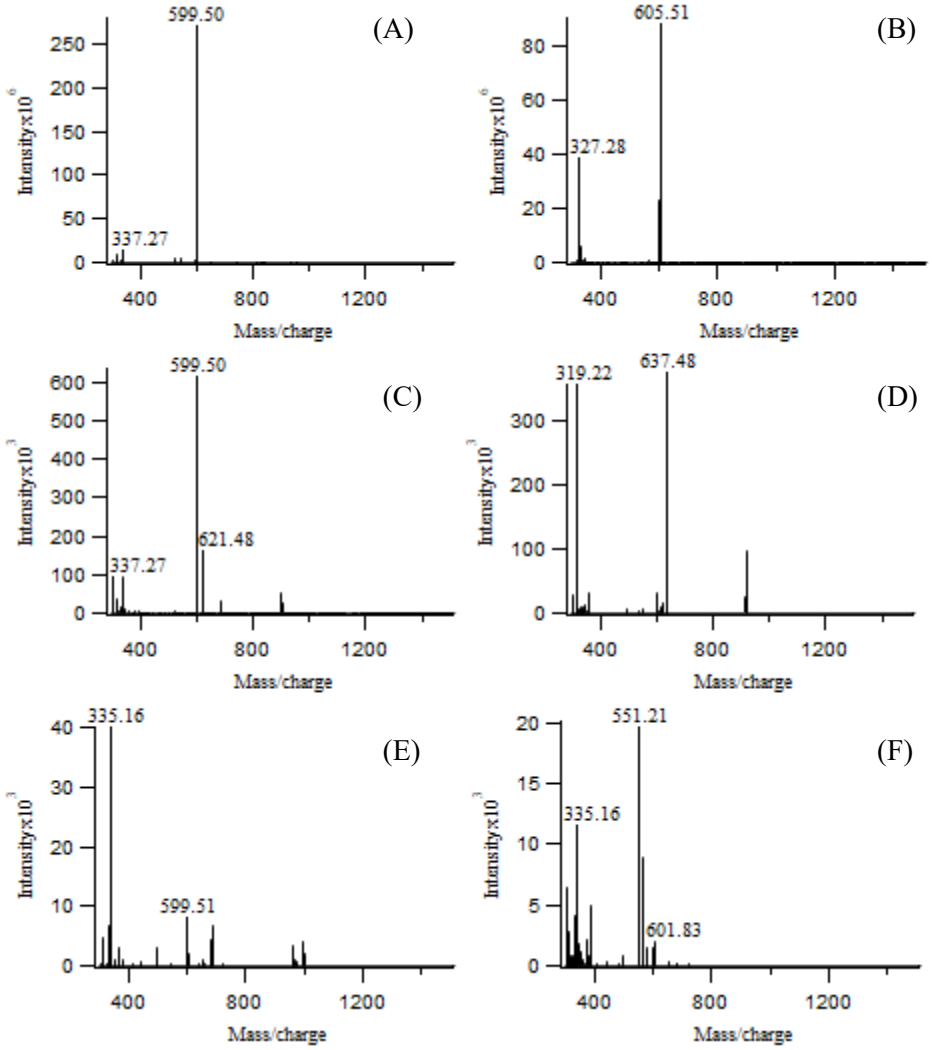

Figure 2.6 Electrospray ionization tandem mass (ESI-MS/MS) spectra of the ammonium and alkali metal adducts of trilinolein collected on the Q-OT mass spectrometer where NH_4 adduct is displayed in panel (A), Li (B), Na (C), K (D), Rb (E) and Cs (F). All fragmentation spectra were collected using a collision energy of 27 eV.

The ammonium-trilinolein precursor (m/z 896; Fig 2.6, A) was selected using the ±2 Da window by the quadrupole mass filter and accumulated in the C-trap prior to fragmentation in the octopole cell of the Q-OT mass spectrometer. Panel A shows a very clean spectrum that is dominated by a protonated DAG molecule, following the loss of ammonia and a C18 acyl chain as expected. Given that trilinolein is a symmetric (i.e., 18:2/18:2/18:2) TAG, the same fragment mass is expected regardless of whether the cleavage occurs at the *sn-1, sn-2* or *sn-3* position. In panel (B), the fragmentation of precursor Li-(18:2/18:2/18:2) (m/z 885) produces two DAG and one MAG product ions. The ion at m/z 605.51 has lithium bound to the DAG, resulting in a loss of $C_{18}H_{32}O_2$ as expected and previously determined by Hsu et al. (2010). Unlike ammonium, lithium is a stable ion, though some protonated DAG molecule (m/z 599.1) is observed in this spectrum. The formation of a protonated fragment from a lithiated precursor is unusual and unexpected for a unimolecular collision with an inert nitrogen collision gas because the lithium adduct is the charge carrier, promoting successful ionization of the molecule. Therefore, the presence of a protonated product ion would result in the loss of lithium while gaining a hydrogen atom. The protonated DAG molecule was previously identified by Hsu et al. (1999) where a proposed mechanism showed lithium leaving with a FA to generate a ring formation on the remaining DAG ion (Figure 2.7).

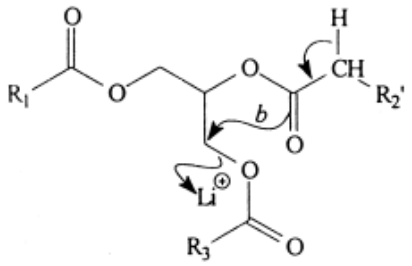

Figure 2.7 Proposed pathway to generate the protonated DAG ion from lithiated precursor trilinolein. This rationalizes the formation of DAG ion arising from elimination of the *sn*-2 FA as a lithiated salt.

The generated MAG ion from lithium dissociation at m/z 327.28 was also previously described by Hsu et al. (1999) and is different than those resulting from NH_4, Na, K, Rb and Cs precursor ions. A rearrangement takes place between the *sn-2* acyl chain and the glycerol backbone that forms an additional double bond and methyl group (Hsu et al. 2010). It is predicted that m/z 327.28 product ion forms from further fragmentation of m/z 605.51 product ion. The loss of the R_3 fatty acyl chain instead of R_1 would produce the same m/z 327.28 product ion.

In panel (C) the fragmentation spectra of sodiated trilinolein shows two DAG ions. Both fragments result from the loss of $C_{18}H_{32}O_2$; however, one DAG, m/z 621.5, has sodium still associated while the other, m/z 599.5, represents the protonated DAG previously seen with ammonium adducts. The mechanism of formation for the protonated DAG has not been determined although it presumably follows the same mechanism as lithiated TAG. At m/z 337.27, the fragment ion represents $C_{22}H_{25}O_3$, which lost two C18 fatty acid chains and is a derivative of a MAG. The product ion m/z 337.27 is a protonated ion which lost the sodium adduct. It is assumed that it is derived from DAG ion m/z 599.51. The MAG derivative appears as a product of ammoniated trilinolein as well (Panel A). Kalo et al. (2006) referred to the MAG derivative from ammoniated TAG

as RCO+74^{+}. Similar nomenclature is used by Neff et al. (1998), who label the product ion with +74. A proposed structure shows cyclization of an oxygen atom originally present on the glycerol backbone (Figure 2.8). Encompassed in red is the additional +74 often referred to by authors such as Neff et al. (1998), McAnoy et al. (2005) and Kalo et al. (2006), while the RCO group outside of that represents the acyl chain.

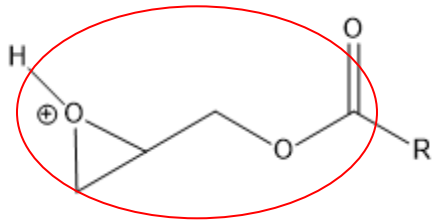

Figure 2.8 Proposed structural diagram of m/z 337.27 monoacylglycerol derivative by Kalo et al., (2006) representing RCO+74. Highlighted in red is the +74 m/z units described. Knowing trilinolein is 18:2/18:2/18:2, R represents *sn-1* or *sn-3*.

Panel (D) with potassium yielded similar results to the lithium adduct, where potassium stayed attached to the DAG ion and there was a protonated MAG fragment; however, the MAG derivative is different than those seen with lithium, sodium or ammonium. The resulting product ion from potassium trilinolein has a m/z of 319.22. A simulated spectrum of m/z 319.22 was used to calculate the loss of H_2O (18 m/z) from m/z 337.27 to yield $C_{22}H_{35}O_2$ that matched the experimental m/z 319.22 collected within a 10 ppm window. Readdressing the proposed structure for m/z 337.27 by Kalo et al. (2006) (Figure 2.8), it is likely that the epoxide ring opened, giving rise to O-H_2 leaving. The proposed MAG derivative of precursor potassiated trilinolein likely arose from fragmentation of m/z 637.5.

The largest adducts, rubidium and cesium, failed to produce extensive fragmentation spectra, with rubidium in panel (E) yielding small amounts of the

protonated DAG, m/z 599.51 and the MAG ion, m/z 335.51, being the dominant fragment. The MAG derivative from rubidium is 2 Th lower than the MAG derivative from sodium and ammonium. The fatty acyl chain in the derivative represents an 18:3 chain rather than 18:2. The mechanism of rearrangement to form an additional double bond is unknown but it can be assumed to undergo rearrangement from further fragmentation of the DAG ion. When fragmenting the cesium adduct of trilinolein, there was a small amount of monoglycerol ion at m/z 335.5, as well as an unidentified ion at m/z 551.21. There was also a small amount of m/z 601.83 that was two mass units higher than m/z 599.51 protonated DAG previously described. Simulating the spectra resulted in a proposed empirical formula of $C_{39}H_{69}O_4$, which would indicate a loss of $C_{18}H_{30}O_2$. The difference in the loss of this C18 chain versus the C18 chain lost with the other five adducts is two more hydrogen atoms on the DAG fragment, which would often indicate one less double bond (i.e., 18:2/18:1). All of these fragments were unexpected as Kato et al. (2021) suggested that FA molecules with cesium adducts cannot produce fragmentation due to the large ionic radius of cesium atom causing the interaction between adduct and glycerol oxygen to decrease as the positive charge is dispersed over a larger sphere. It was also highlighted by Adams et al. (1987) that cesium does not produce successful product ions when fragmenting fatty acid precursors due to the low binding strength of cesium compared to other alkali metals. While fragments were obvious here, very low levels of product ions from cesium and rubidium precursor ions were present, likely due to the loss of adducts at the applied collision energies. Previously in Section 2.3.1, using the same Q-OT, ammoniated trilinolein was shown to form dimeric species of the form $[2TAG+NH_4]^+$. Alkali metal adducts with trilinolein also

form dimer ions in the form of $[2TAG+A]^+$. It is interesting, however, to note that fragmentation of cesium and rubidium dimers resulted in $[TAG+Cs]^+$ and $[TAG+Rb]^+$ product ions since fragmentation of precursor $[TAG+Cs]^+$ and $[TAG+Rb]^+$ ions did not lead to many successful product ions. It may be that the energy applied to fragment the dimer is used to break the TAG-TAG interaction first, allowing cesium and rubidium ions to stay bound to the monomer. In the dimeric form, the adducts could be in a position that is protected from collision energies, resulting in them remaining intact with the TAG ion.

Here, we have provided a qualitative comparative analysis of trilinolein with alkali metal adducts and ammonium using direct-infusion MS and tandem-MS techniques on a Q-OT MS. DAG product ions and proposed MAG structures had previously been identified by Neff et al. (1997) and Kalo et al.(2014) for ammoniated TAG; however, a comprehensive analysis using the six adducts with direct comparison has not been done to our knowledge. Further, successful identification of cesiated and rubidiated TAG product ions has not previously been reported; a comparison of competitive ionization had also not been made until now. The competitive ionization comparison was done to determine the different ionization potentials of the adducts. It was surprising that TAGs have such high affinities for alkali metals in comparison to ammonium.

2.3.5 Thermal Degradation of Intact TAG Standards

The MS inlet in this work was initially set to 25°C to reduce degradation. However, knowing increased inlet temperatures improves signal transmission; the temperature was raised to 275°C on the L-QIT for similar infusion analysis of trilinolein. When the capillary temperature was increased to 275°C, a surprisingly different spectrum was obtained. The higher temperature favoured a dominant ion of m/z 599.67, previously

seen from applied collision energies. Further, the expected ion of ammoniated trilinolein (m/z 896.5) is actually lower than sodiated trilinolein (m/z 901.83). Sodium was not added to the sample; the adduct formed from endogenous sodium in the environment. The increase in inlet temperature unexpectedly and previously unnoted, resulted in the degradation of TAG species. It is important to note the change in signal intensity of $[M+NH_4]^+$ with temperature (Fig 2.9, A and B). If the sample had been initially analyzed at high capillary temperature, the conclusions of adduct ionization would have been very different.

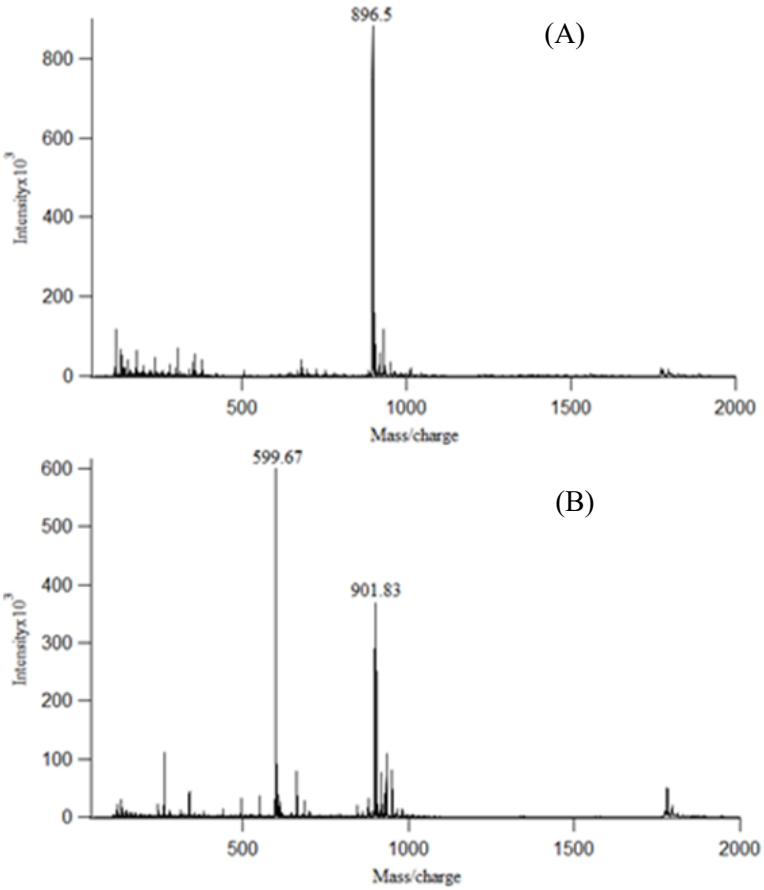

Figure 2.9 Thermal degradation of the ammonium adduct of trilinolein in the heated transfer capillary of a linear quadrupole ion trap (L-QIT). Spectra collected with the transfer capillary at room temperature (panel A) were compared to those at 275°C (panel B).

Finding endogenous sodiated trilinolein at a higher intensity than the ammonium adduct suggested a greater stability of the sodium adduct at higher temperatures compared to ammonium (Figure 2.10). The signal intensity for $[TAG+Na]^+$ greatly increased between panel (A) and (B) as was initially expected. The increase in the monomer (m/z 901.83) can be associated with improved ion transmission at higher temperatures as well as potential decomposition of the dimer. Noting the differences between the two adducts at various temperatures, it can be proposed that the effect of temperature is adduct dependent. While the effect of temperature was greatest with ammonium, other adducts such as Li, Rb, K and Cs also showed degradation occurring, with high amounts of protonated DAG ions observed.

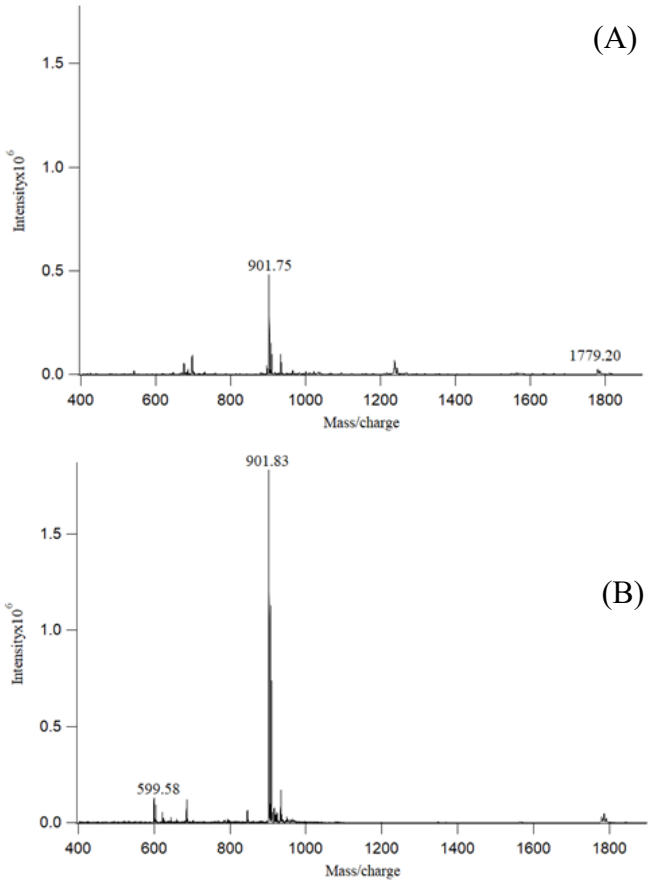

Figure 2.10 Thermal degradation of the sodium adduct of trilinolein in the heated transfer capillary of a linear quadrupole ion trap (L-QIT). Spectra collected with the transfer capillary at room temperature (panel A) were compared to those at 275°C (panel B).

The effect of capillary temperature appears to be more pronounced on the linear trap (LQIT) than was observed on the quadrupole Orbitrap (Q-OT). This may be due to the longer length of the transfer capillary and a reduced linear velocity of the gas into the linear trap. The effect of temperature with the ammonium adduct was further investigated to better understand the temperature at which degradation began to occur. Extraction of the TAG monomer, 896.67, showed a decrease in signal intensity at temperatures above 100°C (Figure 2.11). Furthermore, the DAG ion began to appear at 150°C with a large increase in signal between 150-200°C. The DAG signal surpassed the monomer at 250°C while the endogenous sodium adduct surpassed the monomer signal at 300°C (Figure

2.11). It can be concluded that inlet temperatures below 150 °C provide optimal signal transmission of TAG with reduced degradation. The effect of temperature is heightened with ammoniated TAG, however degradation is still notable with alkali metal adducts. Each tested adduct, except sodium, showed reduced signal intensity for the target monomer ion at increased temperatures, therefore providing a rationale for limiting the use of high MS inlet temperatures.

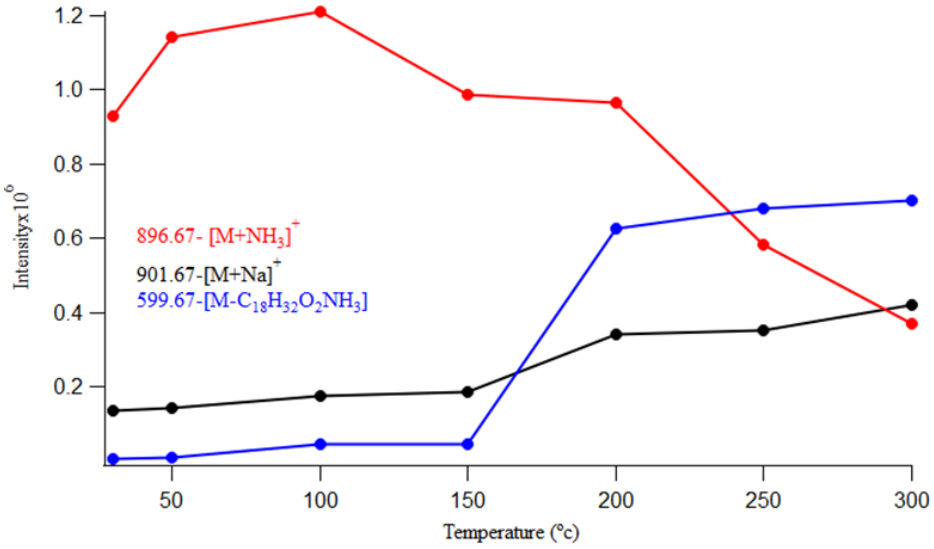

Figure 2.11 Extraction of 896.67 monomer ion of ammoniated trilinolein, 901.67 of sodiated trilinolein and 599.67 degradation of the monomer ion to DAG. Samples were infused on the L-QIT mass spectrometer and signal intensity was recorded for each ion at temperature intervals of 30°C, 50°C, 100°C, 150°C, 200°C, 250°C and 300°C.

2.3.6 Ionization of TAG Oxidation Products (hydroxy trilinolein, hydroperoxy trilinolein and epoxy trilinolein) at 25°C

Each of the alkali metal adducts and ammonium used previously were analyzed again with the oxidation standards at room temperature (25°C) on the Q-OT. This analysis was done on the Q-OT in comparison to the L-QIT for mass accuracy. Especially for MSMS, with potentially unknown product ions, it was advantageous to

perform initial analysis on a HR/AM MS for mass accuracy. Primary oxidation products, hydroperoxides, were first investigated using hydroperoxy trilinolein standard (Figure 2.12). The mixed standard claims to have up to three hydroperoxy groups and 132 potential isomers.

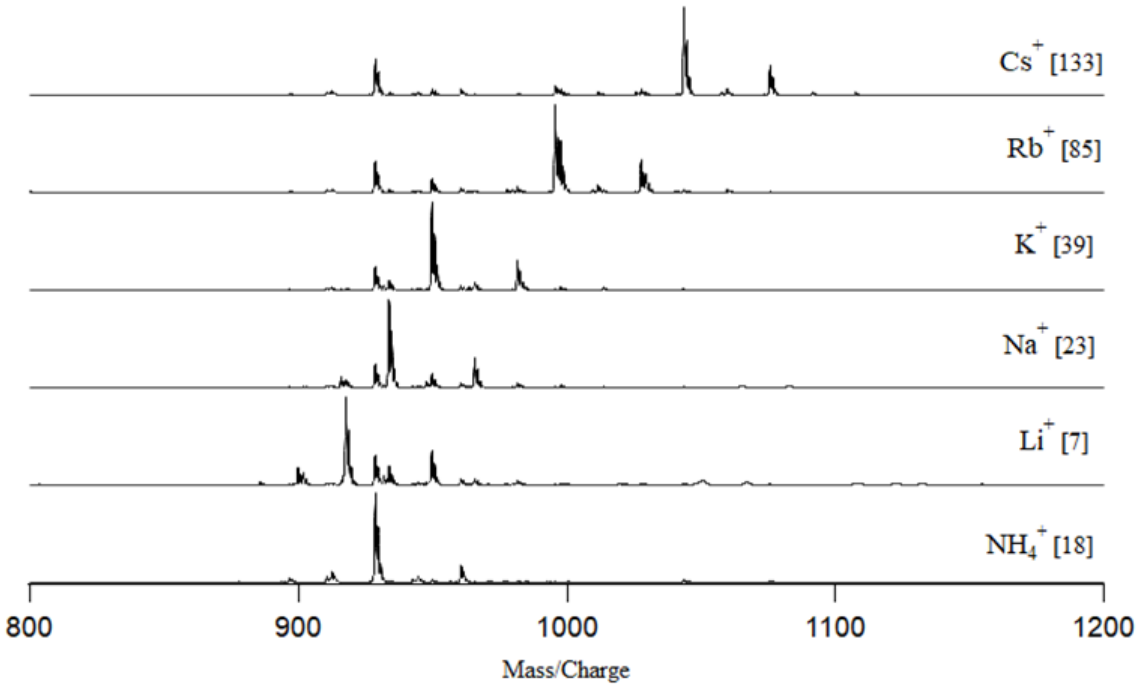

Figure 2.12 Ionization of hydroperoxy trilinolein by direct-infusion MS on the Q-OT with each alkali adduct and ammonium. Hydroperoxy trilinolein has the empirical formula $C_{57}H_{98}O_6AO_2$, where A represents one of the cation adducts displayed.

Similar to trilinolein, ionization of hydroperoxy trilinolein standard at room temperature was successful using each of the six adducts but carry-over between infusion samples continued to be a challenge. It is clear within the six panels that the ammoniated sample is present in all of the other samples at m/z 928.762 (Figure 2.12). At room temperature (25° C) there is no degradation occurring from the source temperature, and the correct monomer ion is identified, without high amounts of DAG present.

Although the mixed standard claims to contain structures with up to three hydroperoxide groups, for each adduct, a maximum of two hydroperoxide groups were identified. Mono- and di- hydroperoxy trilinolein can be described as $C_{57}H_{98}O_6A(2O)$ and $C_{57}H_{98}O_6A(4O)$, respectively, where A represents the corresponding cation adduct. For all adducts, the major peak in the spectra represented mono-hydroperoxy trilinolein with the di-hydroperoxy ion consistently present in lower amounts. Ammoniated mono-hydroperoxy trilinolein and di-hydroperoxy trilinolein had m/z of 928.75 and 960.68, respectively (Figure 2.12). Mono-hydroperoxy products for the other adducts had m/z of 917.74, 933.71, 949.68, 995.62 and 1043.62 for lithium, sodium, potassium, rubidium and cesium, respectively. Di-hydroperoxide products had an increased m/z of 32 Th from the mono-hydroperoxy m/z.

Hydroperoxide functional groups contain two oxygen atoms; therefore, it was surprising to observe oxidation products containing three oxygen atoms. There are small peaks that appear between the mono- and di- hydroperoxy products for each adduct (Figure 2.12). For example, for the sodium adduct, there was a peak with m/z of 949.714 and can be described as $C_{57}H_{98}O_6Na(3O)$. Hydroperoxides are often described as unstable oxidation products and are easily decomposed and susceptible to further reactions. The ability to further react can create other oxidation products or radicals. It is anticipated that although the sample is a standard, there was degradation of the di-hydroperoxide that resulted in formation of a mono-oxygen product such as hydroxy, epoxy or ketone groups. However, it was not possible to determine the structure of this oxygenated TAG using direct infusion analysis only.

The hydroxy standard was similar in composition to the hydroperoxide standard where there are 6 double bonds within the TAG and the standard had 132 potential isomers of mono-, di-, and tri- hydroxy compounds (Figure 2.13).

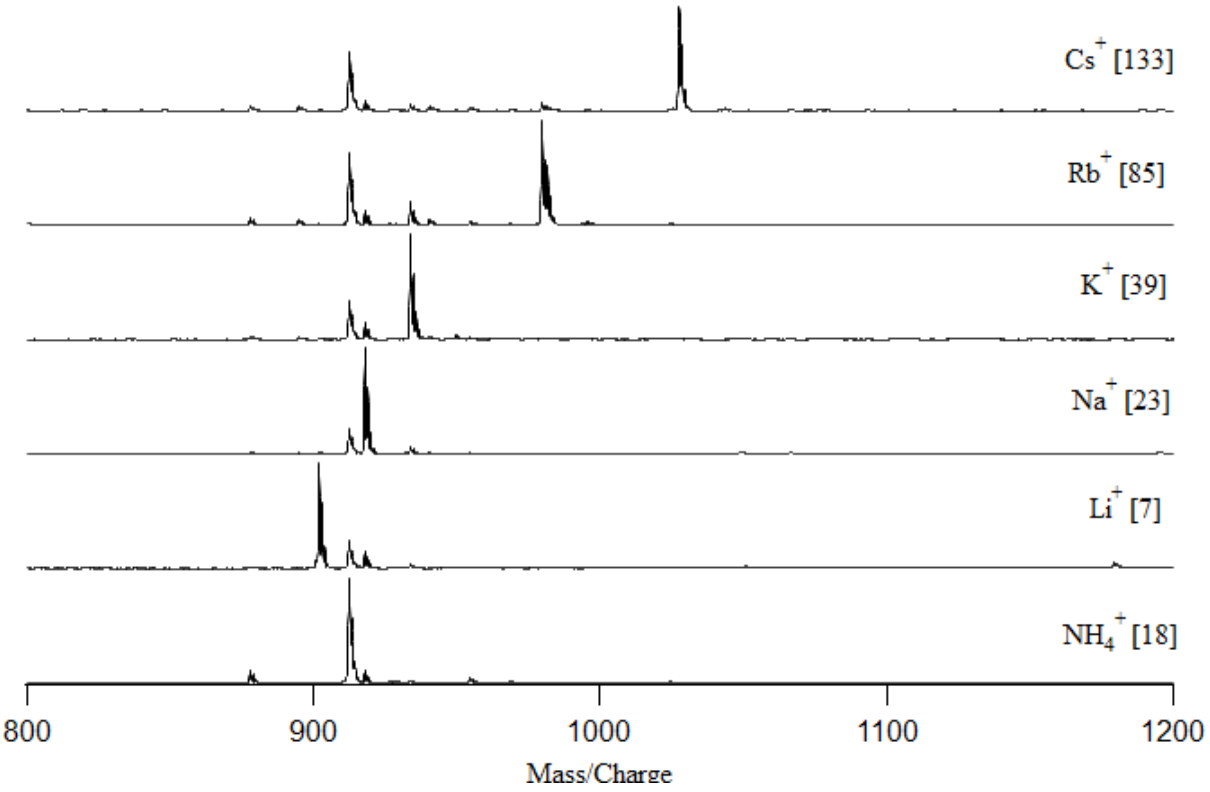

Figure 2.13 Ionization of hydroxy trilinolein by direct-infusion MS on the Q-OT with each alkali adduct and ammonium. Hydroxy trilinolein has the empirical formula $C_{57}H_{98}O_6AO$, where A represents one of the cation adducts displayed.

Mono-hydroxy products have an empirical formula of $C_{57}H_{98}O_6AO$ where A represents the cation adduct. Successful ionization of mono-hydroxy products was confirmed using each adduct, resulting in m/z values of; 912.78 $[NH_4]^+$, 901.74 $[Li]^+$, 917.72 $[Na]^+$, 933.68 $[K]^+$, 979.63 $[Rb]^+$ and 1027.63 $[Cs]^+$ (Figure 2.13). Although the syringe was flushed using 100 % EtOH between consecutive samples there is ammoniated mono-hydroxy trilinolein carry-over at m/z 912.67 in each of the other

samples (Figure 2.13). Unlike the hydroperoxide samples where two hydroperoxy groups were identified, only mono-hydroxy groups were identified for each adduct in this case.

Although di-hydroxy ions were not identified, in a naturally oxidized sample, there would be potential for overlap to occur between mono-hydroperoxy trilinolein and di-hydroxy trilinolein. For example, in ammoniated TAG, di-hydroxy trilinolein would have the formula $C_{57}H_{98}O_6NH_4(2O)$ and m/z 928.768 while mono-hydroperoxy trilinolein has the same formula and m/z. Direct-infusion MS methods alone do not allow differentiation between the isomers. Depending on the complexity of the samples, further overlap between 4-hydroxy and di-hydroperoxy trilinolein might also occur. Worse, the degradation of di-peroxy trilinolein would likely result in the same m/z and empirical formula as tri-hydroxy trilinolein at 944.785 Da. The complexity of a single TAG standard alone is large and becomes increasingly more complex when oxidation products are introduced.

Another type of secondary oxidation product, epoxides, is primarily reported from hydroperoxide decomposition following the mechanism described in Figure 2.14. Epoxides are three membered rings that can form directly in place of a double bond or on the residing allylic carbon atoms (Parker, 1959). It has recently been proposed that epoxide oxidation content in TAG degradation provides a more complete view of total lipid oxidation compared to measuring only hydroperoxides (Gruneis et al. 2019) because, as hydroperoxides begin to decompose, secondary products such as epoxides form (Xia et al. 2015). Epoxides are single oxygen products similar to hydroxides, creating challenges in differentiating between the two degradation products.

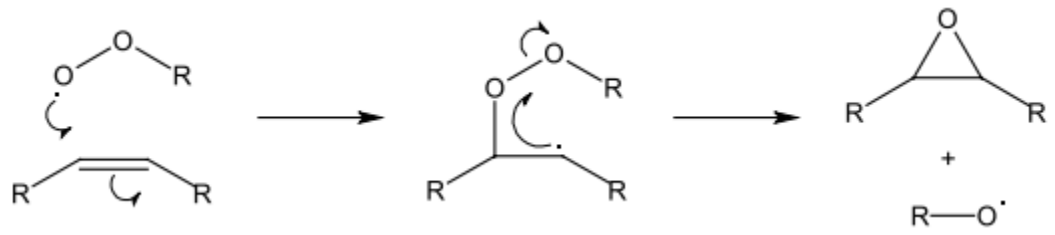

Figure 2.14 Hydroperoxide decomposition mechanism to generate secondary oxidation products, epoxides.

Epoxide standards were not commercially available, unlike hydroperoxide and hydroxide standards. Epoxide products were formed following a method proposed by Xia et al. (2015) using hydrogen peroxide, formic acid and trilinolein standard as described in the experimental section. Trilinolein standard was chosen as the TAG to oxidize in order to have a direct comparison with hydroxide and hydroperoxide standards (Figure 2.15).

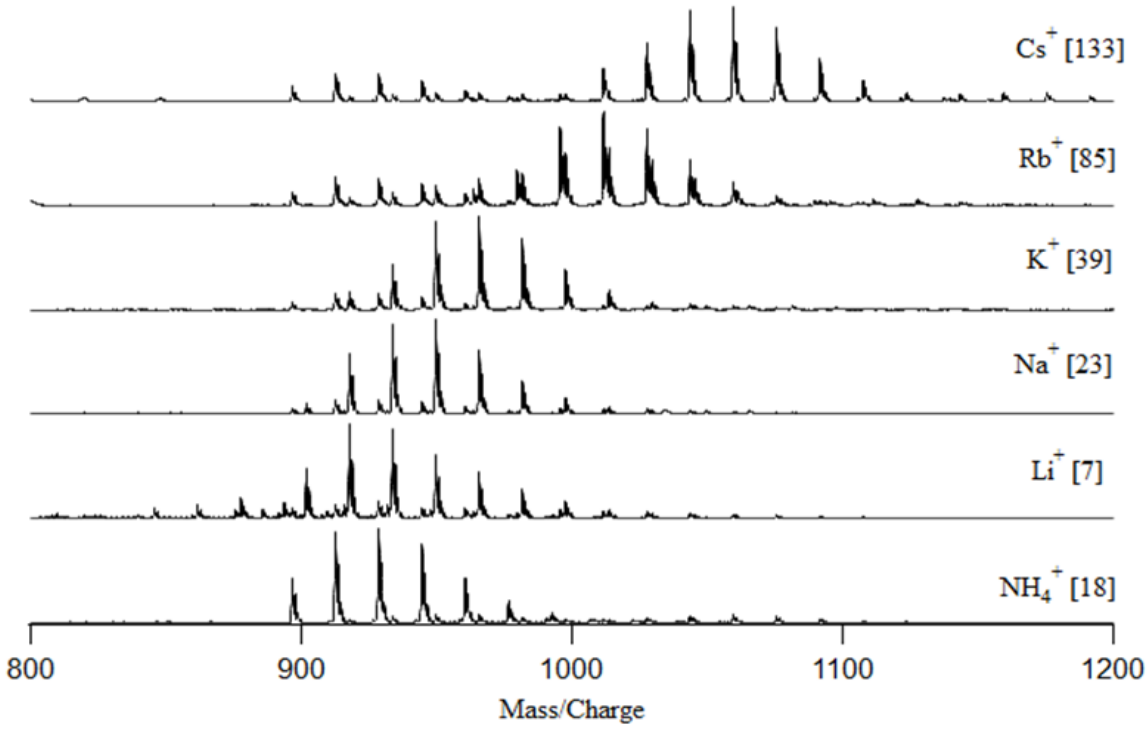

Figure 2.15 Ionization of epoxy trilinolein by direct-infusion MS on the Q-OT with each alkali adduct and ammonium. Epoxy trilinolein has the empirical formula $C_{57}H_{98}O_6AO(1\text{-}6)$, where A represents one of the cation adducts display.

An obvious notable difference in the mass spectra collected at 25° C for epoxidized trilinolein compared to hydroxy or hydroperoxy trilinolein is the multiple peaks within the spectra (Fig 2.15). Since the epoxide sample was made within the lab, the oxidation time was varied to attempt to induce complete oxidation. If the oxidation process were to go to completion, only the 6-epoxy trilinolein would be identified without observing the mono- or other lower number of epoxy groups; however, the spectra clearly showed the presence of 1-6 epoxide products, as well as unaltered trilinolein and higher-ordered epoxidized products (Figure 2.15). Considering first ammoniated epoxy trilinolein, the first peak represents m/z 896.787 which is trilinolein without oxygen (Figure 2.15). Such un-oxidized ions are not identified in hydroxy- and hydroperoxy- trilinolein standards, presumably because they would have been removed from the oxidized products. The six epoxidized products of trilinolein had the following m/z: 912.78- $C_{57}H_{98}O_6NH_4(O)$, 928.75- $C_{57}H_{98}O_6NH_4(2O)$, 944.74- $C_{57}H_{98}O_6NH_4(3O)$, 960.67- $C_{57}H_{98}O_6NH_4(4O)$, 976.78- $C_{57}H_{98}O_6NH_4(5O)$ and 992.75- $C_{57}H_{98}O_6NH_4(6O)$. Signal intensities for [5O] and [6O] were much lower compared to the first four oxidation products. It is interesting to note that mono- and di-epoxy ammoniated trilinolein were present at almost identical signal intensities in contrast to hydroxy- and hydroperoxy trilinolein where mono-hydroxy and mono-hydroperoxy products dominated the spectra. Even tri-epoxy trilinolein is present at high amounts. There were also a series of high-order epoxides produced (7 and 8 oxygens), clearly indicating that the number of oxygen products was not directly correlated with the number of double bonds. The two carbon atoms at either side of the unsaturation are readily available for oxygen binding. It is possible that multiple oxygens are binding near the same unsaturation leading to

increased oxidation products. This can explain why low amounts of seven and eight epoxide products are seen within the spectra. Considering these higher-order products, it is evident that there are multiple mechanisms at work aside from the one presented in Figure 2.14; however, it was not possible to determine the exact mechanisms occurring.

Mass-to-charge overlap is found in abundance between different adducts with epoxidized trilinolein. For example, lithiated di-epoxy trilinolein has a m/z of 917.7407 which is the same nominal mass as sodiated mono-epoxy trilinolein at m/z 917.7205. However, using HR/AM, the difference between the two exact masses is 20.2 ppm. Therefore, differentiation of the two products can be achieved by restricting the mass window to 10 ppm. There is continuous overlap between the two adducts as oxygen atoms are added but all can be distinguished using HR/AM because the empirical formulas are not the same. Parallel situations occur between sodium and potassium adducts. When the previous sample contains molecules with the same m/z as the present sample, it creates added challenges due to memory effects within the infusion syringe. The limitation to simulating spectra for compound identification occurs when the empirical formulae are identical. For example, ammoniated hydroxy trilinolein and ammoniated epoxy trilinolein have the same m/z and empirical formula; therefore, they cannot be differentiated by direct-infusion MS methods alone.

2.3.7 Tandem-MS of Oxidized Trilinolein with Cation Adducts

Lithium, sodium, and ammonium adducts with epoxy, hydroxy and hydroperoxy trilinolein were used to target precursor mono- and di- oxidation products for fragmentation at room temperature. With the application of collision energy, cesium and rubidium failed to provide product ions when epoxy, hydroxy or hydroperoxy precursor

ions were targeted (Fig 2.16; E,F). Using hydroxy-TAG as an example, the cesiated molecule showed much lower signal and a lack of DAG product ions (Figure 2.16). In contrast to the TAG results, rubidium failed to yield MAG product ions when mono-hydroxy trilinolein was fragmented at an initial CE of 33 eV. Further, potassiated mono-hydroxy trilinolein yields a DAG product ion at m/z 653.5; however, the signal intensity highlights the low level of ion abundance. The low signal intensities for product ions do not favour potassium as a promising adduct, leaving only ammonium, lithium and sodium as possible useful adducts.

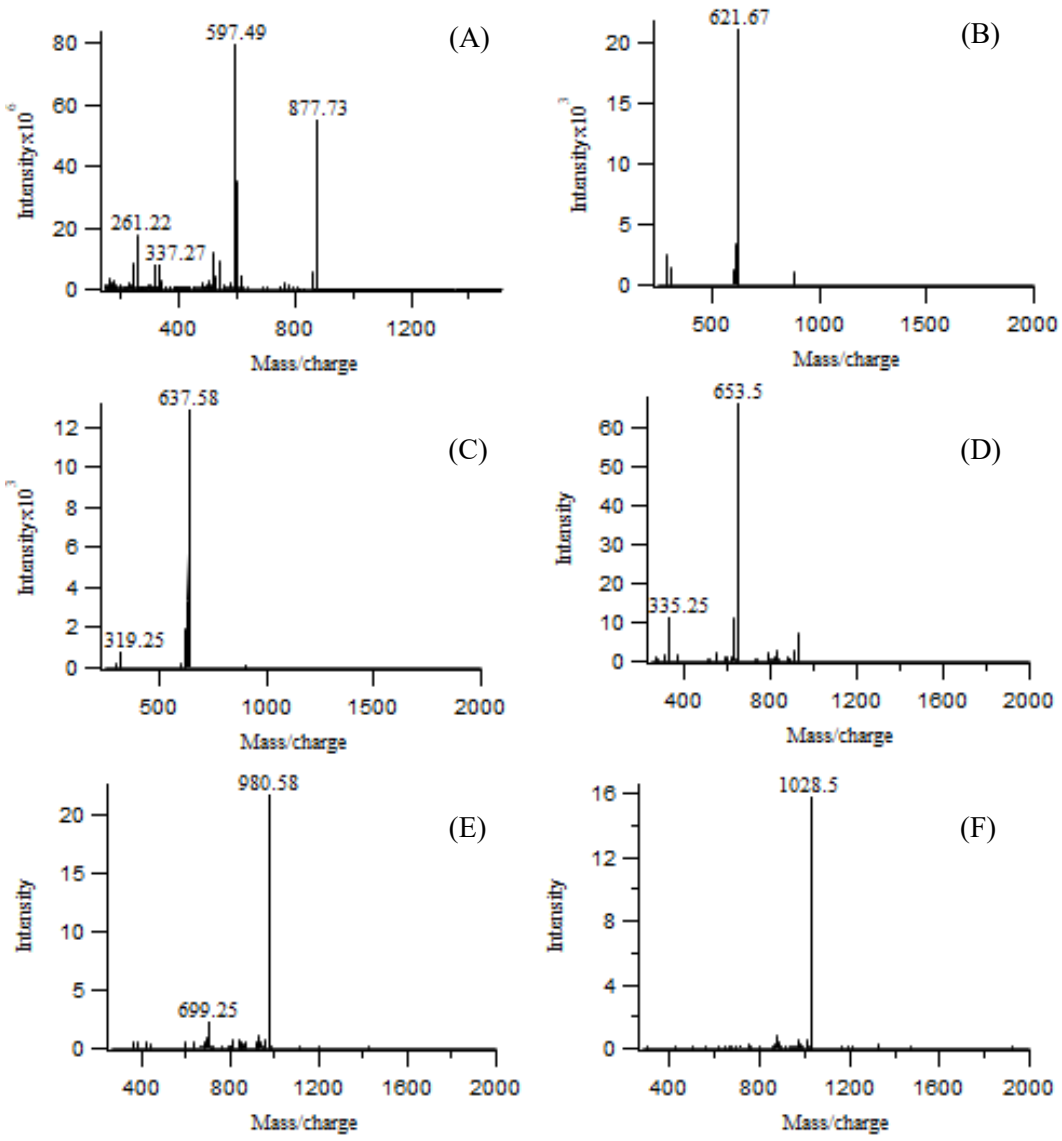

Figure 2.16 Tandem MS of mono-hydroxy trilinolein with respective cation adducts for ionization. CE was set to 33 eV for each sample. Fragmentation with different adducts is shown in panel (A) ammonium $[NH_4]^+$, (B) lithium $[Li]^+$, (C) sodium $[Na]^+$, (D) potassium $[K]^+$, (E) rubidium $[Rb]^+$ and (F) cesium $[Cs]^+$. The samples were prepared at 10 ug mL^{-1} with 0.1 mM of the corresponding adduct. Spectra was collected using direct infusion ESI on the Q-OT MS. Samples were infused in 100 % EtOH at 25 °C.

Qualitatively, tandem-MS of hydroxy trilinolein helps provide structural determination and the location of the hydroxy group. Ammoniated mono-hydroxy trilinolein (m/z 912.78) yielded un-oxidized TAG ($C_{57}H_{97}O_6$) at m/z 877.752 and

protonated DAG at m/z 597.583 ($C_{39}H_{65}O_4$). The empirical formula of the un-oxidized TAG suggests 54:7 or 18:2/18:2/18:3, while m/z 597 DAG ion represents (18:2/18:3). Neff et al. (1998) suggested that the complete loss of an oxidation group can lead neighbouring hydrogen atoms to form an additional double bond. It is assumed that the loss of the hydroxy group is the initial fragment, forming the additional double bond at m/z 877 which undergoes further fragmentation to the DAG product ion at m/z 597. In contrast to ammoniated mono-hydroxy TAG, the lithiated precursor ion targeted at the same CE 33 eV yielded a DAG product ion with the hydroxy group intact ($C_{39}H_{67}O_4LiO$ with m/z 621.67; Figure 2.16; B). Sodium and potassium follow the same trend as lithium with the hydroxy group residing on the DAG product ion, as well as having the adduct remain intact.

Focusing on ammonium, lithium and sodium adducts, tandem MS of hydroperoxy and epoxy standards were also investigated (as with hydroxy standards, Rb and Cs adducts did not generate product ions at useable intensities). Mono-epoxy and mono-hydroxy trilinolein have the same empirical formula $C_{57}H_{98}O_6AO$, where A represents lithium, sodium or ammonium (Table 2.4) but as described above for TAG, tandem MS can often be employed to identify unique product ions. However, for both lithiated and sodiated precursor ions of epoxy *versus* hydroxy trilinolein, there are no unique fragments and the monomers cannot be differentiated using infusion MS methods. The resulting product ions are two DAGs: one with the oxygen (DAG[O]) and one without the oxygen (DAG). DAG[O] product ion is present at a higher intensity than the DAG ion (without the oxygen) indicating that the oxygen is located on a FA in the *sn-2* position since alkyl chains in the *sn*-2 position are less likely to fragment. While DAG product

ions were the most abundant ions when fragmenting mono-epoxy and mono-hydroxy trilinolein, MAG product ions were also present (e.g., $C_{18}H_{33}O_2LiO$ at 303.421 and $C_{18}H_{33}O_2NaO$ at 319.832; Table 2.4). As with DAG ions, the lack of unique fragment ions between MAG product ions prevents them from be unambiguously identified.

Table 2.4 Fragmentation for mono-oxygenated products of trilinolein showing the difference between possible unique fragments using lithium, sodium and ammonium adducts.

Adduct	Target ion and Oxidation Group	Fragment ions
Li^+	***Epoxy trilinolein-*** **$C_{57}H_{98}O_6LiO$, m/z= 901.76**	**621.58,** [M+Li– $C_{18}H_{32}O_2$] **605.75,** [M+Li – $C_{18}H_{32}O_2O$] **599.67 (low),** [M-$C_{18}H_{33}O_2LiO$]
	Hydroxy trilinolein- **$C_{57}H_{98}O_6LiO$, m/z= 901.76**	**621.58,** [M+Li – $C_{18}H_{32}O_2$] **605.75,** [M+Li – $C_{18}H_{32}O_3$] **599.67 (low),** [M-$C_{18}H_{33}O_2LiO$]
Na^+	***Epoxy trilinolein-*** **$C_{57}H_{98}O_6NaO$, m/z= 917.77**	**637.67,** [M+Na+O-$C_{18}H_{32}O_2$] **621.58,** [M+Na+O-$C_{18}H_{32}O_2O$] **599.67 (low),** [M+Na+O-$C_{18}H_{33}O_2NaO$]
	Hydroxy trilinolein- **$C_{57}H_{98}O_6NaO$, m/z= 917.77**	**637.67,** [M+Na+O-$C_{18}H_{32}O_2$] **621.58,** [M+Na+O-$C_{18}H_{32}O_2O$] **599.67 (low),** [M+Na+O-$C_{18}H_{33}O_2NaO$]
NH_4^+	***Epoxy trilinolein-*** **$C_{57}H_{98}O_6NH_4O$, m/z= 912.67**	**615.50,** [M+NH_4+O-$C_{18}H_{33}O_2NH_3$] **599.50,** [M+ NH_4+O-$C_{18}H_{33}O_2NH_3O$] **877.73,** [M+ NH_4+O -NH_3OH_2] **895.74,** [M+ NH_4+O -NH_3]
	Hydroxy trilinolein- **$C_{57}H_{98}O_6NH_4O$, m/z= 912.67**	**597.49,** [M+ NH_4+O -$C_{18}H_{35}O_2NH_3O$] **877.73,** [M+ NH_4+O -NH_3OH_2]

Interestingly, when using ammonium as the cation adduct, unique fragments were achieved when targeting mono-epoxy and hydroxy precursor ions (Table 2.4). Both mono-hydroxy and mono-epoxy trilinolein result in a protonated DAG product ion without oxygen. However the mono-hydroxy spectra shows an additional double bond formed on the DAG ion at m/z 597 representing 18:2/18:3, and the un-oxidized TAG ion at m/z 877 (18:2/18:2/18:3), all without retention of oxygen. The two can be further distinguished because mono-epoxy trilinolein produces a DAG ion that does retain the

oxygen atom (at 615.50 m/z). The most abundant product ion is m/z 615.502, $C_{39}H_{67}O_5$, a (18:2/18:2) DAG ion with the epoxide group remaining, suggesting the epoxide group was positioned at the *sn*-2 position.

A clear distinction between the two overlapping oxidation products has not previously been shown. The ability to differentiate between the two TAG oxidation products will be valuable in elucidating structures in complex samples. The differences in the spectra with respect to ion presence and abundance are well-illustrated in Figure 2.17. It seems that the applied collision energies onto ammoniated hydroxy-TAG ions leads to loss of the hydroxy group, driving the formation of an additional double bond; the same effect is not observed with epoxy-trilinolein. Qualitatively, structures of product ions can be used to differentiate the two oxidation groups whereas quantitatively the amount of each oxidation product can be determined based on the unique fragmentation channels.

In Figure 2.17, panel (A), the precursor ions for mono-hydroxy and mono-epoxy ions are displayed, where they have the exact same m/z at 912.671. When a CE of 33 eV was applied, panel (B) and (C) show the difference in MSMS spectra. In red, the epoxy product ions are dominated by m/z 615.50 and m/z 599.90. In comparison, the black trace in panel (C) shows hydroxy product ions dominated by m/z 877.73 and m/z 597.57. Thus, the two oxidation products are easily distinguishable using tandem MS of the ammoniated precursor ions.

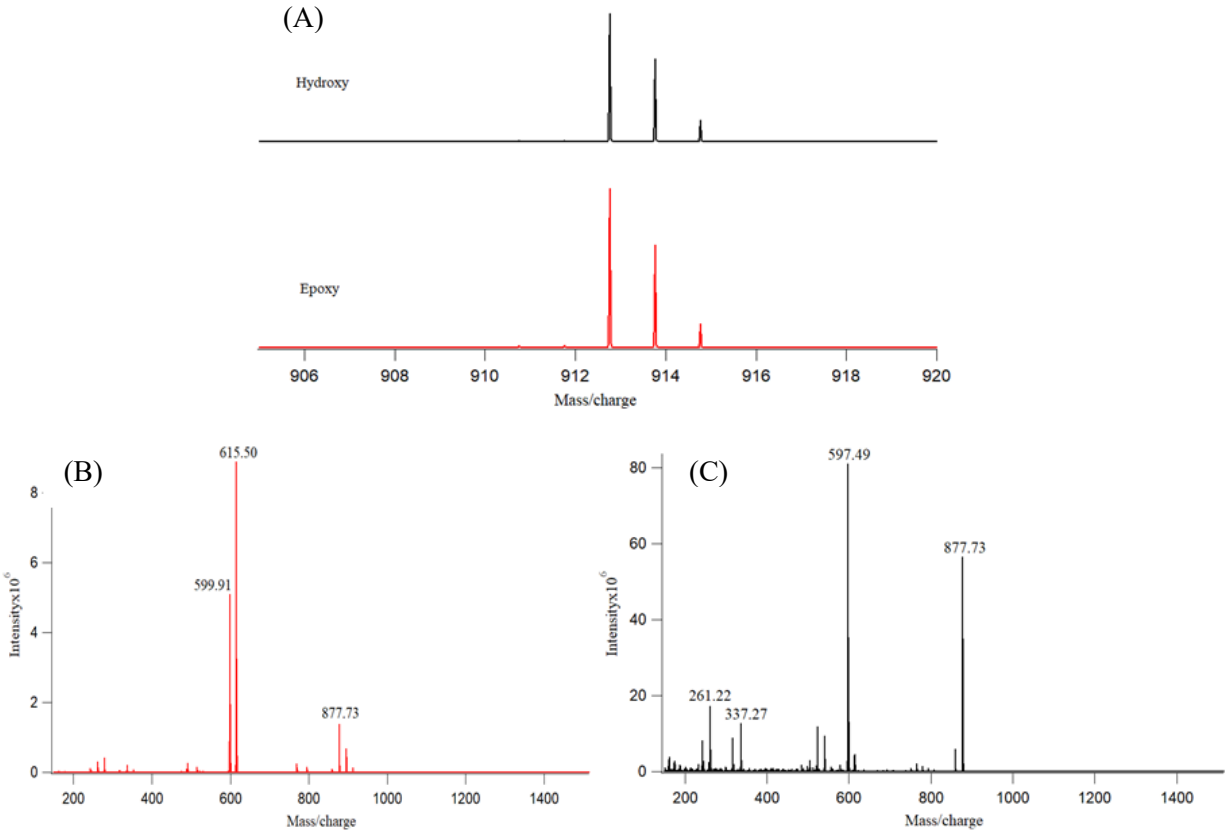

Figure 2.17 Spectra highlighting the unique fragments of mono-hydroxy trilinolein and mono-epoxy trilinolein with ammonium adduct. The precursor ions for mono-hydroxy and mono-epoxy with m/z at 912.671 (A). (B) and (C) show fragment spectra from an applied CE of 27 eV. (B) in red represents MSMS of epoxy monomer and (C) in black represents MSMS of hydroxy monomer.

Product ions can be traced over increasing collision energies to generate a better understanding of when product ions are optimally generated. Un-oxidized TAG (18:2/18:2/18:3; m/z 877.) forms in both fragmentation spectra; however, its intensity is much greater when hydroxy-trilinolein is the precursor. The product ion reaches maximum signal intensity at approximately the same collision energy from both precursors (~20 eV) (Figure 2.18). At the same collision energy from precursor mono-epoxy trilinolein, the loss of ammonia is observed, but the oxygen product is retained. From this product ion (m/z 895), it is assumed that further dissociation results in DAG

ion m/z 615 with the epoxy group (Figure 2.18). The other DAG product ion at m/z 599 is dominant at the same collision energy of ~26 eV and is thought to form from further dissociation of m/z 877. However, it would require the loss of the 18:3 FA chain from m/z 877, whereas in the hydroxy fragmentation spectra, we see the loss of an 18:2 FA to yield DAG product m/z 597 at a higher CE of ~ 38 eV (Figure 2.18, A). Understanding the change in product ion signal at different collision energies allows for an optimal CE to be chosen. For hydroxy trilinolein, a 23 eV would provide good signal for both protonated TAG and DAG product ions whereas 25 eV may be a better CE for epoxy trilinolein. An advantage of direct infusion analysis is the ability to scan CE quickly and obtain the corresponding signal intensities. These results can then be applied to a LC method for optimal results.

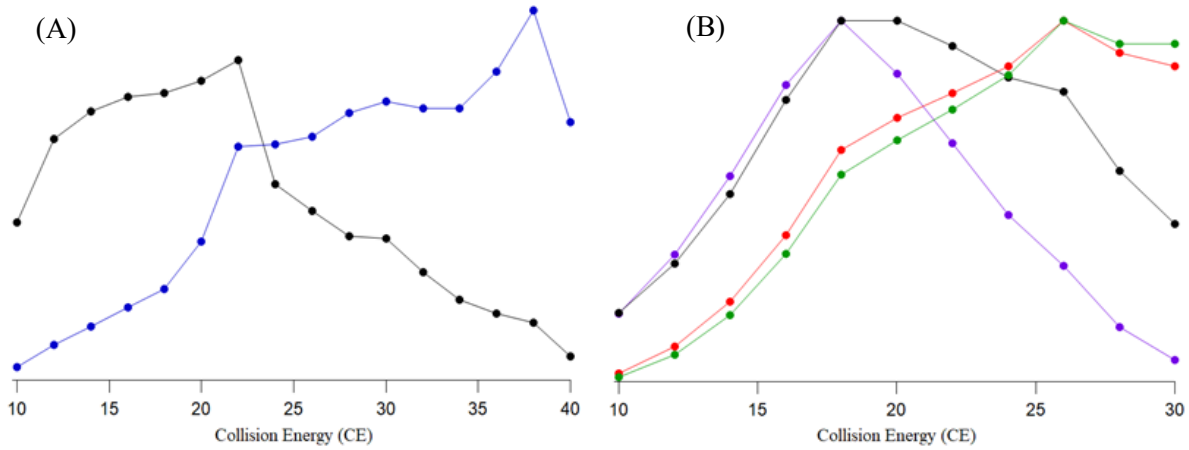

Figure 2.18 Ammoniated mono-hydroxy trilinolein (A) fragmented at increasing collision energies. Product ions 877.7 (black), [M+ NH_4+O -NH_3OH_2] and 597.5 (blue), [M+ NH_4+O -$C_{18}H_{35}O_2NH_3O$] are plotted as signal intensity versus increasing collision energy. Ammoniated mono-epoxy trilinolein (B) fragmented as increasing collision energies. Product ions 895.7 (purple), [M+ NH_4+O -NH_3], 877.7 (black), [M+ NH_4+O -NH_3OH_2], 599.5 (green), [M+ NH_4+O- $C_{18}H_{33}O_2NH_3O$], and 615.5 (red), [M+NH_4+O-$C_{18}H_{33}O_2NH_3$].

Comparing collision energies between different alkali metals showed DAG product ion formation occurring at the same collision energies for a given adduct. Both lithium and sodium adducts fragment to DAG product ions at ~45 eV (Figure 2.19). The collision energy required to achieve the highest product ion signal was higher compared to the CE needed for ammoniated TAG (~25-28 eV). This finding suggests that the alkali metals render the TAG more stable and thus harder to induce fragmentation (Figure 2.19). Two DAG ions were surprisingly identified for rubidiated mono-hydroxy TAG and were monitored over increased collision energies of 10-60 eV. A significant increase in intensity occurred between 40-60 eV and peaked at 58 eV. Although the signal intensity for the two product ions are low compared to other adducts (Li, Na, NH_4), it is important to note because it may explain the prior lack of identification of rubidiated product ions; where the collision energy was simply set too low for their decomposition. Investigation of CE is important when choosing a transition for quantitative analysis. Optimal signal intensities can be determined based on the appropriate CE. Scanning a wide range of CE values was also important in understanding the differences in the energy required for dissociation of different [TAG+A] complexes.

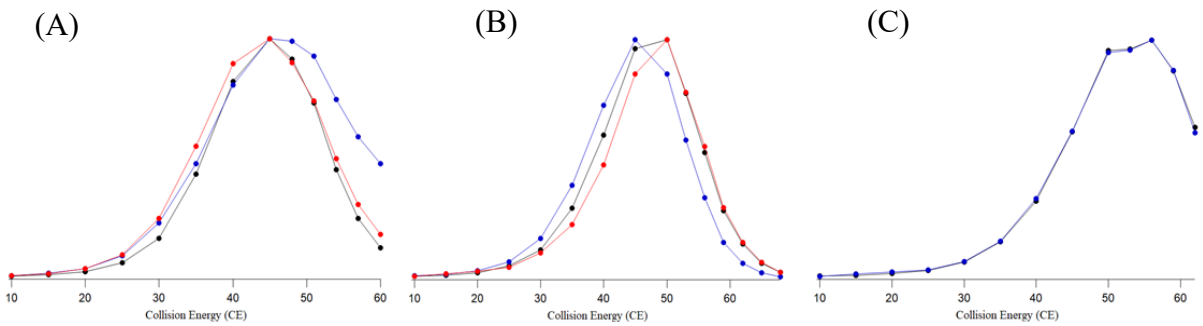

Figure 2.19 (A) represents lithiated mono-hydroxy precursor, and product ions m/z 621.5 [M+Li – $C_{18}H_{32}O_2$] in red, m/z 605.75 in blue, [M+Li – $C_{18}H_{32}O_2O$] and m/z 599.5 in black, [M-$C_{18}H_{33}O_2LiO$]. In (B) precursor sodiated mono-hydroxy trilinolein was targeted. Product ions m/z 637.7 in black, [M+Na+O-$C_{18}H_{32}O_2$], m/z 621.6 in blue, [M+Na+O-$C_{18}H_{32}O_2O$] and m/z 599.7 in red, [M+Na+O-$C_{18}H_{33}O_2NaO$]. In (C) blue product ion m/z 683.5, [M+Rb+O-$C_{18}H_{32}O_2O$] and m/z 699.5 in black, [M+Rb+O-$C_{18}H_{32}O_2$]. The two traces in panel (C) are overlaying.

Hydroperoxide oxidation products contain two oxygen atoms which overlap with the m/z of di-epoxy and di-hydroxy groups. Aside from a single fragment ion, lithium and sodium adducts failed to provide unique fragments to differentiate between di-epoxy, di-hydroxy and hydroperoxide trilinolein (Table 2.5), with lithium and sodium adducts producing the same two DAG ions for all three oxidation products, one with two oxygen atoms (peroxide) and one with one oxygen atom. Both DAG ions were bound to the corresponding adduct.

Table 2.5 Fragmentation for hydroperoxide trilinolein, di-epoxy trilinolein and di-hydroxy trilinolein, showing the difference between possible unique fragments using lithium, sodium and ammonium adducts.

Li+	***Di-Epoxy* trilinolein-$C_{57}H_{98}O_6LiOO$, m/z= 917.76**	**637.50,** [M+Li+2O– $C_{18}H_{32}O_2$] **621.58,** [M+Li+2O– $C_{18}H_{32}O_2O$] **319.37** **599.67 (low),** [M-$C_{18}H_{33}O_2LiOO$]
	***Di-Hydroxy* trilinolein-$C_{57}H_{98}O_6LiOO$, m/z= 917.76**	**637.50,** [M+Li+2O– $C_{18}H_{32}O_2$] **621.58,** [M+Li+2O– $C_{18}H_{32}O_2O$] **319.37** **599.67 (low),** [M+Li+2O-$C_{18}H_{33}O_2LiOO$]
	***Hydroperoxy* trilinolein-$C_{57}H_{98}O_6LiOO$, m/z= 917.76**	**899.83,** [M+Na- H_2O] **637.65,** [M+Li– $C_{18}H_{32}O_2$] **621.50,** [M+Li– $C_{18}H_{32}O_2O$] **319.58**
Na^+	***Di-Epoxy* trilinolein-$C_{57}H_{98}O_6NaOO$, m/z= 933.77**	**653.58,** [M+Na+2O– $C_{18}H_{32}O_2$] **637.67,** [M+Na+2O–$C_{18}H_{32}O_2O$] **335.33**
	***Di-Hydroxy* trilinolein-$C_{57}H_{98}O_6NaOO$, m/z= 933.77**	**653.58,** [M+Na+2O– $C_{18}H_{32}O_2$] **637.67,** [M+Na+2O–$C_{18}H_{32}O_2O$] **335.33**
	***Hydroperoxy* trilinolein-$C_{57}H_{98}O_6NaOO$, m/z= 933.77**	**915.65,** [M+Na-H_2O] **845.75** **653.58,** [M+Na+2O– $C_{18}H_{32}O_2$] **637.48,** [M+Na+2O–$C_{18}H_{32}O_2O$] **335.33**
NH_4^+	***Di-Epoxy* trilinolein-$C_{57}H_{98}O_6NH_4OO$, m/z= 928.76**	**615.50,** [M+NH_4+2O-$C_{18}H_{33}O_2NH_3O$] **613.51,** [M+ NH_4+2O -$C_{18}H_{31}O_2NH_3O$] **599.67,** [M+ NH_4+2O -$C_{18}H_{33}O_2NH_3OO$] **597.77,** [M+ NH_4+2O -$C_{18}H_{31}O_2NH_3OO$] **631.50,** [M+ NH_4+2O -$C_{18}H_{33}O_2NH_3$]
	***Di-Hydroxy* trilinolein-$C_{57}H_{98}O_6NH_4OO$, m/z= 928.76**	**613.48,** [M+ NH_4+2O -$C_{18}H_{31}O_2NH_3O$] **629.38,** [M+ NH_4+2O -$C_{18}H_{31}O_2NH_3$] **599.50,** [M+ NH_4+2O -$C_{18}H_{33}O_2NH_3OO$] **531.40,** [M+ NH_4+2O -$C_{25}H_{44}O_2NH_3$] **491.37**
	***Hydroperoxy* trilinolein-$C_{57}H_{98}O_6NH_4OO$, m/z= 928.76**	**613.48,** [M+ NH_4+2O -$C_{18}H_{31}O_2NH_3O$] **877.73,** [M+ NH_4+2O -NH_3O] **599.50,** [M+ NH_4+2O -$C_{18}H_{33}O_2NH_3OO$]

		597.49, [M+ NH_4+2O - $C_{18}H_{31}O_2NH_3OO$]

There was a single differentiating product ion when fragmenting hydroperoxy trilinolein with sodium or lithium adducts that represented the loss of a H_2O molecule (m/z 899.92). Hydroperoxy groups are unstable; therefore, the loss of H_2O could be the loss of an oxygen and rearrangement to add another double bond. However, signal intensity for this unique product ion is low, limiting its ability to confidently be used to distinguish the overlapping oxidation products.

For ammoniated di-oxygen groups, unique fragment ions were easily identifiable. Di-epoxy trilinolein produces two DAG ions containing one epoxy group, at m/z 615.51 (18:2/18:2[O]) and 613.50 (18:2/18:3[O]), which differ by one double bond, as well as another two DAG ions without oxygen (m/z 599.67 (18:2/18:2) and 597.67 (18:2/18:3)). There is fifth DAG product ion with both epoxy groups remaining at m/z 631.50 (18:2/18:2[2O]). In contrast, the di-hydroxy products only show one protonated DAG ion, 599.50 (18:2/18:2). DAG product ions including one and two hydroxy groups can also be identified at m/z 613.48 (18:2/18:3[O]) and 629.38 (18:2/18:3[2O]). A fourth product generated from di-hydroxy fragmentation at m/z 491.37 represents the loss of C_9H_{18} from the DAG ion and indicates that a hydroxy group was located on C_9 of the fatty acid chain. Since there is no other fragment ion of this type, it can be assumed that both hydroxy groups were located on C_9 positions of fatty acids.

The main unique product ion of hydroperoxy trilinolein is the protonated monomer m/z 877.73, the same product ion observed from fragmentation of mono-hydroxy trilinolein, and represents un-oxidized TAG (18:2/18:2/18:3), having lost the hydroperoxy group. Also useful in identification of hydroperoxy TAG is the lack of a

DAG product ion with two oxygen atoms. Instead, product ion m/z 613.48 represents the loss of [-$C_{18}H_{31}O_2NH_3O$], leaving a single oxygen atom on the ion. This is likely a result of degradation of relatively unstable hydroperoxy groups; it may be that when collision energy is applied to the target ion, the hydroperoxy group degrades into radical oxygens, leading to the formation of epoxides, hydroxides or ketones (+ 14 m/z).

To summarize tandem-MS of oxidation products, potassium and cesium adducts do not produce useful product ions, however, rubidium requires high collision energies to dissociate the precursor ion into low amounts of product ions. In contrast, sodium, lithium and ammonium adducts provide a comprehensive qualitative analysis of TAGs because their product ions represent DAGs from the TAG monomer that help distinguish *sn-1/sn-3* from *sn-2*. It can be concluded that use of ammonium as a cation adduct with TAG oxidation molecules provides unique product ions from tandem-MS to distinguish between m/z overlap in oxidation products. Ammoniated mono-hydroxy TAG and mono-epoxy TAG have key identifying product ions;

(1) Mono-epoxy TAG yields two DAG product ions, one with the epoxy group and one without it.

(2) Mono-hydroxy TAG yields one DAG product ion with an additional double bond that does not contain the hydroxy group, and a protonated TAG monomer with the addition of a double bond.

Further investigation into overlap of oxidized TAG ions of hydroperoxy trilinolein, di-epoxy trilinolein and di-hydroxy trilinolein (m/z 928), showed unique product ions when using the ammonium adduct. In summary;

(1) Di-epoxy (18:2/18:2/18:2) TAG yields two DAG ions without epoxy groups, (18:2/18:2) and (18:2/18:3), and two DAG ions with single epoxy groups, (18:2/18:2/O) and (18:2/18:3/O). A single DAG product ion of (18:2/18:2/2O) with both epoxy groups was also identified.

(2) Di-hydroxy (18:2/18:2/18:2) TAG yields a protonated DAG ion (18:2/18:2), and two oxygenated DAG ions (18:2/18:3/O) and (18:2/18:3/2O). A key product ion from di-hydroxy (18:2/18:2/18:2) is 491.37 which represents loss of C_9H_{18}, indicating the position of hydroxy at C_9.

(3) Hydroperoxy (18:2/18:2/18:2) TAG yields protonated DAGs (18:2/18:2) and (18:2/18:3) as well as oxygenated DAG (18:2/18:3/O). The key unique fragment ion from hydroperoxy TAG is the un-oxidized TAG product ion (18:2/18:2/18:3) and lack of DAG ion containing both oxygen atoms.

It is important to consider that the above techniques were performed on oxidized TAG and the application of a real sample would add to the complexity.

Although the five alkali metal adducts investigated successfully ionized TAGs and TAG degradation products, they did not all produce useful spectra by tandem-MS that allowed elucidation of TAG structure. However, use of ammonium adducts not only produced useful fragment ion signals for quantitation, it also offered unique product ions to distinguish between oxidation products with overlapping precursor m/z.

2.3.8 MS^3 Analysis of Ammoniated TAG Degradation Products

MS^3 analysis was also carried out to compare further product ions between ammoniated mono-epoxy, mono-hydroxy and mono-peroxy trilinolein and generate a better understanding of their degradation mechanisms. Fragmentation of precursor mono-

epoxy monomer, m/z 912, resulted in four major ions (Table 2.6). The ion representing protonated DAG at m/z 599 was isolated and targeted with a collision energy of 27 eV to produce MAG product ions m/z 263.65 and 337.50. Product ion m/z 263.65 represented a single acyl chain with two double bonds (18:2) in protonated form. The second product at m/z 337.50 is often referred to as $RCO+74^+$, or the acyl chain plus 74 mass units (Kalo et al. 2014) and was described in a previous section evaluating fragmentation of trilinolein (Figure 2.8).

In comparison, targeting the corresponding un-oxidized DAG ion (18:2/18:3; 597.58) from MSMS of mono-hydroxy trilinolein failed to produce the acyl chain; instead the $RCO+74^+$ ion was identified (Table 2.6). The $RCO+74^+$ ion at m/z 337.45 has two double bonds, indicating the loss of 18:3 from the DAG precursor. The difference in the two DAG ions, however, is that 597.58 from hydroxy trilinolein is thought to form from m/z 877.77 (18:2/18:2/18:3), providing an extra double bond. This rearrangement potentially limits the ability to identify the protonated acyl chain. Instead, a product ion at m/z 243.33 represents the acyl chain with the loss of H_2O and includes three double bonds, indicating the loss of 18:2 from the DAG precursor ion. Compared to m/z 337.45 ion that represented the 18:2 acyl chain found with the epoxy TAG, m/z 317.33 represents the 18:3 acyl chain, and the loss of H_2O (Table 2.6)

Table 2.6 Direct-infusion MS was performed on the L-QIT MS to employ MS^3 on target TAG precursor oxygen products. Precursor target ions of mono-epoxy trilinolein, mono-hydroxy trilinolein and mono-peroxy trilinolein were first targeted at a CE of 27 eV to yield MS^2 product ions. Un-oxidized DAG product ions from MS^2 were further targeted for MS^3 analysis to yield MAG product ions.

Standard	MS type	$[M+NH_4]^+$	$[(M+NH_4)-H_2O]^+$	$[(M+NH_4)-NH_3]^+$	$[(M+NH_4)-NH_3-H_2O]^+$	$[(M+NH_4)-FA]^+$	$[(M+NH_4)-FA-O]^+$	$[(M+NH_4)-FA-O-H_2]^+$	$[(M+NH_4)-FA-2O]^+$	RCO^+	$(RCO+74)^+$	Other
TAG 54:6 [O] *Epoxide*	**MS**	912.67										
	MS2 912			895.67	877.77	615.54	599.50					
	MS3 912→599									263.65	337.50	
TAG 54:6 [O] *Hydroxy*	**MS**	912.67										
	MS2 912				877.77			597.58				
	MS3 912→597										337.45	317.33[a] 243.33[b] 523.58[c]
TAG 54:6 [OO] *Peroxide*	**MS**	928.77										
	MS2 928		910.52		893.50		613.50		599.50			
	MS3 928→599									263.65	337.50	319.62[a] 523.50[c]

a= $[C_{22}H_{21}O_2]^+$
b= $[Acyl\text{-}H_2O\text{-}H_4]^+$
c= $[(M+NH_4)\text{-}NH_3\text{-}FA\text{-}74]^+$

Un-oxidized DAG at m/z 599 from mono-peroxy trilinolein yielded similar product ions as epoxy-TAG with all three previously identified MAG derivatives; however, all three represent the 18:2 acyl chain. The mono-peroxy could be distinguished because of the product ion m/z 319.62 representing loss of H_2O from $RCO+74^+$. The corresponding ion (m/z 317) was also found for hydroxy-trilinolein, although for the 18:3 acyl chain. Thus, utilizing MS^3 generates a more thorough understanding of the qualitative composition of TAG degradation products and their rearrangements.

2.3.9 Thermal Fragmentation of TAG Oxidation Products

Hydroxy trilinolein standard was evaluated at increased inlet temperatures of 275°C using ammonium adduct where the hydroxy trilinolein monomer, m/z 912.5, decreased significantly compared to analysis done at 25°C (Figure 2.20). The (18:2/18:3)

DAG ion at m/z 597.67 became the dominant ion in the spectra, similar to that observed with un-oxidized trilinolein (Figure 2.20, B).

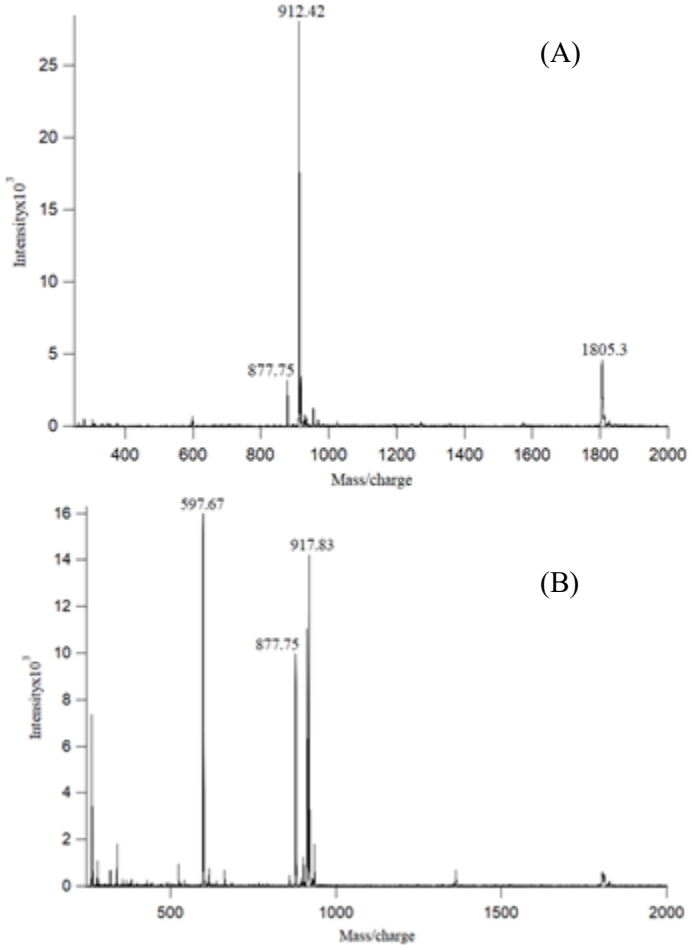

Figure 2.20 Thermal degradation of ammoniated hydroxy trilinolein where panel (A) represents spectra collected at room temperature (25°C) and panel (B) shows spectra collected at 275°C.

Here, m/z 597.67 product ion arose (Fig 2.20, B) solely from an increase in temperature, without collision energy applied. Again, at an inlet temperature of 275°C, the sodiated monomer ion is more abundant than the ammoniated ion. It is ironic to note that applied temperature decreases the amount of oxidation product identified to ions in the gas-phase, when to induce oxidation of TAGs they are exposed to heat in the condensed phase.

Further investigation into the effect of temperature was done for each of the six potential adducts. It had previously been discovered that MSMS analysis of cesium and rubidium did not produce significant product ions when bound to trilinolein. Cesiated hydroperoxy trilinolein monomer has a m/z of 1043.7 and appears at low signal intensity in panel (F) of Figure 2.21. Dominating the spectra is free cesium ion at m/z 133.0. The loss of free cesium at high temperatures highlights the instability of cesium as an adduct. At room temperature there were no obvious amounts of free Cs^+. Revisiting tandem-MS of cesiated TAG, it can be assumed that the application of collision energy causes cesium to leave the ion. When this occurs, the product ions cannot be identified because there is no charge mechanism. It can be inferred that rubidium follows the same trend, although the rubidium ion could not be identified within the 100-2000 m/z range.

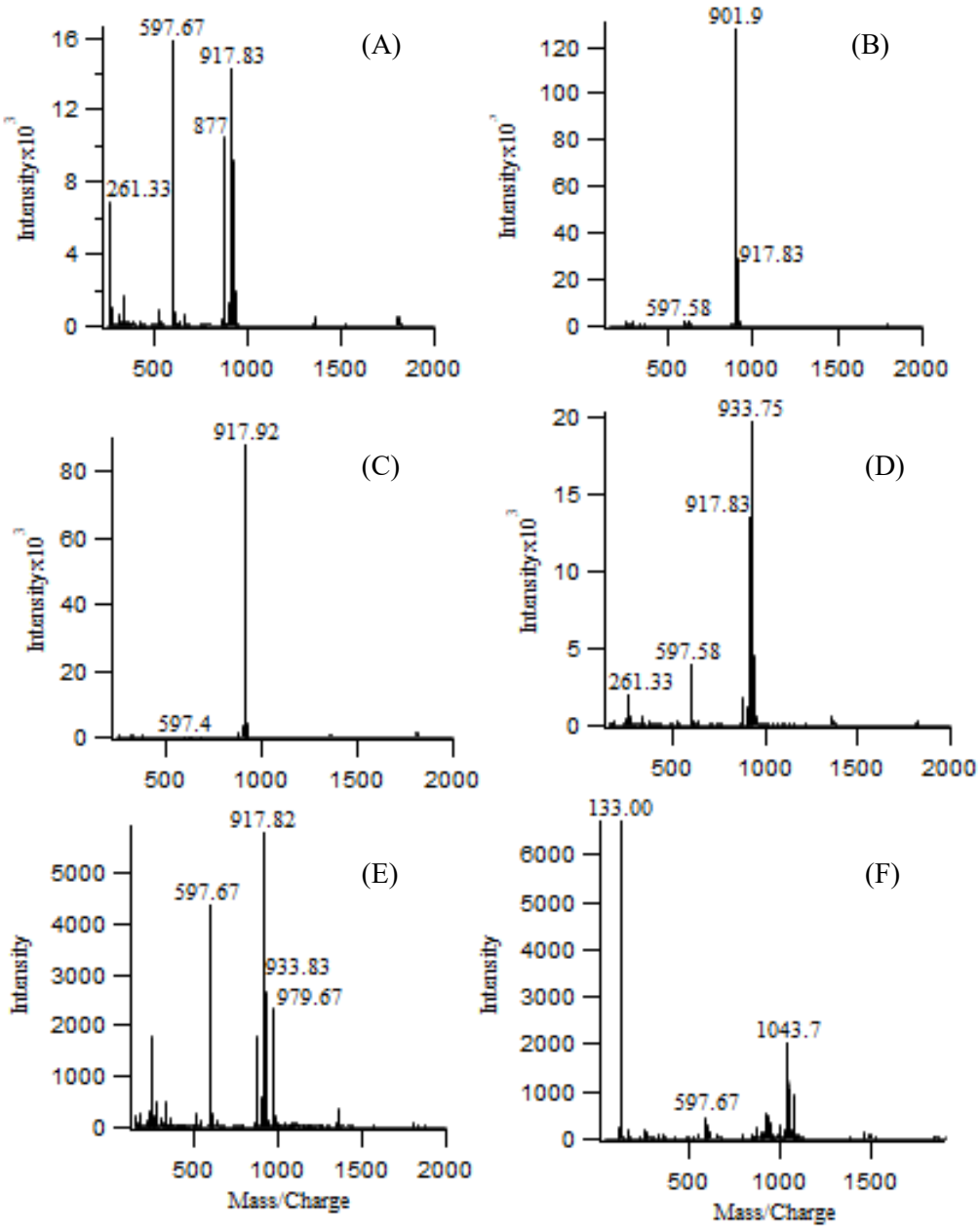

Figure 2.21 Hydroxy trilinolein at 275°C as the inlet temperature with 0.1 mM NH_4 in panel (A), Li in panel (B), Na in panel (C), K in panel (D), Rb in panel (E) and cesium in panel (F).

A commonality of thermal fragmentation between the six tested adducts, aside from cesium, is the appearance of a sodiated monomer ion within the spectra. For example, the rubidium hydroxy monomer at m/z 979.67 was present at low signal intensity (Figure 2.21, E) with the spectra dominated by m/z 917.82, representing the

sodiated hydroxy monomer. A potassiated hydroxy monomer was also present at m/z 933.83 within the rubidium spectra. Sample carry-over within infusion MS is an ongoing issue, and the potassium sample was infused before rubidium. Two 250 uL flushes of 100 % EtOH were used to clean the syringe between samples. It can be assumed that the potassiated ion represents endogenous potassium from the environment or a small amount of sample carry-over. Nonetheless, identifying potassium in the rubidium sample at high temperature highlights the stability of potassium adduct compared to rubidium. Lithium, sodium and potassium hydroxy monomers continued to be the most abundant ions in their corresponding spectra (Figure 2.21, B, C, D), with only small amounts of DAG ions appearing. In panel (B), although the lithiated hydroxy monomer remains the most dominant ion within the spectra, the signal intensity has significantly decreased in comparison to spectra collected at room temperature. The only adduct that promoted increased intensity at higher inlet temperatures is sodium. Ammonium, rubidium and cesium adduct show most drastic effects from high inlet temperature. Degradation of the monomer ions leads to high amounts of protonated DAG ion at m/z 597.5, indicating the loss of the adduct.

An interesting result of thermal fragmentation is the resulting DAG fragment ions. For each of the six cation adducts, at an inlet temperature of 275°C, a common protonated degradation DAG ion is produced of the form (18:2/18:3) at m/z 597.5. Formerly, tandem-MS methods showed DAG ions with intact alkali metal adducts. Also, since the monomer ion has an oxidation group, most of the adducts had produced DAG ions with the hydroxy group. Degradation to a DAG (18:2/18:3) had to include the addition of a double bond on one of the fatty acid chains. Predictably, m/z 597.67 is arising from the

degradation of m/z 877.67 (18:2/18:2/18:3) which is identified in small quantities at 275°C. The product ions generated are different between thermal fragmentation and collision induced fragmentation.

Changing the MS inlet temperature resulted in unexpected results. The effect of inlet temperature has not previously been reported for TAG or TAG oxidation products. The results determined in the present study from the effect of inlet temperature are important for the complete analysis of TAG oxidation products. Direct infusion of TAG oxidation products have not previously been reported, while LC or GC techniques have always accompanied MS for their analysis. Perhaps if prior direct-infusion methods were done, they were completed at common inlet temperatures of 275°C. If this was the case, the amount of oxidized products could have been too low to detect due to degradation.

2.4 Conclusion

Successful ionization of TAG and TAG oxidation products was achieved using alkali metals (Li, Na, K, Rb, Cs) and ammonium acetate. Competitive ionization environments concluded that the metal adducts with a larger atomic radius had a better binding affinity in binary mixtures. Ammonium was determined to be the weakest bound adduct, and easily evaporated at applied collision energies or increased inlet temperatures to produce protonated TAG and DAG molecules. Tandem-MS of intact TAG molecules provided qualitative information using each adduct, where rubidium and cesium yielded reduced amounts of product ions. An important finding in direct-infusion analysis of TAG and TAG oxidation products was sample degradation highlighted at high capillary inlet temperatures (275° C). The majority of direct-infusion analysis is performed at inlet temperatures greater than 250° C which we determined to cause degradation, resulting in

lower signal intensities, DAG formation, and increased levels of endogenous sodium peaks. It is important to understand the effect of inlet temperature as it significantly alters the obtained results.

CHAPTER 3 HIGH-FIELD ASYMMETRIC WAVEFORM ION MOBILITY SPECTROMETRY ANALYSIS OF TAGS AND TAG OXIDATION PRODUCTS

3.1. Introduction

High-field asymmetric waveform ion mobility spectrometry (FAIMS) is an established ion filtering technology most commonly used with atmospheric pressure ionization mass spectrometry. It is a technique that separates gas-phase ions at atmospheric pressure and room temperature. Ion mobility spectrometry (IMS) and FAIMS both operate at atmospheric pressure and are analogous to time-of-flight and quadrupole mass spectrometry respectively. FAIMS is similar to conventional IMS since both techniques are based on the motion of ions induced by electric fields at atmospheric pressure (Purves et al. 1999). In conventional IMS, either decreasing or increasing dc voltages are applied to a series of metal plates creating a uniform electric field (Smith et al. 2020). IMS separates ions based on their drift velocities through the tube, normally at low field conditions. In IMS, ions arrive at the detector at different times depending on their mobilities and there is no ion filtering in the classical sense that transmission is pulsed, rather than continuous. The use of high electric fields differentiates FAIMS from IMS. At high electric fields, the drift velocity is not proportional to the applied electric field, leading to ion mobility (*K)* becoming dependent on the applied field. The dependence of *K* on the strength of the applied electric field is the basis of FAIMS development. The behaviour of ion mobility at high-electric fields is also compound dependent. FAIMS separates ions on the difference in the mobility of an ion at high field relative to its mobility at low field (Purves et al. 1999). This difference can be reflective

of the size and shape of the ion, the position of the charge, its interaction with the bath gas and its structural rigidity (Purves et al. 1999).

An ion's mobility at a given electric field can be defined by Equation 3.1, where *f(E)* describes the functional dependence of ion mobility on the electric field (K_h).

$$K_h(E) = K[1 + f(E)] \qquad \text{Equation 3.1}$$

There are three defined types of ions separated based on how their mobility changes as a function of electric field. Type A, type B and type C are displayed in Figure 3.1 below. As demonstrated, the mobility of a type A ion increases with electric field strength whereas the mobility of a type C ion decreases. Most ions are either type A or type C ions; however, there are cases of type B ions whose mobility increase initially before decreasing at yet higher fields. Large flexible ions, including those of peptides and proteins tend to display type C behaviour (Purves et al. 1999) while smaller and more rigid ions behave as Type A. Type B ion mobility behaviour can be induced for type A ions by modifying the separation gas with helium (Barnett et al. 2011).

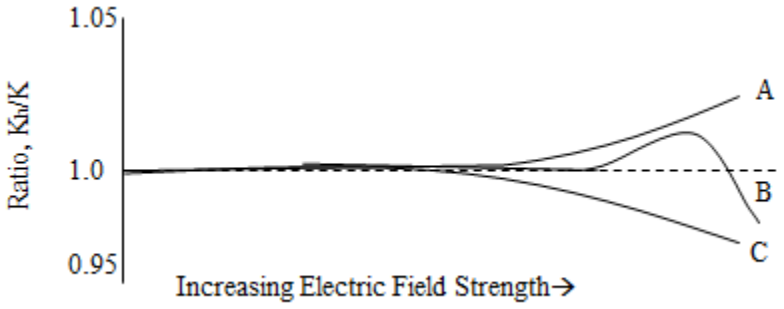

Figure 3.1 Hypothetical dependence of ion mobility on electric field strength for three different types of ions. K_h is ion mobility at high electric fields and K is ion mobility.

An asymmetric high-voltage waveform is applied between FAIMS electrodes to take advantage of the changes in mobility at high and low electric fields. The waveform is comprised of a high voltage component that is applied for a short period of time followed by the opposite polarity, low voltage, being applied for a longer time. In a simplified depiction of the waveform presented in Figure 3.2 below, it shows the magnitude of the high voltage being twice as high as the magnitude of the low voltage. The duration of the low voltage pulse is twice as long as the duration of the high voltage. Therefore, the integrated voltage-time product applied to the electrodes during a complete cycle of the waveform is equal to zero (i.e., $V_{high}t_{high}+V_{low}t_{low}=0$). When the waveform is applied to the electrodes, it causes cations of type A to move as shown by the dashed line in Figure 3.2. During the high voltage portion of the waveform, the ion will move toward the lower electrode. When the low voltage portion of the waveform is applied the ion will move back in the opposite direction; however, it fails to return to its starting position if the mobility is lower. If the ion trajectory is left uncorrected, the ion will eventually strike the lower electrode and be neutralized. A constant negative dc voltage known as the "compensation voltage" (CV), can be applied to reverse (or compensate) for the net drift of the ion. If the CV is wrong the ions may drift towards either electrode and be neutralized (i.e., if CV is too high they hit the top electrode and if it is too low they hit the bottom electrode) (Figure 3.2). FAIMS is therefore regarded as an ion filter where selective transmission of only ions with the correct CV will have stable trajectories through the electrodes and be detected by the MS. Unlike IMS, it is not necessary to inject discrete packs of ions into the FAIMS ion filter. The correct combination of DV

and CV can be used to deliver ions for detection indefinitely. The CV can also be scanned over a linear range to provide a complete picture of the sample ion population.

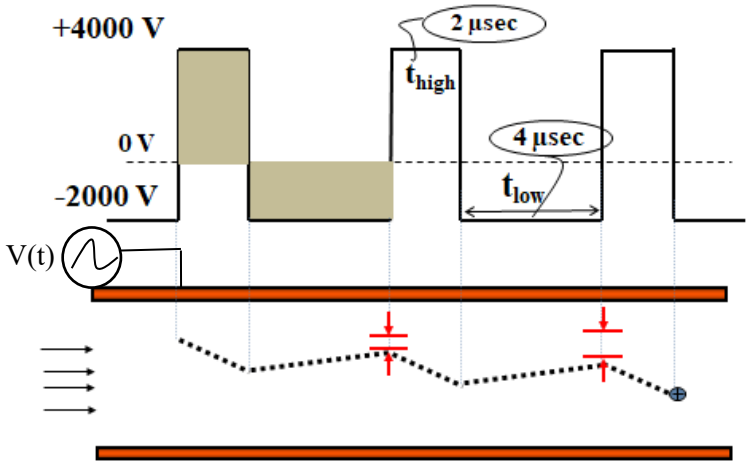

Figure 3.2 Illustration of the ion movement between two plates during an applied electric field shown as *V(t)*. The ion is transported horizontally by a gas flow (distance is not to scale).

The FAIMS waveform is the summation of a sine wave and its first harmonic. The two asymmetric waveforms shown in Figure 3.3 are of opposing polarities. The maximum voltage of the waveform is defined as the dispersion voltage (DV). The dispersion voltage can be either positive or negative. A waveform with a positive DV transmits ions of mode P1 and N2 whereas a negative DV (and opposing polarity waveform) transmits P2 and N1 ions. N and P represent negative and positive ions respectively whereas mode 1 represents type A or small ions and 2 represents type C or large ions.

There are different FAIMS geometries including flat plates and cylindrical arrangements. The modes described above only apply when using cylinders. As the DV potential is increased, there is an inherent ion focusing mechanism within concentric FAIMS cylinders. With increasing DV, ion intensities increase along with increases in

CV. This does not occur within flat plate geometries. Flat plates, differential mobility spectrometry (DMS) or SelexION do not have these modes.

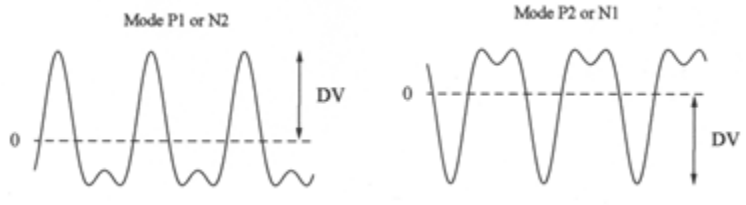

Figure 3.3 Asymmetric waveforms used in FAIMS. The maximum value of the waveform is called the dispersion voltage (DV).

This study focuses on the application of cylindrical FAIMS electrodes (Figure 3.4). Cylindrical electrodes have non-uniform electric fields that allow atmospheric pressure ion focusing. Atmospheric pressure ion focusing is the result of the asymmetric waveform with sufficiently high voltages to induce changes in ion mobility and the non-uniform electric field in space due to electrode geometry.

The FAIMS filter is positioned between the ion source and the mass spectrometer inlet; therefore, ionization suppression or other ion source effects are not affected by the FAIMS filter (Figure 3.4). FAIMS separation occurs on a timescale of seconds, making it suitable for coupling with mass spectrometry (MS), wherein detection usually occurs within seconds (Guevremont et al. 1998). In FAIMS, lipid ions traverse the FAIMS electrodes for separation prior to MS detection. ESI-MS alone only provides information about the total carbon number and unsaturation index from molecular ion peaks but does not identify the specific molecular species composition of TAGs due to the presence of multiple isobaric species. The addition of FAIMS with ESI-MS presents an opportunity to separate isobaric species, which could improve TAG analysis.

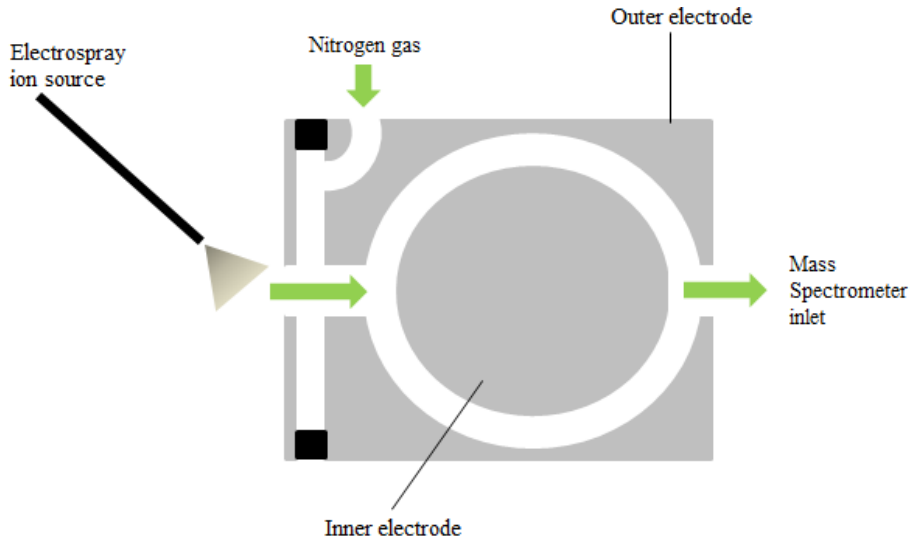

Figure 3.4 A front-on view of cylindrical FAIMS geometry highlighting the inner and outer electrodes and the gas inlet. Ion trajectory direction is highlighted by green arrows.

While FAIMS with a concentric design has not yet been applied to lipid analysis, IMS in combination with mass spectrometry applications have recently begun to emerge. IMS has been used to determine the collision cross section (CCS) to help measure the conformational structure of lipid ions which helps improve the confidence of lipid identification. This analysis was done using drift-tube IMS (Stow et al. 2017) and traveling wave (TW) IMS (Sinclair et al. 2018), which is a different type of ion mobility than FAIMS. Ion mobility has also been used with CID to improve specificity of MSMS based lipid analysis. Further studies have shown IMS-MS improving the peak capacity and signal-to-noise ratio compared to traditional analysis methods (Fouque et al. 2019). Theoretical applications of IMS-MS-based shotgun lipidomic approaches have been proposed by Paglia et al. (2015); however, the experimental application of the technique is not common. A study by Sala et al. (2016) separated TAG regioisomers using the SelexION DMS cell. The DMS cell is similar to FAIMS, where it is positioned between the MS interface and the ion source; however, it is a flat plate device. The study

concluded successful separation of four pairs of TAG regioisomers of both unsaturated and saturated TAG. They optimized different experimental parameters such as flow rate and ion dwell time. Lintonen et al. (2014) also used DMS for lipid analysis, where they focused on the separation of different phospholipids with the help of n-proponal as transport gas. DMS coupled with liquid chromatography and MS separation was used to separate phospholipids by Baker et al. (2014). Separation of phospholipids is the most popular area in ion mobility applications within lipidomics. FAIMS has only touched the surface of lipidomic applications and is new to TAG analysis (Bowman et al. 2017).

The aim of the experiment was to investigate the CV profiles for any notable changes in CV values or differences in ionograms depending on the alkali metal or ammonium used with TAGs. FAIMS was incorporated in an attempt to generate a better understanding of binding mechanisms between alkali metals and TAGs. This study focused on FAIMS' ability to separate endogenous TAG standards and TAG oxidation products in alkali-adduct forms. FAIMS was also used to better understand the effect that MS inlet temperature has on TAGs that was previously investigated in Chapter 2.

3.2. EXPERIMENTAL

3.2.1 Materials and Methods

TAG standards and TAG oxidation standards previously described in Chapter 2 were prepared in the same manner for the experimental procedures in the present chapter. Alkali metal adducts and ammonium acetate were also prepared as described in Chapter 2. All standard samples were analyzed at concentrations of 10 μg mL^{-1}.

3.2.2 Instrumentation

High-field Asymmetric Waveform Ion Mobility Spectrometry (FAIMS)

A set of cylindrical geometry FAIMS electrodes using a domed terminus on the inner electrode was interfaced to the L-QIT MS. Lipid samples were introduced to the FAIMS ion filter by direct-infusion to an electrospray ion source (ESI). A high voltage was supplied to the source through a pin connecter (Label (E) in Figure 3.5), to the MS high voltage supply. No heat was applied to the source. The inlet and outlet of the outer electrode were 2.00 mm in diameter where the outlet was approximately 3 cm from the ion inlet of the mass spectrometer. The outer electrode was 20 mm in diameter creating an analytical gap width of 2 mm between the outer and inner electrodes. The nebulizing gas (nitrogen) rate was set to approximately 9 L min^{-1}. FAIMS (Label (B) in Figure 3.5) was positioned 180° relative to the MS inlet (Label (F) in Figure 3.5), where the ESI source (Label (D) in Figure 3.5) was at 90° relative to the MS inlet. Figure 3.5 demonstrates the FAIMS set up on the L-QIT interface.

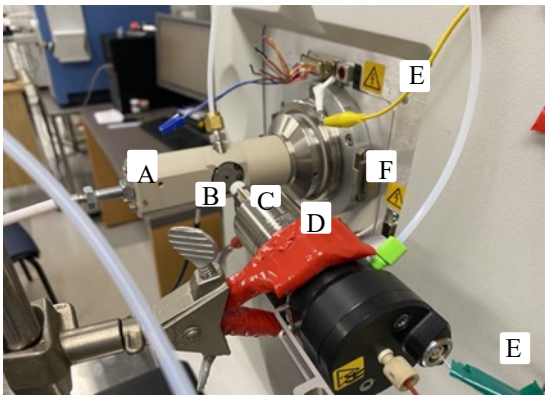

Figure 3.5 Diagram of the experimental setup of the dome-style FAIMS device mounted on the L-QIT MS interface. Label (A) represents the connection between FAIMS electrodes and the rf voltages. (B) represents the PEEK insulator which encompasses the FAIMS electrodes and (C) highlights the FAIMS ion inlet. (D) shows the electrospray ion source and its orientation relative to the mass spectrometer inlet shown by label (F). (F) also represents the mounting bracket created to align and hold FAIMS in position to the MS inlet. Labels (E) represent the high voltage connections from the MS to the source.

A custom waveform generator, Modular Intelligent Power Sources (MIPS), was supplied by GAA Custom Electronics, LLC. The waveform generator was used to supply the dispersion voltage (DV), compensation voltage (CV), curtain plate voltage and outer bias voltage (OBV) to the electrode set. The maximum DV was limited to -4.6 kV as values greater than that would cause an electrical discharge to occur between the electrodes. Electrical discharge was also observed when the voltage gap between the outer electrode and curtain plate was greater than 2.3 kV. The inlet orifice of the curtain plate was 2 mm in diameter. FAIMS voltages were altered under manual control using either the MIPS interface or the MIPS software to input specific values. The waveform was auto-tuned by the MIPS interface each time the system was activated (connection highlighted by Label (A) in Figure 3.5). The shape of the waveform was monitored visually using a Tektronix oscilloscope. Fine tuning was performed manually. The

waveform shape was adjusted slightly until the temperature of the RF electronics was equilibrated. This required approximately 15 minutes of operation. For lipid analysis the waveform was set to P2/N1 mode which generally provides optimal transmission for large positively charged ions with the application of a negative compensation voltage. Nitrogen gas was passed through a charcoal/molecular sieve filter to remove water and any volatile organic compounds (VOCs). This nitrogen gas was used as desolvation gas and as a carrier gas through the electrodes. The gas flow rate through FAIMS was determined by the vacuum of the MS and the dimensions of the inlets and outlets of FAIMS electrodes. The flow rate of nitrogen gas was controlled and adjusted using a 0-10 L min^{-1} ball flow meter from Omega (Los Angeles, California). A comprehensive list of FAIMS parameters used throughout this study is detailed in Table 3.1. The novel MIPS power source, along with novel FAIMS electrodes and a multi-source FAIMS instrument, was developed during the present study and many parameters were optimized.

Table 3.1 List of FAIMS parameters used for this study.

Parameter	**Value**
Dispersion Voltage	(4.10- 4.40)
Outer bias voltage	(+ 100 V)
Curtain plate voltage	1000 V
Outer electrode inlet diameter	2.0 mm
Outer electrode outlet diameter	2.0 mm
Outer electrode length	60.00 mm
Inner electrode length	85.00 mm
Curtain gas flow rate	4.5 L min^{-1}
Curtain gas	Nitrogen
Electrode temperature	RT
Inner electrode outer diameter	16.00 mm
Outer electrode inner diameter	20.00 mm
Analytical gap with	2.0 mm

Chromatographic resolution in FAIMS is calculated using the same formula as in liquid chromatography (LC); however, the parameters represent transmission CV values (CV_A and CV_B) (Equation 3.2). PW_A and PW_B represent the peak widths at half maximum (Equation 3.2).

$$R_s = \frac{2(CV_B - CV_A)}{(PW_A + PW_B)} \qquad \text{Equation 3.2}$$

Mass spectrometry

The L-QIT mass spectrometer previously described in Chapter 2 was used with FAIMS, maintaining the same parameters as described above.

3.3 Results & Discussion

3.3.1 Effect of Dispersion Voltage (DV) on Compensation Voltage (CV)

The required CV for ion transmission through FAIMS is a reflection of the deviation in the ion mobility ratio (K_h/K) that results from the changing electric fields. The CV for optimal transmission of trilinolein (54:6) TAG was not predictable and, therefore, determined experimentally. The CV scan for 54:6 TAG was determined by collecting a total-ion-current of MS spectra while scanning CV over a wider range (+5 to -20 V). CV values for optimal ion transmission are dependent on the magnitude of the DV, the shape of the applied asymmetric waveform, the distance between concentric cylinders and the pressure and temperature. No heat was applied to the MS transfer capillary since ion desolvation occurs at the FAIMS inlet instead of in the capillary. Initial acquisition was done while collecting CV spectra at different DV settings (Figure 3.6, A). As the DV increased, CV values increased as expected for molecules with C type mobility behaviour. This was done in P2 mode with negative polarity waveform. Both

monomer [TAG] and dimer [2TAG] ions were isolated to show the separate responses at increased DV environments (Figure 3.6, A, B). Comparison of the two plots showed a steeper curve for the monomer ion. That is to say that the CV required for ion transmission through FAIMS is lower for TAG clusters. In further comparison of the two plots, the separation between the two ions increased with DV. As well, peak widths increased with increasing DV due to focusing. The ionograms (CV versus intensity) were plotted as a function of intensity versus CV where the peak widths notably increase as the CV value increases (Figure 3.6, B). It is important to note that flat plate instrumentation leads to a decrease in signal as DV values increase. With cylindrical FAIMS, signal intensity is able to increase as DV values increase (Fig 3.6, B). At DV -4.45 kV the signal intensity decreased could be explained by multiple conformations of the ion, different positions of the cationic adduct, possible ion dissociation induced by the high electric fields (ion heating) or loss of ion extraction efficiency. Therefore, it is advantageous to have a high DV setting to gain advantages in separation and sensitivity.

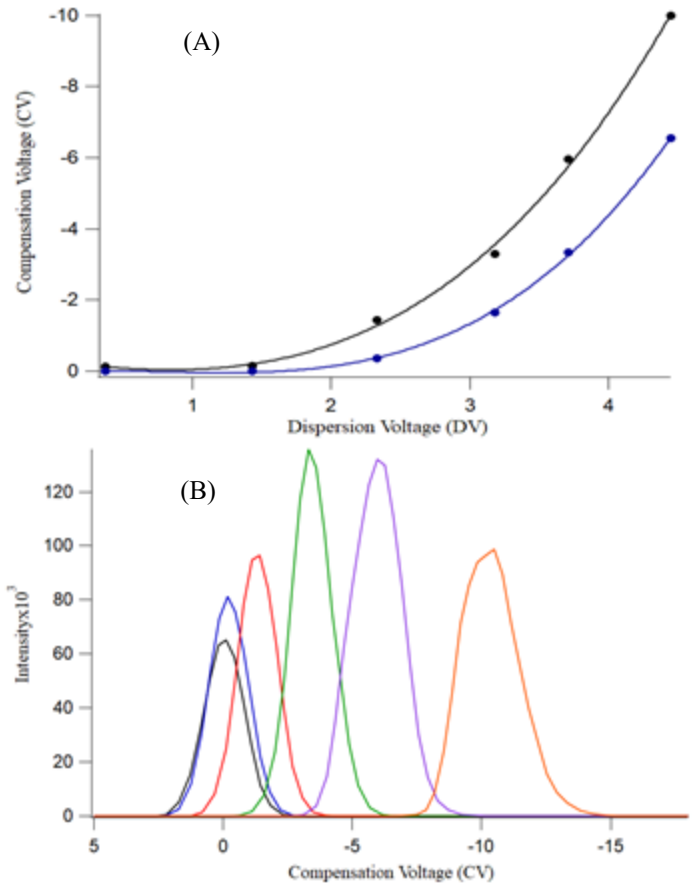

Figure 3.6 In panel (A) CV is plotted as DV values increase. Ammoniated trilinolein (54:6) monomer (black) m/z 896 and ammoniated trilinolein dimer (blue), m/z 1773 are plotted against CV. Panel (B) shows CV ionograms of 54:6 monomer at DV values of -0.37 (black), -1.43 (blue), -2.33 (red), -3.18 (green), -3.71 (purple) and -4.45 kV (orange).

An advantage of using FAIMS is the increased signal-to-noise (S/N) ratio. Since CV is unique to ions' mobility, when the ion of interest is isolated, there is often reduced background noise due to target ions having a different CV response than other ions. Hydroxy-trilinolein was analyzed both with FAIMS at a DV of -4.2 kV and without FAIMS under the same MS conditions (Figure 3.7, A,B). In the MS spectra without FAIMS, a dimer ion was present at m/z 1805.3, as well as increased background noise. With FAIMS applied, the dimer ion disappears and background noise was greatly reduced. Although the target ion in this case was abundantly present in both spectra, it is

easy to imagine the improvements that FAIMS can offer within complex sample media. The ability to increase S/N is advantageous in TAG analysis since they are generally investigated in complex samples that contain high background levels. The application may be particularly useful with oxidized TAG samples where analysis is often limited by low levels of oxidation products. To generate a more confident analysis of the oxidation products, FAIMS can be used to provide cleaner spectra for the target ions by eliminating interfering background ions. This could be a specific application of FAIMS to the field of TAGs, where some analyses have required an off-line separation step to concentrate the amount of oxidized products prior to MS analysis (Gruneis et al. 2019)

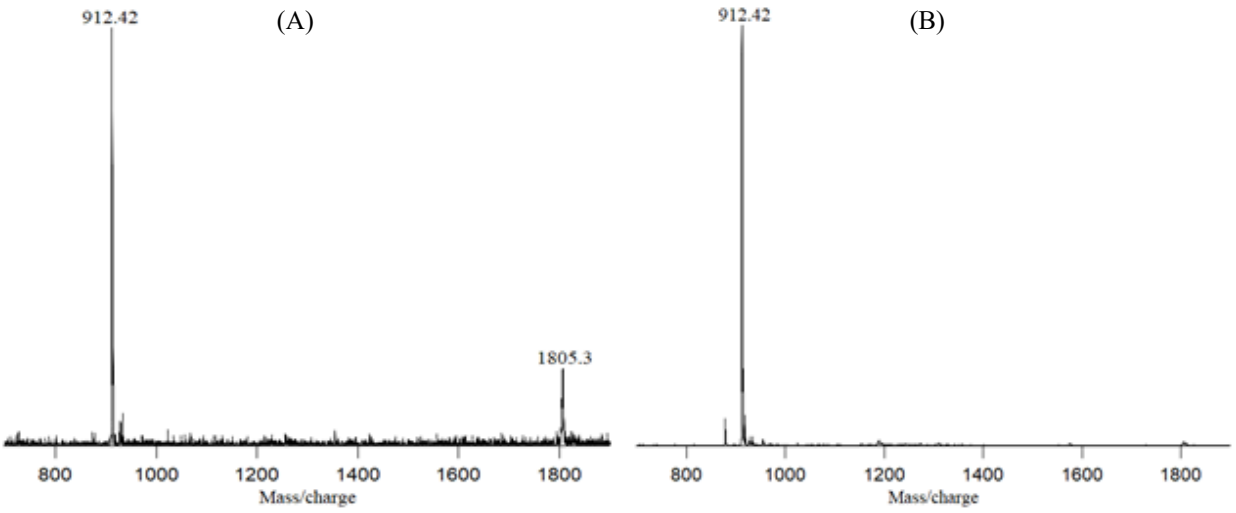

Figure 3.7 (A) Full MS spectra acquired on the L-QIT without FAIMS of ammoniated hydroxy 54:6 versus (B) ammoniated hydroxy 54:6 at a DV of -4.2 kV.

3.3.2 FAIMS transmission of (54:6) and (54:3) TAG

It was of interest to compare two standard TAGs with different numbers of double bonds to evaluate their separation by FAIMS. Resolution in FAIMS can be defined in two ways: spectroscopic resolution and chromatographic resolution. Spectroscopic

resolution can also be referred to as resolving power and is defined as the CV of transmission divided by the CV peak width at half maximum (Barnett et al. 2011). In comparison, chromatographic resolution is analogous to resolution calculated by LC. This study will focus on chromatographic resolution for comparison to LC methods. CV was scanned at a DV of -4.25 kV where triolein (54:3 TAG) had a resulting CV of -9.8 V and trilinolein (54:6 TAG) had a CV of -7.0 V. R_s was calculated as 1.02, which does not meet baseline resolution of 1.5. There is obvious overlap between the two ionograms, and scope for improved resolution (Figure 3.8). Peak resolution in FAIMS can be increased by controlling the temperature of the electrodes (Barnett et al. 2007), using dopants or gas additives, or adjusting the size of the concentric cylinders (Barnett et al. 2000), and future work should evaluate these options. It should also be noted that only two TAGs were evaluated, and the implementation of other TAG standards could show an increased resolution.

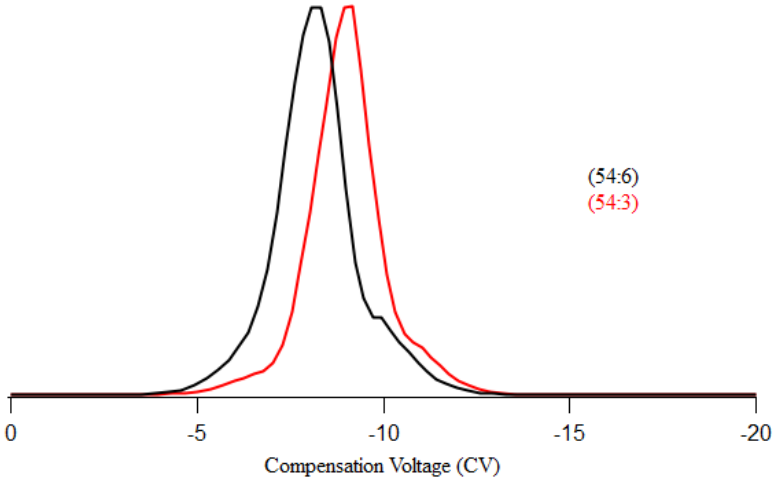

Figure 3.8 CV chromatograms of trilinolein, (54:6) and triolein, (54:3) using FAIMS.

3.3.3 Ion-selective Compensation Voltage Spectra of TAG and TAG Oxidation Products Using Alkali Metal Adducts

Here, the separation of TAG and TAG oxidation products in CV space using FAIMS was explored. FAIMS may offer insight into differences in binding position or different adduct species. With the inlet capillary set to 25 °C, ionograms were extracted for the six potential adducts with trilinolein using a DV of -4.4 kV (Figure 3.9). Different adducts could potentially lead to less flexible or more rigid TAG structures depending on the binding mechanism and FAIMS transmission could reflect the position of the charge. It can be assumed that if the binding site was significantly different between adducts (i.e., oxygen vs. double bond) then the resulting CV profiles would be different. Comparison of the six adducts shows that NH_4^+ and Na^+ profiles were similar (CV = ~ -8 V) while K^+ had a CV of -9.8 V, Rb^+ was -10.4 V and Cs^+ -11 V with similar peak widths and shape (Figure 3.9), while Li^+ TAG resulted in a narrower ionogram at a CV of -11 V. The increased width of CV peaks could indicate the presence of isomers although that cannot be concluded with certainty. The different CV profiles hint at different binding mechanisms between the different alkali metals and ammonium with trilinolein. Han et al. (2001) suggested that the ion binds at either an oxygen on the glycerol backbone or at a double bond to form the adduct. The atomic radii of the alkali metals are often used to describe the binding mechanisms where the larger adducts entail weaker bonds (Hsu et al. 2010). The larger adducts did show similar ionograms; however, lithiated TAG showed a more similar ionogram to the larger adducts compared to sodium and ammonium. There is also the argument that a small ion like lithium could bind more readily to double bonds in comparison to larger ions that may not easily fit in that conformation. Since there is no standard data from FAIMS with TAGs, the different ionogram profiles cannot be directly

correlated to increased or decreased ion mobility. However, it was clear that relative ion mobility for the same TAG was adduct dependent.

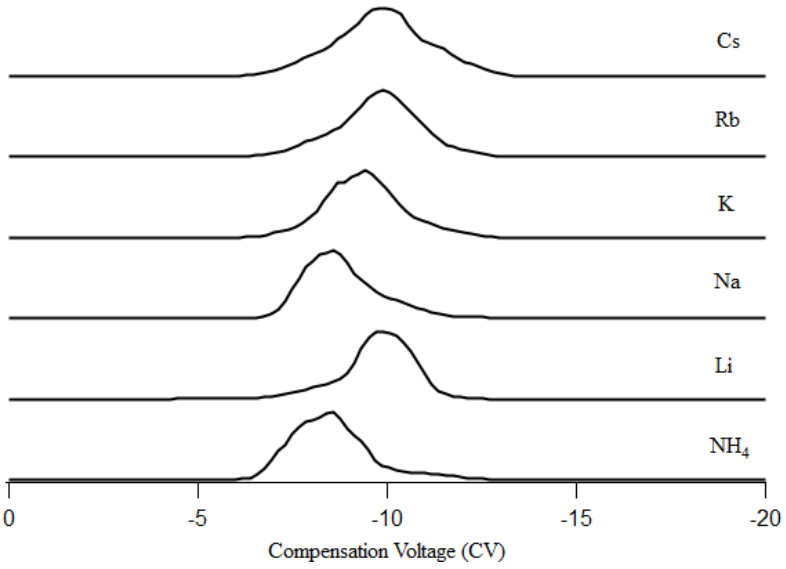

Figure 3.9 Trilinolein CV scans using different alkali salt adducts and ammonium acetate using FAIMS. CV chromatograms were extracted for the ion $C_{57}H_{98}O_6A$ where A represents the adduct. The MS inlet was set to room temperature (23°c) and the DV was set to -4.4 kV while scanning CV from 0 to -20 V.

Further comparison of the adducts with an oxidized TAG (Figure 3.11) showed that Cs^+, Rb^+ and K^+ hydroperoxy TAG resulted in similar CV values of -11.1 V, -10.4 V and -9 V respectively, as with trilinolein. The peak widths were seemingly narrower in hydroperoxy TAG for the three adducts than with trilinolein; however, the position of the metal cannot be concluded based on the widths of the peaks (Figure 3.10 and Figure 3.11). Hydroperoxy trilinolein showed a different ionogram shape with sodiated ox-TAG compared to the other adducts. It was also clearly different than the intact trilinolein profile with sodium. It can be proposed that the addition of oxygen atoms changes the binding mechanism between the metal and TAG, changing the ionogram profile, but the exact charge mechanisms cannot be concluded.

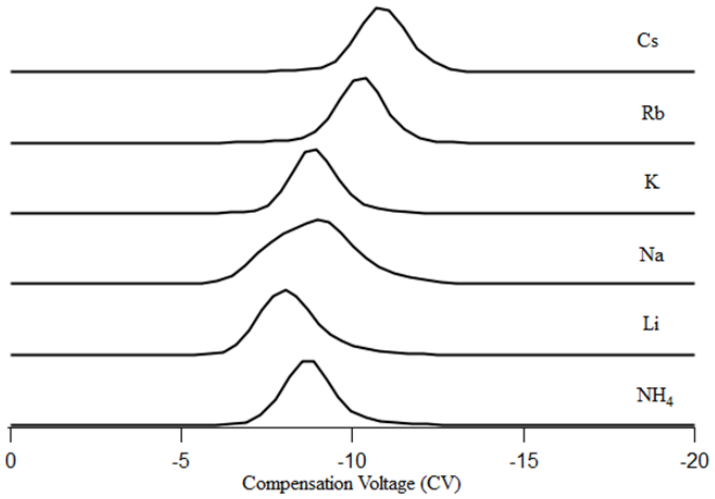

Figure 3.10 Hydroperoxy trilinolein CV scans using different alkali salt adducts and ammonium acetate with FAIMS. CV chromatograms were extracted for the ion $C_{57}H_{98}O_6AO_2$ where A represents the adduct. The MS inlet was set to room temperature (23°c) and the DV was set to -4.4 kV while scanning CV from 0 to -20 V.

Considering lithiated trilinolein showed a different CV profile compared to the other metals, it was of interest to further investigate lithium's characteristics using oxidized standards of hydroxy, epoxy and hydroperoxy trilinolein. If the metal was only binding to the glycerol backbone, it could be assumed that the CV profiles of trilinolein and oxidized trilinolein would be very similar. Therefore, it was surprising to see a difference in CV between mono-hydroxy, mono-epoxy, mono- peroxy and intact trilinolein (Figure 3.11). The oxidation products favour lower CV values (-5.7 V hydroperoxy, -6.8 V epoxy and -7.2 V hydroxy) where intact TAG shows a higher CV value at -11 V. It is interesting to note that the three molecules show a greater change in relative mobility (higher CV) as the number of oxidation products decreases. The four ion-selective CV spectra are generally symmetrical, aside from hydroxy trilinolein that shows evidence of a shoulder and increased width. A limitation of dome-style FAIMS relative to flat plates is reduced resolution, albeit the sensitivity is generally higher. At

increased resolution potential, or with flat-plate FAIMS, the hydroxy trilinolein ionogram could potentially resolve into two peaks. It is anticipated that the oxidized standards have many potential isomers where a symmetrical peak indicates that the different positions of the oxygen group does not affect the ions relative mobility changes.

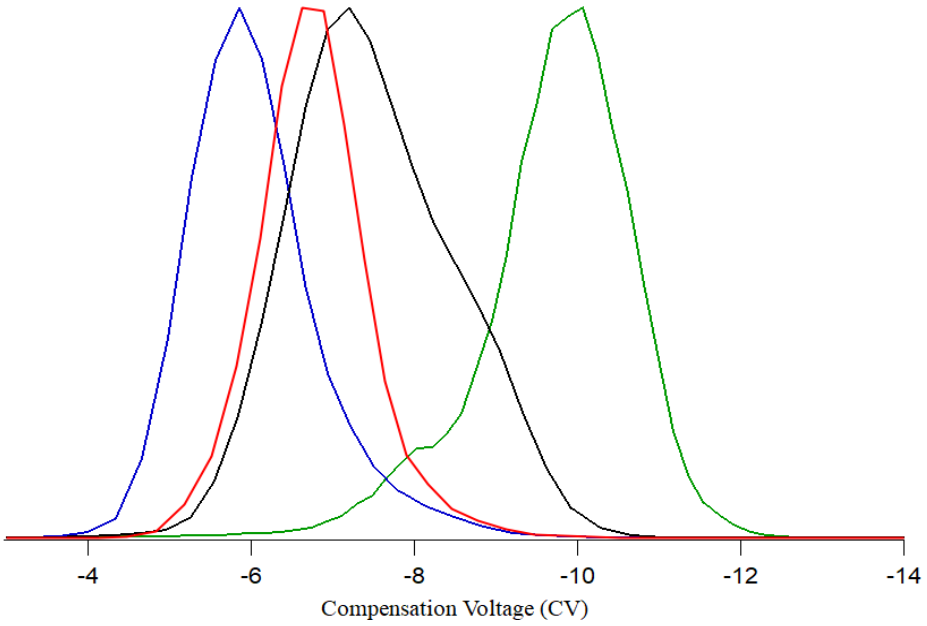

Figure 3.11 Comparison of lithiated trilinolein (green), lithiated hydroxy trilinolein (black), lithiated epoxy trilinolein (red) and lithiated hydroperoxy trilinolein (blue) CV traces at DV-4.25 kV.

To further compare the different oxidation products, ammoniated hydroxy, hydroperoxy and epoxy trilinolein were analyzed. Ammonium was chosen as the charge carrier because the ionogram between intact trilinolein and hydroperoxy trilinolein were similar and ammonium is the adduct of choice for LCMS analysis, so it was of interest to understand more. By comparing only one adduct, any change in mobility would be due to the change in oxidation group. CV values of -10.2 V, -9.7 V and -9.5 V were obtained for ammoniated mono-hydroxy, mono-epoxy and mono-hydroperoxy trilinolein respectively. The intact trilinolein trace was not included in the figure as it overlapped with

hydroperoxy and epoxy trilinolein at a CV of -8 V, which made it a challenge to view the changes between oxidation products.

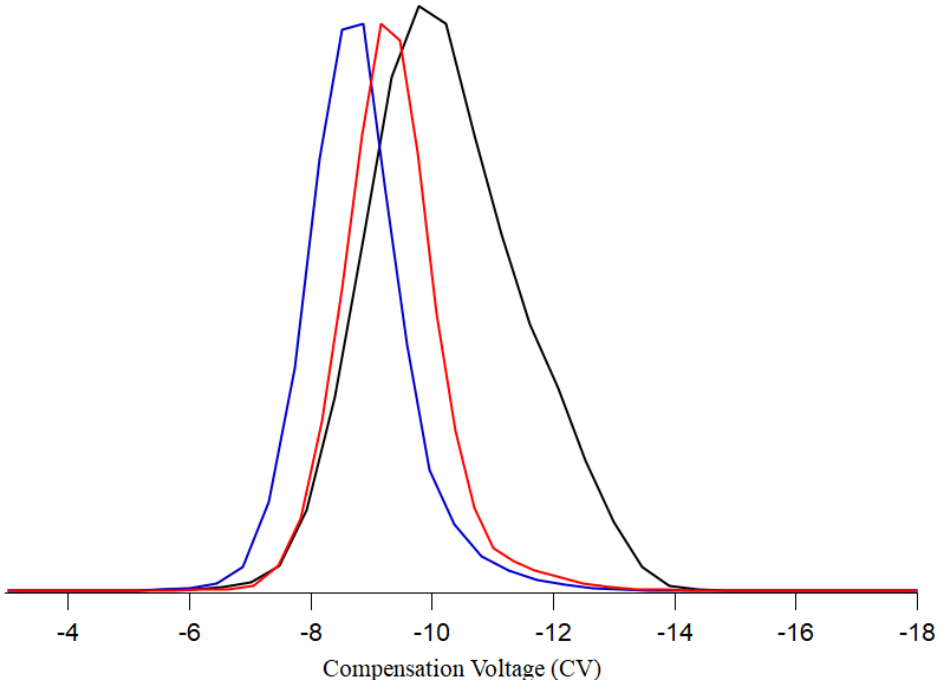

Figure 3.12 Comparison of CV profiles of ammoniated mono-hydroxy trilinolein (black), mono-hydroperoxy trilinolein (blue) and mono-epoxy trilinolein (red) at a DV of -4.25 kV.

Similar to the results obtained from the comparison with lithium (Figure 3.10), mono-hydroxy trilinolein had a higher CV compared to mono-peroxy trilinolein (Figure 3.12). Furthermore, the hydroxy ionogram was wider than the hydroperoxy ionogram, as with lithiated mono-hydroxy trilinolein. The difference in CV between the groups is less (0.7 V) than the change in CV observed using lithium (3.3 V). However, it can be concluded that there is a trend in mobilities between hydroxy and peroxy trilinolein with both adducts where hydroxy trilinolein shows a higher CV compared to hydroperoxy. Epoxy trilinolein did not have a clear trend between the two tested adducts.

3.3.4 Thermal Degradation of Oxidized TAG at High Inlet Temperatures

Chapter 2 described degradation of TAG and TAG oxidation products occurring at elevated MS inlet temperatures (>150 °C). Oxidized TAGs showed more degradation compared to intact TAGs. The effect due to temperature was first observed while performing analysis with FAIMS. FAIMS is operated with the inlet set to room temperature (~25 °C) because desolvation of the analytes is achieved by the flow of curtain gas, and does not require high MS inlet temperatures for further desolvation. With the inlet temperature set to 25 °C, a much cleaner MS spectrum was achieved. The MS inlet temperature can be changed without affecting the temperature of FAIMS in order to evaluate thermal degradation of gas-phase TAG molecules. The complexity from the effect of temperature comes from dissociation of TAG in the MS inlet rather than from the solution itself.

Ion-selective compensation voltage spectra for hydroperoxy-trilinolein were acquired using a DV of -4.25 kV (Figure 3.13). The monomer ion (m/z 928) was extracted to show a symmetric ionogram at CV -10 V with an inlet temperature of 25 °C. The dimer ion at m/z 1805.3, $[2TAG+NH_4]^+$, was also observed but at a lower CV of -7.4 V. When the MS inlet temperature was increased, the DAG ion (m/z 597) appeared at a CV of -11 V. Furthermore, some monomer ions started to appear at a CV of -7.4 V. There was very little observed dimer ion in the spectra. The monomer ion identified at 275 °C appeared at the same CV value as the dimer ion at 25 °C. Similarly, the DAG ion present at 275 °C has a similar profile and CV as the monomer ion at 25 °C. The slight change in CV can be attributed to variability in the manual triggering of the CV scan and the MS data acquisition. Since FAIMS is positioned between the ion source and the MS inlet, when the ions go through FAIMS they are not affected by the inlet temperature.

Residual heat from the MS inlet could also impact the FAIMS transmission if the temperature of the electrodes changes. In practice, we do not observe a significant change in electrode temperature over the course of these relatively brief measurements. Therefore, since the CV and ionogram peaks match between the monomer ion at 25 °C and the DAG at 275 °C, we can conclude that the real monomer ion (18:2/18:2/18:2[OOH]) is degrading into the DAG ion (18:2/18:3) identified at 275 °C. In addition, the 'monomer' ion present in the spectra at 275 °C is actually a degradation product of the dimer ion at 25 °C and not the true monomer ion from solution. This finding is very important because if analysis was performed initially at 275 °C, the wrong ion would be quantified leading to incorrect conclusions. Furthermore, the presence of multiple peaks for the monomer ion at 275 °C could falsely lead to the conclusion that isomers were being resolved. The same degradation trend is observed for both hydroxy and epoxy TAG.

Large amounts of DAG were identified from degradation with ammonium as the charge carrier. In Chapter 2, we previously determined that there was less of an effect from high inlet temperatures when analyzing TAG with lithium. However, at 275 °C, there is a second peak in the extracted ionogram of the monomer ion showing that some degradation from the dimer ion is still occurring (Figure 3.13). There is also a small amount of DAG ion at the same CV of -10.5 V where the monomer ion was identified at 25 °C. The metal least affected by temperature was sodium. Only a small shoulder appeared with the extracted monomer ionogram at 275 °C.

Elevated inlet temperature also had obvious influence on dimer and DAG presence, with the other three adducts formed with K^+, Rb^+ and Cs^+; the adduct formed

with cesium had the most degradation and was comparable to ammonium. Presumably cesium is lost when the adduct is met with high temperatures, with this in turn leading to loss of oxygen. Oxygen is thought to leave as H_2O, generating a protonated TAG at m/z 877 as (18:2/18:2/18:3). Further degradation of this protonated TAG leads to the DAG at m/z 597 as (18:2/18:3). In Chapter 2, ammonium was determined to be a weakly binding species and several studies have identified cesium as a weakly bound metal due to its large atomic radius (Renaud et al. 2013 & Han et al. 2001). Therefore, it is intuitive that adducts formed from both were affected most by high inlet temperatures. These adducts are more likely to dissociate at applied temperatures, allowing the TAG to be more susceptible to degradation. In comparison, it can be proposed that sodium and lithium are more tightly bound, protecting the TAG in a sense from degradation.

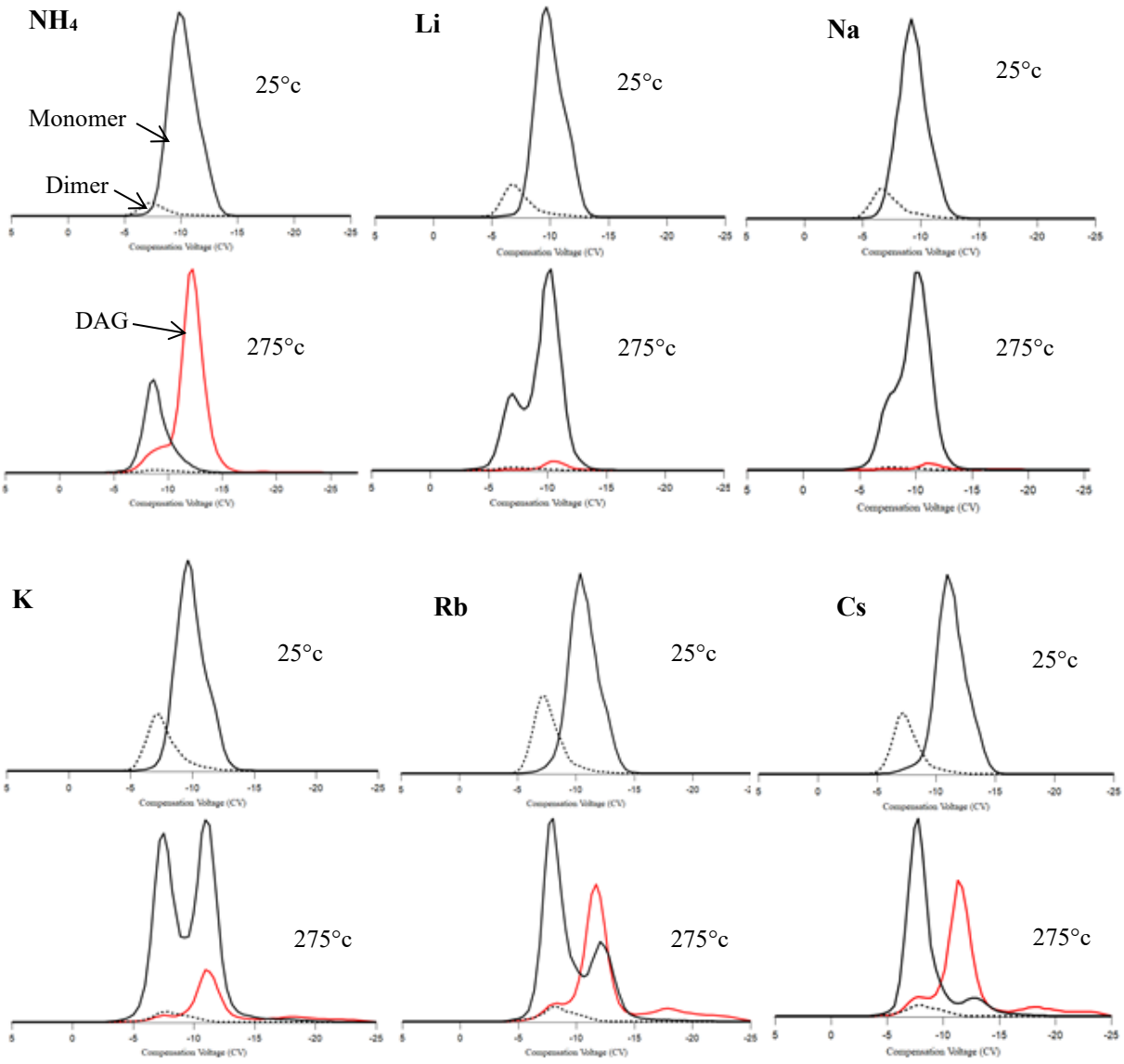

Figure 3.13 FAIMS analysis of hydroperoxy-trilinolein with each adduct; NH_4^+, Li^+, Na^+, K^+, Rb^+ and Cs^+ at 25 °C and 275 °C. Monomer ions, $[TAG(OOH) + A]^+$ are plotted in black, dimer ions $[2TAG(OOH) + A]^+$ as the dashed trace and DAG, $[18:2/18:3]^+$ in red, where A represents the corresponding adduct.

A study by Sala et al. (2015) studied TAG regioisomers through a SelexION differential ion mobility device. The study claimed to separate TAG isomers OSO (18:1/18:0/18:1) and SOO (18:0/18:1/18:1). However, they failed to provide standard ionograms of the isomers individually and they performed the analysis at an MS inlet

temperature of 225 °C. Understanding the effect of inlet temperature, the two peaks they identify as isomers are more likely to be degradation from a dimer with some monomer remaining. In the present study, it was presented that a single TAG species created two peaks at high inlet temperatures. The present study provided important information for the field of lipidomics that has not been discovered prior. High inlet temperatures are most likely leading to misidentification of the target ion, allowing quantitation of the wrong species. The effect of degradation was more severe in oxidation products than intact TAGs; however, the same phenomenon was observed where degradation of the monomer ion into DAG and dimer into monomer occurs at high temperatures. Since lithium and sodium adducts showed the least degradation, they may be better choices as adducts for analysis of TAG oxidation products, as opposed to ammonium or other alkali metals. However, the argument could also be made to use ammonium at a low inlet temperature where it provides structural insight by MSMS.

3.4 Conclusions

The application of a dome-style FAIMS showed similar ionograms between K^+, Rb^+, Cs^+ with intact TAG while Li^+ showed a narrower profile. NH_4^+ and Na^+ resulted in lower CV values compared to the other alkali metals. The different profiles indicate that the charge carrier affected the mobility of the intact TAG species. Different mobilities were shown between hydroxy and hydroperoxy TAG with lithium, where hydroperoxy TAG had a CV of -5.7 V and hydroxy at -7.2 V. The same trend was observed for ammoniated TAG where hydroperoxy had the lowest CV value. High (>150 °C) MS inlet temperature was determined to cause degradation of oxidized TAG standards, where monomer ions degraded to protonated DAGs and dimers degraded to monomer ions.

Ammonium, rubidium and cesium were shown to be most influenced by high inlet temperatures while sodium and lithium were the least affected. The use of high inlet temperature may be leading to misinterpretation of TAG spectra and TAG oxidation products and inaccurate quantification. Considering that the phenomenon is dependent on the charge carrier, the temperature of the inlet and the adduct employed should be important factors to consider prior to native or oxidized TAG analysis.

CHAPTER 4 LIQUID CHROMATOGRAPHY MASS SPECTROMETRY OF TAG AND TAG DEGRADATION PRODUCTS

4.1 INTRODUCTION

Historically, thin layer chromatography (TLC) and gas chromatography (GC) were chromatographic methods of choice for lipid analysis (Hou et al. 2008). Due to the non-volatile nature of TAGs and TAG oxidation products, intact analysis by GC is not an option (Levison et al. 2013). Analysis by GC requires several sample preparation steps including derivatization and transmethylation that break TAG molecules into fatty acids and then methyl ester constituents (FAME) (Kail et al. 2012). The lengthy sample preparation steps also scramble structural information of TAGs thereby inhibiting the collection of accurate structural information. Another limitation of GC is the inability to identify hydroperoxide oxidation products due to their instability (Pavlica et al. 2021). In more recent years, liquid chromatography (LC) coupled with mass spectrometry (MS) has become the method of choice for TAG analysis (Xia et al. 2017). LC-MS/MS offers three methods of separation; by hydrophobic properties, by mass-to-charge (m/z) and by collision induced dissociation (CID). The main advantage of LC-MS is the ability to identify intact TAG molecules which provide better structural insight. LC offers advantages in efficiency and selectivity while the addition of MS and tandem-MS improve specificity and analytical sensitivity compared to other detectors such as UV (Zheng et al. 2018).

TAGs can be infused into the ESI source of the MS in the absence of chromatography which is a technique known as ‘shotgun lipidomics’ (Griffiths et al. 2020). Shotgun lipidomics can be an advantageous technique due to its speed of analysis

and simplicity in sample preparation (Griffiths et al. 2020). However, the addition of chromatographic separation to MS, such as LC, reduces some of the limitations associated with shotgun lipidomics. Such limitations include resolution of isomers and ion-suppression effects caused by analytes competing for ionization. Ion suppression is reduced because the application of LC separates analytes prior to the MS so the number of competing molecules entering the source at the same time is decreased (Christie and Han. 2010). Normal phase LC (NPLC) has been used for TAG analysis where TAGs are separated based on their polar oxidation groups or double bonds. However, the solvents required for NPLC separation are not compatible with electrospray ionization (ESI) and require atmospheric pressure chemical ionization (APCI). APCI limits the amount of molecular ions produced where fragment ions often dominate the spectra. APCI produces ions through a heated needle making it an unfavourable technique for thermally labile compounds (Lee et al. 2015). ESI is the favourable ionization technique for TAG analysis as intact ions can be identified with the addition of cation metals or ammonium. Therefore, reversed phase LC (RPLC) is the most common chromatographic method for the separation of TAGs, because it is compatible with ESI and separates TAGs based on their no-polar acyl chains.

The order of elution of TAGs by RPLC depends on the length of the FA chains and the number of double bonds and oxidation products (Lazardi et al. 2021). In RPLC, TAG molecules are separated based on their equivalent carbon number (ECN) as described in Equation 4.1 below (Rigano et al. 2018).

$$ECN = \text{Total carbon number} - (2*DB) \qquad \text{Equation 4.1}$$

There remains to lack a comprehensive overview of how different TAG oxidation products affect the order of elution in RPLC.

One of the main drawbacks of LC is that it is time consuming. The majority of TAG analysis by LC have employed gradient elution methods, where the composition of the mobile phase changes with time and can be upwards of 90 minutes long (Petronilho et al. 2021, Han et al. 2021). Gradient methods were developed to deal with the "general elution problem" by dealing with wide ranges in retention time. Gradients have to be chosen carefully to ensure sufficient resolution at low retention times. Gradients allow the analysis of a wider array of chemicals on the same column. However, gradient methods generally require at least two solvents and lengthy column re-equilibration times (Petronilho et al. 2021 & Doreshl, 2002 & Guan et al. 2016). Isocratic methods maintain the same composition of mobile phase for the duration of the method. Isocratic elution is generally less expensive as methods can be run with a single pump and simple control system. Less preparatory work may be needed to optimize the analysis and no time and solvent are wasted re-equilibrating columns between sample runs (Christie and Han. 2010). TAG analysis by isocratic methodology was previously shown by Zeb et al. (2010) for the successful separation of intact TAGs in cameilla oil where they used a mobile phase composition of 18 % isopropanol in methanol over 35 minutes (Zeb et al. 2010).

Quantitation of TAGs was typically performed using GC coupled with flame ionization detection (FID) on their FAME constituents (Levison et al. 2013 & Grebenteuch et al. 2021). This approach is limited because it does not actually identify TAG molecules but rather the percentage of individual fatty acids present within the

TAG. Quantitation of TAGs by LCMS continues to be an analytical challenge due to the complexity of TAGs in real samples and the lack of reliable standards. Han et al. (2021) stated that the number of internal standards required for accurate quantitation of TAGs depends on the variables of the methodology, including collision energy (CE), number of unknowns and availability of isotopically labeled standards.

Acidified ammonium acetate can be included in the LC mobile phase to form $[TAG+NH_4]^+$ adducts for efficient ionization (Kato et al. 2017). Alkali metal salts are not typically used with LC to avoid precipitation in the column and clogging the MS inlet with involatile salt residue. Ammonia and acetic acid are both volatile components that are easily evaporated from solution and therefore do not form salt clusters (Paciga et al. 2014). In this study, a quick isocratic ESI-MS method is presented to separate intact TAG and TAG oxidation products with overlapping mass-to-charge ratios. The method aims to provide a higher throughput for TAG samples in comparison to classic LC methods while continuing to resolve TAG isomers and regioisomers. Furthermore, separation of overlapping m/z TAG oxidation products was determined.

4.2 EXPERIMENTAL

4.2.1 Materials

The TAG and TAG oxidation standards (triolein, trilinolein, hydroxy trilinolein, hydroperoxy trilinolein, epoxy trilinolein) used in Chapter 2 are used for the present study. Ethanol, ammonium acetate and formic acid in Chapter 2 Table 2.1 are used for the present study.

4.2.2 Liquid chromatography

A list of details of the high performance liquid chromatography (HPLC) methodology used in this study is provided in Table 4.1. The LC platform used in this study was an Agilent 1260 II Quaternary LC (Agilent Technologies, Santa Clara, CA). A 10 minute 95 % ethanol (EtOH) with 0.1 % formic acid and 0.1 mM ammonium acetate, isocratic method was used for TAG analysis. A RPLC Avantor® HPLC C8 column was used. The same LC method and column was used for the duration of experimental procedures in this Chapter.

Table 4.1 Agilent 1260 Infinity II, LC parameters used in this study.

Parameter	**Value**
Mobile phase flow rate	40 µL min^{-1}
Solvent A (Isocratic flow)	95% EtOH, 0.1 mm AA, 0.1% Formic acid
Column chemistry	C8
Column diameter	1.0 mm
Column length	15.0 cm
Packing diameter	5 µm
Column temperature	RT
Injection volume	5 µL
Column back pressure	~1500 psi
Mobile phase time	1.4 minutes
Column manufacturer	Avantor® HPLC/UHPLC Columns
Column distributer	VWR
Column catalog number	88394
LC sample Vials (Low-Bind)	Canadian Life Science, Clean Vial (2 mL)

LC-MS results are presented as intensity *versus* time chromatograms. A full-MS scan continuously collects data over a wide mass range for the entire LC elution. The MS scan time depends on the variable ion trap fill time and the resolution (transient) of the orbitrap (i.e., 512 ms for R=140,000). LC coupled to Q-OT permits several filters for data extraction including total ion chromatogram (TIC), base peak chromatograms (BP), extracted ion chromatograms (XIC) and selected reaction monitoring (SRM). A TIC

shows the sum of signals from all masses in any given spectrum (Figure 4.1, A). The BP chromatogram shows the signal for the most intense peak in each spectrum where the most intense peak can change with every scan (Figure 4.1, B). This filter represents the intensity of the most intense peak at every point in the analysis. The most common filter used for this study is XIC which provides the signal from a single mass of interest, unrelated to whether that mass is the most intense ion at that given time (Figure 4.1, C). A SRM filter targets a known analyte where one of the fragment ions of interest is extracted and provides signal for that single fragment mass of interest (Figure 4.1, D).

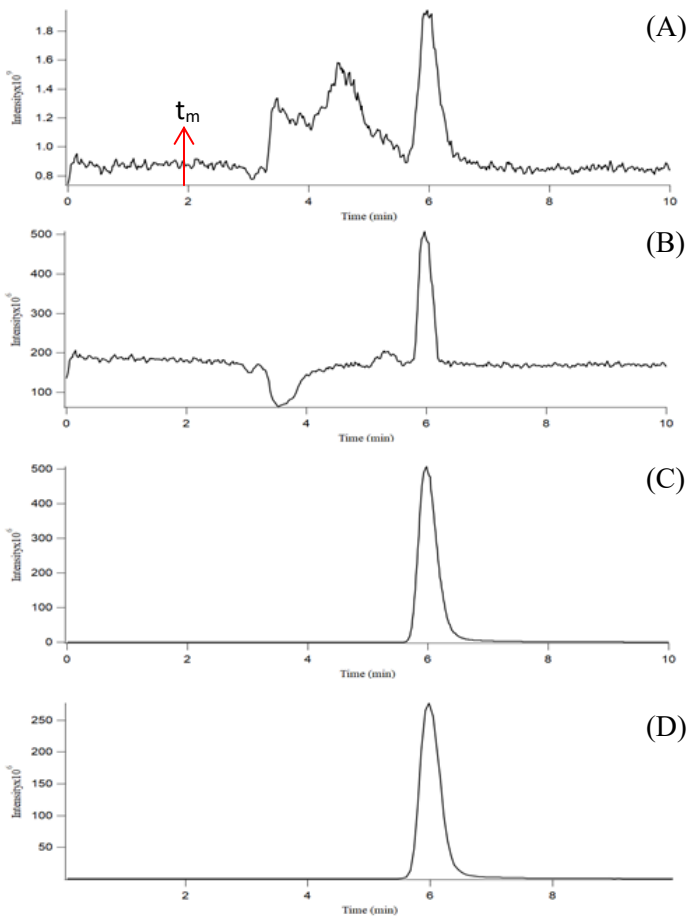

Figure 4.1 LC chromatogram of 5 ug/mL of trilinolein standard using a 10 minute 95% ethanol method with 0.1 mM ammonium acetate and 0.1% formic acid. Scan filters are shown with a total ion chromatogram (TIC) in panel (A), and base peak (BP) filter in panel (B). In panel (C) an extracted ion chromatogram (XIC) of trilinolein m/z 896.771 to a 10 ppm window. A selected reaction monitoring scan of the precursor ion 896.771 to fragment 599.502 is shown in the bottom panel (D). The mobile phase is highlighted in red at 1.4 minutes in panel (A).

Chromatographic resolution can be calculated for LC using Equation 4.1 below.

$$R = \frac{t_{R2} - t_{R1}}{\frac{1}{2}(W_1 + W_2)} \qquad \text{Equation 4.1}$$

Resolution is calculated using the retention time for the later eluting analyte, (t_{R2}) and subtracting the earlier eluting analyte, (t_{R1}). The two peak widths (W_1, W_2) are summed and multiplied by ½ to achieve the peak widths at half height.

4.2.3 Mass spectrometry

The quadrupole orbitrap MS (Q-OT) was used as the detector for the LC method. A maximum resolution setting of 140,000 was used for the duration of this study. Q-OT parameters used for the present study are the same as described in Chapter 2.

4.2.4 Sample preparation

Triolein (18:1/18:1/18:1) and trilinolein (18:2/18:2/18:2) are prepared to 5 ug mL^{-1} in 95 % EtOH from stock solutions of 5 mg mL^{-1}. Hydroxy, and hydroperoxide trilinolein standards are also prepared to 5 ug mL^{-1} from 5 mg mL^{-1} stock solutions. Epoxide trilinolein was prepared following the method proposed by Wei & Budge (2015) to 5 ug mL^{-1}. Calibration curves were created using a range of samples prepared from 5 mg mL^{-1} TAG stocks.

4.3 Results and Discussion

4.3.1 Isocratic Elution of TAG and TAG Oxidation Products

A 95 % EtOH, 10-minute isocratic method was used with 0.1 mM ammonium acetate and 0.1 % formic acid. The method produced successful elution of TAG and TAG oxidation standards over a short duration of 10 minutes. Using the Q-OT, the MS inlet temperature was set to 275 °C for the increased sample flow rate (40 uL min^{-1}) used with LC. The effect of inlet temperature will be notably less with increased flow rate and decreased capillary length (5 cm) relative to the L-QIT (10 cm) used in chapters 2 and 3.

Triolein (18:1/18:1/18:1, m/z=902.876) is separated from trilinolein (18:2/18:2/18:2, m/z= 896.674) where extracted ion chromatograms (XIC) are plotted based on their individual mass-to-charge ratios (Figure 4.2). Based on their equivalent carbon numbers (ECN), it was expected that trilinolein would elute earlier with an ECN

value of 45 compared to triolein with a value of 48. This indicates that TAGs with a higher number of double bonds are more polar molecules than TAGs with less double bonds. Previous LC analysis of triolein by Petronilho et al. (2021) showed a retention time of 27 minutes for triolein. Their method used a C30 RP column and a 45 minute solvent gradient using 50:50 water/acetonitrile as solvent A and isopropanol/acetonitrile/water (85:10:5) as solvent B that was increased over the duration of the gradient. The study did not include results on resolution as they only focused on triolein. The short isocratic method implemented in this study allows for a quicker analysis time and higher sample throughput while maintaining baseline resolution. The extracted mass spectra for the two standard TAGs also contain low amounts of dimer ion, $[2TAG+NH_4]^+$, at the same retention time at m/z 1775.50 and 1787.60 for trilinolein and triolein, respectively (Figure 4.2). The levels of observed dimer ions can increase at elevated lipid concentrations and their detection can also be affected by inlet conditions including lens voltages and transfer capillary temperature.

The retention factor for trilinolein standard can be calculated using the mobile phase time at 1.4 minutes. *k*' is determined to be 2.79 for trilinolein and 3.79 for the later eluting triolein peak. LC methods typically aim for *k'* values between 2.0 and 20, therefore the proposed LC method is appropriate. When developing a new LC method it is important to ensure *k*' values are within the expected range so that adequate retention is achieved. It was previously reported by multiple authors that successful resolution was achieved between TAGs with different numbers of double bonds (Fasciotti et al. 2010 & Kato et al. 2017 & Nagai et al. 2019). The resolution value was calculated for the two TAG standards in this study using Equation 4.1. Triolein and trilinolein resulted in a

resolution value of 2.78. Baseline resolution is achieved at values of 1.5 and higher for symmetric peaks with no tailing. The chromatographic resolution from LC proved to be superior to chromatographic resolution with FAIMS calculated in Chapter 3.

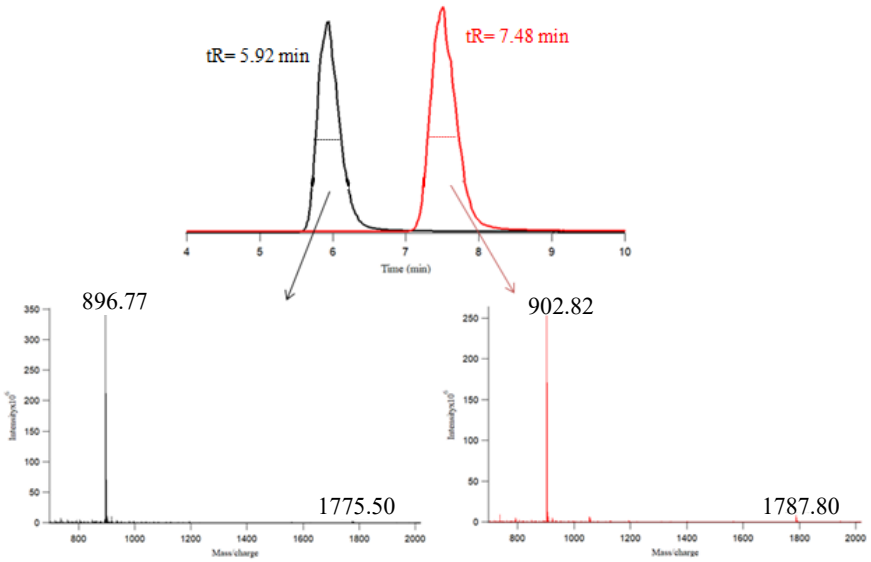

Figure 4.2 Trilinolein (black) and triolein (red) standards on LC-QOT. Extrapolating the chromatogram peaks yield MS spectra at the corresponding retention time. At tR=5.92 min, MS spectra yields 896.77 [$C_{57}H_{98}O_6NH_4$] and 1775.50 [$2M+NH_4$], confirming trilinolein standard. At tR 7.48 min, MS spectra yields 902.82 [$C_{57}H_{104}O_6NH_4$] and 1787.60 [$2M+NH_4$]. The two standard samples were normalized to max intensity in the top panel.

In Chapter 2, several oxidation products had overlapping m/z, including mono-epoxy and mono-hydroxy trilinolein as well as hydroperoxide trilinolein and di-epoxy or di-hydroxy trilinolein. Mono-epoxy and mono-hydroxy trilinolein standards have the same empirical formula, $C_{57}H_{98}O_6NH_4O$ and therefore the same m/z value of 912.671, where use of HR/AM alone was not able to differentiate the two products. We concluded that unique fragment ions are produced from MS/MS of precursor ammoniated mono-hydroxy and mono-epoxy groups, providing an alternative means for their identification. Infusion mass spectrometry would produce chimeric fragmentation spectra from the co-

isolation of multiple precursor ions. This limitation of infusion (shotgun) mass spectrometry for analysis of TAGs provides motivation for the development of liquid chromatographic methods despite the reduced throughput.

A survey of epoxy trilinolein by infusion MS showed six epoxy oxidation products were expected. XIC of the six epoxide groups proved an increase in oxidation products yields shorter retention times. Hexa-epoxy trilinolein [$(TAG+NH_4+6O)^+$, m/z=992.58] resulted in a retention time (t_R) of 3.52 minutes whereas mono-epoxy trilinolein [$(TAG+NH_4+O)^+$, m/z=912.67] eluted at 5.19 minutes. The order of elution of epoxide products suggests that more oxidation products create a more polar TAG. A previous study by Petronilho et al. (2021) provides the same conclusions where they see more hydroperoxy products resulting in lower retention times.

It is important to note that each epoxide oxidation product produced a symmetrical chromatographic peak. With multiple possible binding locations (double bonds), it would not be surprising if the presence of isomers lead to multiple peaks for the same m/z value. For example, it is presumed that epoxides form by attacking the double bond so tri-epoxy trilinolein $(TAG+NH_4+3O)^+$ would have several positions where the three epoxide groups could form. There is also the possibility that epoxides are forming on the adjacent allylic carbon, which creates even more potential permutations. A single chromatographic peak either indicates that the oxidation groups are always positioned at the same location or the difference in position is not distinguished chromatographically. The intensity decreases for each additional epoxide product. It can be inferred that the epoxide reaction had not gone to completion or each oxidation product would have been present at the same intensity.

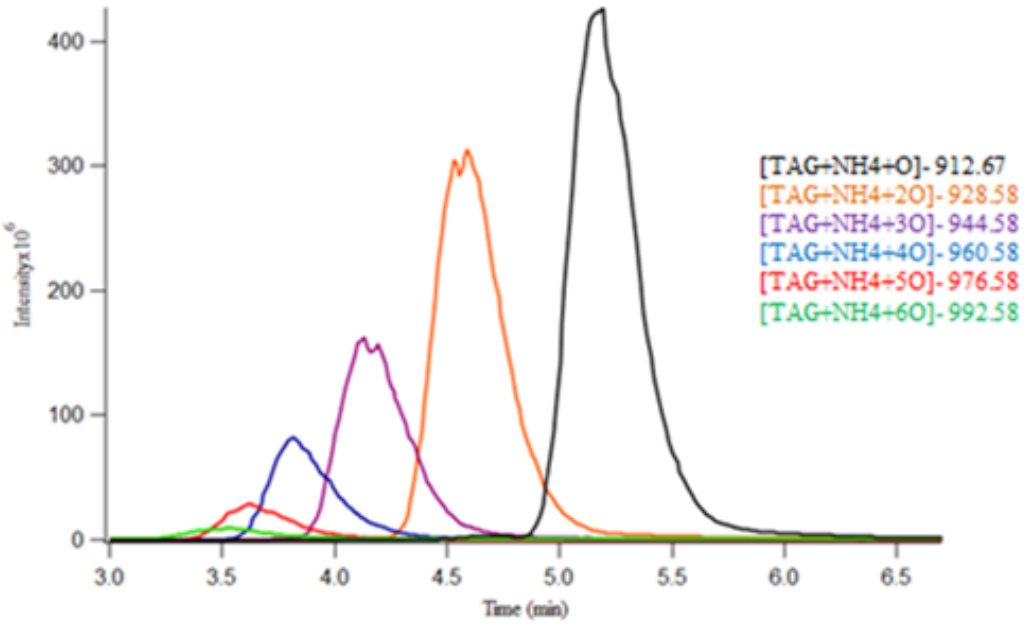

Figure 4.3 Epoxidized trilinolein with 0.1 mM ammonium acetate. LC separation of the six oxidation products is shown over an isocratic (95% ethanol) period of 10 minutes.

Previous investigation of TAG oxidation products by LCMS have shown limited comparisons between different oxidation groups (Gruneis et al. 2019 & Petronilho et al. 2021). The identification of different oxidation products within oil samples have shown an overlap in retention time (Gruneis et al. 2019). For the present study, a comparison was done using hydroxy trilinolein and epoxy trilinolein standards. There has not been a direct comparison of hydroxy and epoxy oxidation products previously by LC. Mono-epoxy trilinolein eluted at a retention time of 5.19 minutes while mono-hydroxy trilinolein has a retention time of 4.62 minutes (Figure 4.4). Further analysis of the two overlapping products resulted in di-epoxy trilinolein eluting at a retention time of 4.60 minutes and di-hydroxy at 4.40 minutes. It was concluded that hydroxy products yield a more polar, earlier eluting TAG than epoxy oxidation products. The two oxidation products lead to symmetric peaks of approximately the same width (~0.6 minutes)

(Figure 4.4). It is important to note the characteristics or differences between the two chromatographic peaks as they can be further applied to complex samples.

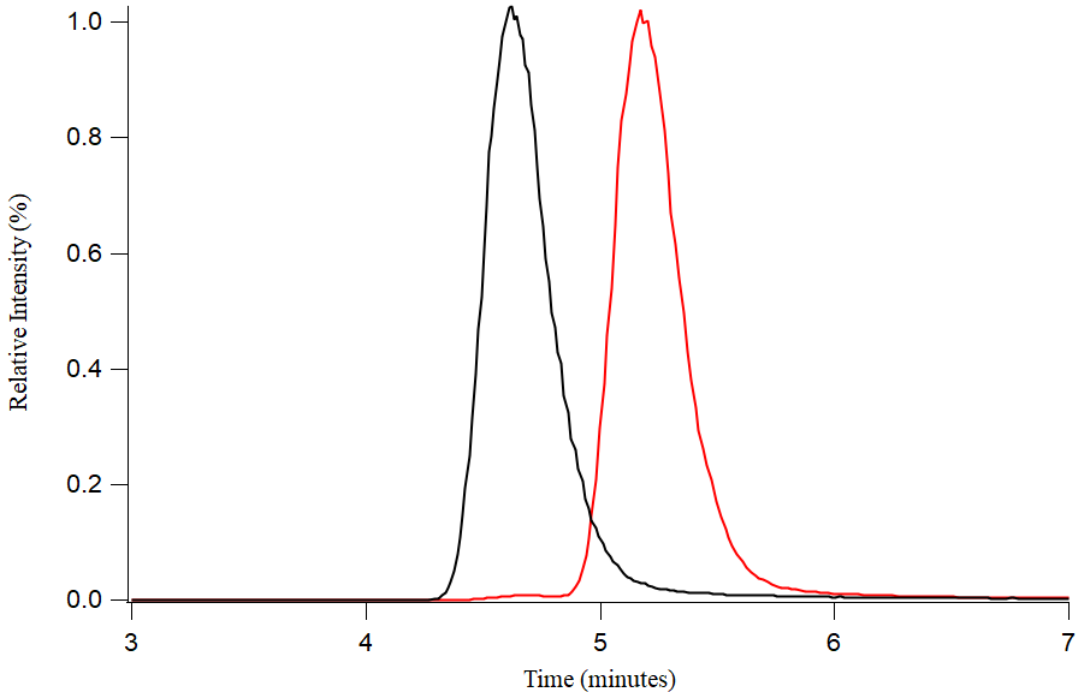

Figure 4.4 Separation of mono-epoxy trilinolein (red) and mono-hydroxy trilinolein (black). The molecules were ran separately and extracted with a m/z of 912.67 within 10 ppm.

Mono-, di- and tri-hydroperoxy products were identified using hydroperoxy trilinolein standard. Mono-peroxy trilinolein [TAG+(2O)+NH_4, m/z 928.76]$^+$ eluted at a retention time of 4.64 minutes, which was 0.24 minutes later eluting than di-hydroxy trilinolein [TAG+(2O)+NH_4, m/z 928.76]$^+$. There was very little chromatographic difference between hydroperoxy-trilinolein and di-epoxy trilinolein (~0.04 minutes). The peak widths were also the same at ~0.6 minutes. This indicates that the two oxidation products have similar hydrophobic properties. The similar orders of retention make it difficult to distinguish between peroxide products versus epoxides with the same m/z. A complete list of retention times for the three oxidation groups is given in Table 4.2.

Table 4.2 Epoxy, hydroxy and hydroperoxy trilinolein standard retention times. XIC for each oxidation product was done using a 10 ppm window to provide accurate retention times.

Oxidation group	Chemical formula and m/z	t_R (min)	Peak widths (min)
Epoxy trilinolein	$C_{57}H_{98}O_6NH_4O$ m/z=912.786	5.19	0.65
	$C_{57}H_{98}O_6NH_4(2O)$ m/z=928.762	4.60	0.65
	$C_{57}H_{98}O_6NH_4(3O)$ m/z=944.785	4.13	0.70
	$C_{57}H_{98}O_6NH_4(4O)$ m/z=960.681	3.82	0.60
	$C_{57}H_{98}O_6NH_4(5O)$ m/z=976.788	3.63	0.60
	$C_{57}H_{98}O_6NH_4(6O)$ m/z=992.759	3.52	0.70
Hydroxy trilinolein	$C_{57}H_{98}O_6NH_4O$ m/z=912.786	4.62	0.60
	$C_{57}H_{98}O_6NH_4(2O)$ m/z=928.762	4.40	0.80
	$C_{57}H_{98}O_6NH_4(3O)$ m/z=944.785	3.84 4.28	1.10
Hydroperoxy trilinolein	$C_{57}H_{98}O_6NH_4O$ m/z=912.786	4.74	1.00
	$C_{57}H_{98}O_6NH_4(2O)$ m/z=928.762	4.64	0.70
	$C_{57}H_{98}O_6NH_4(3O)$ m/z=944.785	3.92 4.34	1.20
	$C_{57}H_{98}O_6NH_4(4O)$ m/z=960.681	3.77	0.75
	$C_{57}H_{98}O_6NH_4(5O)$ m/z=976.788	3.68	0.70
	$C_{57}H_{98}O_6NH_4(6O)$ m/z=992.759	3.38	0.70

The XIC of tri-hydroxy trilinolein resulted in two peaks at t_R of 3.84 minutes and 4.28 minutes (Figure 4.5). Three oxidation products present the possibility of multiple arrangements of the three hydroxides. The appearance of multiple peaks enables a

possibility to discriminate structural or positional isomers using tandem-MS. A collision energy of 30 eV was applied to precursor ion m/z 944.785 which resulted in product ions m/z 507.27 and m/z 491.37. Product ion m/z 491.37 had a later t_R of 4.30 minutes compared to m/z 507.27 which eluted at 3.85 minutes. The two product ions are used to determine the location of the oxidation group, where m/z 491.37 represents a hydroxy group on C9 and m/z 507.27 represents a hydroxy group on C10. The two different positions of the oxidation products lead to two different retention times. In comparison, tri-epoxy trilinolein resulted in a single symmetrical peak, allowing the two different peak shapes to be a tool in distinguishing the two overlapping m/z oxidation products.

Although, epoxy and hydroperoxy products do not resolve, hydroxy and hydroperoxy products do resolve chromatographically. Di-hydroxy and mono-hydroperoxy both have an m/z of 928.76 and are partially resolved (Figure 4.5). Di-hydroxy TAG is a more polar, earlier eluting product than mono-hydroperoxide TAG. Extracted chromatograms for hydroxy TAG and hydroperoxy TAG produce symmetrical peaks except for tri-hydroxy (Figure 4.5).

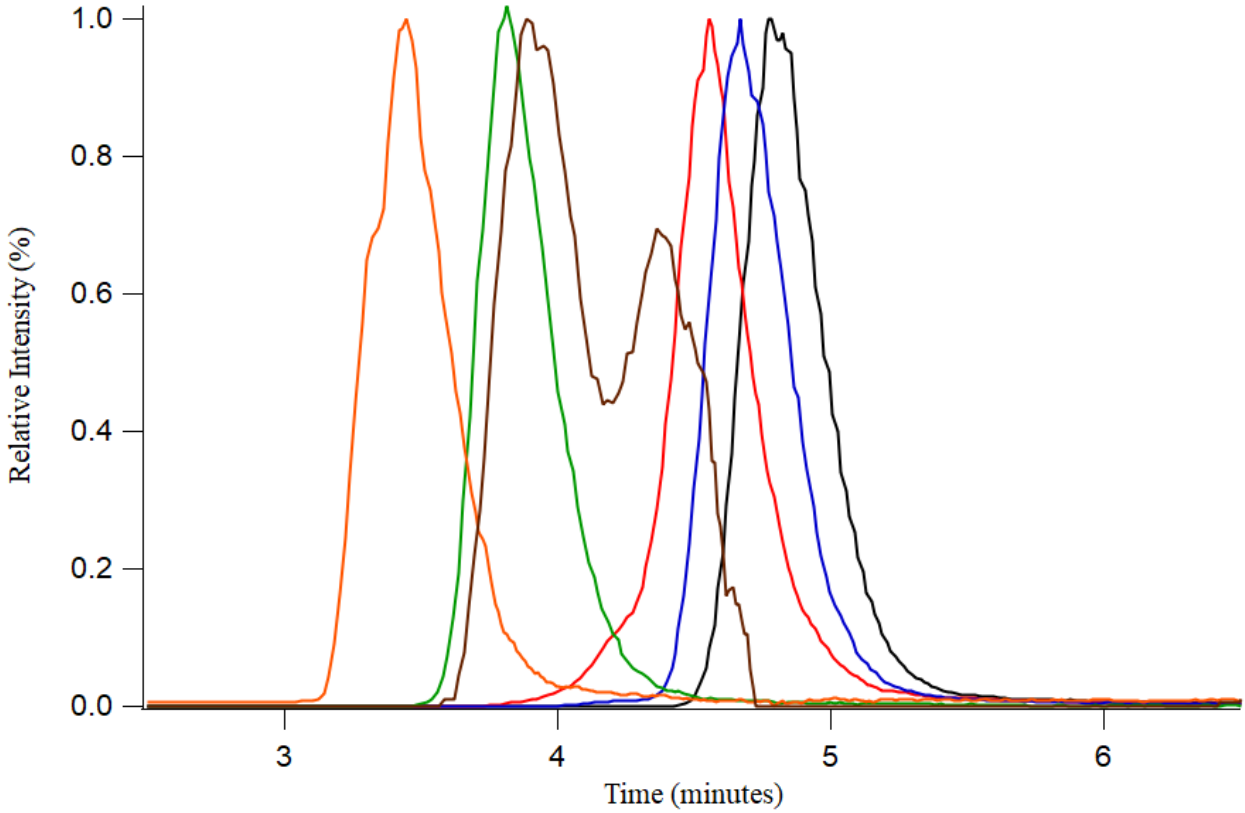

Figure 4.5 Hydroxy and hydroperoxy trilinolein XIC for mono-hydroxy ($C_{57}H_{98}O_6NH_4(O)$, m/z=912.67, black) di-hydroxy ($C_{57}H_{98}O_6NH_4(2O)$, m/z=928.76, red) and tri-hydroxy ($C_{57}H_{98}O_6NH_4(3O)$, brown). Mono-hydroperoxy ($C_{57}H_{98}O_6NH_4(2O)$, m/z= 928.76, blue), di-hydroperoxy ($C_{57}H_{98}O_6NH_4(4O)$, m/z=960.68, green) and tri-hydroperoxy ($C_{57}H_{98}O_6NH_4(6O)$, m/z=992.76, orange) are extracted within 10 ppm.

The ability to successfully resolve intact TAGs in a quick and reproducible method increases sample throughput. In the same method that intact TAGs are identified, oxidized TAG products can also be resolved and identified. It was important to distinguish between epoxy-TAG and hydroxy-TAG in a method that can be applied to a complex sample. Understanding that hydroxy products are more polar provides some additional information for specification of the two products.

4.3.2 Calibration Curves for TAG Degradation Products

Calibration curves are produced to understand signal response as TAG concentration changes. Initial curves were done using a concentration range of 0.001 ug mL^{-1} - 5 ug mL^{-1} for hydroxy trilinolein (Figure 4.6). There is no internal standard used for the extracted calibration curves, therefore signal response is approximate. The resulting calibration curves did not adhere to a linear fit, with data points at lower concentration's not aligning with higher concentrations. At this concentration range the data aligned with an polynomial fit (Figure 4.6, red). It is assumed that the formation of dimers and/or trimers happens readily between TAG molecules especially at elevated concentrations. Trimers and larger multimers would not be detected by the mass spectrometer because they are simply too heavy. The ability to form dimers increases as a function of concentration, where at high concentrations of TAG it is anticipated that some of the monomer ion is being generated from degradation of dimer within the mass spectrometer inlet. Therefore, there was seemingly a limit of saturation above 1 ug mL^{-1} (Figure 4.6). The "roll-off" of signal is likely due to the formation of multimers. They can still contribute to the signal since they can dissociate but it is 2 for 1 at best. At high enough concentrations the formation of micelles in solution might even be expected.

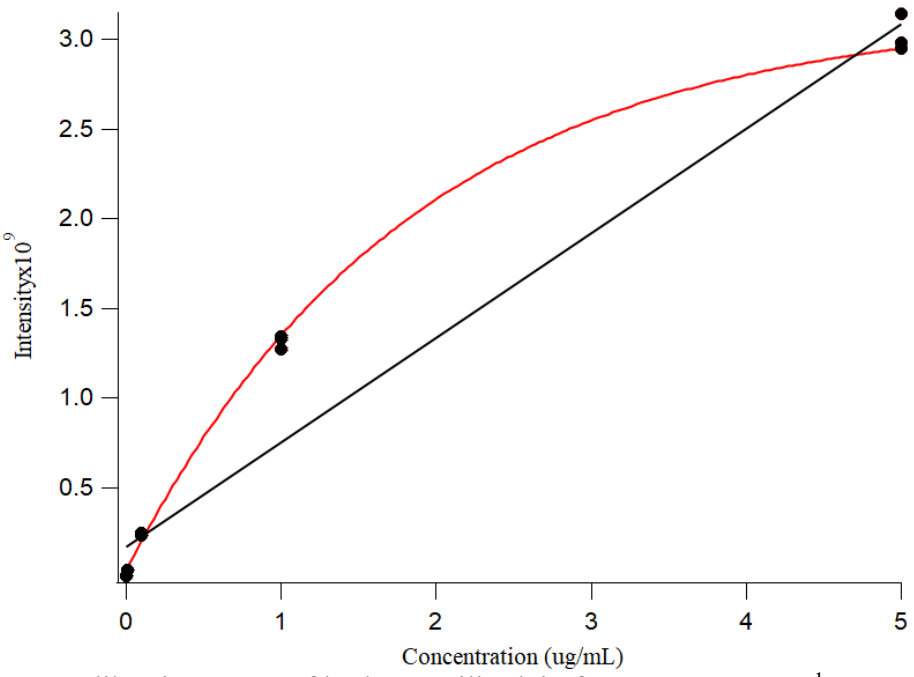

Figure 4.6 Calibration curve of hydroxy trilinolein from 0.001 ug mL^{-1} – 5 ug mL^{-1} where mono-hydroxy trilinolein, m/z 912.67 is extracted and plotted. The analysis was done in triplicate. Red-polynomial fit, black-linear fit.

Further investigation into a potential linear response was done at a lower concentration range of 0.001 ug mL^{-1} – 1.0 ug mL^{-1} (Figure 4.7). The signal response for the oxidized TAG was linear over a 1000-fold dynamic range (Figure 4.7). The ability to have a linear range at low concentrations is advantageous in the sense that small amounts of sample can be analyzed since high concentration samples can always be diluted. The limit of detection (LOD) can be calculated by multiplying the standard deviation of the blank or background signal by a factor of 3 and dividing by the slope of the linear equation. The LOD for hydroxy trilinolein is determined to be 24 pg mL^{-1}. The LOD for this study is much lower in comparison to the LOD resulted from GCMS analysis by Xia et al. (2017) and Mubiru et al. (2013) at 30 ug/g and 1.45 ug/g respectively. The lower LOD can be attributed to minimal sample preparation steps and the sensitivity of the LCMS. Sample carry over is common with LCMS where column flushing or blanks are

needed to clean the system. However, with TAGs and TAG oxidation products it is easy to get blanks as there is limited carry over and memory between samples, even after injecting high analyte concentrations.

Han et al. (2001) stated that longer chain lengths and a lower saturation index resulted in lower sensitivity of the TAG molecule in positive-ion ESI. However, signal responses for triolein (54:3) and trilinolein (54:6) resulted in nearly identical signals, with triolein being slightly higher. Comparing single responses between different oxidized trilinolein resulted in a 1.6-fold increase in signal response for hydroperoxy compared to hydroxy TAG (Figure 4.7). The linear range for hydroperoxy trilinolein ranges from 0.001 ug mL-1 – 0.5 ug mL^{-1}. The linear dynamic range is therefore 500-fold in comparison to hydroxy trilinolein at 1000-fold. The different responses for different oxidation products have not previously been described but are nonetheless important for quantitative analysis.

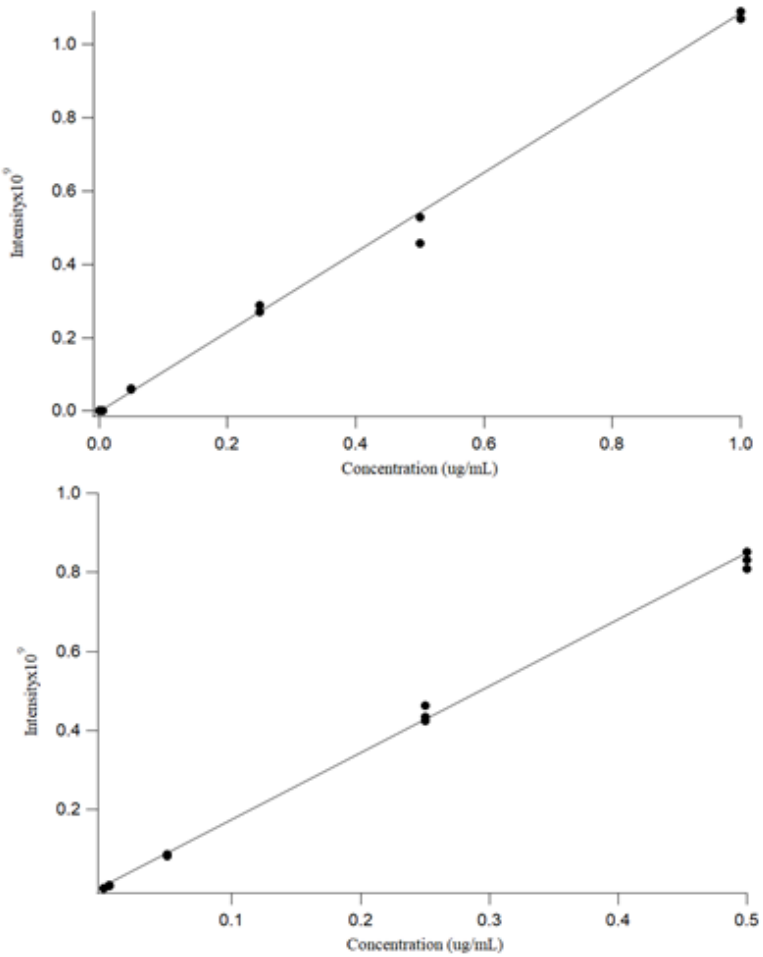

Figure 4.7 Hydroxy trilinolein at concentrations from 0.001 ugmL-1 to 1 ug mL-1, where m/z 912.786 is plotted from XIC less than 10 ppm (A). Hydroperoxy trilinolein at concentrations from 0.001 ugmL-1 to 1 ug mL-1, where m/z 928.762 is plotted from XIC less than 10 ppm (A).

4.4 CONCLUSION

A novel isocratic RPLC method using 95 % ethanol was successful in resolving intact TAG and TAG oxidation products. The 10-minute method easily resolved triolein and trilinolein standards. Furthermore, epoxy-TAG and hydroxy-TAG resolved as hydroxy products were determined to be more polar, earlier eluting compounds than epoxides. Isomeric species of tri-hydroxy were identified by incorporating MSMS to specify two different binding locations of the hydroxy products. This method further provided a low concentration linear regime with a LOD of 24 pg mL-1. Assuming high

concentrations of TAG in edible oil, the present method creates a large region of analytical space for the detection of oxidation products within complex samples.

CHAPTER 5 IDENTIFICATION OF TRIACYLGLYCEROL DEGRADATION IN CANOLA OIL USING ESI-LC-MSMS

5.1 INTRODUCTION

Edible oils and fats are essential components of the human diet for their contribution of essential fatty acids. An imbalance of oil and fat intake or increased intake of oxidized oil can lead to health issues such as coronary heart disease, obesity and others (Xu et al. 2018). Aside from negative health conditions, oxidized TAGs lead to the deterioration of foods in terms of flavour, smell and taste. Therefore, it is important to understand the composition of TAGs and TAG oxidation products that compose these edible oils (Gruneis et al. 2019). Multiple analytical methods have attempted the daunting task.

Lipid oxidation is a very complex process that facilitates formation of multiple oxidation products. The extent of lipid oxidation is dependent on temperature, atmospheric oxygen, light and the amount of double bonds (Petronilho et al. 2021). TAGs oxidize to hydroperoxide TAGs as the primary oxidation product which further oxidize to various secondary oxidation products (Kato et al. 2018). While the secondary oxidation products are responsible for negative health effects and deterioration of food quality, their formation proceeds through hydroperoxides, so the majority of oxidation studies have focused on the cause of their generation to limit deterioration (Zeb, 2010; Kato et al. 2018). More recently, a number of studies have looked at epoxides as potential markers for lipid oxidation as they were determined to be more detrimental to health and nutrition than other secondary oxidation products like hydroxides and aldehydes (Gruneis et al. 2019).

The majority of analytical methods for TAG analysis in oils used complicated LC gradients which are often time consuming and require complex solvent compositions.

Zeb (2010) implemented a more efficient LCMS method which incorporated a 35 minute isocratic method at 18 % isopropanol in methanol. They characterized the unoxidized oils by assigning DAG product ions and proposed FA distributions of TAGs (Zeb, 2010). Zeb (2010) also identified the position of double bonds within the TAG based on DAG product ions. Gruneis et al. (2019) focused on oxidized canola oil and margarine using a 30 minute LCMS gradient. They estimated concentrations for hydroperoxide products and epoxide products over a short heating period of 60 minutes. The confirmation of an epoxy product versus hydroxy or ketone was not stated nor were hydroperoxy groups distinguished from di-epoxy or di-hydroxy groups. FA positions on the glycerol backbone were not determined nor were the position of the oxidation groups. Previous studies focused on the oxidation products at one data point after heat was applied, but did not track the progression of oxidation over time (Zeb et al. 2010; Petronilho et al. 2021; Kato et al. 2017).

This study presents a longitudinal LC-ESI-MSMS method to resolve TAGs and TAG epoxy, hydroxy and hydroperoxy oxidation products simultaneously in canola oil. Improvements from prior work are made by reducing analysis time as well as eliminating the need for a separation step by limiting sample preparation to a single 100,000 fold dilution of the oil. Retention times and MSMS product ions from oxidized TAG standards are used to identify potential oxidation products in oxidized canola oil. Oxidation was monitored in real time as the heated oil sample was analyzed periodically over 21 days to achieve a better understanding of the oxidation taking place at specific time points.

5.2 EXPERIMENTAL

5.2.1 Materials

Compliments brand "100% Pure Canola Oil" was used. Ammonium acetate and formic acid were purchased from Sigma-Aldrich and used in the LC buffers at 0.1 mM and 0.01 % respectively. 95% ethanol from Greenfield Global was used for the LC mobile phase and sample dilution solvent.

5.2.2 Mass Spectrometry

Mass spectrometry detection for LCMS analysis was performed using a high-resolution/accurate mass (HR/AM) quadrupole-orbitrap (Q-OT), from Thermo-Fisher Scientific (San Jose, CA). Instrumental details used in this study are the same as described in Chapter 2, Table 2.3. HR/AM MS detection is the method of choice for the complex canola sample to assign accurate molecular weight and molecular formulas to TAG species. The L-QIT MS used in Chapter 2 was also incorporated in this chapter for MS^3 analysis. The MS parameters used for the present study are the same as those presented in Chapter 2, Table 2.2.

5.2.3 Liquid Chromatography

The details of the high performance liquid chromatographic (HPLC) methodology used in this study are given in Table 5.1. The liquid chromatography platform used in this study was an Agilent 1260 Infinity II Quaternary LC (Agilent Technologies, Santa Clara, CA). A 10 minute 95 % ethanol (EtOH) with 0.1 % formic acid and 0.1 mM ammonium acetate, isocratic method was used for TAG analysis. Reversed-phase chromatography was used with an Avantor® HPLC C8 column. The same LC method and column was used for the duration of experimental procedures in this Chapter.

Table 5.1 Agilent 1260 Infinity II, liquid chromatography parameters used in this study.

Parameter	Value
Mobile phase flow rate	40 uL min^{-1}
Solvent A	95 % EtOH, 0.1mm AA, 0.1 % Formic acid
Isocratic flow	100 % A
Column chemistry	C8
Column diameter	1.0 mm
Column length	15.0 cm
Packing diameter	5 uM
Column temperature	RT
Injection volume	5 uL
Column back pressure	~1500 psi
Mobile phase time	1.56 minutes
Column manufacturer	Avantor® HPLC/UHPLC Columns
Column distributer	VWR
Column catalog number	88394
LC sample Vials (Low-Bind)	Waters Quan Recovery, 12 x 32 mm

5.2.4 Sample preparation

100 uL of *Compliments* brand Canola oil was pipetted into one, 1.5 mL LoBind Eppendorf tube. The tube was placed on a heating block set to 60°C with the Eppendorf caps open to allow oxygen in. The sample was tested after 24 hours (day 1), 48 hours (day 2), 72 hours (day 3), 96 hours (day 4), 102 hours (day 4), 120 hours (day 5), 144 hours (day 6), 168 hours (day 7), 240 hours (day 10), 360 hours (day 15) and 504 hours (day 21). The dilution steps were as follows: 1uL of stock canola into 999 uL EtOH (1000-fold dilution), creating Sample 1 and then vortexed for 30 seconds. 10 uL of Sample 1 was diluted into 990 uL EtOH (100-fold dilution), creating Sample 2 and vortexed for 30 seconds. 500 uL of Sample 2 was pipetted into a 2 mL glass sample vial from Canadian Life Sciences. The vial was then placed in the LC-autosampler which was set to 15°C for analysis.

5.3 Results and Discussion

5.3.1 Identification of Unoxidized TAG in Canola Oil

Our prior work in Chapter 4 has demonstrated the use of a 10-minute isocratic method using 95% ethanol to effectively separate TAG standards and TAG oxidation standards in a quick and efficient LCMS method. The previous tools for identification and quantification of TAG oxidation products were applied to a complex sample of canola oil that was composed of many different TAG species. TAG is the main component of edible oils, and therefore it can be assumed that there is an incalculable amount of isomers of TAG oxidation products within oxidized canola oil. A focus was put on hydroxy, epoxy and hydroperoxy oxidation products due to prior analysis with these standards.

The first step in characterizing the oil sample was to analyze it prior to any heating or degradation, at day 0. Kato et al. (2018) found that the main fatty acids in unoxidized canola oil were oleic acid (18:1), linoleic acid (18:2) and linolenic acid (18:3). It was assumed that the majority of TAG in the unoxidized sample was composed of some combination of the three main fatty acids. LCMS analysis of the day 0, unheated canola oil lead to the identification of twelve intact TAG species with signal intensities greater than 1E7 (Figure 5.1). Using HR/AM, predicted empirical formulas for each TAG were matched within 10 ppm. The most abundant TAG molecules were identified as 54:3, 54:4, 54:5, 54:6 and 54:7 TAG. Following the expected patterns considering polarity due to number of double bonds (DB), 54:7 was the earliest eluting molecule at a retention time of 5.64 minutes and 54:3 was the latest at 6.94 minutes (Figure 5.1, A). TAGs at m/z 874 and 876 represented 52:3 and 52:2 TAG within a 10 ppm window. TAG 52:3 eluted at an earlier retention time than 54:3 TAG and 52:2 eluted earlier than

54:2 indicating shorter FA chain lengths within the TAG cause the molecule to be more polar (Han et al. 2021). TAGs with longer FA chains were identified at m/z 928, 930 and 932 and likely represented 56:3, 56:2 and 56:1 TAG, respectively. The three TAGs eluted slightly later than the TAGs with the same double bond distribution and shorter chain lengths (Figure 5.1,B). It should be noted that only one of the three fatty acid chains were longer/shorter and it is assumed that having 2 or 3 longer/shorter fatty acids within the TAG would affect the retention more. The order of elution of the observed TAG species coincides with the results concluded by Zeb et al. (2010) in their analysis of intact TAG of canola and sunflower oil.

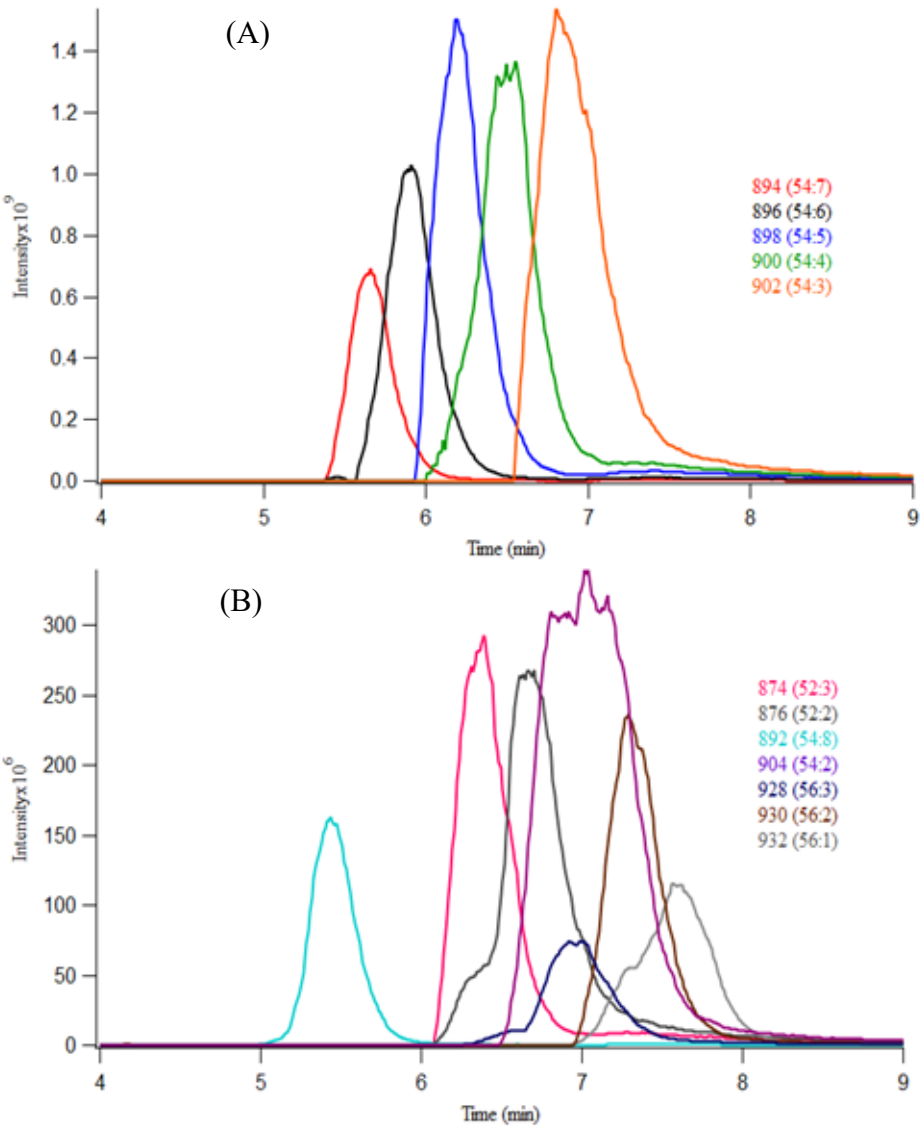

Figure 5.1 Endogenous TAG identified in un-oxidized canola oil analyzed using a 10 minute 95% EtOH isocratic method coupled to a HR/AM Q-OT MS. Panel (A) displays the 5 most abundant TAG identified, where the colour corresponds to that in the legend. Panel (B) highlights 7 less abundant identified TAGs.

A peak at 6.82 minutes with a m/z value of 902.767 was the most abundant within the sample (Figure 5.1). A proposed empirical formula of $C_{57}H_{104}O_6NH_4$ matched within 5 ppm to the experimental spectra and suggested a 54:3 TAG, the same empirical formula as the triolein standard. In previous investigation using TAG standards, we determined

triolein to elute at a retention time of 7.30 minutes. The triolein standard had a known fatty acid distribution of (18:1/18:1/18:1), where as in canola oil, although the m/z and empirical formula match with triolein, the fatty acid distribution is not necessarily homogenous. Direct comparison of the two chromatograms shows a slightly earlier eluting peak at 6.97 minutes from the extracted 54:3 ion of canola. Formerly, we determined that increasing the number of double bonds within a TAG results in an earlier retention time. With identification of the empirical formula, it is known that there are three double bonds in some distribution within the TAG. It can be proposed that multiple double bonds within one chain compared to an even distribution can contribute to the TAG being more polar and resulting in a shorter retention time as observed with the 54:3 TAG of canola. Therefore, it can be assumed that 54:3 TAG of canola represents multiple isomers composed of different FA distributions. A previous study on the composition of canola oil defines 54:3 TAG as 18:1/18:1/18:1 or 18:0/18:2/18:1, based on their product ions (Zeb et al. 2010).

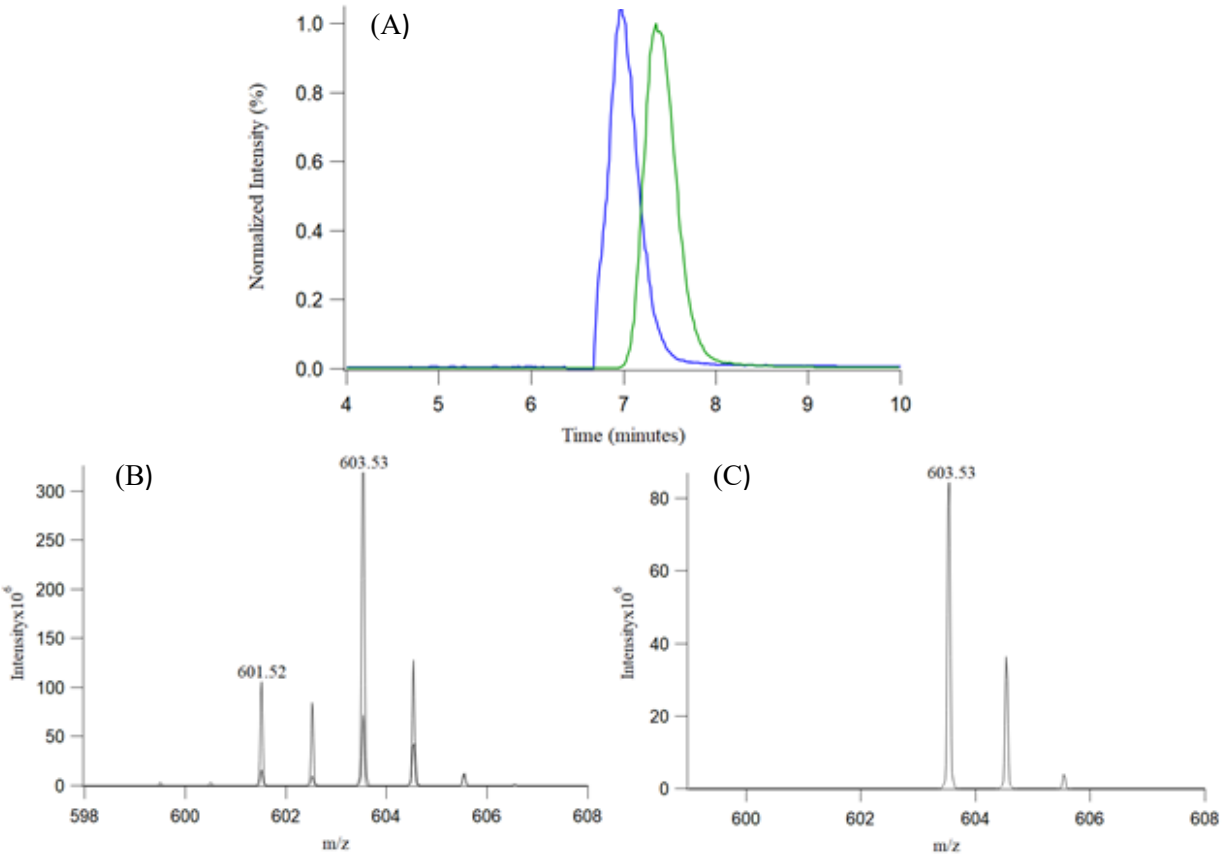

Figure 5.2 Comparison in panel (A) of 54:3 TAG of un-oxidized canola oil (blue) to triolein standard (green), analysis with Q-OT MS detection in Full MS scan mode detecting $[TAG+NH_4]^+$ ions. Tandem-MS targeted precursor m/z 902 at a CE of 30 eV for both TAG where product ions are shown in panel (B) of 54:3 TAG of canola oil and (C) triolein standard.

Applying tandem-MS provides a better qualitative comparison of the two TAG molecules. An applied collision energy of 30 eV on precursor triolein monomer ion (902 m/z) resulted in a single DAG product ion of 603 m/z (18:1/18:1), which represents the loss of 18:1 fatty acyl chain as expected (Figure 5.2, B,C). Targeting precursor m/z 902 in canola oil yielded two product ions of m/z 603 and m/z 601 (Figure 5.2, B,D). m/z 601 represented a DAG with three double bonds, confirming the presence of isomers in 54:3 TAG of canola oil, where the 54:3 TAG molecule is likely composed of some combination of 18:0, 18:1, 18:2 and 18:3. Since the product ion m/z 601 had three double

bonds, it means an 18:0 FA was lost. Therefore, the remaining DAG ion is an 18:1/18:2 DAG or 18:3/18:0 DAG. The challenge with TAG analysis is that even the product ion at m/z 603 does not mean that one of the isomers is (18:1/18:1/18:1). However, previous analysis on canola oil composition determined the main component of canola oil is oleic acid (18:1) (Guan et al. 2015). Therefore, we can assume that the majority of m/z 603 is (18:1/18:1), with less contribution from (18:2/18:0). Linoleic acid (18:2) was determined to be the second most abundant FA in canola by Guan et al. (2015), with stearic acid (18:0) and linolenic acid (18:3) present in slightly lower amounts. Presumably, the presence of different FA distributions of 54:3 causes the shift in retention time in comparison to triolein standard. It should also be noted that the precision of retention times could be affected by an automated start on the LC instrument. Although minor, this could have led to variability in the retention time.

To further investigate the FA distribution of 54:3 TAG of canola, direct-infusion MS^3 analysis was done using the L-QIT MS. Our analysis switched between the Q-OT and L-QIT due to the MS^n function of the L-QIT that is not present on the Q-OT. Using this MS, m/z 603 DAG product ion of canola was targeted as the precursor ion to undergo further fragmentation. Resulting MAG product ions were identified at m/z 267.24 (18:0), m/z 265.25 (18:1), m/z 263.64 (18:2) (Figure 5.3, A). Knowing the MAG ions that compose m/z 603 DAG, it was concluded that the DAG is composed of the two isomers (18:1/18:1) and (18:2/18:0).

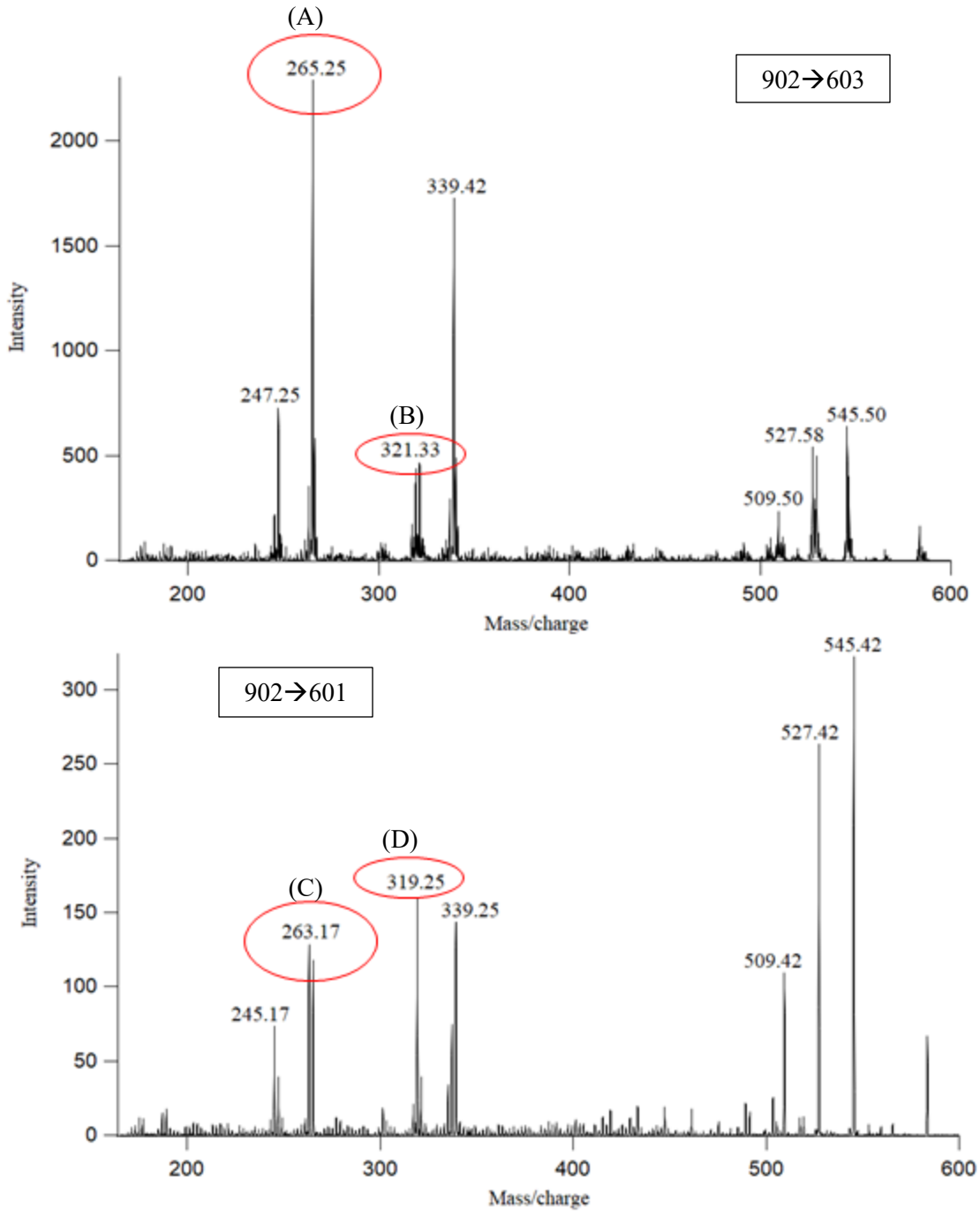

Figure 5.3 Un-oxidized canola oil analyzed on the LQIT MS using MS^3 to target 54:3 TAG. The top panel displays fragment ions from m/z 902→603 fragmentation channel to produce MAG product ions m/z 265.25 (18:1) (A) and m/z 321.33 $C_{22}H_{37}O_2$ (B), which contains the glycerol backbone. In the bottom panel, MAG product ions are highlighted as m/z 263.17 (18:2) with m/z 265.25 (18:1) present as well beside m/z 263 (C) and m/z 319.25 $C_{22}H_{35}O_2$ (D).

Targeting m/z 601 product ion using MS^3 analysis resulted in m/z 263.17 (18:2) MAG ion as the most abundant with comparable amounts of m/z 265.25 (18:1) MAG ion (Figure 5.2). There is not an identifiable ion at m/z 261.20 (18:3) indicating that m/z 601 precursor has to be composed of 18:2/18:1. This also indicates that this isomer of 54:3 TAG is of the form (18:2/18:1/18:0). Prior identification of 54:3 in canola oil was based on MSMS analysis and did not use MS^3. The ability to identify the specific MAG ions allows for the isomers to be more confidently determined.

A complete list of identified TAG in un-oxidized canola oil is provided where empirical formulae are matched within a 10 ppm window (Table 5.2). Tandem-MS was done for each TAG using a CE of 30 eV to identify DAG product ions. The FA lost was identified for each DAG product ion.

Table 5.2 Endogenous TAG of canola oil with MSMS product ions.

Endogenous TAG (m/z) <10 ppm	Empirical formula	Carbon # and Unsaturation #	Retention time (tR), (min)	Tandem MS fragment ions *	FA dissociated
874.7858	$C_{55}H_{100}O_6NH_4$	(52:3)	6.38	575.52, (M-$C_{18}H_{34}O_2NH_3$) 603.53, (M-$C_{16}H_{30}O_2NH_3$) **577.50, (M-$C_{18}H_{32}O_2NH_3$)** 601.52, (M-$C_{16}H_{32}O_2NH_3$)	(C18:1) (C16:1) (C18:2) (C16:0)
876.8015	$C_{55}H_{102}O_6NH_4$	(52:2)	6.66	**577.52, (M-$C_{18}H_{34}O_2NH_3$)** 603.53, (M-$C_{16}H_{30}O_2NH_3$) 575.50, (M-$C_{18}H_{32}O_2NH_3$) 601.52, (M-$C_{16}H_{32}O_2NH_3$)	(C18:1) (C16:1) (C18:2) (C16:0)
892.7389	$C_{57}H_{94}O_6NH_4$	(54:8)	5.44	595.47, (M-$C_{18}H_{32}O_2NH_3$) 597.49, (M-$C_{18}H_{30}O_2NH_3$) **599.50, (M-$C_{18}H_{28}O_2NH_3$)**	(C18:2) (C18:3) (C18:4)
894.7545	$C_{57}H_{96}O_6NH_4$	(54:7)	5.64	595.47, (M-$C_{18}H_{34}O_2NH_3$) 597.50, (M-$C_{18}H_{32}O_2NH_3$) **599.50, (M-$C_{18}H_{30}O_2NH_3$)** 601.51, (M-$C_{18}H_{28}O_2NH_3$)	(C18:1) (C18:2) (C18:3) (C18:4)
896.7702	$C_{57}H_{98}O_6NH_4$	(54:6)	5.93	597.49, (M-$C_{18}H_{34}O_2NH_3$) **599.50, (M-$C_{18}H_{32}O_2NH_3$)** 601.52, (M-$C_{18}H_{30}O_2NH_3$) 603.53, (M-$C_{18}H_{28}O_2NH_3$)	(C18:1) (C18:2) (C18:3) (C18:4)
898.7858	$C_{57}H_{100}O_6NH_4$	(54:5)	6.21	597.49, (M-$C_{18}H_{36}O_2NH_3$) **599.50, (M-$C_{18}H_{34}O_2NH_3$)** **601.52, (M-$C_{18}H_{32}O_2NH_3$)** 603.53, (M-$C_{18}H_{30}O_2NH_3$)	(C18:0) (C18:1) (C18:2) (C18:3)
900.8015	$C_{57}H_{102}O_6NH_4$	(54:4)	6.50	599.50, (M-$C_{18}H_{36}O_2NH_3$) **601.50, (M-$C_{18}H_{34}O_2NH_3$)** 603.53, (M-$C_{18}H_{32}O_2NH_3$) 605.54, (M-$C_{18}H_{30}O_2NH_3$)	(C18:0) (C18:1) (C18:2) (C18:3)
902.8171	$C_{57}H_{104}O_6NH_4$	(54:3)	6.82	601.52, (M-$C_{18}H_{34}O_2NH_3$) **603.53, (M-$C_{18}H_{32}O_2NH_3$)**	(C18:1) (C18:2)
904.8328	$C_{57}H_{106}O_6NH_4$	(54:2)	7.02	601.52, (M-$C_{18}H_{36}O_2NH_3$) **603.53, (M-$C_{18}H_{34}O_2NH_3$)** 605.55, (M-$C_{18}H_{32}O_2NH_3$)	(C18:0) (C18:1) (C18:2)
928.8328	$C_{59}H_{106}O_6NH_4$	(56:4)	6.97	599.50, (M-$C_{20}H_{40}O_2NH_3$) 601.52, (M-$C_{20}H_{38}O_2NH_3$) 603.53, (M-$C_{20}H_{36}O_2NH_3$) 627.50, (M-$C_{18}H_{34}O_2NH_3$) **629.55, (M-$C_{18}H_{32}O_2NH_3$)** 631.57, (M-$C_{18}H_{30}O_2NH_3$)	(C20:0) (C20:1) (C20:2) (C18:1) (C18:2) (C18:3)
930.8484	$C_{59}H_{108}O_6NH_4$	(56:3)	7.28	601.52, (M-$C_{20}H_{40}O_2NH_3$) 603.53, (M-$C_{20}H_{38}O_2NH_3$) **631.56, (M-$C_{18}H_{34}O_2NH_3$)** 633.58, (M-$C_{18}H_{32}O_2NH_3$)	(C20:0) (C20:1) (C18:1) (C18:2)
932.8641	$C_{59}H_{110}O_6NH_4$	(56:2)	7.61	603.53, (M-$C_{20}H_{38}O_2NH_3$) 605.54, (M-$C_{20}H_{36}O_2NH_3$) 631.57, (M-$C_{18}H_{34}O_2NH_3$) **633.58, (M-$C_{18}H_{32}O_2NH_3$)**	(C20:1) (C20:2) (C18:1) (C18:2)

*Bold = most abundant product ion.

Targeting precursor ion m/z 874 showed the loss of (18:1) to result in DAG m/z 575.50 composed of (16:0) and (18:2). The loss of (18:2) is highlighted by DAG product

ion m/z 577.52, which is composed of (16:0) and (18:1). DAG ion m/z 577.52 was the most abundant product ion, indicating 18:2 is positioned on *sn*-1/*sn*-3, and FA 18:1 was positioned on *sn*-2, resulting in lower amounts of product ion m/z 575.50. Identification of multiple product ions for each TAG species highlights the complexity of the oil sample.

TAG within canola oil were identified by Guan et al. (2011) who also found 54:3 TAG as the most abundant TAG within un-oxidized oil. Their analysis was not able to provide any data using tandem-MS; therefore, the fatty acid composition of identified TAG molecules was limited to intact mass and prior FA analysis done by GC. The present method is able to gather intact LCMS data and tandem-MS data at the same time, in a short isocratic method, increasing sample throughput. Application of MS^3 analysis by infusion can be done to further target known TAG molecules.

Kalo et al. (2006) studied the composition of MAG, DAG and TAG molecules in canola oil where they identified a number of 52- and 54- carbon TAGs. They also included MSMS analysis that identified some of the same product ions as the present study. However, their analysis did not highlight the potential isomers of certain intact TAGs. For example, the dissociation of (18:4) from 54:8 TAG resulted in the most abundant DAG product ion of m/z 599.50 (Table 5.2). Knowing the molecule is composed of 18:2, 18:3 and 18:4 FA molecules, one of the TAG isomers must be 18:4/18:2/18:2. Kalo et al. (2006) only identify 18:3/18:2/18:3 as the structural composition of 54:8 TAG. Zeb et al. (2010) identified many of the same intact TAG molecules and highlighted product ions. This study did identify isomers of 54:3 and 54:6 TAG, but failed to identify isomers for other intact TAGs including 52:3 and 54:2 TAG.

The lack of referenced isomers could be attributed to low signal intensities for these molecules, as they were less abundant than 54:3 and 54:6 TAG. Both studies agree in general with 54:3 TAG being the most abundant TAG in canola oil.

5.3.2 Thermal Oxidation of TAG in Canola Oil

Canola oil was heated at 60°C over a period of 21 days where it was sampled periodically. An untargeted analysis of canola oil was done to identify changes between the unoxidized canola oil sample and the canola oil sample after heating at 60°C for 24 hours and after 15 days. Base peak (BP) chromatograms were extracted where there was a notable difference in the base peak retention profile between the three time points (Figure 5.4). Prior LCMS analysis of TAG oxidation products required the use of a Sep-Pak separation step, to concentrate the oxidation products as they are often present at low levels in comparison to intact TAG (Gruneis et al. 2019). The initial untargeted analysis was done to see if oxidation products could be identified above the baseline signal without the need for separation. The ability to eliminate the extra sample preparation step not only saves analysis time but also reduces the risk of contaminating or deteriorating the sample.

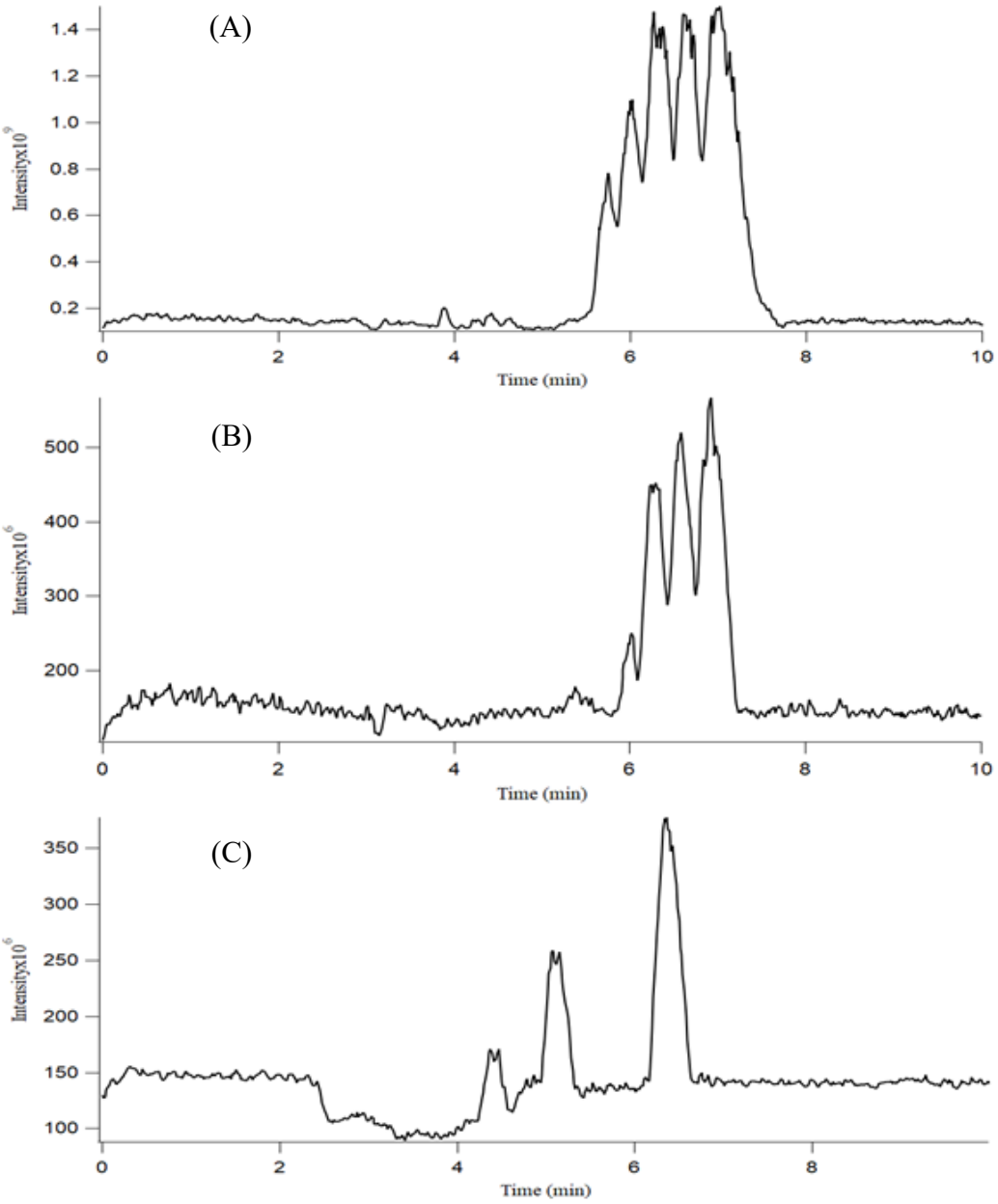

Figure 5.4 Base peak chromatograms of un-oxidized canola oil (A), canola oil heated (60°C) for 24 hours (B) and heated for 15 days (C).

Unoxidized canola produced a large cluster of peaks between 5 and 8 minutes and represented the twelve TAGs previously identified (Figure 5.4, A). After heating the sample for 24 hours, the same cluster of endogenous TAG decreased in signal intensity (Figure 5.4, B). A decrease in intact TAG signal as temperature was applied was

expected as the unsaturated TAGs began to oxidize (Figure 5.4, B). However, at 24 hours there was insufficient oxidized TAG to appear on the base peak chromatogram. Oxidized TAGs are expected to elute earlier than un-oxidized TAG. After 15 days there is a single peak present at ~6.5 minutes, representing 54:3 and 54:4 TAG. The two un-oxidized TAG molecules still appeared at high signal intensities; however, compared to their starting points in panel (A), they have decreased by a factor of approximately 4. Although the other intact TAGs are not identified above baseline signal, it does not mean they are not present in the sample. A targeted analysis of the m/z for the intact TAGs would show the corresponding peaks but at low signal intensities. The ability to identify a decrease in intact TAG molecules is not often noted in previous work. Appearing in the base chromatogram at Day 15 was two peaks between 4-5.25 minutes. These two peaks represented mono- and di-oxygenated 54:3 TAG which are the most abundant oxidation products identified in the present study. Considering oxidized TAG could be identified by BP chromatograms, it was not necessary to include a separation step. Methods often focus on either intact TAGs or oxidized TAGs as they are required to separate them to concentrate oxidized TAGs (Gruneis et al. 2019; Neff et al. 1998). The ability to look at both TAG molecules in the same method provides a simple and quick analysis.

A focus was placed on potential oxidation products of 54:3 TAG, due to it being the most abundant TAG in canola oil. It is assumed that the other TAG molecules previously identified will follow similar trends to those identified for 54:3. Predicted oxidation products for 54:3 TAG were generated for up to six oxygen groups (Table 5.3). The predicted m/z values can be used as search targets in the heated canola sample using

the proposed LC-MS conditions, where oxidized TAG was detected as $[M+NH_4]^+$ adduct ions, which were also selected as precursor ions for MS/MS analysis.

Table 5.3 Predicted m/z values and empirical formulas for mono-, di-, tri-, tetra-, penta- and hexa-oxygenated products onto 54:3 TAG.

902.8171	$C_{57}H_{105}O_6NH_3$	918.8120	O	$C_{57}H_{105}O_6NH_3O$
		934.8069	2 x O	$C_{57}H_{105}O_6NH_3(2O)$
		950.8018	3 x O	$C_{57}H_{105}O_6NH_3(3O)$
		966.7967	4 x O	$C_{57}H_{105}O_6NH_3(4O)$
		982.7916	5 x O	$C_{57}H_{105}O_6NH_3(5O)$
		998.7866	6 x O	$C_{57}H_{105}O_6NH_3(6O)$

After 24 hours of heating, there was no obvious oxidation peaks present in the BP chromatograms (Figure 5.4). This is because the BP chromatogram shows the signal for the most intense peak in each spectrum, where the oxidation products were not the most intense at this point. However, the exact m/z values (Table 5.3) can be used to search for the expected oxidation products. After 24 hours, mono- and di-oxygen products were identified. Searching for the other predicted oxidation products (Table 5.3) did not lead to successful identification at 24 hours. Mono-oxygen was identified with a signal intensity of 3.95e6 and di-oxygen was identified at 3.49e6. In attempts to provide qualitative analysis of the mono- and di-oxygen products, tandem-MS was done on precursor ions m/z 918 (mono-) and m/z 934 (di-) using a CE of 30 eV. Precursor m/z 918 produces DAG fragment ions m/z 601.52 and m/z 603.53. There was no DAG product ion with the oxygen product remaining. Previously, when investigating TAG degradation standards in Chapter 2, the hydroxy oxygen was determined to leave at applied collision energies, failing to produce DAG products with the hydroxy product remaining. This finding was unlike what was found with overlapping m/z mono-epoxide products, where the epoxide

group remained intact on the DAG product ion. Therefore, a tentative ID of mono-hydroxy 54:3 can be made at 24 hours.

When targeting the di-oxygen precursor m/z 934 at 24 hours, two peaks appeared in the PRM channel at 4.47 minutes and 7.37 minutes (Figure 5.5). Product ions arising from the peak at 4.47 included DAG m/z 603.54 and DAG m/z 615.51. We previously determined that mono-hydroperoxy products fragment into a protonated DAG ion without oxygens attached and a DAG ion with one oxygen attached (Figure 5.6).

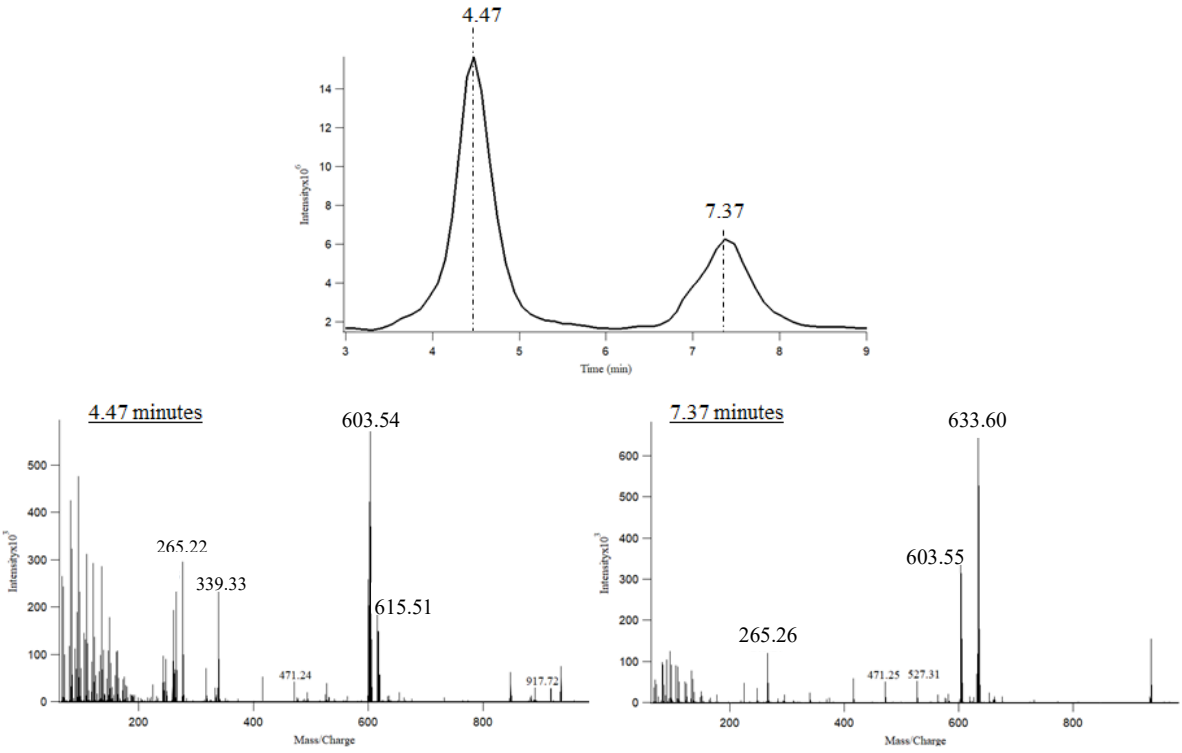

Figure 5.5 MSMS SIM channel of precursor ion 934 at CE=27 eV. A peak at 4.47 minutes represents two oxygen atoms bonded within 54:3 TAG and produces fragment ions 603.54 [M+NH_4+2O-FA-NH_3-2O] and 615.51 [M+NH_4+2O-FA-NH_3- O]. The peak at 7.37 minutes represents endogenous 56:1 TAG ion with corresponding fragment ions 603.55 [M+NH_4-C_{20} FA-NH_3] and 633.6 [M+NH_4-C_{18} FA-NH_3].

The mechanism for hydroperoxide decomposition is not agreed on in the literature with several different proposed mechanisms (Gruneis et al. 2019; Petronilho et al. 2021;

Kato et al. 2017). Based on the findings in the present study, the proposed mechanism agrees with that of Gruneis et al. (2019) where the initial decomposition step is the hydroperoxide group forming an epoxide (Figure 5.6, B). A similar formation of an epoxide from hydroperoxide decomposition was stated by Zeb, (2012) when looking at hydroperoxide products of Camelia oil. The loss of an un-oxidized FA chain results in the oxidized DAG ion at m/z 615, which contains the epoxide group (Figure 5.6, C). The other DAG ion arises from the dissociation of the FA with the epoxide group, resulting in the protonated DAG at m/z 603 (Figure 5.6, D). Hydroperoxides do not result in DAG ions with two oxygens remaining. The CE required for dissociation of an acyl chain is presumably greater than the energy required for degradation of the hydroperoxide group itself; therefore, the likelihood of an acyl chain dissociating without degrading the hydroperoxy group is low. Our previous results using MSMS also show di-epoxide and di-hydroxy products have a DAG ion with two oxygens. Therefore, it is predicted that the identified oxidation product at m/z 934 after 24 hours represents mono-hydroperoxy 54:3 TAG.

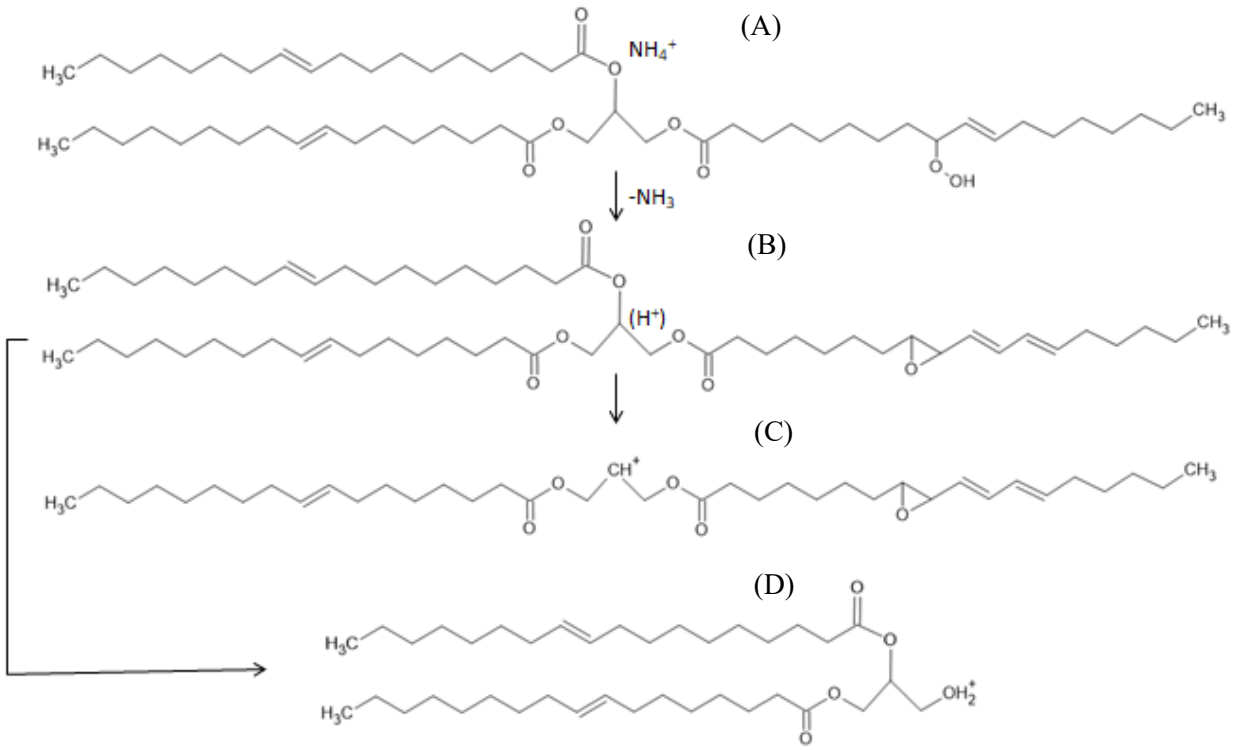

Figure 5.6 Proposed mechanism for the decomposition of hydroperoxy triolein (A) to form protonated epoxy TAG (B), epoxy DAG (C) and protonated DAG (D).

The peak at 7.37 minutes resulted in two DAG product ions m/z 603.55 and m/z 633.6. It was determined to be a small amount of 56:1 unoxidized TAG with a m/z of 934 (Figure 5.5). DAG product ions represented the loss of 20:0 FA (m/z 603) and the loss of 18:1 fatty acyl chain (m/z 633) (Figure 5.5). This unoxidized TAG was not included in the previous description of unoxidized TAG because it was present at trace levels.

Gruneis et al. (2019) used tandem-MS analysis on 54:5 and 54:3 TAG of canola oil with a focus on hydroperoxide products. Their results showed similar DAG fragment ions to those resulted from di-oxygenated TAG at 24 hours of heating. Gruneis et al. (2019) identified DAG product ions with two oxygens remaining although they did not include a mechanism for the formation of that DAG ion. The different product ions could

be due to the different heating temperatures, where their canola sample was heated at 180 °C compared to the present study at 60 °C.

5.3.3 Mono-oxygenated Degradation Products of 54:3 TAG

LC-MS has the ability to identify sample components at multiple time points throughout thermal treatment of the sample. For example, extracting mono-oxygenated 54:3 TAG (m/z 918.81) from canola collected at different sampling times highlighted important changes within the chromatogram (Figure 5.7). At 72 hours, the extracted ion chromatogram (XIC) of m/z 918.81 showed another peak beginning to appear at a later retention time of ~5.6 minutes. At 96 hours the two peaks are present at the same intensity. After 102 hours, the later eluting peak dominates the XIC as shown at 504 hours (Figure 5.7).

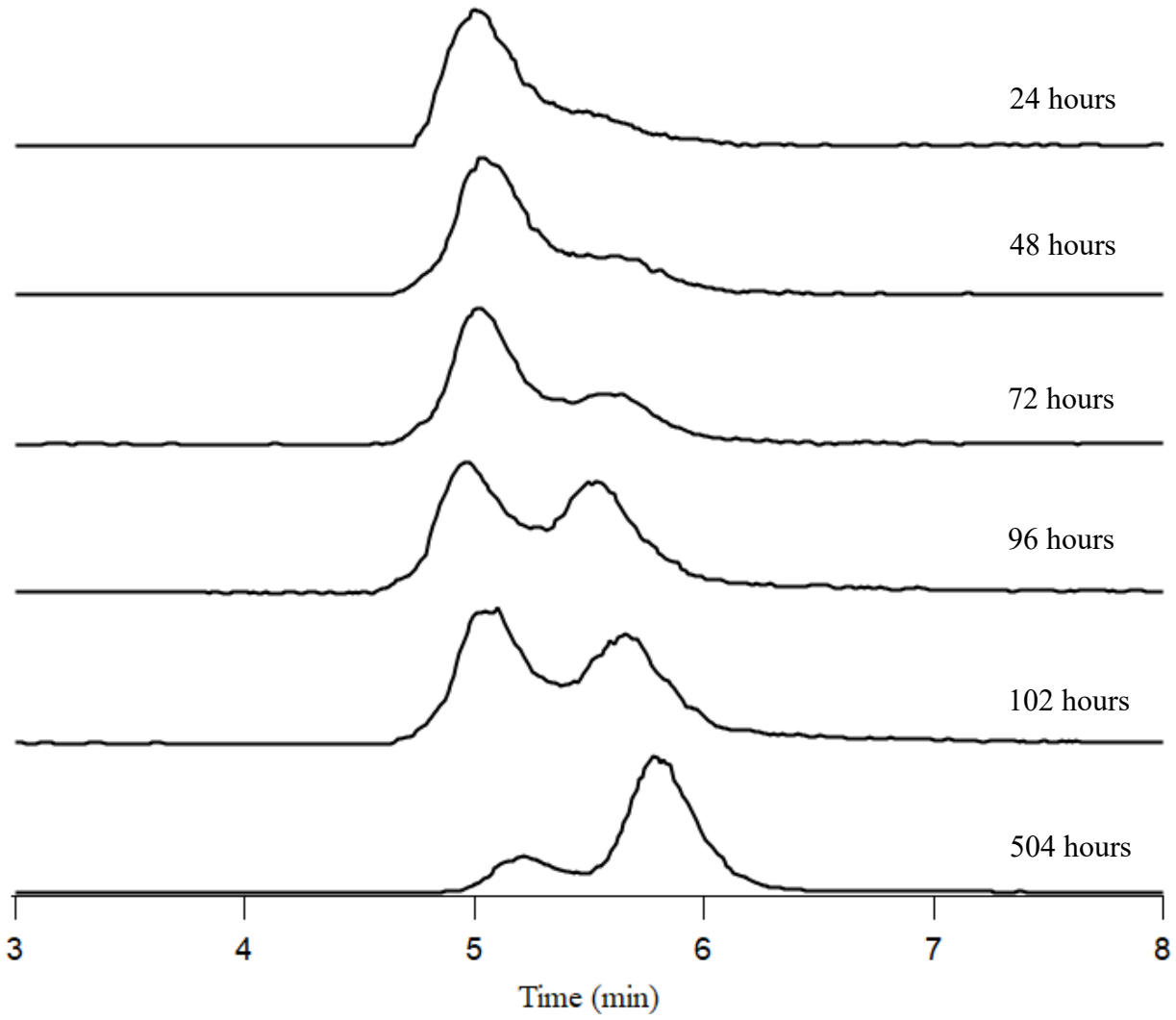

Figure 5.7 XIC of mono-oxygenated (54:3) after 24 hours, 48 hours, 72 hours, 96 hours, 102 hours and 504 hours. Mono-oxygenated 54:3 was extracted at m/z 918.81 within a 10 ppm window.

The appearance of a second peak increasing over time hinted at potentially different oxidation groups forming on the TAG. It is important to note that the appearance of different chromatographic peak shapes during thermal treatment of an oil sample has not previously been reported. Tandem-MS was applied to precursor m/z 918 to generate a qualitative understanding of the TAG structure at the two peaks (Figure 5.8). After 24 hours, m/z 918 was tentatively identified as hydroxy 54:3 TAG. The

appearance of a second peak at a later retention time produced two DAG product ions different from the earlier eluting peak. At a retention time of 5.8 minutes, product ions m/z 603.55 and m/z 619.54 were produced. Prior investigation into epoxide standards in Chapter 2 showed MSMS products of a DAG ion with the epoxide and a protonated, un-oxidized DAG ion. The protonated unoxidized DAG resulting from MSMS of epoxide standards was 2 m/z units higher than the DAG product ion from hydroxy standards. As well, we previously showed epoxide oxidation products are less polar (later eluting) compounds than hydroxides (earlier eluting). Therefore, using tandem-MS and previously determined retention times, it is anticipated that the second mono-oxygen containing peak forming after 72 hours is an epoxide product. Epoxides are said to form from degradation of hydroperoxides (Zeb, 2012 & Neff et al. 1998 & Gruneis et al. 2019 & Kato et al. 2017). Thus, it is assumed that after some amount of hydroperoxides had formed, their degradation begins at an increased rate, leading to the appearance of epoxide products. Although epoxides are greater in relative abundance compared to hydroxides after 102 hours, over all signal intensity still increases for hydroxides. Based on these facts, it can be assumed that some degradation of hydroperoxides is also leading to continued hydroxide formation.

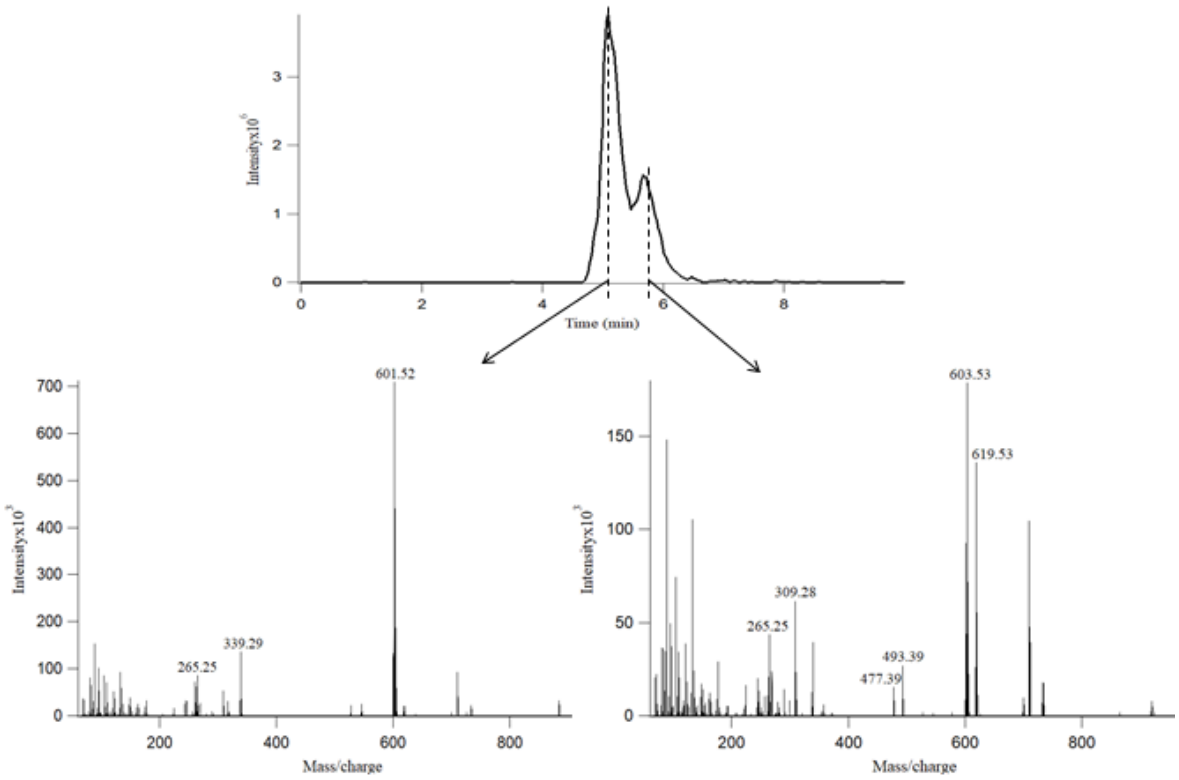

Figure 5.8 m/z 918.81 mono-oxygen product after 96 hours of heating at 60°C (A). MSMS on precursor m/z 918 with a CE of 30 eV. Product ions from the two peaks are presented in (B) for t_R at 5.01 minutes and (C) at 5.8 minutes.

Interest in epoxides in the field of lipid oxidation is growing, wherein their presence is being used to determine the extent of oxidation. Epoxides have been determined to pose more detrimental health effects in comparison to other secondary oxidation products such as aldehydes and hydroxides (Gruneis et al. 2019). Therefore, it is important to be able to specify epoxides within a complex sample. Gruneis et al. (2019) previously suggested that epoxides form before hydroperoxides. However, based on our results obtained, it is more likely that epoxides are formed through degradation of hydroperoxides, as more commonly reported in the literature (Xia et al. 2017).

From 168 hours to 504 hours, the epoxide product was consistently present at a relative amount of ~ 80% of the two potential mono-oxygenated products of 54:3 TAG,

compared to the hydroxide product at ~20 % (Figure 5.9). At the start of the study, the hydroxide was the dominant product. Absolute signal intensity showed that the amount of hydroxy products slowly increased over time as the sample was heated, but does not increase to the same intensity levels as epoxy products. Therefore, we can propose that the degradation of hydroperoxide products into radical oxygens to form hydroxy oxidation products occurred readily without the need to be heated for long durations (Figure 5.9). The formation of epoxides from these radicals is proposed to require more heating, but to accumulate at higher amounts once they start to form (Xia et al. 2017). The greater abundance of epoxides in comparison to hydroxides agrees in general with the study by Xia et al. (2017), where epoxy FAs were deemed more abundant than hydroxy FAs in canola. In contrast, the study showed epoxy concentration was consistently greater than hydroxides, whereas the present study proved the abundances varied.

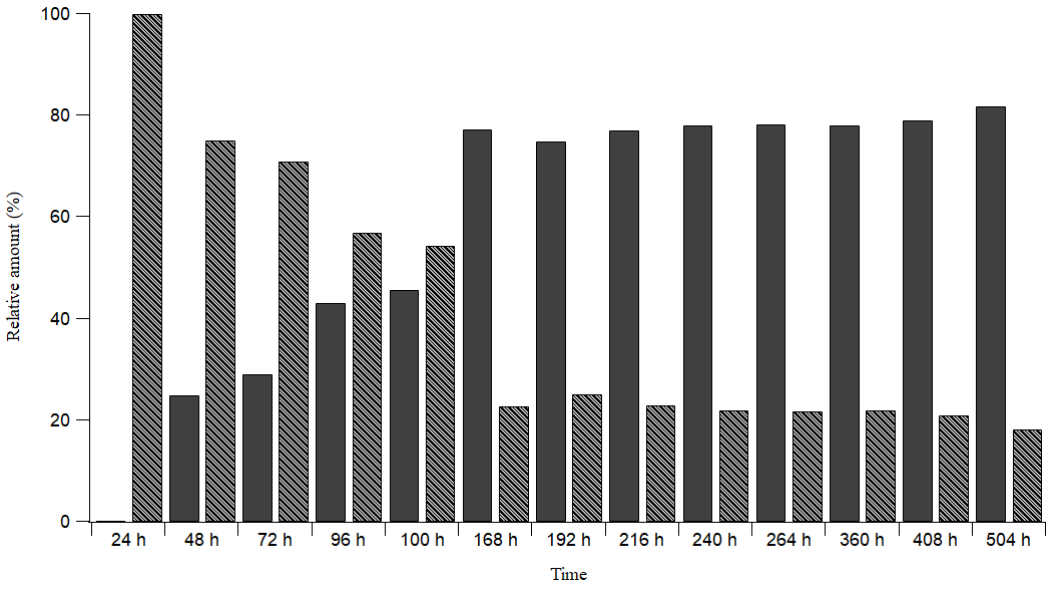

Figure 5.9 Proposed mono-hydroxy 54:3 TAG in canola represented by diagonal grey stripes versus proposed mono-epoxy 54:3 TAG in canola represented by solid black.

The change in oxidation products over time is an important result. The overlapping m/z oxidation products can easily be misinterpreted as the wrong oxidation product. Unique product ions and retention times allow for a better understanding in how oxidation proceeds. Furthermore, the later appearance of epoxide products provides insight into when these oxidation products should be measured and how they are forming.

5.3.4 Di-oxygenated Degradation Products of 54:3 TAG

Investigation of the appearance of di-oxygen products of 54:3 TAG (m/z 934) elute earlier than mono-oxygenated TAG at ~4.95 minutes. XIC of m/z 934 produced a single chromatographic peak until 168 hours of heating (Figure 5.10). After this time point, a shoulder began to appear at an earlier retention time of ~ 4.3 minutes. It should also be noted that the time points of 144 and 168 hours produced a thinner peak than the other time points (Figure 5.10). It can be proposed that the wider chromatographic peaks form from multiple isomer products, whereas the thinner peaks contain fewer isomers. The different chromatographic profiles indicate that some isomers degrade faster or more preferentially than others.

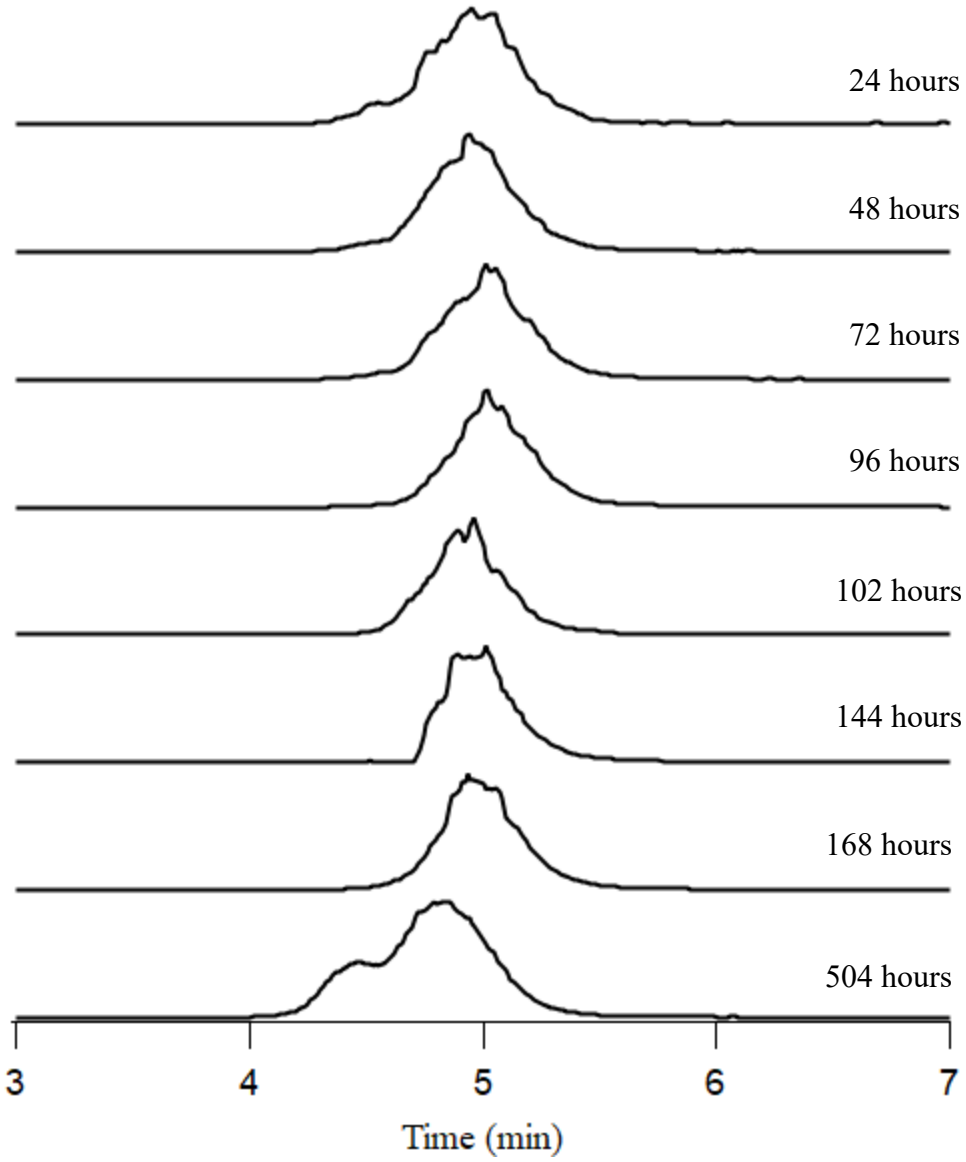

Figure 5.10 XIC of di-oxygenated 54:3 TAG of canola after heating at 60°C for 24 hours, 48 hours, 72 hours, 96 hours, 102 hours, 144 hours, 168 hours and 504 hours.

A collision energy of 30 eV was applied to precursor m/z 934 to generate a better qualitative understanding of the TAG degradation structures after 504 hours. Previously, the MSMS spectrum of precursor m/z 934 was shown after 24 hours, where expected DAG product ions were produced and m/z 934 was determined to be mono-

hydroperoxide 54:3 TAG (Figure 5.11). After 504 hours, it was determined that di-epoxy and di-hydroxy products had formed to result in the shoulder on the XIC of m/z 934.

It was previously determined in Chapter 2 that MSMS of hydroperoxides does not produce a DAG product ion with the peroxide group intact at an amount that could be identified. Previous studies by Gruneis et al. (2019) and Neff et al. (1998) report very low amounts of DAG product ions containing a peroxy group although both used different analytical methods than this work: APCI MS and Sep-Pak separation mechanisms. Initial MSMS analysis after 24 hours of heating led to the identification of m/z 934 as hydroperoxides. Therefore, it was unexpected to see higher amounts of DAG product ions at m/z 633 and m/z 635, with two oxygens attached when MSMS was done at 504 hours (Figure 5.11). The product ions at both retention times, 4.3 and 4.7 minutes are more similar to di-epoxide or di-hydroxide product ions than hydroperoxide (Figure 5.11). The appearance of multiple DAG-[O] ions and DAG-[2O] ions is expected from di-epoxide degradation products and di-hydroxide degradation products, based on the analysis in Chapter 2. The shift in retention time is also in correlation with the results obtained from di-hydroxy standard, which eluted slightly earlier than di-epoxy and hydroperoxy standards. However, the resolution and product ions are not resolved enough to distinguish di-epoxy from di-hydroxy. The initially identified DAG product ions at 24 hours, m/z 603 and m/z 615, are still present at 4.7 minutes after 504 hours, however they are present in lower amounts compared to the newly identified DAG ions. Therefore, it is anticipated that hydroperoxides were degrading into both di-epoxide and di-hydroxide product ions, leading to the shift in retention time and different MSMS

spectra. However, the presence of hydroperoxides is still identified at 504 hours, but in lower abundance compared to di-epoxides and di-hydroxides.

It is predicted that as the canola sample is heated, the hydroperoxides reach their highest concentration and then they begin to further degrade into secondary oxidation products, generating multiple oxidation products at the same m/z (Grebenteuch et al. 2021). After 24 hours, an initial comparison of the results was made to Gruneis et al. (2019) where they had identified a DAG with two oxygens intact. With the results after 504 hours, it is likely Gruneis et al. (2019) were identifying di-epoxide or di-hydroxide products rather than hydroperoxides. Their study was completed at frying temperature (180°C) that would presumably lead to increased rates of oxidation, where the hydroperoxides were degrading into epoxides and hydroxides.

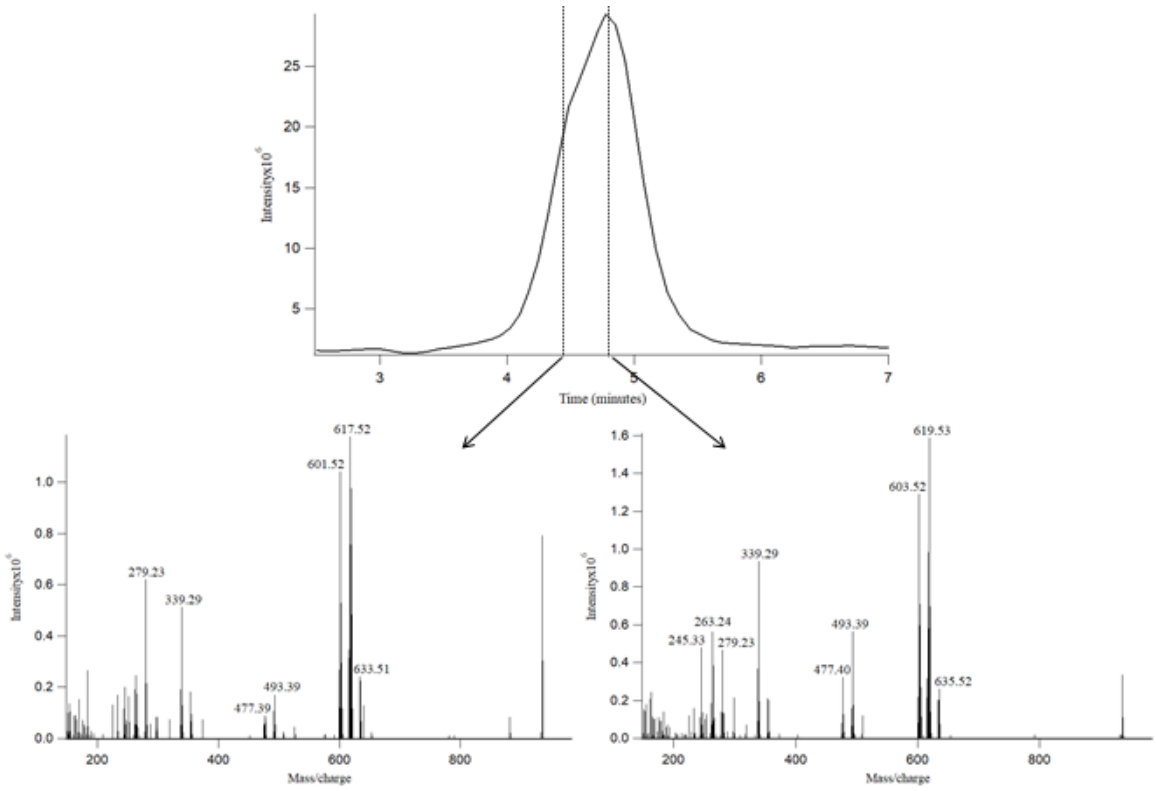

Figure 5.11 54:3 TAG with two oxygen atoms bound for a m/z of 934.81. Panel (A) shows the MSMS SRM window of m/z 934 at 504 hours of heating, where there is an appearance of a shoulder at 3.75 minutes that was not present in the previous days. Corresponding MSMS spectra are shown in panel (B) for 4.3 minutes and panel (C) for 4.70 minutes.

Product ions at m/z 477.40 and 493.39 represent the loss of parts of the acyl chain where there is an epoxide/hydroxide group. These fragment ions reveal that epoxide or hydroxide products were located on carbon-8 and carbon-9 of the fatty acyl chain.

5.3.5 Identification of Multiple Oxidation Products on 54:3 TAG

Identification of tri-oxygen 54:3 TAG at m/z 950 appeared after 96 hours of heating at 60°C. After four days, the tri-oxygenated group continued to steadily increase in signal intensity, reaching a maximum of 1.52e8 after 504 hours. Tetra-oxygenated 54:3 at m/z 966 was not identified until 168 hours where penta-oxygen at m/z 982 was 192 hours. Hexa-oxygenated 54:3 TAG at m/z 998 was identified at low amounts after 240

hours of heating. Previous identification of oxidation products with up to six oxygens has not been reported from complex oil samples. It is evident from the collected results that it requires very long oxidation times to form higher numbers of oxidation products. Mono- and di-oxidation products show chromatographic changes as the heating process evolves but the other oxidation products do not follow the same trend (Figure 5.12). Symmetrical chromatographic peaks are identified up to 504 hours, the last time point tested. Due to the lower amounts of oxidation products identified for tri-, tetra-, penta- and hexa-oxygenated 54:3, it can be assumed that if the sample were heated for a longer duration, chromatographic peaks for these oxidation products could show evidence of multiple peaks as well. However, when heating canola oil, the sample reached a point where it began to polymerize and coagulate on the heating block. This led to difficulties in accurate pipetting of the sample and to the conclusion of the time-course at 504 hours. It should also be noted that after 240 hours at 60°C, the oil sample turned a darker shade of yellow/gold which is an indication of oxidation (Jaarin & Kamisah, 2012). Incorporation of a separation step to isolate oxidation products could lead to easier identification of multiple oxidation products, however un-oxidized TAG information would be lost.

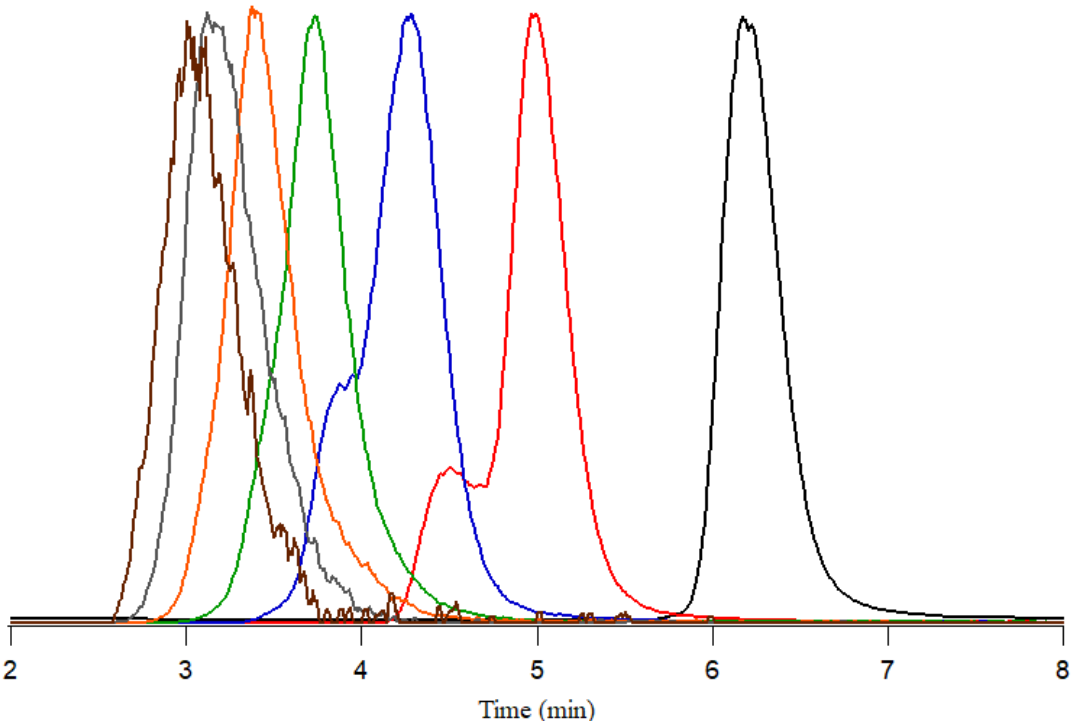

Figure 5.12 XIC of un-oxidized 54:3 TAG at m/z 902.78 in black, 54:3[O] at m/z 918.82 in red and 54:3[2O] at m/z 934.81 in blue. The green trace represents 54:3[3O] at m/z 950.80, the orange trace represents 54:3[4O] at m/z 966.79 and the grey trace represents 54:3[5O] at m/z 982.78. In brown is 54:3[6O] at m/z 998.78. The XIC were taken at 240 hours. Peaks are normalized to their maximum.

Precursor ions m/z 950.80, 966.79, 982.78 and 998.78 were targeted at a collision energy of 30 eV (Figure 5.13). The resulting fragmentation spectra were populated with multiple product ions and isomers. Precursor m/z 950 resulted in three main DAG ions previously identified from precursor m/z 934 (Figure 5.13, A). However, it is clear from the spectra that there were other DAG ions present at 2 m/z units lower, highlighting an additional double bond. Based on the product ions, it cannot be determined whether m/z 950 is composed of hydroxy, epoxy or hydroperoxy products. The DAG ions represent a protonated DAG (m/z 601.52), a mono-oxygenated DAG (m/z 617.51), a di-oxygenated DAG (m/z 633.51) and a small amount of tri-oxygenated DAG (m/z 649.50). Based on these facts, the positions of the oxidation products on the FA chains are present in

multiple different conformations. There are FA chains with 3 oxidation groups, with 2, with 1 and with no oxidation groups. There is immense complexity within oxidized TAG, which continues to increase as oxidation products increase. The DAG product ions are similar for each of the other oxidation products (Figure 5.13). Even with tetra-, penta- and hexa-oxidation products, the largest DAG was the tri-oxidized DAG. Therefore, formation of more than three oxidation products onto the same FA chain seems unfavourable.

MAG product ions were identified at m/z 265.24 (18:1) as the most abundant in each fragmentation spectra, while m/z 261.24 (18:3) and 263.5 (18:2) were present at lower amounts (Figure 5.13, A,B,C,D). The product ions at m/z 477.4, m/z 493.4 and m/z 509.39 formed due to cleavage of the carbon-carbon bond in proximity to the oxidation product on DAG ion m/z 601.54. This indicated the position of the functional groups at C9 and C10.

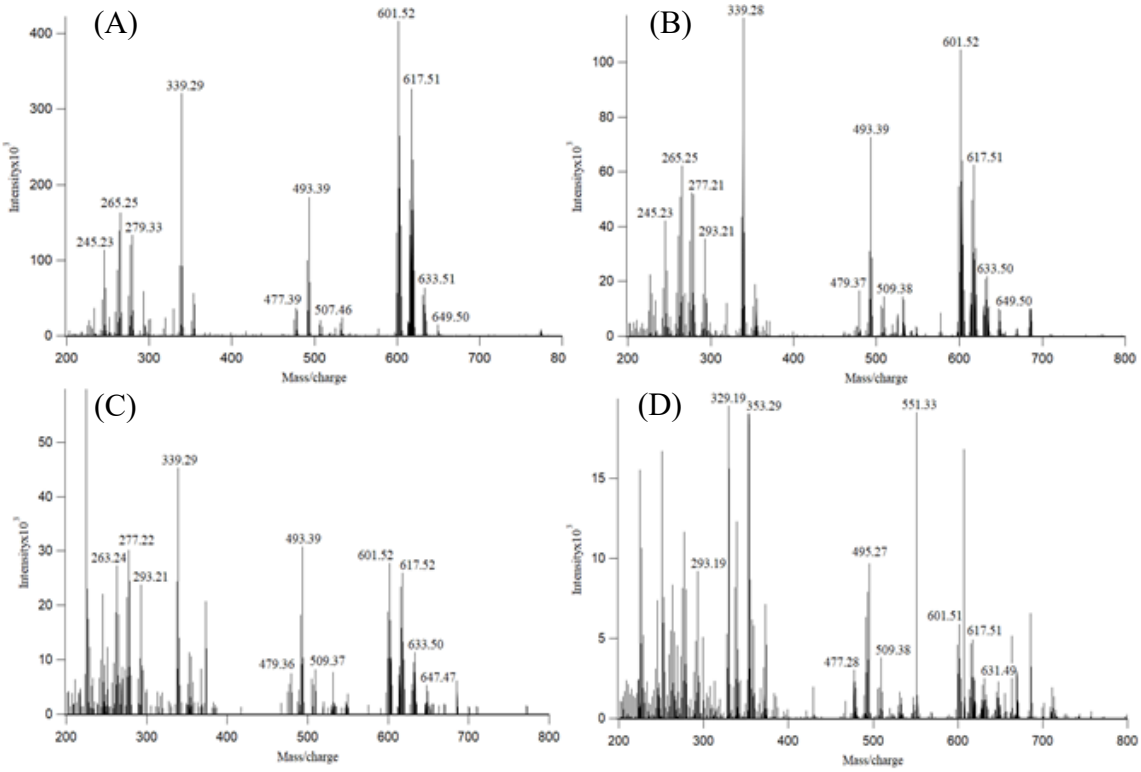

Figure 5.13 MSMS of precursor ions m/z 950.8; $C_{57}H_{105}O_6NH_3$(3O) in panel (A), m/z 966.5; $C_{57}H_{105}O_6NH_3$(4O) in panel (B), m/z 982.5; $C_{57}H_{105}O_6NH_3$(5O) in panel (C) and m/z 998.5;$C_{57}H_{105}O_6NH_3$(6O) in panel (D). Product ion at m/z 601.53 represents $C_{39}H_{69}O_4$ and 617.52 represents $C_{39}H_{69}O_5$. Product ion m/z 633.52 represents $C_{39}H_{69}O_5$ and 649.51 represents $C_{39}H_{69}O_6$. Product ions m/z 509.39, 493.4 and 477.4 represent $C_{32}H_{61}O_4$, $C_{31}H_{57}O_4$ and $C_{31}H_{57}O_3$, respectively.

Absolute signal intensity was extracted for each potential oxidation group, including the identification of mono-hydroxy versus mono-epoxy 54:3 TAG. As the sample was continuously heated the amount of oxidation products in general was anticipated to increase. Extracting each oxidation product separately provided a more in-depth analysis of the rate of oxidation for each type of individual oxidation product. When grouped together over the entire time duration, signal levels over the first 100 hours are not easily shown due to higher signal intensities at 168 hours to 504 hours (Figure 5.14). It is important to note the increase in oxidation products from 100-168

hours. At some time between 100 and 168 hours, the oxidation rate increased sharply for most products and then stayed relatively consistent with the exceptions of mono-epoxy 54:3 and the di-oxygen products that began to increase in signal again from 360-504 hours. In section 5.3.4, it was determined that m/z 934 was composed of di-epoxides/hydroxides and primary hydroperoxide products after 504 hours. It can be proposed that the decrease in m/z 934 at 216-360 hours is primary hydroperoxide oxidation products degrading. It was previously stated by Grebenteuch et al. (2021) that hydroperoxides reach a lag time, where the amount of hydroperoxides forming is less than the amount degrading (Grebenteuch et al. 2021). Based on this evidence, it is anticipated that at 216 hours, hydroperoxides had reached their lag time. In addition, when m/z 934 was decreasing, the formation of epoxide products (Figure 5.14, blue striped) increased. The evidence supporting the formation of epoxides at this time includes the unique product ions and the shift in retention time. As time passes and more mono-epoxides form, the amount of di-oxygen (m/z 934) begins to increase again at 408 hours. At this time, there is evidence of the formation of di-epoxide/di-hydroxides which is assumed to contribute to the increase in m/z 934. The study was done in physical triplicates while each oxidation product followed the same general trend for each replicate (Appendix A).

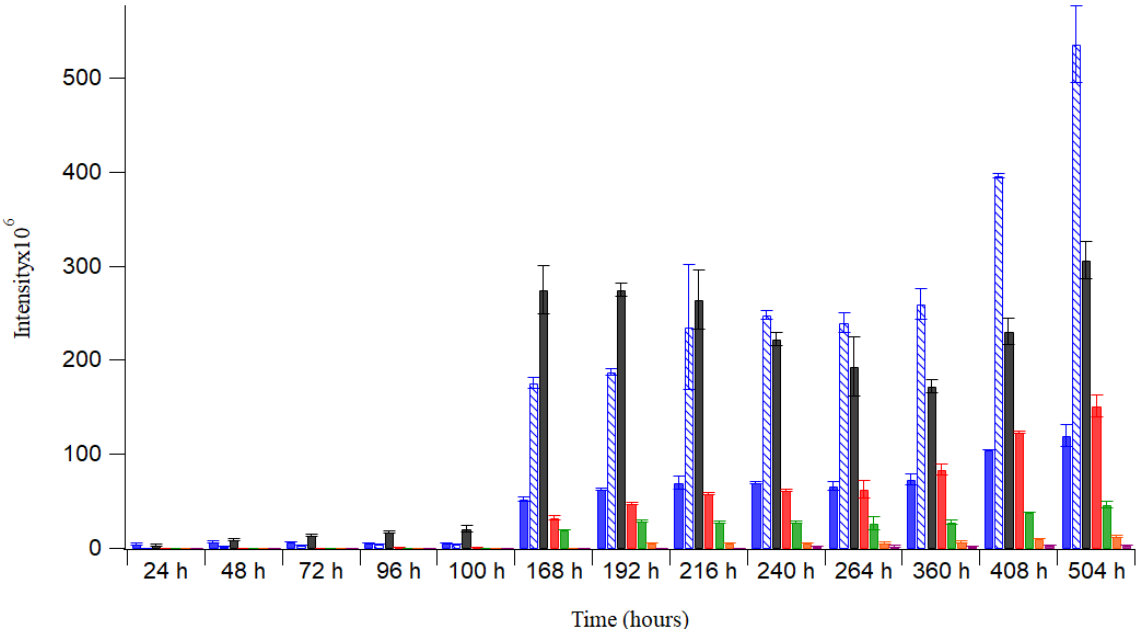

Figure 5.14 Absolute signal intensities for six potential oxidation products of 54:3 TAG in canola oil over a period of 504 hours. The bar in solid blue represents mono-hydroxy 54:3, while the blue striped bar is the proposed mono-epoxy 54:3 TAG. In black is di-oxygen 54:3, red is tri-oxygen 54:3, green is tetra-oxygen 54:3, orange is penta-oxygen 54:3 and purple represents hexa-oxygen 54:3. The relative amount was expressed as a percentage where the overall amount of oxidation within the sample is 100 %. Each sample was tested in triplicate where error bars are included based on the standard deviation.

Signal for m/z 950, tri-oxygen, steadily increases from 168-504 hours. Penta- and hexa- oxidation products were present in much lower amounts compared to the other products, as they required more time to form. It can be assumed that if the sample integrity remained intact over a longer period of time without polymerizing, higher amounts of penta- and hexa- oxidation products would be identified. Relative amounts of the oxidation products were calculated for different time points to highlight the oxidative composition of canola oil at that time (Figure 5.15). On Day 1, the sample was only composed of mono-hydroxy (53%) and di-oxygen 54:3 TAG (47%) in terms of oxidation products. On day 2 and 3, >50% of the sample was composed of di-oxygen (hydroperoxy) products, while the remainder was composed of mono-hydroxy and mono-

epoxy products. The relative amount of mono-hydroxy products compared to others within the sample, steadily decreased after Day 1 to only 9 % by Day 7. At that point, there was approximately three times more of the mono-epoxy product (30%) than the mono-hydroxy product. From Day 10 to Day 20, mono-epoxy TAG was the most abundant oxidation product within the sample. Tri-oxygen products reached a maximum amount of 16 % on Day 20 while 4-, 5- and 6- oxygen products remained below 10 % throughout the duration of the study.

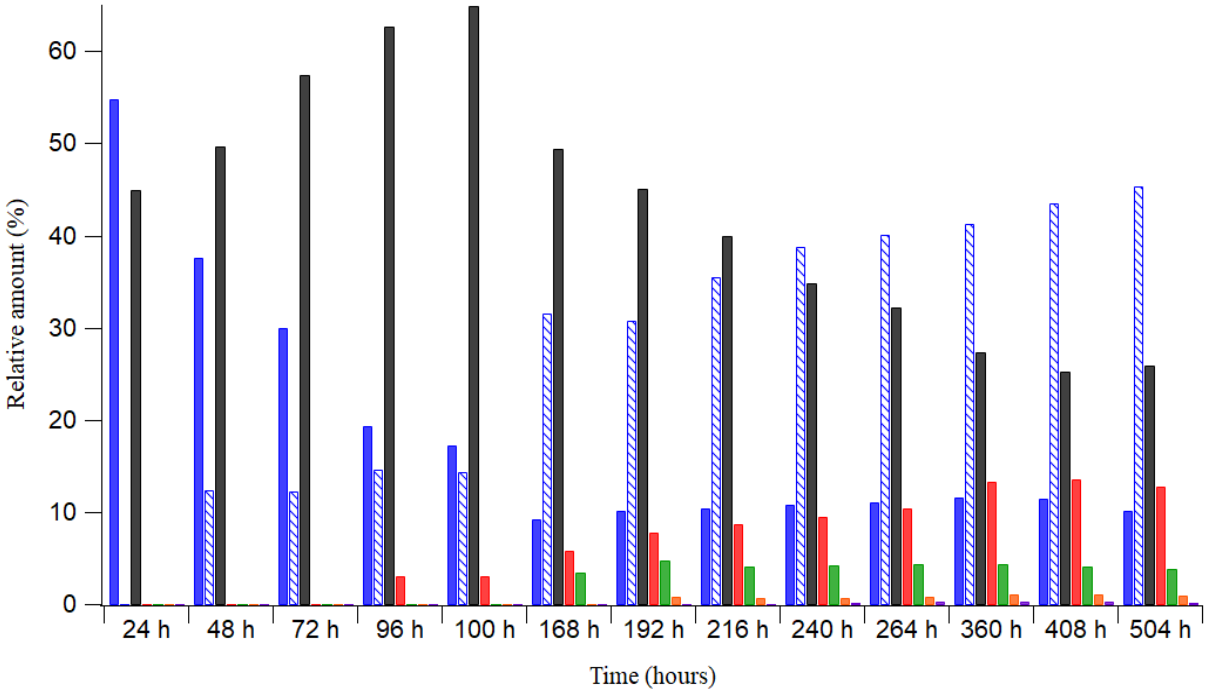

Figure 5.15 Relative amounts of six potential oxygen atoms onto 54:3 TAG in canola oil. Mono-oxygen product is represented in two columns due to the predicted appearance of both hydroxy and epoxy products. Relative amounts are calculated based on an average value calculated from three replicates taken. Mono-oxygen at an earlier tR (predicted hydroxy product) is the black column while the later retention time (predicted epoxy group) is represented by the dashed column. di-oxygen products is the blue column, tri-oxygen is in red, tetra-oxygen is in green, penta-oxygen is in orange and hexa-oxygen is in pink.

Multiple oxidation products are not commonly reported in the literature. Previous studies on the oxidation of TAG focus on single time points after thermal or light treatments (Levison et al. 2013). This often limits the ability to understand the complete process of oxidation. It is also common to heat lipid samples at frying temperatures to monitor the oxidation products over a shorter period of time (~1 hour) (Kato et al. 2017; Petronilho et al. 2021). However, even in the short time studies, the appearance of multiple m/z overlapping oxidation products was not identified. The present work demonstrates the different times and rates at which different oxidation groups are formed and degraded. The ability to generate a qualitative analysis of these lipid oxidation products provides a more thorough understanding of how, when and what oxidation products are forming. Incorporation of tandem-MS provided positional determination of where the oxidation products are located which is important to determine potential biological effects (Zeb, 2015).

5.4 Conclusion

A quick isocratic, LC-MSMS method used for a longitudinal analysis of canola oil degradation. Furthermore, the LC-MSMS method was also able to identify hydroxy, epoxy and hydroperoxy oxidation products within the same method. Canola oil was heated over 21 days and was tested at several different time points to identify the appearance of oxidation products. It was concluded that 54:3 TAG was the most abundant TAG in the canola sample. The presence of mono-oxygenated 54:3 TAG showed a second peak appearing at 72 hours of heating at 60 °C. Based on the previous results with oxidized TAG standard, it was concluded that hydroxy TAG was the first mono-oxygenated product formed, followed by the appearance of mono-epoxy TAG at

72 hours. Mono-epoxy TAG was identified as the most abundant product after 168 hours of heating. It was further determined that degradation of hydroperoxide products arises after 216 hours of heating, where di-epoxides and di-hydroxides began to form. The identification of different oxidation products forming while heated for a period of time has not previously been done. The study was important in highlighting the formation of epoxide products in comparison to the more commonly measured hydroperoxides. The short and simple LC-MSMS method can be further applied to other complex samples for identifying the formation of oxidation products over time.

CHAPTER 6 CONCLUSIONS

6.1 GENERAL CONCLUSIONS

The ability to generate a qualitative and quantitative understanding of TAGs and TAG oxidation products has been hindered by a lack of reliable analytical methods. The greatest challenge is arguably the complexity of TAG molecules. The potential number and locations of double bonds along with the number and types of oxidation products create an enormous amount of isomers that pose a significant analytical road block. A multi-analytical method is required to address these issues. This thesis addressed ways to deal with the complexity of TAGs using ESI-MS/MS, liquid chromatography and FAIMS.

The initial step in understanding TAG and TAG oxidative degradation was to optimize the ionization of standard molecules using alkali metals and ammonium as the charge carrier. Successful ionization was achieved using each of five alkali metals and ammonium; however, tandem-MS failed to successfully produce product ions with cesium and rubidium cations. Investigation into a number of isomeric oxidized TAG molecules led to the conclusion that ammonium was the best adduct for producing unique product ions. Unique product ions can be used to differentiate between the isomeric oxidation groups. Lithium and sodium did produce product ions for oxidized TAG; however they did not distinguish between oxidized TAGs with overlapping mass-to-charge ratios. Acidified ammonium was chosen as the best option for ionization due to its volatility and its ability to differentiate overlapping parent ions by tandem mass spectrometry.

Early, during the investigation of TAG ionization, the effect of inlet temperature presented as a prominent factor in the analysis of TAG. Initial analysis at an MS inlet

temperature of 275°C for ammoniated TAG suggested that the standard sample had degraded due to the presence of high amounts of DAG ions. However, after further analysis at a decreased inlet temperature of 25°C, the degradation was not present and higher signal intensities of the ammoniated monomer ion were identified as initially expected. Further investigation was carried out with ammoniated TAG, where the effect of temperature appeared to be even greater on oxidized TAG molecules. Sodium and lithium showed minimal effects from temperature, whereas temperature significantly reduced the monomer ion intensity for potassium, rubidium, cesium and ammonium adducts. High amounts of free cesium metal ion were observed at the elevated inlet temperature.

A FAIMS ion filter was incorporated to better understand the effect of MS inlet temperature since FAIMS can be used to fractionate gas-phase ions based on relative mobility before introduction to the mass spectrometer. First, FAIMS was shown to separate TAG dimers (i.e., $[2M+NH_4]^+$) from monomeric species (i.e., $[M+NH_4]^+$). Based on compensation voltage profiles acquired at different temperatures, FAIMS showed that elevated inlet temperatures (>150 °C) led to degradation of the gas-phase monomer ion into DAG and the TAG dimer ion into a monomeric species. The previously unobserved effect of temperature is important for the field of TAG analysis as it offers a suggestion to the limited knowledge of TAG oxidation products currently available in the literature. The observed instability of gas-phase TAGs and their oxidized products may have important implications for gas chromatographic techniques wherein high temperatures are critical for analyte vaporization in the sample injection port.

FAIMS was also used to look at the different ion mobilities of TAG and TAG oxidation products with alkali metals and ammonium. The ionogram profiles showed different compensation voltage (CV) values between hydroxy, epoxy and hydroperoxy oxidation products. The ionograms also varied adduct used. Different mobility profiles indicated that the different cations behaved differently, or caused the molecule to behave differently within FAIMS. FAIMS had not previously been used for TAG oxidation products, and we have only begun to scratch the surface of FAIMS potential.

Further steps to tackle the complexity of TAGs included the development of a 10 minute isocratic LCMS method. The LC method successfully resolved isomeric TAG degradation standards, offering another method for their differentiation. The LCMS method was applied to a complex sample of canola oil to monitor the degradation products over a period of 21 days. From the chromatographic profiles and MSMS analysis it was determined that there were overlapping m/z mono-epoxy and mono-hydroxy products present in canola oil, where mono-epoxy products were shown to form later than the mono-hydroxy products. Furthermore, hydroperoxy products were among the most abundant oxidation product until 240 hours when the proposed mono-epoxy product began to dominate. The longitudinal sampling and testing of the canola sample at multiple time points provided a more thorough understanding of oxidation as the products were generated. Advantages of LC-MSMS for this analysis include the direct detection of TAG species, minimal sample preparation and the extremely high sample dilution factor (100 000-fold). This study demonstrates the complexity within a real sample with the presence of multiple oxidation products having the same m/z. Incorporation of the previous MSMS and LC method allowed for assumptions to be made as to the oxidation

products present, based on fragmentation and relative retention times. These results could help guide studies using other analytical methods that require more extensive sample preparation. This methodology could also be extended to other oils or the study of a range of oxidation conditions.

In comparison to classical TAG analysis by GC, the method presented in this study provides an insight into hydroperoxide oxidation products and intact TAG molecules that are not possible by GC. The advantage of identifying hydroperoxide products is the ability to identify the start of oxidation. The ability to identify intact TAG molecules reduces the variability of TAG identification as GC relies on the identity of the FA constituents. However, the present method is limited by the vast amount of data, and potential isomers within a complex sample. Intact TAG identification limits the ability to distinguish an 18:1/18:1/18:1 TAG from a 18:2/18:0/18:1 TAG. GC would be able to identify the corresponding FA as well as the FA that contained the oxidation product. A potential combination of the two methods would increase the confidence of isomer identification.

6.2 FUTURE WORK

The initial goals of this study were to generate a better qualitative understanding of TAG and TAG degradation products and to create a multi-inlet (multi-source) FAIMS prototype for increased analyte signal intensity.

The complexity of TAGs continues to be an ongoing challenge. Tandem mass spectrometric, liquid chromatographic and FAIMS tools were introduced to address isomeric oxidation products. Further study into these techniques should be applied to different TAG standards, including those with a heterogeneous distribution of double

bonds. By addressing these gaps, a better understanding of the unique product ions and depth of this technique would be explored. Use of an appropriate MS inlet temperature is imperative to the reduction in spectral complexity, stabilization of TAG oxidation products and the minimization of heat-induced spectral artifacts.

Future studies should focus on the development of the multi-inlet/multi-source FAIMS for sensitivity enhancements, the optimization of LC-MS duty cycle using indexed sources and the discrete introduction of calibration standards. Proof of source indexing was achieved; however the use of both sources at the same time was limited by the current FAIMS ion sampling efficiency. Future FAIMS electrode designs should address issues with ion sampling and ion source design. Three-dimensional (3D) printing offers significant reductions in cost for the production and testing of new FAIMS prototypes over conventional CNC manufacturing. Outer and inner electrodes can be created using conductive polymer while the insulating electrode body can be created from polylactic acid (PLA).

FAIMS successfully transmitted intact TAG molecules with little resolution between 54:3 and 54:6 TAG. Therefore, low-resolution FAIMS might be useful as a TAG-specific filter. Future work could look into an LC-FAIMS-MS combined method, where CV is set to transmit TAG ions, reducing possible background interferences. A method using multi-inlet FAIMS prototype could potentially increase the overall signal for TAGs and would be very useful in complex matrices.

A short LC method was established for adequate separation of TAG and TAG oxidation products. However, all of the molecules eluted between 3 and 8 minutes. Future investigation should include potential gradient options where the percent ethanol is

gradually increased to 100 %. Slowly increasing the percent ethanol could lead to increased resolution between epoxide and hydroxide oxidation products in complex samples. Switching to a gradient elution will increase method duration; however, if high throughput is not necessary, the potential for increased resolution could be an advantage.

BIBLIOGRAPHY

Abeyrathne, E. D. *et al*. Analytical methods for lipid oxidation and antioxidant capacity in food systems. *Antioxidants* **10,** 1587 (2021).

Adams, J. & Gross, M. Energy Requirements for Remote Charge Site Ion Decompositions and Structural Information from Collisional Activation of Alkali Metal Cationized Fatty Alcohols. *Journal of the American Chemistry Society* **108**, 6915-6921 (1986).

Andrikopoulos, N. K. Triglyceride species compositions of common edible vegetable oils and methods used for their identification and quantification. *Food Reviews International* **18,** 71–102 (2002).

Baba, T. *et al*. Structural identification of triacylglycerol isomers using electron impact excitation of ions from organics (EIEIO). *Journal of Lipid Research* **57,** 2015–2027 (2016).

Baker, P.R.S. *et al*. Three-dimensional enhanced lipidomics analysis combining UPLC, differential ion mobility spectrometry, and mass spectrometric separation strategies. *Journal of Lipid Research* **55**, (2014).

Barnett, D. *et al.* Application of ESI-FAIMS-MS to the Analysis of Tryptic Peptides. *Journal of American Society for Mass Spectrometry* **13**, 1282-1291 (2002).

Barnett, D. *et al*. Elimination of the helium requirement in high-field asymmetric waveform ion mobility spectrometry (FAIMS): beneficial effects of decreasing the analyzer gap width on peptide analysis. *Rapid Communications in Mass Spectrometry* **25**, 1-13 (2011).

Bayly, G. R. Lipids and disorders of lipoprotein metabolism. *Clinical Biochemistry: Metabolic and Clinical Aspects* 702–736 (2014). doi:10.1016/b978-0-7020-5140-1.00037-7

Belford, M. *et al.* Characterization of FAIMS Waveform With Regards to Amplitude, Frequency, Phase, and Electrode Temperature. *Thermo Fisher Scientific* (2015).

Berdeauz, O. *et al.* Selection of methylatioin procedures for quantitation of short-chain glycerol-bound compounds formed during thermoxidation. *J Chromatogr A* **863**, 171-181 (1999).

Bird, S. S. *et al*. Separation of cis–trans phospholipid isomers using reversed phase LC with high resolution MS detection. *Analytical Chemistry* **84,** 5509–5517 (2012).

Brzhozovskiy, A. *et al*. The Parallel Reaction Monitoring-Parallel Accumulation-Serial Fragmentation (prm-PASEF) Approach for Multiplexed Absolute Quantitation of Proteins in Human Plasma. *Analytical Chemistry* **94**, 2016-2022 (2022).

Byrdwell, W. C. & Neff, W. E. Analysis of genetically modified canola varieties by atmospheric pressure chemical ionization mass spectrometric and flame ionization detection. *Journal of Liquid Chromatography & Related Technologies* **19,** 2203–2225 (1996).

Cai, S.-S. & Syage, J. A. Comparison of atmospheric pressure photoionization, atmospheric pressure chemical ionization, and electrospray ionization mass spectrometry for analysis of lipids. *Analytical Chemistry* **78,** 1191–1199 (2006).

Cajka, T. & Fiehn, O. Comprehensive analysis of lipids in biological systems by liquid chromatography- mass spectrometry. *Trends in Analytical Chemistry* **61**, 192-206 (2014).

Chakrabarti, P. Systematics in the interaction of metal ions with the main-chain carbonyl group in protein structures. *Biochemistry* **3**, 651-658 (1990).

Christie, W. W. & Han, X. *Lipid analysis: Isolation, separation, identification, and lipidomic analysis*. (The Oily Press, 2010).

Christie, W. W. *Lipid analysis*. (Pergamon Press, 1982).

Cody, R.B. Electrospray ionization mass spectrometry: history, theory and instrumentation. *Applied Electrospray Mass Spectrometry* (2002).

Cohn, J. Oxidized fat in the diet, postprandial lipaemia and cardiovascular disease. *Current Opinions in Lipidomics* **13**, 19-24 (2002).

Denisov, E. *et al*. Orbitrap mass spectrometry with resolving powers above 1,000,000. *International Journal of Mass Spectrometry* **325-327,** 80–85 (2012).

Dorshel, C. Characterization of the TAG of Peanut Oil by Electrospray LC-MS-MS. *Journal of the American Oil Chemists' Society* **79** (2002).

Douglas, D.J. Linear ion trap in mass spectrometry. *Mass Spectrometry Review* **24,** 1-29 (2004).

Duffin, K. L. *et al*. Electrospray and tandem mass spectrometric characterization of acylglycerol mixtures that are dissolved in nonpolar solvents. *Analytical Chemistry* **63,** 1781–1788 (1991).

Echegaray, N. *et al.* Lipid oxidation of vegetable oils. *Food Lipids* 127–152 (2022). doi:10.1016/b978-0-12-823371-9.00009-5

Endo, Y. *et al*. Autoxidation of Synthetic Isomers of Triacylglycerol Containing Eicosapentaenoic Acid. *Journal of the American Oil Chemists' Society* **74** (1997).

Fasciotti, M. *et al.* Optimization and application of methods of triacylglycerol evaluation for characterization of olive oil adulteration by soybean oil with HPLC-APCI-MS-MS. *Talanta* **81**, 1116-1125 (2010).

Fouque, K. *et al*. Effective liquid chromatography-trapped ion mobility spectrometry-mass spectrometry separation of isomeric lipid species. *Analytical Chemistry* **91**, 5021-5027(2019).

Frankel, E. N. Chemistry of free radical and singlet oxidation of lipids. *Progress in Lipid Research* **23,** 197–221 (1984).

Frankel, E. N. *Lipid oxidation*. (The Oily Press, 1998).

Frankel, E.N. Antioxidants and Hydroperoxides: from Soybean Oil to Red Wine. *Inform* **10**, 889-896 (1999).

Frankel, EN. Secondary products of lipid oxidation. *Chem Phys Lipids* **44**, 73–85 (1987).

Gaskell, S. J. Electrospray: Principles and practice. *Journal of Mass Spectrometry* **32,** 677–688 (1997).

Gaskell, S.J. Electrospray: principles and practice. *J. Mass Spectrom* **32**, 677-688.

Gerbig, S. & Takats, Z. Analysis of triglycerides in food items by desorption electrospray ionization mass spectrometry. *Rapid Communications in Mass Spectrometry* **15,** 2186-2192 (2010).

Gray, J. I. Measurement of lipid oxidation: A Review. *Journal of the American Oil Chemists' Society* **55,** 539–546 (1978).

Grebenteuch, S. *et al*. Formation of secondary and tertiary volatile compounds resulting from the lipid oxidation of rapeseed oil. *Foods* **10**, (2021)

Griffiths, W.J. *et al.* Lipidomics Basics. *Lipidomics: Current and Emerging Techniques*, 1-24 (2020)

Grossert, J.S. *et al.* Studying the Chemistry of Cationized Triacylglycerols Using Electrospray Ionization Mass Spectrometry and Density Functional Theory Computations. *Journal of the American Society for Mass Spectrometry* **25**, 1421-1440 (2014).

Grüneis, V. *et al.* Simultaneous analysis of epoxidized and hydroperoxidized triacylglycerols in canola oil and margarine by LC-MS. *Journal of Agricultural and Food Chemistry* **67,** 10174–10184 (2019).

Guan, M. *et al*. A study on triacylglycerol composition and the structure of high-oleic rapeseed oil. *Engineering* **2**, 258-262 (2016).

Guevremont, R. *et al.* High Field Asymmetric Waveform Ion Mobility Spectrometry-Mass Spectrometry: An Investigation of Leucine Enkephalin Ions Produced by Electrospray Ionization. *Journal of the American Society for Mass Spectrometry* **10**, 492-501 (1999).

Hamilton, R. J. *Chemistry of free radicals in lipids*. (Society of Chemical Industry, 1993).

Hamilton, R. J. *et al.* Chemistry of free radicals in lipids. *Food Chemistry* **60,** 193–199 (1997).

Han, X. & Gross, R. W. Quantitative analysis and molecular species fingerprinting of triacylglyceride molecular species directly from lipid extracts of biological samples by electrospray ionization tandem mass spectrometry. *Analytical Biochemistry* **295,** 88–100 (2001).

Han, X. & Ye, H. Overview of lipidomic analysis of triglyceride molecular species in biological lipid extracts. *Journal of Agricultural and Food Chemistry* **69,** 8895–8909 (2021).

Horman, I. & Traitler, H. Pseudo-molecular ions in ion trap detector electron impact mass spectra: practical consequences. *Anal. Chem* **61**, 1983-1984 (1989)

Hsu, F.-F. & Turk, J. Structural characterization of triacylglycerols as lithiated adducts by electrospray ionization mass spectrometry using low-energy collisionally activated dissociation on a triple stage quadrupole instrument. *Journal of the American Society for Mass Spectrometry* **10,** 587–599 (1999).

Hsu, F-F. Mass spectrometry-based shotgun lipidomics- a critical review from the technical point of view. *Journal of Analytical and Bioanalytical Chemistry* **410,** 6387-6409(2018).

Indelicato, S. *et al*. Triacylglycerols in edible oils: Determination, characterization, quantitation, chemometric approach and evaluation of adulterations. *Journal of Chromatography A* **1515**, 1-16 (2017).

Jaarin, K. & Kamisah, Y. Repeatedly heated vegetable oils and lipid peroxidation. *Lipid Peroxidation* **10**, (2012).

Jedrychowski, M. P. *et al.* Evaluation of HCD- and CID-type fragmentation within their respective detection platforms for murine phosphoproteomics. *Molecular & Cellular Proteomics* **10,** (2011).

Jenske, R. & Vetter, W. Gas chromatography/ electron-capture negative ion mass spectrometry for the quantitative determination of 2- and 3-hydroxy fatty acids in bovine milk fat. *J Agric Food Chem* **56**, 5500-5505 (2008).

Jurowski, K. *et al.* Analytical Techniques in Lipidomics: State of the Art. *Critical Reviews in Analytical Chemistry* **0**, 1-20 (2017).

Kail, B.W. *et al*. Determination of Free Fatty Acids and Triacylglycerides by Gas Chromatography Using Selective Esterification Reactions. *Journal of Chromatographic Science* **50**, 934-939 (2012).

Kalo, P.J. *et al*. Identification of molecular species of simple lipids by normal phase liquid chromatography-positive electrospray tandem mass spectrometry, and application of developed methods in comprehensive analysis of low erucic acid rapeseed oil lipids. **254**, 106-121 (2006).

Kanner, J. Dietary advanced lipid oxidation endproducts are risk factors to human health. *Molecular Nutritional Food Research* **51**, 1094-1101 (2007).

Kato, S. *et al*. Determination of Triacylglycerol Oxidation Mechanisms in Canola Oil Using Liquid Chromatography-Tandem Mass Spectrometry. *Npj Sci Food* **2**, 1 (2018).

Kato, S. *et al.* Determination of triacylglycerol oxidation mechanisms in canola oil using liquid chromatography–tandem mass spectrometry. *npj Science of Food* **2,** (2018).

Kato, S. *et al.* Structural analysis of lipid hydroperoxides using mass spectrometry with alkali metals. *Journal of the American Society for Mass Spectrometry* **32,** 2399–2409 (2021).

Keilhauer, E. C. HCD fragmentation of glycated peptides. *Journal of Proteome Research* (2016). doi:10.1021/acs.jproteome.6b00464.s003

Khor, Y.P. *et al*. Oxidation and Polymerization of Triacylglycerols: In-Depth Investigations towards the Impact of Heating Profiles. *Foods* **8**, 1-15 (2019)

Kruve, A. & Kaupmees, K. Adduct formation in ESI/MS by mobile phase additives. *Journal of The American Society for Mass Spectrometry* **28**, 887-897 (2017)

Lazardi, E. *et al.* A Comprehensive Two-Dimensional Liquid Chromatography Method for the Simultaneous Separation of Lipid Species and their Oxidation Products. *Journal of Chromatography* A **1644** (2021).

Lee, H.R. *et al*. Comparison of Electrospray Ionization and Atmospheric Chemical Ionization Coupled with Liquid Chromatography-Tandem Mass Spectrometry for the Analysis of Cholesteryl Esters. *International Journal of Analytical Chemistry* **2015** (2015).

Levison, B. *et al*. Quantification of fatty acid oxidation products using online high-performance liquid chromatography tandem mass spectrometry. *Free Radical Biology and* Medicine **59**, 2-13 (2013).

Li, L. *et al*. Mass Spectrometry Methodolgy in Lipid Analysis. *International Journal of Molecular Sciences* **15**, 10492-10597 (2014).

Liang, C. *et al.* Simple and sensitive method for the quantitative determination of lipid hydroperoxides by liquid chromatography/mass spectrometry. *Antioxidants* **11,** 229 (2022).

Liebisch, G. *et al.* Update on lipid maps classification, nomenclature, and shorthand notation for MS-derived lipid structures. *Journal of Lipid Research* **61,** 1539–1555 (2020).

Lim, J.H. *et al.* Simultaneous Quantification of Oleins (triolein, diolein and monoolein) in Mouse Feces using Liquid Chromatography-Electrospray Ionization/Mass Spectrometry. *Mass Spectrometry Letters* **3,** (2012).

Lin, J.T. *et al.* Analysis of Regiospecific Triacylglycerols by Electrospray Ionization-Mass Sepctrometry^3 of Lithiated Adducts. *Journal of Agricultural and Food Chemistry* **56,** 4909-4915 (2008).

Lintonen, T. *et al*. Differential mobility spectrometry-driven shotgun lipidomics. *Analytical Chemistry* **86**, 9662-9669 (2014).

Mansbach, C. M. Fat digestion and absorption. *Encyclopedia of Gastroenterology* 23–30 (2004). doi:10.1016/b0-12-386860-2/00263-x

McAnoy, A. M. *et al*. Direct qualitative analysis of triacylglycerols by electrospray mass spectrometry using a linear ion trap. *Journal of the American Society for Mass Spectrometry* **16,** 1498–1509 (2005).

Mottram, H. R. & Evershed, R. P. Elucidation of the composition of bovine milk fat triacylglycerols using high-performance liquid chromatography–atmospheric pressure chemical ionisation mass spectrometry. *Journal of Chromatography A* **926,** 239–253 (2001).

Mubiru, E. *et al.* Improved gas chromatography-flame ionization detector analytical method for the analysis of epoxy fatty acid. *J Chromatogr A* **1318**, 217-225 (2013).

Neff, W. E. & Byrdwell, W. C. Characterization of model triacylglycerol (Triolein, trilinolein and trilinolenin) autoxidation products via high-performance liquid chromatography coupled with atmospheric pressure chemical ionization mass spectrometry. *Journal of Chromatography A* **818,** 169–186 (1998).

Neff, W. E. *et al.* Autoxidative dimerization of methyl linolenate and its monohydroperoxides, Hydroperoxy epidioxides and dihydroperoxides. *Journal of the American Oil Chemists' Society* **65,** 616–623 (1988).

Paciga, A. *et al*. Effect of Ammonia on the Volatility of Organic Diacids. *Environmental Science and Technology* **48**, (2014).

Pavlica, D. *et al.* Quantification of Hydroperoxides by Gas Chromatography with Flame Ionization Detection. *Acta Chimica Slovenica* **3**, 728-735 (2021).

Payne, A. H. & Glish, G. L. Tandem Mass Spectrometry in quadrupole ion trap and ion cyclotron resonance mass spectrometers. *Methods in Enzymology* 109–148 (2005). doi:10.1016/s0076-6879(05)02004-5

Pelley, J. W. Fatty acid and triglyceride metabolism. *Elsevier's Integrated Review Biochemistry* 81–88 (2012). doi:10.1016/b978-0-323-07446-9.00010-6

Petronilho, S. *et al*. Characterization of Non-volatile Oxidation Products Formed from Triolein in a Model Study at Frying Temperature. *Journal of Agriculture and Food Chemistry* **69**, 3466-3478 (2021).

Poad, B. *et al*. Online Ozonolysis Combined with Ion Mobility-Mass Spectrometry Provides a New Platform for Lipid Isomer Analyses. *Journal of Analytical Chemistry* **90,** 1292-1300 (2018).

Postel, A.D. Electrospray mass spectrometry of lipids. *Lipid Technology* **18**, 181-185.

Purves, R.W. & Guevremont, R. Electrospray Ionization High-Field Asymmetric Waveform Ion Mobility Spectrometry-Mass Spectrometry. *Journal of Analytical Chemistry* **71**, 2346-2357 (1999).

Qian, Y. *et al*. Determination of triacylglycerols by HTGC-FID as a sensitive tool for the identification of rapeseed and olive oil adulteration. *Molecules* **25,** 3881 (2020).

Renaud, J.B. *et al*. Energy and entropy at play in competitive dissociations: The case of uneven positional dissociation of ionized triacylglycerides. *International Journal of Mass Spectrometry* **352**, 77-86 (2013).

Rigano, F. *et al*. High-performance liquid chromatography combined with electron ionization mass spectrometry: A review. *Trends in Analytical Chemistry* **118**, (2019)

Rossi, D. *et al*. Tandem-in-Time Mass Spectrometry as a Quantitative Bioanalytical Tool. *Journal of Analytical Chemistry* **69**, 4519-4523 (1997).

Saguy, I.S. *et al*. Integrated approach to deep fat frying: engineering, nutrition, health and consumer aspects. *Journal of Food Engineering* **56**, 143-152.

Sala, M. *et al*. Determination of triacylglycerol regioisomers using differential mobility spectrometry. *Rapid Commun. Mass Spectrom* **30,** 256-264 (2016).

Schaich, K. M. Challenges in analyzing lipid oxidation. *Lipid Oxidation* 53–128 (2013). doi:10.1016/b978-0-9830791-6-3.50005-9

Schaich, KM. Lipid oxidation: theoretical aspects. *New York: John Wiley & Sons, Inc* **6**, 269–355 (2005).

Schaich, KM. Thinking outside the classical chain reaction box of lipid oxidation. *Lipid Technol* **24**, 55–8 (2012).

Schneider, C. An update on products and mechanisms of lipid peroxidation. *Molecular Nutrition & Food Research* **53,** 315–321 (2009).

Schwudke, D. *et al*. Shotgun lipidomics on high resolution mass spectrometers. *Cold Spring Harbor Perspectives in Biology* **3,** (2011).

Shu-ling, X. *et al*. Research advances based on mass spectrometry for profiling of triacylglycerols in oils and fats and their applications. *Journal for Electrophoresis* **39**, 1558-1568 (2018).

Simas, R.C. *et al*. Triacylglycerols Oxidation in Oils and Fats Monitored by Easy Ambient Sonic-Spray Ionization Mass Spectrometry. *Journal of the American Oil Chemists' Society* **89**, 1193-1200 (2012).

Sinclair, E. *et al*. Monilising ion mobility mass spectrometry for metabolomics. *Analyst* **19**, (2018).

Smith, B. L. *et al.* Flexible drift tube for high resolution ion mobility spectrometry (FLEX-DT-IMS). *Analytical Chemistry* **92,** 9104–9112 (2020).

Somgoyi, Á. R. P. Á. D. Mass spectrometry instrumentation and techniques. *Medical Applications of Mass Spectrometry* 93–140 (2008). doi:10.1016/b978-044451980-1.50008-2

Stow, S.M. *et al.* An Interlaboratory Evaluation of Drift Tube Ion Mobility-Mass Spectrometry Collision Cross Section Measurements. *Analytical Chemistry* **17**, 9048-9055 (2017).

Strupat, K. *et al.* High-Resolution, Accurate-Mass Orbitrap Mass Spectrometry-Definitions, Opportunities, and Advantages. *Thermo Fisher Scientific* (2016).

Sullivan Ritter, J. *et al.* Oxidation Rates of Triacylglycerol and Ethyl Ester Fish Oils. *Journal of the American Oil Chemists' Society* **92**, 561-569 (2015).

Sutton, P. A. & Rowland, S. J. High temperature gas chromatography–time-of-flight-mass spectrometry (HTGC–TOF-MS) for high-boiling compounds. *Journal of Chromatography A* **1243,** 69–80 (2012).

Volmer, D. A. *et al.* Ion suppression :A major concern in mass spectrometry. *LCGC North America* **24**, 498-510 (2006).

Watson, J.T. Introduction to Mass Spectrometry. *Lippincott-Raven* **3**, (1997).

White, D. A. *et al*. Genetic determinants of plasma lipoprotein levels and their dietary response. *Prostaglandins, Leukotrienes and Essential Fatty Acids* **57,** 455–462 (1997).

Xia, W. & Budge, S. M. Techniques for the analysis of minor lipid oxidation products derived from triacylglycerols: Epoxides, alcohols, and ketones. *Comprehensive Reviews in Food Science and Food Safety* **16,** 735–758 (2017).

Xia, W. & Budge, S. Simultaneous quantification of epoxy and hydroxy fatty acids as oxidation products of triacylglycerols in edible oils. *Journal of Chromatography A* **1537**, 83-90 (2018).

Xia, W. *et al*. 1H-NMR Characterization of Epoxides Derived from Polyunsaturated Fatty Acids. **Journal of the American Oil Chemists' Society 93**, 467-478 (2016).

Xu, C. & Shanklin, J. Triacylglycerol metabolism, function, and accumulation in plant vegetative tissues. *Annual Review of Plant Biology* **67,** 179–206 (2016).

Yang, L. *et al.* Recent advances in Lipidomics for Disease Research. *Journal of Separation Science* **39,** 38–50 (2015).

Yoshinaga, K. *et al.* Quantification of triacylglycerol molecular species in edible fats and oils by gas chromatography-flame ionization detector using correction factors. *Journal of Oleo Science* **66,** 259–268 (2017).

Zeb, A. & Murkovic, M. Analysis of triacylglycerols in refined edible oils by isocratic HPLC-ESI-MS. *Journal of Lipid Science* **112**, 844-851 (2010).

Zeb, A. & Murkovic, M. Characterization of the effects of β-carotene on the thermal oxidation of triacylglycerols using HPLC-ESI-MS. *European Journal of Lipid Science* Technology **112**, 1218-1228 (2010).

Zeb, A. Chemistry and liquid chromatography methods for the analyses of primary oxidation products of triacylglycerols. *Free Radical Research* **49,** 549–564 (2015).

Zeb, A. Triacylglycerols composition, oxidation and oxidation compounds in camellia oil using liquid chromatography-mass spectrometry. *Chemistry of Physics of Lipids* **5**, 608-614 (2012).

Zheng, X. *et al.* Recent Advances in Lipid Separations and Structural Elucidation Using Mass Spectrometry Combined with Ion Mobility Spectrometry, Ion-Molecule Reactions and Fragmentation Approaches. *Curr Opin Chem Biol* **42**, 111-118 (2017).

Zubarev, R. A. & Makarov, A. Orbitrap Mass Spectrometry. *Analytical Chemistry* **85,** 5288–5296 (2013).

APPENDIX A PHYSICAL REPLICATES OF CANOLA OIL DEGRADATION STUDY

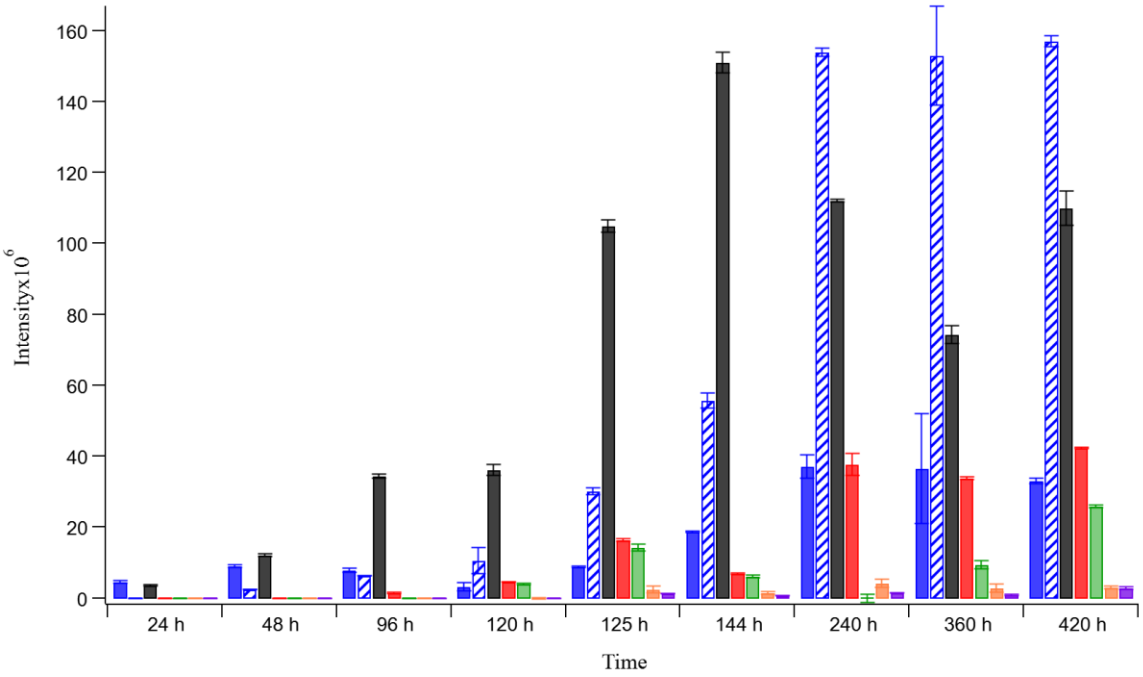

Figure A1. Absolute signal intensities of Canola oil degradation replicate 1, with hydroxy (blue), epoxy (blue striped), di-oxygen (black), tri-oxygen (red), tetra-oxygen (green), penta-oxygen (orange) and hexa-oxygen (purple). Error bars are the standard deviation of the technical replicates.

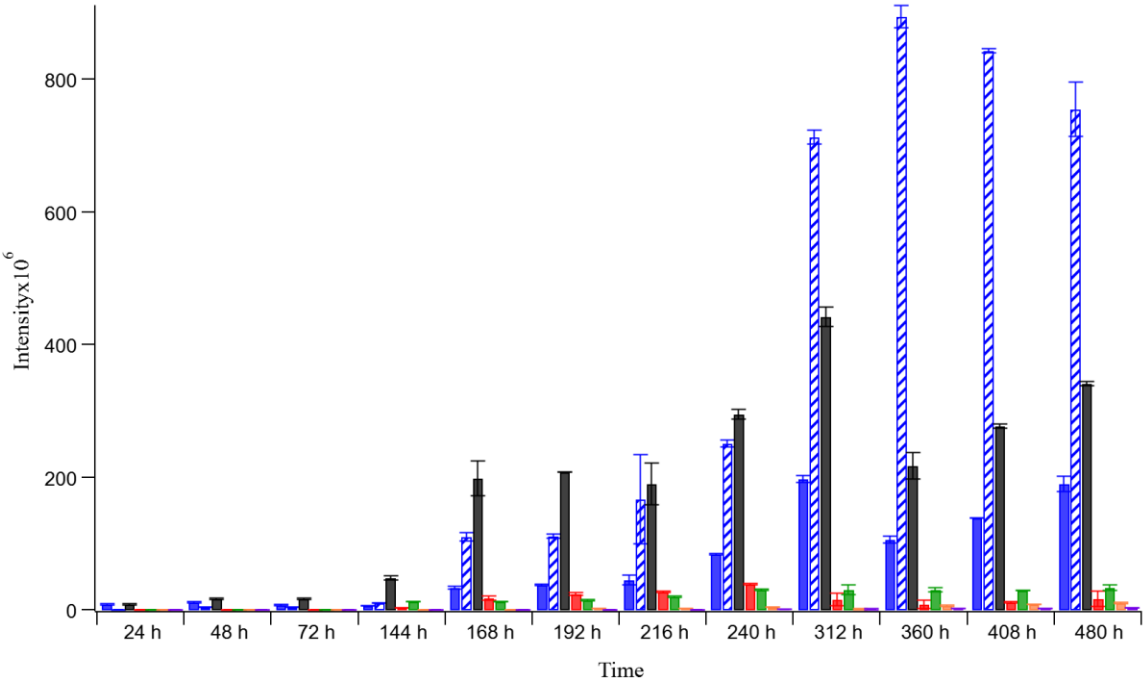

Figure A2. Absolute signal intensities of Canola oil degradation replicate 2, with hydroxy (blue), epoxy (blue striped), di-oxygen (black), tri-oxygen (red), tetra-oxygen (green), penta-oxygen (orange) and hexa-oxygen (purple). Error bars are the standard deviation of the technical replicates.